The role of the lysine-specific demethylase 1 during oligodendrocyte differentiation and its novel function in nuclear redox signaling

Inaugural-Dissertation

zur Erlangung des Doktorgrades
der Mathematisch-Naturwissenschaftlichen Fakultät
der Heinrich-Heine-Universität Düsseldorf

vorgelegt von
Thomas Hildebrandt
aus Göttingen

Düsseldorf, September 2020

Aus der Klinik für Neurologie
der Heinrich-Heine-Universität Düsseldorf

Gedruckt mit der Genehmigung der
Mathematisch-Naturwissenschaftlichen Fakultät der
Heinrich-Heine-Universität Düsseldorf

Berichterstatter:
1. **Univ.-Prof. Dr. Orhan Aktas**
(Klinik für Neurologie der Heinrich-Heine-Universität Düsseldorf)
2. **Univ.-Prof. Dr. Andreas Reichert**
(Institut für Biochemie und Molekularbiologie I der Heinrich-Heine-Universität Düsseldorf)

Tag der mündlichen Prüfung: 31.03.2021

I Declaration

Ich versichere an Eides Statt, dass die Dissertation von mir selbständig und ohne unzulässige fremde Hilfe unter Beachtung der „Grundsätze zur Sicherung guter wissenschaftlicher Praxis an der Heinrich-Heine-Universität Düsseldorf“ erstellt worden ist. Darüber hinaus versichere ich, dass diese Dissertation noch keiner anderen Fakultät zur Prüfung vorgelegen hat.

Düsseldorf

(Thomas Hildebrandt)

II Acknowledgement

Der größte Dank gebührt meiner Familie, die mir meine Ausbildung ermöglicht hat, mich unterstützt hat und ohne die es nicht möglich gewesen wäre, diese Doktorarbeit abzuschließen.

I would like to thank Prof. Dr. Orhan Aktas for giving me the opportunity to do a doctoral thesis in his research group. Furthermore, I would like to thank him for the suggestion to change the focus from neurogenesis to OPCs development. I thank Prof. Andreas Reichert for his help and for accepting the task as a second supervisor. I thank PD Dr. Carsten Berndt for showing complete confidence in my work and for giving me the opportunity to take advantage of collaborations that were essential to develop a PhD project. In addition, I would like to thank all members of the AG Aktas. In particular, Klaudia for her support and motivation! Jan Schmitz for his help with the redox-blots and belgian beers, and finally, Tim for his selfless help, his responsibility and scientific exchange.

I am very grateful to Ben for giving me the opportunity to pursue experiments in his lab over a long period of time. During the time in Bonn I felt very warmly welcomed and always had the feeling of being part of the group. Except for the long journey, I was always very happy to come to Bonn. Many thanks to Tobi, Felix, Bhuvi, Enrico, Funda and Öznur. Without your help the experiments in Bonn would not have been possible.

I would like to thank Lars Bräutigam for the opportunity to spend 2 very nice weeks in Stockholm. It is a pity that the EMBO application did not work out. Many thanks also to Linda Pudelko for the experiments in the glioblastoma cells and all the best for your future career.

I am extremely appreciative for Gereon Poschmann, who supported me throughout my doctoral thesis with the numerous mass spectrometric measurements that were essential for the development of both parts of my work.

In the last third of my doctoral thesis I had the luck to be a guest in Ilka Wittig's lab 2 times. I would like to thank Ilka, Juliana and Jana Meisterknecht. Your advices to perform a co-IP and a redoxome analysis were essential to develop the LSD1/oxidase project. Your willingness to help was incredible. In particular, Jule

and Jana for their help in the lab and Ilka for the evaluation of all measurements. Beyond that I was impressed by your hospitality and responsibility!
I thank Qu Jiang for her help with the LSD1 mice and wish her all the best for the future.

Finally, I would like to thank Elena Vasyutina, who tragically passed away this year. I am very grateful for your responsibility and for your selfless help you offered, although we barely knew each other.

III Abstract

The lysine-specific demethylase 1 (LSD1) is a flavin-dependent histone demethylase that is implicated in transcriptional activation and repression. Beside its role as a unifying transcriptional regulator during development and cancer progression, it produces the second messenger hydrogen peroxide (H_2O_2) as a by-product, whose fate and function is largely unexplored.

The present study suggests LSD1 as an essential epigenetic regulator during oligodendrocyte development in mouse-derived oligodendrocyte progenitor cells, cerebellar slice cultures and *in vivo* in the zebrafish spinal cord. It could be shown that LSD1 is recruited by ZFP516 during initiation of differentiation to convey its function as a transcriptional regulator in mouse-derived OPC. Furthermore, an untargeted and targeted approach revealed that LSD1 regulates its own redox state, possibly leading to an oligomeric arrangement via disulfide bond formation. Furthermore, hundreds of proteins involved in transcriptional regulation and RNA processing were identified as less oxidized upon knockout or inhibition of LSD1 activity. Therefore, beyond its role as a transcriptional regulator, LSD1 could serve as a key player in nuclear redox signaling, broadening its regulatory function to a yet unknown extent. These results do not only provide a first link between epigenetics and redox signaling, but also introduce the first oxidase to the field of redox signaling.

IV Zusammenfassung

Die Lysin-spezifische Demethylase 1 (LSD1) ist eine Flavin-abhängige Histon-Demethylase, die Geneexpression sowohl aktiviert als auch abschaltet. LSD1 spielt in vielen Abschnitten der Entwicklung und der Krebsentstehung eine wichtige Rolle. Während der Demethylierungsreaktion entsteht Wasserstoffperoxid (H_2O_2) als Nebenprodukt, dessen Funktion bisher allerdings ungeklärt ist. In dieser Arbeit konnte gezeigt werden, dass LSD1 eine Schlüsselrolle in der Oligodendrozytendifferenzierung einnimmt. Sowohl in primären Oligodendrozytenvorläuferzellen der Maus, Schnittkulturen des Kleinhirns, als auch *in vivo* im Rückenmark des Zebrafisches ließ sich zeigen, dass die Differenzierung nach Inhibierung der Enzymaktivität oder dem Knockdown signifikant eingeschränkt war. Unmittelbar nach Beginn der Differenzierung wird LSD1 von dem Zinkfingerprotein ZFP516 rekrutiert. Das deutet darauf hin, dass diese Interaktion eine entscheidende Rolle während der Entwicklung von Oligodendrozytenvorläuferzellen spielt.

Darüber hinaus wurden klare Hinweise für eine neue Funktion von LSD1 als Oxidase in der redox-vermittelte Signaltransduktion erbracht. Zunächst konnte gezeigt werden, dass LSD1 durch Eigenoxidation seinen eigenen Redoxstatus reguliert, möglicherweise unter Oligomerenbildung. Darüber hinaus führten der Knockout und die Inhibierung zu einer Anreicherung von weniger oxidierten Proteinen im Zellkern. Der Großteil der differenziell oxidierten Proteine, die hier gefunden wurden, ist an der Transkriptionsregulation und der RNA-Verarbeitung beteiligt. Die hier gewonnenen Daten bringen LSD1 erstmals mit der Redox-Signaltransduktion im Zellkern in Verbindung und erweitern so das Funktionsspektrum dieser Flavin-abhängigen Demethylase. Diese Erkenntnisse verbinden Redoxregulation mit Epigenetik und führen zudem zur Identifikation einer der ersten Oxidasen im Bereich der Redox-Signaltransduktion.

V List of abbreviations

AEP	Anterior entopeduncular area
aOPC	Adult oligodendrocyte progenitor cell
ATP	Adenosine triphosphate
BAF	Brg1/Brm associated factor
BIAM	Biotinylated iodoacetamide
C491	Cysteine 491
CHD7	Chromodomain helicase DNA-binding protein 7
CLDK	Claudin k
CNPase	2′, 3′-cyclic nucleotide-3′-phosphodiesterase
CNS	Central nervous system
co-IP	Co-immunoprecipitation
CTBP1	C-terminal-binding protein 1
CTRL MO	Control morpholino
DNA	Deoxyribonucleic acid
DOX	Doxycycline
dpf	Day postfertilization
DRGN	Dorsal root ganglion neuron
DTT	Dithiothreitol
EGFP	Enhanced green fluorescent protein
EGFR	Epidermal growth factor receptor
ESC	Embryonic stem cell
FAD	Flavin adenine dinucleotide
FGF	Fibroblast growth factor
GAPDH	Glycerinaldehyde 3-phosphat dehydrogenase
GATAD2A	GATA zinc finger domain containing 2A
GFAP	Glial fibrillary acidic protein
GFP	Green fluorescent protein
GO	Gene Ontology
H_2O_2	Hydrogen peroxide

H3K4	Lysine 4 of histone 3
H3K9	Lysine 9 of histone 3
H3K9me2	Dimethylated lysine 9 of histone 3
HDAC	Histone deacetylase
hpf	Hour postfertilization
ICC	Immunocytochemistry
IgG	Immunoglobulin G
JmjC	Jumonji C
LSD1	Lysine-specific demethylase 1
MAO	Monoamine oxygenase
MBP	Myelin basic protein
MGE	Medial ganglionic eminence
MN	Motor neuron
MO	Morpholino
mRNA	Messenger ribonucleic acid
MTA2	Metastasis-associated protein 2
MYT1	Myelin transcription factor 1
NCC	Neural crest cell
NCL	Nucleolin
NEM	N-ethylmaleimide
NG2	Neural/glial antigen 2
NGN1	Neurogenin 1
NGN2	Neurogenin-2
NOX	Nicotinamide adenine dinucleotide phosphate oxidase
NSC	Neural stem cell
NuRD	Nucleosome remodeling and deacetylase complex
O-2A	Oligodendrocyte type 2 astrocyte
OL	Oligodendrocyte
OLIG2	Oligodendrocyte transcription factor 2
OPC	Oligodendrocyte progenitor cell
OSC	Organotypic slice culture

PDGF	Platelet-derived growth factor
preOL	Premature oligodendrocyte
PRX 2	Peroxiredoxin 2
PTEN	Phosphatase and tensin homolog
qRT-PCR	Quantitative real-time polymerase chain reaction
RBBP7	Retinoblastoma binding protein 7
RCOR1	REST corepressor 1
SDF1	Stromal cell-derived factor 1
SDS PAGE	Sodium dodecyl sulfate polyacrylamide gel
SHH	Sonic hedgehog
shRNA	Short hairpin ribonucleic acid
siRNA	Small interfering RNA
SMARCA4	ATP-dependent chromatin remodeler SMARCA4
SOX10	Transcription factor SOX-10
SV2	Synaptic vesicle glycoprotein 2
SWI/SNF	Switch/sucrose non-fermentable
TCA	Trichloroacetic acid
TCEP	Tris (2-carboxyethyl) phosphin
TRX1	Thioredoxin 1
UI	Uninjected
VZ	Ventricular zone
ZFP516	Zinc finger protein 516
gt	Goat
ms	Mouse
rb	Rabbit
gp	Guinea pig
do	Donkey
LGE	Lateral ganglionic eminence
MGE	Medial ganglionic eminence
div	Day *in vitro*

VI List of figures

VII List of tables

1 Introduction

1.1 Oligodendrocyte development

Neuronal function in mammals and most vertebrates is characterized by a rapid impulse propagation compared to invertebrates. This is facilitated by the insulation of axons with myelin and endows higher organisms with the capacity to carry out complex motoric, sensory and cognitive functions. Oligodendrocytes (OLs) are differentiated glial cells responsible for the production of myelin in the central nervous system (CNS) and are generated from oligodendrocyte progenitor cells (OPCs) at late embryonic stage after the neurogenic phase (Lu et al., 2002; Jackson et al., 2006; Kessaris et al., 2006). Myelin is the multilayered plasma membrane extension of OLs and consists of myelin specific lipids and proteins. Historically, myelin has been appreciated solely as an insulator and myelination as a static process which is completed during postnatal development. However, myelination is a selective process and exhibits a high degree of plasticity (Fields, 2015). Not every axon is myelinated to the same extent or myelinated at all. By selectively controlling myelin homeostasis, OLs orchestrate neural function and cognitive regulation throughout life. Intriguingly, not all OPCs differentiate during development. A subpopulation of OPCs become evenly dispersed all over the adult CNS and persists as adult OPCs (aOPCs) (Nishiyama et al., 2009; Dimou and Gallo, 2015). Those aOPCs continuously sense their environment for perturbations of the myelin homeostasis. If necessary, they extensively proliferate and give rise to myelinating OLs to re-establish the myelin sheath, prevent neuronal death and restore their function. This is of particular importance during demyelinating diseases such as multiple sclerosis as its devastating pathology is attributed to inflammatory demyelinated lesion areas and neuronal death (Bradl and Lassmann, 2010). Differentiation of aOPC in response to demyelinating injuries recapitulates many aspects of developmental OL differentiation (Fancy et al., 2004). It is therefore of vital importance to understand the biology of OL development, as OPCs are considered as the endogenous source of cells responsible for regeneration.

1.1.1 Experimental models

In the past decade, a variety of experimental models has been established to study the process of OPC differentiation on different levels. In this study, a combination of different experimental models has been selected to investigate the multifaceted aspects of OL development and myelination.

The zebrafish is a vertebrate model for embryonic development and frequently used to study myelination *in vivo* (Preston and Macklin, 2015). The zebrafish shares a high degree of homology with mammals and has characteristics that provide exceptional advantages over other *in vivo* models (Lieschke and Currie, 2007). One of the unique advantages is that embryogenesis occurs externally and is comparable fast. First OPCs appear after 1 day postfertilization (dpf) and formation of myelin becomes visible by day 4 dpf. Its transparent nature and the availability of transgenic reporter lines allow non-invasive investigations. Genetic manipulation induced by morpholinos and global administration of small chemical compounds affects protein level and function in all cell types. Therefore, it should be considered that effects on myelination are not only attributed to developmental changes in OPCs and OLs but also other neural and non-neural cells.

Organotypic slice cultures (OSCs) of the cerebellum offer an *ex vivo* approach to carry out investigations in a rodent model (Gähwiler et al., 1997). The system is still complex and secondary effects exerted by manipulation of other cell types cannot be excluded, but the time point of preparation provide full control over the developmental stage. When isolated at postnatal day 3, neurogenesis is completed and the cerebellum is invaded by OPCs prone to differentiate into OLs. When isolated at later time points, myelination is completed and mechanisms of de- and remyelination can be investigated.

Primary OPCs enriched from cortical cell preparations by magnetic cell sorting against specific epitopes provide a valuable tool to carry out mechanistic investigations specifically in progenitor cells. A2B5 is a marker for oligodendrocyte type 2 astrocyte (O-2A) progenitor cells which are considered as the ancestors of neural/glial antigen 2 (NG2) expressing OPCs (Baracskay et al., 2007; Strathmann et al., 2007). Thus, A2B5 is suitable to identify and obtain an early oligodendroglial committed cell population *in vitro*. Although the resulting cell culture mainly

consists of bipolar OPCs, it may also contain small subpopulations of more advanced, pre-myelinating cells and, to a small extent, also astrocyte fated cells. Differentiation can be induced by mitogen removal, the addition of retinoic acid and thyroids hormones. The simplicity of the system, e.g. absence of neurons and morphogen attraction, should be considered when it comes to the interpretation of the results.

1.1.2 Oligodendrocyte differentiation

The OL developmental program begins with specification of OPCs that derived from self-renewing neural stem cells (NSCs) during late embryonic gestation. In the developing brain and spinal cord, NSCs reside in the epithelial surface lining the lateral ventricle, the ventricular zone (VZ) (Lee and Jessell, 1999). Upon delamination from the VZ, OPCs proliferate and migrate throughout the developing CNS by following morphogen gradients (Kessaris et al., 2006). Migratory OPCs can be identified by the expression of the platelet-derived growth factor receptor (PDGFr) (Pringle and Richardson, 1993). During migration, OPCs establish contacts with the endothelial surface of the vasculature. The interaction is established and maintained by WNT pathway activation in OPC (Tsai et al., 2016). WNT is a receptor/ligand induced signaling pathway important for cell differentiation and organogenesis in general. WNT is believed to inhibit OL differentiation and thereby allowing OPCs to migrate and proliferate. Activation of WNT in OPCs leads to the expression of the chemokine receptor CXCR4. CXCR4 recognizes its ligand, the stromal cell-derived factor 1 (SDF1), which is expressed by the endothelium. Blood vessels thereby provide a physicochemical scaffold for migration and prevent differentiation during this stage in a WNT-dependent manner. Downregulation of WNT signaling triggers the release from the endothelium and OPCs develop into oligodendrocyte marker O4 (O4) expressing pre-myelinating oligodendrocytes (preOLs). Once they reach their final destination, preOLs differentiate into myelinating OLs (**Figure 1**).

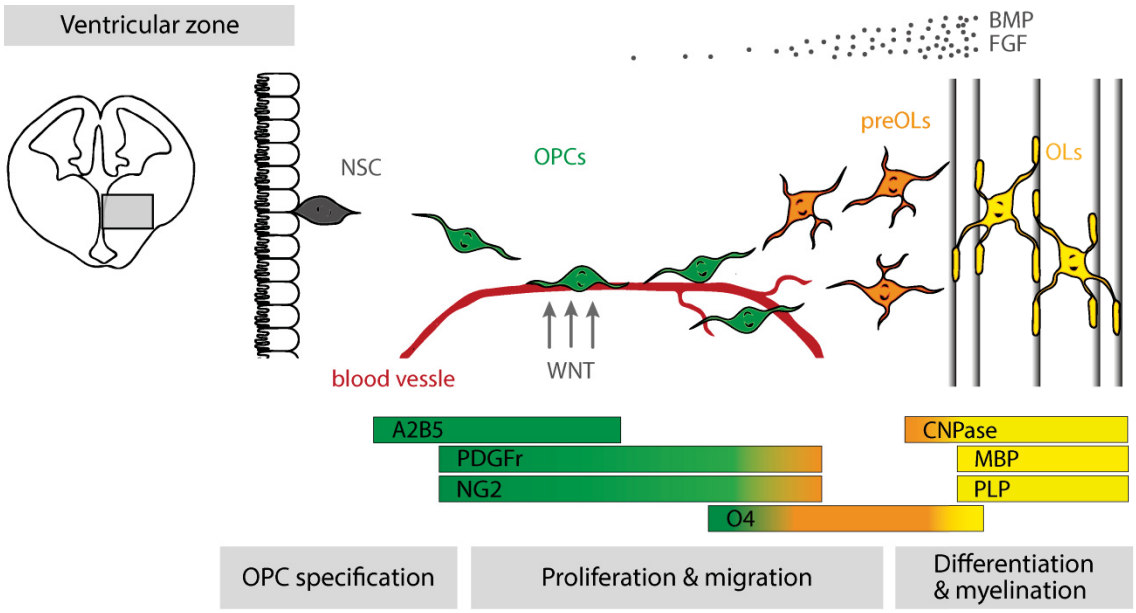

Figure 1 | OPC specification and differentiation
OPC specification occurs during delamination of NSC from the VZ. Shortly after specification, OPCs express stage specific A2B5 and PDGFr and associate with the abluminal endothelial surface to migrate along the blood vessels in the direction of morphogen gradients. Physical contact with the endothelial promotes migration and prevents OPCs to exit the cell cycle in a WNT dependent manner. Soon before terminal differentiation, OPCs enter a post-mitotic premyelinating stage characterized by the expression of O4. Terminal differentiated OLs can be identified by the expression of myelin-specific genes MBP, PLP and CNPase (Figure adapted from van Tilborg et al. 2018).

1.1.3 Oligodendrocyte differentiation in the forebrain

In the past decades, it became evident that the generation of OPCs occurs in sequentially emerging waves that arise in distinct regions of the VZ (**Figure 2**) (Kessaris et al., 2006). The temporal regulation of these waves varies between species and regions. In the developing forebrain of mice, the first wave emerges around embryonic day 12.5 (E12.5) from the anterior entopeduncular area (AEP) and the medial ganglionic eminence (MGE) (Pringle and Richardson, 1993; Tekki-Kessaris et al., 2001). OPCso originating from this most ventral niche arise in dependency of the diffusible glycoprotein sonic hedgehog (SHH). This observed in the ventral spinal cord as well as discussed in the following chapter in more detail. OPCs induced by the morphogen SHH can be identified by the expression of NKX2.1. Upon release, they migrate into all directions and invade the entire telencephalon and the cerebral cortex. A second wave arises from the VZ of the lateral ganglionic eminence (LGE) at E15.5 (Kessaris et al., 2006). OPC residing in the LGE are characterized by the expression of the homebox protein GSH2. They specify and spread out independent of SHH cues. Shortly after birth, EMX1 expressing OPCs in

the dorsal VZ expand and initiate the third stream that evades the neocortex. While OPCs derived from the SHH-dependent `NKX2.1 domain´ entirely differentiate to OLs, OPCs originating from the LGE and the dorsal EMX1 domain give either rise to OLs or persist as adult OPCs (aOPCs) throughout life.

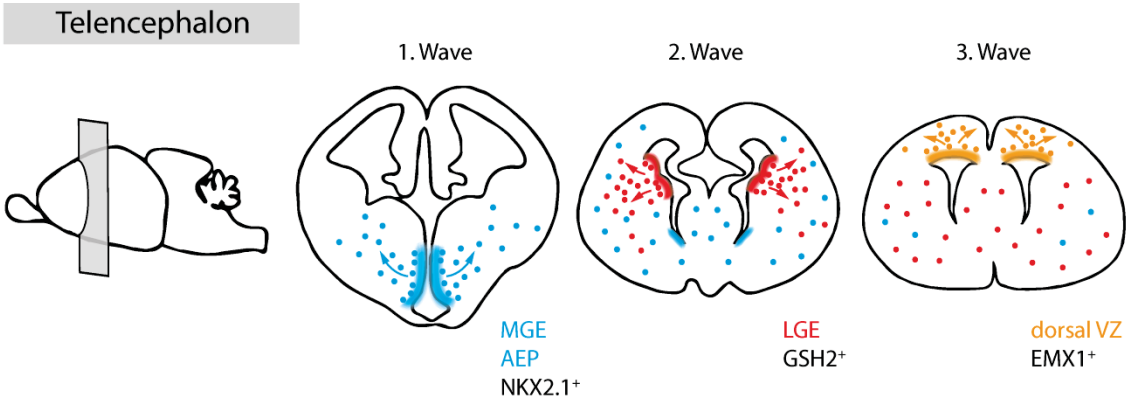

Figure 2 | OPC development in the telencephalon
OPCs emerge in 3 consecutive waves from the neuroepithelial zones of the developing brain depicted in different colors. Each wave of OPCs can be identified by the expression of niche-specific transcriptional regulators. The population of OPC that emerge from the 1. wave entirely differentiate into OLs, while OPCs that emerge from the 2. and 3. wave only partially differentiate into OLs. A subset persists as adult OPCs throughout life (Figure adapted from van Tilborg et al. 2018).

Intriguingly, although every progenitor population can be characterized by a specific transcriptional profile and respond to distinct signaling cues, they give rise to OLs that appear to be functionally equivalent (Clarke et al., 2012). Abolishing one of the niches in mice revealed that the remaining OPCs sources can take over as those mice develop normally, form myelin and exhibit no behavioral defects (Kessaris et al., 2006). Therefore, different OPC pools compete for the supply of the brain with OLs rather than providing unique niche-specific subtypes with different functional properties. Although compensatory mechanisms exist during development, the heterogeneity of OPCs is undisputed and subject of ongoing research (Spitzer et al., 2019).

1.1.4 Oligodendrocyte differentiation in the spinal cord

The process of OL development in the spinal is largely conserved in mammals and remarkably similar to that in vertebrates (Jeserich et al., 2008; Howe et al., 2013). The majority of spinal cord OLs originate from OPCs that reside in the ventral motor neuron progenitor domain (pMN), exemplarily shown for the zebrafish spinal cord

in **Figure 3** (Cai et al., 2005; Park et al., 2007). OPC specification within the pMN domain is completed by 30 hours postfertilization (hpf) in zebrafish, E12.5-14 in rodents and E45 in humans (Pringle and Richardson, 1993; Timsit et al., 1995; Hajihosseini et al., 1996). The specification of functional distinct regions within the ventricular zone of the spinal cord, e.g. the ventral OPC containing pMN domain, is orchestrated by a gradient of SHH. SHH is secreted by ventral residing neuroeptithel-derived floor plate cells. It binds to its receptor expressed by cells residing in the ventricular zone and initiates intracellular signaling pathways with either activating or repressing function depending on the extent of activation. Thus, the establishment of a SHH gradient along the dorsoventral axis facilitates the establishment of distinct zones with sharp boundaries and unique transcriptional profiles (Lupo et al., 2006).The pMN domain is established by high levels of SHH and therefore, located adjacent to the SHH secreting floor plate cells. SHH is opposed by bone morphogenetic proteins (BMPs), which are secreted by cells that reside in the ventral roofplate.

OPC commitment becomes evident by the expression of transcription factor SOX-10 (SOX10) and OLIG2 (Lu et al., 2000; Britsch et al., 2001). The expression of both markers persists in premature and mature OLs.

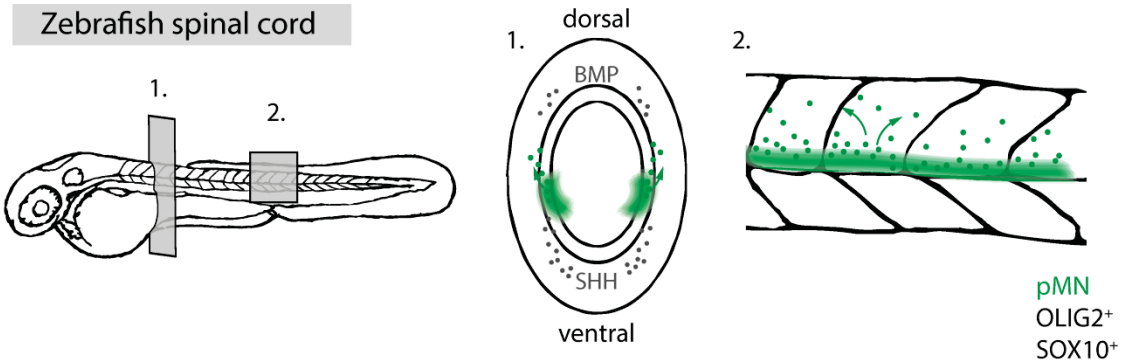

Figure 3 | OPC differentiation in the zebrafish spinal cord
SHH signaling cues secreted from ventral floor plate (depicted in grey colour) regulate specification and positioning of OPCs in the pMN domain (green hatched area). Ventral SHH signaling is antagonized by BMP morphogens secreted from the roof plate to initiate dorsal migration of OPCs.

OLIG2$^+$ OPCs in the spinal cord give rise to motor neurons (MNs) first, before they become gliogenic and produce OLs starting from 48 hpf in zebrafish and E16.5 in mice (Blader et al., 2003; Masahira et al., 2006). The fact that pMN-derived OPCs

exhibit an early neurogenic potential indicate a high degree of functional plasticity during this stage. OLIG2 is expressed in OPCs, MNs and in OLs. Therefore, OLIG2 exhibits a bifunctional pro-neurogenic and pro-oligogenic role that is rather unusual among the bHLH transcription factor family, as they are known to unequivocally regulate cell identity. On the molecular level, this could be explained by a serine phosphorylation site in the helix-loop-helix domain that is decisive whether OLIG2 forms a heterodimer with the pro-neuronal neurogenin-2 (NGN2) or a pro-oligogenic homodimer (Lee et al., 2005c).

1.1.5 Epigenetics of oligodendrocyte development

OL fate acquisition is a stepwise process in which OPCs pass through a series of distinct stages which can be defined by stage-specific transcriptional regulators (Wegner, 2008; Emery and Lu, 2015). It is suggested that these consecutive cell fates and their inherent transcriptional signatures are established and stabilized by epigenetic factors. On the mechanistic level, epigenetic regulation comprises covalent modifications of deoxyribonucleic acid (DNA) and histone proteins, as well as adenosine triphosphate (ATP)-dependent remodeling of DNA-nucleosome contacts. While some regulators might act individually, it is generally assumed that epigenetic regulation occurs in concerted and intertwining manner and essentially determines the accessibility of genes and their regulatory elements to the transcriptional machinery. Most epigenetic enzymes require metabolic co-factors to carry out their function. This regulatory link provides an attractive explanation how metabolic activity and extrinsic stimuli impact on cellular identity and function (**Figure 4**).

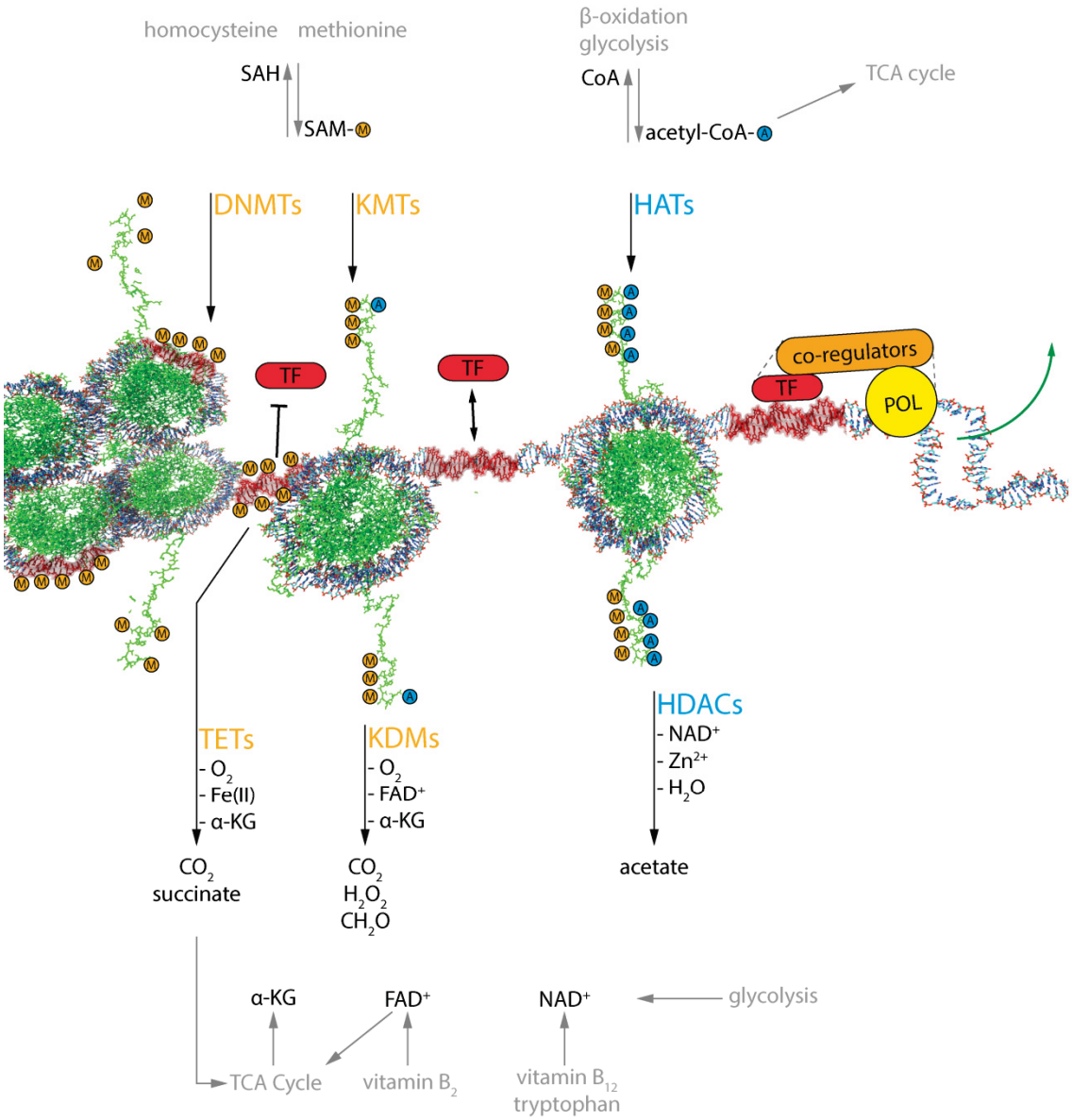

Figure 4 | Epigenetic regulation of DNA accessibility and metabolic interplay
The transition of repressive chromatin (left) via a permissive intermediate state (middle) results in chromatin opening and active gene transcription (right). The process is driven by transferases and erasers. Transferases (top) deploy their substrates derived from metabolic processes on the histone tails and DNA. Erasing of histone marks and methylated DNA require metabolic co-factors and yield by-products that could potentially be fed back into metabolic circuits. Many types of modifications have been described so far. For simplification only methylation and acetylation are shown here. Lysine methylation is implicated in both, transcriptional activation and repression, depending on the specific lysine residue. Acetylated lysines are exclusively found near transcriptional active genes. Schematic illustration created with VMD. (Abbreviations: α-KG- α-ketoglutarate, A- acetyl, DNMT- DNA methyltransferase, HAT- histone acetylase, KMT- lysine methyltransferase, M- methyl, TET- ten-eleven translocation methylcytosine dioxygenase and TF- transcription factor.

N-terminal histone tails can be modified in many different ways comprising acetylation, methylation, phosphorylation, citrullination or simply said: most known posttranslational modifications have been identified on histone tails as well.

Only a minority could be put in a functional context so far. It is suggested that histone modifications alter the electrostatic and hydrophobic properties of the histone tail leading to repulsive or attractive interaction towards the negatively charged DNA backbone (Clark and Kimura, 1990). Some modifications serve as anchors for adaptor proteins that recruit regulatory complexes, indicating that the overall modification code determines complex composition and its repressive or activating function.

The epigenetic regulation of oligodendrocyte development and myelination has been investigated in more detail in the past decades. Multiple lines of evidence suggest that histone deacetylase 1 (HDAC1) and HDAC2 are required for OL development (Marin-Husstege et al., 2002; Ye et al., 2009). HDACs remove acetyl groups from specific lysine residues of histone tails leading to chromatin compaction and repressed gene expression. Pharmacological inhibition with pan-HDAC inhibitors and genetic ablation revealed that HDAC activity is required during early differentiation of OPCs *in vitro* and *in vivo*. Several studies indicate that HDAC1 and HDAC2 (HDAC1/2) co-occupy regulatory elements of genes important for OL differentiation. In this regard, HDAC1/2-dependent decommissioning of the WNT/TCF7L/β-catenin complex appears to be the driving force (Ye et al., 2009). However, multiple other putative targets and interacting proteins have been suggested, indicating that HDACs initiate OL lineage progression in multiple ways (Swiss et al., 2011).

A general observation in developing OLs is that the overall chromatin structure is extensively reorganized (Nielsen et al., 2002; Marie et al., 2018). This is, in part, attributed to the activity of ATP-dependent chromatin remodeling enzymes (Yu et al., 2013). Mammalian switch/sucrose non-fermentable (SWI/SNF) complexes, also called Brg1/Brm associated factor (BAF) complexes constitute multisubunit machineries that assemble on nucleosomes guided by stage-specific transcriptional regulators (Jenuwein and Allis, 2001; Becker and Hörz, 2002). In such complexes, ATP is hydrolyzed to remove DNA histone contacts leading to the formation of transient DNA loops that are propagated out of the nucleosome and finally dissolve. In the resulting situation, the nucleosome is repositioned, repressive DNA-histone contacts dissolved and re-established respectively. In addition to repositioning

movements, SWI/SNF complexes can exchange histone variants or eject whole nucleosomes leading to the exposure of larger DNA segments (**Figure 5**).

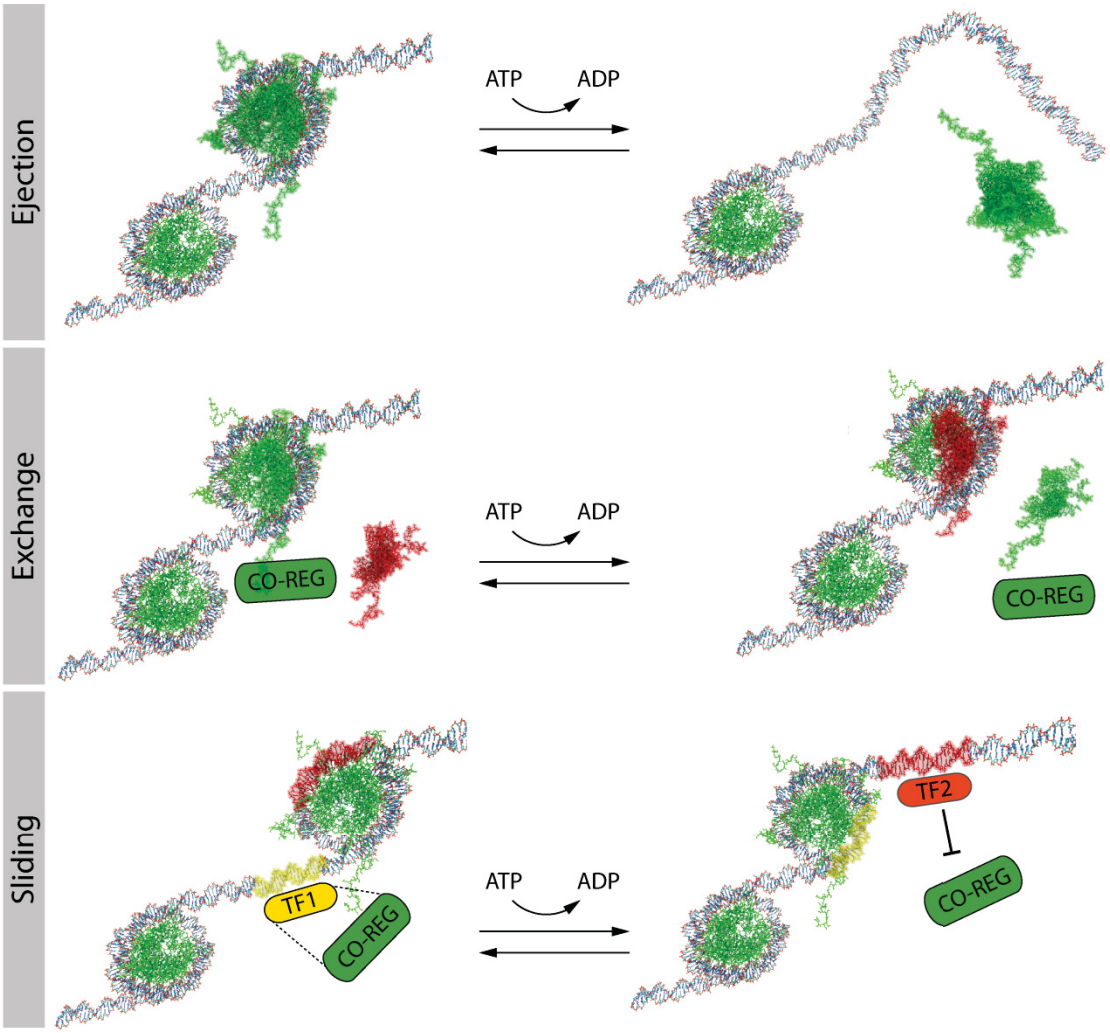

Figure 5 | Mechanisms of chromatin remodeling
ATP-dependent chromatin remodeling mediated by SWI/SNF complexes comprise ejection of histone core proteins leading to exposure of large DNA fragments (top). Exchange of histone units confers novel structural and functional properties to the nucleosome (middle). Sliding of nucleosomes unwraps and/or wrap regulatory elements, respectively (bottom; CO-REG- co-regulator and TF- transcription factor).

ATP-dependent chromatin remodeler SMARCA4/BRG1 (SMARCA4) with its intrinsic ATPase activity is a core subunit of the mammalian SWI/SNF complex. It has been shown that SMARCA4 co-occupies OL-specific enhancers together with OLIG2 to promote OL fate commitment (Yu et al., 2013). During final stage, when preOLs become mature OLs, the ATP-dependent chromodomain helicase DNA-binding protein 7 (CHD7) cooperates with SOX10 to initiate myelinogenic program (He et al., 2016). Therefore, chromatin remodeling is necessary in all steps of OL

development. A dynamic change of the histone methylation pattern during OPC lineage progression has been recognized as well and strongly suggests that methyltransferases and demethylases must be involved (Liu et al., 2015). However, no particular demethylase has been described in this context so far.

1.1.6 Lysine-specific demethylase 1

It has long been assumed that histone methylation is irreversible until the discovery of the first histone demethylase, the lysine specific demethylase1 (LSD1) (Shi et al., 2004).

Later, several other de-metylases have been discovered. All of them belong to the jumonji C (JmjC) domain-containing family that comprises more than 20 members. The reaction mechanism of the JmjC demethylases is compatible with mono-, di-. and the trimethylated substrates. It consumes oxygen as well, but uses α-ketoglutarate and bivalent iron to produce the demethylated lysyl residue, formaldehyde, succinate and carbon dioxide (Culhane and Cole, 2007). LSD1 and also LSD2 are flavin adenine dinucleotide (FAD)-dependent demethylase and closely related to the monooxygenase family. LSD1-dependent demethylation requires the protonation of the methylated nitrogen hence, LSD1 can demethylate mono- and dimethyl but not trimethyl lysines (Forneris et al., 2006). The unique FAD-dependent reaction consumes molecular oxygen and leads to the formation of hydrogen peroxide (H_2O_2), formaldehyde and water as by-products.

Initial studies on the regulatory function of LSD1 have shown that LSD1 engages with the HDAC1/2 and REST corepressor 1 (RCOR1 or COREST) containing co-repressor complex to permanently repress pro-neural genes in non-neural cells (Andrés et al., 1999; Lee et al., 2005a). Its repressive function is achieved through the removal of mono- and dimethyl marks (me1 and me2) from lysine 4 of histone 3 (H3K4). Beside its function as a long-term repressor in fully differentiated cells, LSD1 also functions as a transient repressor to stabilize cell fates in a spatiotemporal manner. In embryonic and hematopoietic stem cells, LSD1 shuts down the self-renewal program and facilitates lineage restriction (Sprüssel et al., 2012; Whyte et al., 2012; Kerenyi et al., 2013). In NSCs, LSD1 associates with the TLX receptor to maintain NSCs in their proliferative state by repressing cell cycle inhibitors P21 and the phosphatase and tensin homolog (PTEN) (Yokoyama et al., 2008). Knockdown

of LSD1 leads to premature neural differentiation indicating that LSD1 is important for NSCs maintenance. These are only a few examples of the multifaceted function of LSD1 during development. Like other histone modifying enzymes, LSD1 demethylates non-histone substrates to regulate their function and stability e.g. P53 and DNMT1 (Huang et al., 2007; Wang et al., 2009a; Wu et al., 2017). This adds yet another level of complexity to its regulatory potential.

LSD1 is overexpressed in several cancer types comprising e.g. leukemia, neuroblastoma, prostate and breast cancer where it essentially contributes to disease progression. Soon after the discovery of LSD1, its function as a transcriptional activator has been described in the context of prostate cancer (Metzger et al., 2005). Here, LSD1 engages with the androgen receptor to remove the repressive H3K9me1 and H3K9me2 mark. Once more, this indicates how adaptor proteins convey substrate specificity to epigenetic modulators. In contrast to oncogenic mutations in genes, aberrant transcriptional regulation caused by epigenetic enzymes can in theory be "corrected" by small chemical compounds targeting their activity or complex assembly. Due to the high degree of similarity of the catalytic domain of LSD1 to monoamine oxygenases (MAOs), most of the compounds targeting MAO activity inhibit the reaction of LSD1 as well (Schmidt and McCafferty, 2007). Thus, MAO inhibitors comprising e.g. phenelzine and tranylcypromine serve as a starting point to develop LSD1 specific inhibitors. These comprise e.g. ORY-1001, a tranylcypromine derivate that is currently in phase IIa clinical trial for safety and tolerability assessment in patients with acute myeloid leukemia and small lung cancer, respectively (Clinical Trials Register EudraCT 2018-000482-36 and 2018-000469-35) (Maes et al., 2018). Unbiased approaches based on screenings of small molecule libraries have led to the identification of e.g. SP2509 (Fiskus et al., 2014). Molecular docking studies suggest that SP2509 interacts with LSD1 by hydrogen bonding near the active site.

Although a plethora of LSD1 inhibitors with strong effects on proliferation of cancer cells have been developed to date, only a few entered clinical trials (Niwa and Umehara, 2017). An obvious assumption is that progress in this field is hampered by the lack of specificity. This might be in part true but it seems also reasonable to assume that (unknown) inhibitor specific off-target effects could also contribute to the beneficial outcome. Thus, unwanted and beneficial off-target effects need to be

defined for existing inhibitors and considered in the development of new derivatives. This could either help to increase specificity to the designated target or to the refinement of the off-target effect. One example is the MAO B inhibitor selegiline (L-deprenyl). Long after its approval for treatment in Parkinson's disease, it became evident that it exerts its neuroprotective effect independent of its designated function to inhibit MAO B (Tatton and Chalmers-Redman, 1996; Suuronen et al., 2000). It is suggested that selegiline directly binds to GAPDH and prevents its nitrosylation (Kragten et al., 1998). Thereby it interferes with a novel pro-apoptotic pathway involving the nuclear translocation of nitrosylated GAPDH (Hara et al., 2005). This finding has the lead to the development of omigapil (TCH346), a derivate which lacks MAO B affinity, but has a refined ability to bind to GAPDH and prevent its translocation (Tatton and Chalmers-Redman, 1996).

1.2 Redox signaling

Functional sites of proteins are often decorated with cysteines as they are highly reactive under physiological pH. The reactivity is attributed to the thiol side chain that acts as a strong nucleophile. Cysteines can be directly involved in the enzymatic reaction by performing a nucleophilic attack on the substrate or coordinate metal containing co-factors. Due to their reactivity some thiols, in particular those that exists as a thiolate anion, are subjected to a series of redox-mediated modifications (Poole et al., 2004). Redox-sensitivity is defined by the local microenvironment that favors the fully deprotonated state. In particular, positively charged amino acids can stabilize the negatively charged thiolate anion in its redox-sensitive state. The oxidation of the thiolate anion is initiated by the reaction with the second messenger H_2O_2 and leads to the formation of a sulfenic acid (**Figure 6**).

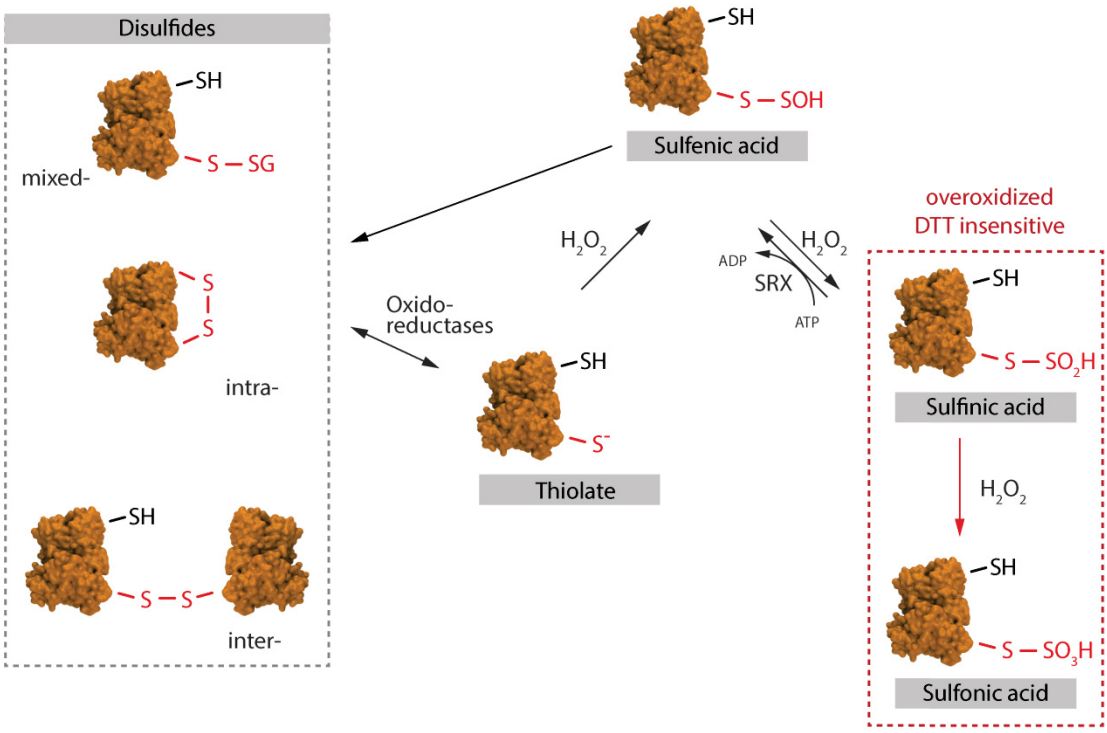

Figure 6 | Redox regulation through H_2O_2-modified cysteine residues
H_2O_2 reacts with the cysteine thiolate to the reactive sulfenic acid (-SOH). Sulfenic acids are transient intermediates that immediately react with other thiols or thiol containing low molecular weight molecules to form mixed-, intra- or inter-disulfide bonds. The reaction of sulfenic acids with thiols is an autocatalytic reaction solely driven by the high reactivity of the sulfenic acid. The reversal reaction needs the specific activity of oxidoreductases of the thioredoxin superfamily, which leads to the formation of the thiolate anion. Vice versa, some oxidoreductases can directly oxidize the thiolate anion to form disulfides. Upon prolonged exposure to H_2O_2 sulfenic acids may also further react to sulfinic ($-SO_2H$) and sulfonic acids ($-SO_3H$). Sulfinic and sulfonic acids are overoxidized and cannot be reduced by the DTT. Whereas sulfonic acids are irreversible oxidized, sulfinic acids may be reduced by ATP-dependent sulfiredoxins (SRX).

Prolonged exposure to H_2O_2 leads to the formation of the hyperoxidzed sulfinic and sulfonic acids. Whereas the latter is irreversible oxidized and considered as a dead end-product, sulfinic acids can be reduced by sulfiredoxins under consumption of ATP (Biteau et al., 2003). Noteworthy, both hyperoxidized species are not reducible by common chemical reducing agents e.g. dithiothreitol (DTT), tris (2-carboxyethyl) phosphin (TCEP) or β-mercaptoethanol. The reversible oxidized sulfenic acid is a highly reactive and unstable intermediate that reacts with other thiols to form more stable products comprising intra- and intermolecular disulfide bonds and mixed disulfides with glutathione. In either case, the reaction can have profound consequences for protein function and structure. Intriguingly, the reverse reaction is driven by the specific activity of enzymes. Small oxidoreductases of the thioredoxin superfamily are able to restore the reduced state of a redox-sensitive

thiol and its associated function (Arnér and Holmgren, 2000). Hence, thiol redox states are subjected to specific regulation conveyed by the chemistry of the target site on the one hand, and specific enzymatic reduction on the other. This observation has greatly advanced the concept of redox signaling.

1.2.1 LSD1 and its potential role in redox signaling

A variety of physiologically relevant thiol switches has been discovered in recent years and the observation that numerous redox-sensitive cysteines exist throughout the proteome, suggests a yet unappreciated number of biological processes that could be redox regulated (van der Reest et al., 2018). The oxidation of redox-sensitive thiols by H_2O_2 is an autocatalytic process. To ensure productive thiol oxidation, a reasonable amount of redox equivalents needs to reach the target site. How specificity is achieved during this process is currently under debate. Sources of H_2O_2 are known and comprise e.g. cellular respiration, activity of enzymes e.g. nicotinamide adenine dinucleotide phosphate oxidases (NOXs), and neutrophil phagocytosis. Peroxiredoxins are highly abundant proteins and exhibit a remarkable affinity to H_2O_2. They out-compete the reactivity of every known redox-sensitive thiol towards H_2O_2. (Cox et al., 2009; Manta et al., 2009) Inevitably, this leads to two possible yet not mutually exclusive mechanisms of thiol oxidation. First, peroxiredoxins not only detoxify H_2O_2 via the thioredoxin system but are also directly involved in redox signaling by conveying oxidation equivalents to other targets. This scenario would provide a satisfying explanation as it introduces enzymatic specificity and could explain how compartmentalized sources of reactive oxygen species are connected to more distant targets. Indeed, oxidation of signal transducer and activator of transcription 3 (STAT3) which leads to the formation of transcriptional inactive oligomeric form is mediated by peroxiredoxin 2 (PRX2) (Sobotta et al., 2015; Stöcker et al., 2018). Second, a H_2O_2 producing enzyme could come in close proximity to its putative target protein. In this scenario, specificity would be conveyed by the microenvironment created by the oxidase, its target protein and possible interacting partners. Thus, large protein complexes that sterically exclude peroxiredoxins and create a redox insensitive microarchitecture could provide ideal conditions. In contrast to the peroxiredoxin model, the diffusion model provides a straightforward explanation for the oxidation of active site

cysteines that are often deeply buried in protein cavities and might not be accessible for peroxiredoxins. However, direct protein oxidation could not be demonstrated so far.

LSD1 produces the second messenger H_2O_2 and formaldehyde as by-products during its catalytic cycle and is known to interact with proteins that are subjected to redox modifications e.g. P53, HDAC1/2 and SIRT1 (Forneris et al., 2006; Velu et al., 2007; Doyle and Fitzpatrick, 2010; Bräutigam et al., 2013). It seems reasonable to speculate about a direct oxidation of target proteins by LSD1 for several reasons. First, it resides in large protein complexes. Although complete crystal structures are not available it seems to be very likely that the entire surface of LSD1 is occupied by interacting partners and the H_2O_2 is released to their surfaces. Second, the presence of peroxiredoxins in such complexes could not be shown so far. Third, LSD1-mediated demethylation exerts a considerable high evolutional pressure as H_2O_2 and formaldehyde are potentially harmful and produced in close proximity to the DNA. It is very likely that nature has evolved physiological relevant routes for detoxification in addition to the peroxiredoxin system. In estrogen responsive breast cancer cell lines, LSD1 associates with the estrogen receptor to demethylate H3K9 and positively controls the expression of estrogen responsive genes (Perillo et al., 2008). Intriguingly, demethylation leads to localized DNA oxidation. The DNA repair machinery modulates the chromatin DNA topology for excision of oxidized nucleotides and thereby facilitates the attachment of DNA polymerase. Thus, perhaps due to short distances to the redox target, the peroxiredoxin system is not sufficient to prevent oxidation and instead, a redox based mechanism has evolved that promotes cell growth. Taken together, it is reasonable to assume, that LSD1 mediates oxidation of many other targets. Thus, LSD1 could link epigenetic regulation with nuclear redox signaling.

1.3 Aims of study

The transition of proliferating OPCs to myelinating OLs is probably one of the most impressive differentiation processes with regard to the extent of the morphological and functional changes. It is not surprising that this process is accompanied by an substantial rearrangement of the chromatin architecture, driven by histone modifications and ATP-dependent remodeling. Although the methylation pattern of histones is dynamically regulated during the development of OLs, no particular demethylase has been investigated in this context so far. LSD1 is an important regulator of neural stem cell proliferation and neuronal differentiation. The role of LSD1 in OL differentiation, however, remains to be defined. Therefore, the study aims:

(I) to investigate the role of LSD1 during the development of the zebrafish CNS *in vivo*, and specifically, in OL differentiation and myelination,

(II) to dissect the cellular effects of LSD1-dependent demethylation during differentiation *in vitro*, and

(III) to identify stage-specific LSD1-containing complexes in OPC and preOLs.

Moreover, reversible thiol modifications induced by H_2O_2 are considered as essential cell-signaling events. While the reduction of oxidized cysteines is regulated by enzymes and well-described, it is largely unknown how oxidation of thiols is achieved in a specific manner. LSD1 produces the second messenger H_2O_2 as a by-product and could potentially adopt a key role in nuclear redox signaling. Thus, an additional aim of this study is:

(IV) to investigate the potential role of LSD1 in nuclear redox signaling.

2 Materials and methods

2.1 Materials

2.1.1 Chemicals

Table 1: Chemicals

Name	Provider	Catalog number
5,5-Dimethyl-1,3-cyclohexanedione	Merck	38490
Acetic acid	VWR International	1.00056.2500
Acetonitrile	Merck	45983
Agarose	Merck	A9539
Agarose, low gelling temperature	Merck	A4018
Albumin bovine serum (BSA)	Merck	A4737
Albumin Fraktion V, ≥98 %, biotinfrei	Carl roth	0163.3
Ampuwa®	Fresenius	B23067A
Any kD™ Mini-PROTEAN® TGX™ Precast Protein Gels, 15-well	Bio-Rad Laboratories	4569036
BC Assay Protein Quantitation Kit (BCA)	Interchim	UP40840A
Bio-Gel P-6 Gel	Bio-Rad Laboratories	1504134
Bizine	Axon Medchem	Axon2306
Bovine Serum Albumin, cell culture tested	Merck	A9418
cDNA Reverse Transcription Kit	Applied Biosystems	4368813
CellTiter-Blue® Cell Viability Assay	Promega	G8081

cOmplete™, Mini, EDTA-free Protease Inhibitor Cocktail	Merck	4693159001
CutSmart® Buffer	New England Biolabs	B7204S
Cy5 Maleimide	GE Healthcare	PA25031
DEPC-Treated Water	Thermo Fisher Scientific	AM9906
Dimedone	Merck	D153303
Dimethyl pimelimidate dihydrochloride	Merck	D8388
Dimethyl sulfoxide	Merck	D5879
Disuccinimidyl suberate (DSS)	Merck	21655
DL-Dithiothreitol (DTT)	Merck	D0632
Dynabeads™ Protein G	Thermo Fisher Scientific	10003D
EDTA UltraPure™ 0.5M	Thermo Fisher Scientific	15575020
Ethanol absolut	supelco	107017
Ethidium bromide~95% (HPLC)	Merck	E8751
Ethyl 3-aminobenzoate methane sulfonate $C_{10}H_{15}NO_5S$ (MS222)	Fluka	A5040
Ethylene glycol bis (succinimidyl succinate) (EGS)	Merck	21565
Ethylenediaminetetraacetic acid (EDTA)	Merck	E9884
FAP-1	Chang lab, Berkeley	(Brewer and Chang, 2015)
Formaldehyde	Merck	F8775
GeneJET RNA Purification Kit	Thermo Fisher Scientific	K0731
Glycerin≥99,7 %	Carl Roth	6962

GoTaq® DNA Polymerase	Promega	M3001
Guanidine hydrochloride	Merck	G3272
Hematoxylin Solution, Mayer's	Merck	MHS32
Hydrochloric acid (37%)	Merck	1003175000
Hydrogen peroxide	Merck	H3410-500ML
Immu-Mount™	Fisher Scientific	9990412
Iodoacetamide	Merck	I1149
Isofluran Piramal	Piramal Critical Care	30372.00.00
Kynurenic acid ≥98%	Merck	K3375
LS Columns	Miltenyi Biotec	130-042-401
Methanol ≥99.8%	VWR International	20847.320
Methylene blue $C_{16}H_{18}ClN_3S$	Merck	6040
Mini-PROTEAN TGX precast gels	Bio-Rad Laboratories	4569036
N-Ethylmaleimide	Merck	E3876
Neural Tissue Dissociation Kit (P)	Miltenyi Biotec	130-092-628
Normal Goat Serum (NGS)	Thermo Fisher Scientific	PCN5000
N-Phenylthiourea $C_6H_5NHCSNH_2$ (PTU)	Merck	P7629
Phenol red solution (0.5 %)	Merck	P0290
PhosSTOP™	Merck	4906845001
Pierce™ Streptavidin Agarose Resin	Thermo Fisher Scientific	20347
Power SYBR™ Green PCR Master Mix	Applied Biosystems	4368702
Propidium iodide (PI)	Merck	P4170

Protein Sample Loading Buffer (4x)	LI-COR Bioscience	928-40004
Protein-Marker V ('Prestained')	VWR International	27-2210
RIPA Lysis and Extraction Buffer	Thermo Fisher Scientific	89900
Roti®-Histofix (4 %) (PFA)	Carl Roth	P087
SDS ultra-pure ≥99 %	Carl Roth	2326
Silver nitrate	Merck	209139
Sodium acetate	Merck	S2889
Sodium carbonate	Merck	1613757
Sodium chloride ≥99.0%	Merck	S9888
Sodium citrate	Merck	1613859
Sodium thiosulfate	Merck	72049
SP2509	Cayman Chemicals	15487
Sucrose	Merck	SX1075
Taqman Master Mix	Applied Biosystems	4369510
TERGITOL™ solution	Merck	NP40S
Tissue-Tek® O.C.T.™	Sakura Finetek	4583
Trans-Blot® Turbo™ Mini PVDF	Bio-Rad Laboratories	1704156
Trichloric acid	Merck	T6399
Triethanolamine ≥99.0%	Merck	90279
Tris hydrochloride	Merck	10812846001
Tris/Glycine/SDS (10x)	Bio-Rad Laboratories	1610772
TRISPUFFERAN® ≥99,9 %	Carl Roth	4855
Triton X-100	Merck	T9284
UltraPure™ TBE Buffer, 10X	Invitrogen™	15581028

2.1.2 Kits and assays

Table 2: Kits and assays

Name	Provider	Catalog number
Anti-A2B5 MicroBeads, human, mouse, rat	Miltenyi Biotec	130-093-388
cDNA Reverse Transcription Kit	Applied Biosystems	4368813
CellTiter-Blue® Cell Viability Assay	Promega	G8081
GeneJET RNA Purification Kit	Thermo Fisher Scientific	K0731
Neural Tissue Dissociation Kit (P)	Miltenyi Biotec	130-092-628

2.1.3 Cell culture and experimental organisms

Table 3: Cell culture reagents and supplements

Name	Provider	Catalog number
3,3′,5-Triiodo-L-thyronine sodium salt≥95% (T3)	Merck	T2752
B-27™ Supplement (50X), minus vitamin A (B27-)	Thermo Fisher Scientific	12587001
B-27™ Supplement (50X), serum free (B27+)	Thermo Fisher Scientific	17504-044
D-(+)-Glucose solution (45%)	Merck	G8769
Doxycycline hyclate	Merck	D9891
DPBS w/o Ca^{+} & Mg^{+} (1x)	Thermo Fisher Scientific	14190250
Dulbecco's Modified Eagle F-12, no glutamine (DMEM/ F-12	Thermo Fisher Scientific	21331020

Dulbecco's Modified Eagle Medium, high glucose, pyruvate (DMEM/HG)	Thermo Fisher Scientific	41966-029
Fetal bovine serum, Gibco™	Thermo Fisher Scientific	10500064
GlutaMAX™ supplement	Thermo Fisher Scientific	35050061
HBSS $Ca^{+}Mg^{+}$ (1x)	Thermo Fisher Scientific	24020083
HEPES (1 M)	Thermo Fisher Scientific	15630080
Horse serum	Thermo Fisher Scientific	26050088
L-Thyroxine≥98% (HPLC) (T4)	Merck	T2376
Minimum Essential Medium	Thermo Fisher Scientific	11090081
Minimum Essential Medium Eagle (MEM)	Merck	M2279
Neurobasal™-A medium	Thermo Fisher Scientific	10888022
Non-essential amino acids (NEAA)	Millipore	K0293
Penicillin-streptomycin (P/S) (10,000 U/mL)	Thermo Fisher Scientific	15140122
rm FGF-b (FGF)	ImmunoTools	1234362
rm PDGF-AA (PDGF)	ImmunoTools	12343687
StemPro™ Accutase™	Thermo Fisher Scientific	A1110501
Trypsin-EDTA (0.05%)	Thermo Fisher Scientific	25300054

Table 4: Cell lines

Name	Provider	Reference
MCF-7	SIGMA	(Soule et al., 1973)
SN4741		(Son et al., 1999)

Table 5: Zebrafish strains

Strain	Provider	Reference
AB wildtype fishline	EZRC, KIT	n/a
Brass wildtype fishline	EZRC, KIT	n/a
Tg(-8.4*neurog1*:GFP)	EZRC, KIT	(Blader et al., 2003)
Tg(*cldnk*:EGFP)	Becker lab, Edinburgh	(Münzel et al., 2012)
Tg(*cldnk:*TDTOMATO-caax)		
Tg(kdrl:EGFP)		(Jin et al., 2005)
Tg(*mbp*:GFP)	Lyons lab, Edinburgh	(Almeida et al., 2011)
Tg(*mnx2b*:GFP)	Kawakami lab, Mishima	(Asakawa et al., 2012)
Tg(*olig2:GFP*)	Becker lab, Edinburgh	(Shin et al., 2003)
TL wildtype fishline	EZRC, KIT	n/a
TU wildtype fishline	EZRC, KIT	n/a

2.1.4 Mouse

Mice were bred in the animal facility of the Heinrich-Heine-University of Düsseldorf (Zentrale Einrichtung für Tierversuche und Tierschutzaufgaben; ZETT) under pathogen-free conditions on, 12 h light/dark cycle with access to pelletized dry food and germ-free water.

Table 6: Mouse strains

Strain	Provider	Reference
C57BL/6	Jackson Laboratory	n/a
Tg(plp:GFP)	Göbels lab, Düsseldorf	(Sobottka et al., 2011)
Tg(tetO-shRNA:kdm1a)	Schüle lab, Freiburg	(Zhu et al., 2014)

2.1.5 Antibodies

Table 7: Antibodies

Target antigen	Host	Dilution			Provider	Catalog number
		WB	ICC	IHC		
Alexa Fluor 594 mouse IgG	gt			1:1000	Thermo Fisher Scientific	R37121
BRG-1	ms	1:1000			Santa Cruz	SC-17796
Cleaved Caspase-3	rb			1:200	Cell Signaling	9662
CNPase	ms		1:1000		Merck	C5922
CoREST1	rb	1:3000			Abcam	ab32631
Dimedone	rb			1:500	Custom-made	
GFAP	gp	1:2000			Synaptic Systems	173 004
Glutathione	ms				ViroGen	101-A
Guinea pig IgG 800CW	do	1:20000			LI-COR	926-32411
Guinea pig IgG-Cy5	do		1:500		Merck	AP193S
HDAC1	ms	1:1000			Santa Cruz	sc-81598
LSD1	rb	1:1000		1:1000	Abcam	ab17721
LSD1	rb	1:1000			Cell Signaling	2139
MBP		1:1000	1:500	1:500	Merck	MAB386
Mouse IgG 680RD	gt	1:20000			LI-COR	926-68070
Mouse IgG 800CW	do	1:20000			LI-COR	926-32212

NF200	ms		1:1000	Merck	N0142
NG2	rb	1:1000		Millipore	AB5320
Normal rabbit IgG	rb			Merck	12-370
O4		1:500		R & D Systems	MAB1326
Olig2	rb		1:500	Merck	AB9610
PCNA	ms		1:1000	Merck	P8825
PDGFRα	ms		1:200	Merck	CBL1366
Rabbit IgG 680RD	gt	1:20000		LI-COR	926-68071
Rabbit IgG 800CW	do	1:20000		LI-COR	926-32213
Rat IgG 680RD	gt	1:20000		LI-COR	926-68076
SV2	ms		1:250	Hybridoma Bank - DSHB	Buckley, K.M.
Tubulin, acetylated	ms		1:250	Merck	T6793
β-Actin	ms	1:5000		Merck	A5316

2.1.6 Equipment and consumables

Table 8: Equipment

Device	Provider	Identification number
7500 Pro Real-Time PCR Systems	Applied Biosystems	4357362
Bandelin Sonopuls UW 2070	BANDELIN electronic	
Biometra TGradient Thermocycler	Analytik Jena AG	Biometra 050-801

BTX Gemini SC2	BTX Molecular Delivery Systems	452043
Confocal Laser Scanning Microscope	Leica	DMi8
Cryostat	Leica	CM 1900 CV
DynaMag™-2 Magnet	Thermo Fisher Scientific	12321D
EnSight™ multimode plate reader	Perkin Elmer	HH34000000
Fluorescence microscope 1	Nikon	AZ100
Fluorescence microscope 2	Olympus	BX51
HulaMixer™ Sample Mixer	Thermo Fisher Scientific	15920D
Mcilwain tissue chopper	Campden Instruments	Model TC752
Nanodrop 2000 Spectrophotometer	Thermo Fisher Scientific	ND-2000
Odyssey Infrared Imaging System	LI-COR	
Shaking incubator, Thriller	VWR International	
Standard Power Pack Biometra P25	Analytik Jena	846-040-800
Standard Power Pack P25T	Analytik Jena	846-040-850
Tecan Genios Pro	Tecan Group	
Trans-Blot® Turbo™ Transfer System	Bio-Rad Laboratories	1704150
Two-photon light sheet microscope	Custom-built	Manuscript in preparation
Two-photon point scanning microscope	LaVision	Trimscope II
Typhoon™ Imager	GE Healthcare	9400

Table 9: Plastic and glasware

Name	Provider	Catalog number
13 mm Ø cover glasses	Paul Marienfeld	0111530
15 µ-Slide 2 well co-culture	ibidi	81806
50 ml, 15mL CELLSTAR® polypropylene tube	Greiner Bio One	227261, 188261
Cell culture dish (uncoated), 100 x 20 mm	Greiner Bio-One	664160
Cell culture dish, 100 x 20 mm	Sarstedt	83.3902
Electroporation cuvettes	VWR International	732-1137
Eppendorf safe-lock tubes, (2 mL, 1.5 mL, 0.5 mL)	Eppendorf	003012- 0094, -0086, -1023
Frosted slides (glass slides)	Engelbrecht	11102
Millicell cell culture insert	Merck	PICM03050
Poly-l-lysine hydrobromide	Merck	P9155
Protein LoBind tubes	Eppendorf	0030122356
VWR® PCR 8-well tubes	VWR International	53509-304

2.1.7 Buffers/Solutions/Media

Table 10: Buffers/Solutions/Media

Buffers / Solutions / Media	Formulation
BIAM-DAB buffer	8 M Urea, 5 mM EDTA, 0.5% SDS, 50 mM Tris/HCL, pH 8.5, 50x molar excess BIAM
BIAM-IP buffer	5 mM EDTA, 50 mM Tris/HCL, 1% Triton-X-100, 1% SDS, pH 8.5

BIAM-IP elution buffer	6M GdmCl, 50 mM Tris/HCl, pH 8.5
Danieau (3x)	2.9M NaCl, 60mM $Ca(NO_3)$ 2 × 4 H_2O 40 mM, $MgSO_4$, 70mM KCl, 0,5M Hepes
DTT-DAB buffer	8 M Urea, 5 mM EDTA, 0.5% SDS, 50 mM Tris/HCL, pH 8.5, 3 mM DTT
Electroporation buffer	21 mM Hepes, 137 mM NaCl, 5 mM KCl, 0.7 mM Na_2HPO_4, 6 mM D-Glucose, pH 7.15
Elution buffer (4x)	30 % Glycerin, 12 % SDS, 150 mM Tris Base, 0.5 % bromphenol blue, pH 7.0 (RT)
ICC/IHC blocking buffer	5 % NGS and 0.5 % Triton-X-100 in PBS
MCF-7 medium	MEM (Merck), 10 % FCS, 2 mM GlutaMAX™, 1x NEAA, 100 U/mL P/S
Native lysis buffer	50 mM Tris/HCL,150 mM NaCl, 0,5 mM EDTA, 1 % NP-40, 1 Tablette complete mini (Roche) w/o EDTA/10ml and PhosSTOP™
NEM-DAB buffer	8 M Urea, 5 mM EDTA, 0.5% SDS, 100 µM Neocuproine, 50 mM Tris/HCL, and 50x molar excess NEM, pH 8.5
OPC differentiation medium	DMEM/F12, 1x B27+, 2mM GlutaMAX™, 100 U/mL P/S, 8 mM Hepes; 400 ng/mL T3, 400 ng/mL T4
OPC proliferation medium	DMEM/F12, 1x B27-, 2mM GlutaMAX™, 100 U/mL P/S, 8 mM Hepes; 20 ng/mL PDGF, 10 ng/mL FGF
OSC dissection medium	1 x HBSS $Ca_2^+Mg_2^+$, 100 U/mL P/S, 1mM kynurenic acid, 0.5 % Glucose, pH 7.2-7.4 (4°C)
OSC medium with horse serum	Neurobasal-A™, 2mM GlutaMAX, 25 % Heat inactivated horse serum, 100 U/mL P/S
OSC medium without horse serum	Neurobasal-A™, B-27™ Supplement, 2mM GlutaMAX™, 0.5% glucose, 100 U/mL P/S

OSC washing medium	0.5 x HBSS $Ca_2^+Mg_2^+$, 0.5 x Minimal essential medium, 100 U/mL P/S, 25 mM HEPES
PLL-coating solution	1mg/ mL PLL ,100 U/mL P/S, PBS
Resolubilization buffer	10% SDS, 150 mM NaCl, 50 mM HEPES pH 7.8
SG buffer A	50 % (v/v) ethanol, 10 % acetic acid (v/v)
SG buffer B	30 % (v/v) ethanol, 500 mM sodium acetate, 8 mM sodium thiosulfate in destilled water
SN medium	DMEM HG, 10 % FCS, 100 U/mL P/S, 2 mM glutamine
Tail lysis buffer	100 mM Tris/HCl pH 7.5, 5 mM EDTA, 2% SDS (w/v), 200 mM NaCl
Tris-buffered saline (10x)	1.5 M NaCl, KCl 30 mM, 250 mM

2.1.8 Oligonucleotides

Table 11: Oligonucleotides

Target gene	Sequence 5'-3'
cnp	*Fw: TGCTGCACTGTACAACCAAATTC* *RV: GAGAGCAGAGATGGACAGTTTGAA*
gapdh	*Fw: CTCAACTACATGGTCTACATGTTCCA* *RV: CCATTCTCGGCCTTCACTAT* *Probe: (Fam)TGACTCCACTCACGGCAAATTCAACGT(TAMRA)*
hkdm1a siRNA	*FW: CCACGAGUCAAACCUUUAUTT* *RV: AUAAAGGUUUGACUCGUGGTT*
hscrambled CTRL siRNA	*FW: UUCUCCGAACGUGUCACGUTT* *RV: ACGUGACACGUUCGGAGAATT*
LSD_TetO insert	*FW: CCATGGAATTCGAACGCTGACGTC* *RV: TATGGGCTATGAACTAATGACCC*

LSD_WT	*FW: AGCATGCTCTTTTCCAGCAT* *RV: CTCAGGCTGGCCTAAAACTG*
mbp	*Fw: CACAGAGACACGGGCATCCT* *RV: TCTGCTTTAGCCAGGGTACCTT*
plp	*Fw: GTATAGGCAGTCTCTGCGCTGA* *RV: AAGTGGCAGCAATCATGAAGG*
zfkdm1a MO	*CTGACTTCTTATTGGACAACATCAC*

2.1.9 Software

Table 12: Software

Name	Provider
Adobe Illustrator CS6	Adobe Systems
Citavi 6 (6.0.02)	Swiss Academic Software
ClusterONE plugin	(Nepusz et al., 2012)
Cytoscape	(Shannon et al., 2003)
Fiji Is Just ImageJ	(Schindelin et al., 2012)
GraphPad Prism 5	GraphPad Software
Image Studio™ Lite Software	LI-COR Bioscience
Leica Application Suite X (LAS X)	Leica
Magellan™ Data Analysis	Tecan Group
Office 2010	Microsoft Corporation
Sequence detection software 1.5.1	Applied Biosystems
Visual Molecular Dynamics (VMD 1.9.3)	(Humphrey et al., 1996)

2.2 Methods

2.2.1 Zebrafish imaging

Embryos were anaesthetized in 0.3 x Danieau + PTU containing 1:1000 MS222 and mounted in 1.25 % low melting agarose (0.3 x Danieau + PTU). For the *Tg(olig2:GFP)*, a custom-built two-photon light sheet microscope was used (manuscript in preparation). For this purpose, zebrafish larvae were mounted inside of fluorinated ethylene propylene (FEP) tube with an inner diameter of 1mm and an outer diameter of 1.6 mm. The *Tg(cldnk:TDTOMATO-caax)*, *Tg(cldnk:EGFP)* and *Tg(mbp:GFP)* and the whole mounted larvae were imaged with a two-photon point scanning microscope. For this purpose, zebrafish larvae were mounted on a 100 x 20 uncoated cell culture dish. The *Tg(-8.4neurog1:GFP)* and *Tg(mnx2b:GFP)* were mounted on a 15 µ-Slide 2 Well Co-Culture slide for confocal images. Brightfield images were used to crop the image to 4 spinal segments above the egg yolk extension. Maximum intensity projected images were blinded and cells of interest were counted using the Fiji Cell counter plugin (Kurt De Vos, University of Sheffield). For quantification of dorsal migrated cells, positive cells above and not touching the pMN domain were considered. For high-throughput images, the EnSight™ multimode plate reader was used. Anaesthetized embryos were placed in 96-well clear bottom plate with one larva positioned in the centre of each well. The overall length growth was recorded with a novel coded algorithm embedded in the Kaleido© Software (unpublished data). Time-lapse measurements were performed with the help of Enrico Mingardo and Felix Häberlein (University Bonn).

2.2.2 Morpholino injections

The translational blocking *kdm1a* anti-sense MO was dissolved to 3 mM in Ampuwa®. The working solution contained 75 µM LSD1 MO and 0.5x CutSmart® Buffer in Ampuwa® with Phenol red. The drop size was adjusted to 150 µm in mineral oil corresponding to ~1.8 µL injection volume containing 1.1 ng LSD1 MO.

2.2.3 FAP-1

Small droplets of FAP-1 (5mM) were injected intracranial in 3 dpf larvae. After 2 h, injected larvae were washed 3 times with Danieau and imaged using the

fluorescence microscope 1. For incubation, 3 dpf embryos were incubated with 12.5 or 25 µM FAP-1 for 20 h in Danieau. They were then washed 3 times and mounted in low gelling agarose for confocal imaging.

2.2.4 Immunochemistry

2.2.4.1 Whole mount staining

Anesthetized 3 dpf larvae were washed in PBS and fixed in 4 % paraformaldehyde (PFA) overnight. Larvae were washed 3 times in PBS for 10 min and dehydrated through a series of 25 %, 50 %, 75 % and 100 % methanol for 10 min each. Embryos were stored in 100 % methanol and rehydrated in a series of 100 %, 75 %, 50%, 25 % methanol diluted in PBS containing 0.005% Tween (PBS-T) for 10 min each. Larvae were then washed in PBS-T (3 x 5 min) and subsequently 3 times in 150 mM Tris-HCL (pH 9) for 5 min each step. Embryos were then equilibrated in the same buffer for 15 min at 70 °C and washed 2 times for 5 min in PBS-T. They were then permeabilized using 5 µg/mL ProteinaseK in PBS for 50 min, fixed again using 4 % PFA for 20 min and washed in PBS-T (2 x for 5 min). Fixed embryos were blocked in 10 % normal goat serum (NGS) and 2 % bovine serum albumin (BSA) in PBS-T at 4 °C for 4 hours. Larvae were then incubated in 2 % NGS and 2% BSA in PBST with either 1:250 anti-synaptic vesicle protein 2 (SV2) antibody or 1:500 anti-acetylated tubulin antibody for 72 h at 4 °C. Stained embryos were then washed 4 x in PBS-T for 1 h followed by 2 washing steps for 30 min in PBS-T at RT. They were then subjected to secondary antibody stainings for 48 h at 4 °C using goat anti-mouse IgG (H+L) Alexa Fluor 594 (1:1000). Stained larvae were first washed 6 x for 15 min in PBS-T and then washed 5 x for 5 min at RT. Finally, stained larvae were mounted in agarose and images obtained from a two-photon point scanning microscope.

2.2.4.2 Paraffin sections

Zebrafish larvae were fixed as described above and embedded in paraffin. Stainings were done by Dr. Anna Japp (University of Bonn, Institute of Neuropathology). In brief, paraffin sections were stained with either 1:1000 PCNA or 1:200 cleaved caspase 3 and counterstained with haematoxylin.

2.2.4.3 Cryosection sections

Mice were anaesthetized using isoflurane and perfused with PBS. Dissected brains were postfixed with 4 % PFA for 16 h, followed by dehydration in a 25–30 % (v/v) sucrose solution. Tissue samples were cryopreserved in TissueTek at −80 °C. Brains were cut in 20 µm slices were using a cryostat, permeabilized with 0.5 % (v/v) Triton X-100. After blocking in 5 % (v/v) horse serum and 1 % (v/v) bovine serum albumin in PBS for 2 h, slices were subjected to the same staining protocol as described for OSCs.

2.2.4.4 OSCs and cell culture

OSCs and cells were fixed in Roti®-Histofix (4 %) for 30 min and 10 min respectively, and wash twice with PBS. After incubated in ICC/IHC blocking buffer for 2h at RT, primary antibody was added in 0.5 x ICC/IHC blocking buffer in PBS at 4 °C overnight. After 3 washing steps in PBS 0.5 % Triton-X-100, OSCs and cells were incubated with the secondary antibody in 0.5 x ICC/IHC blocking buffer in PBS for 1 h at RT. For immunocytochemistry experiments, nuclei were stained with a 1:20000 Hoechst followed by 3 washing steps. Stained OSCs and cells on cover slips were mounted on glass slides using Immu-Mount™. Images were acquired from the confocal laser scanning microscope or the fluorescence microscope 2 on the next day. OSCs were exposed to the indicated concentrations of bizine for 8 days. OSCs were then incubated with 3 µM propidium iodide for 10 min and washed in PBS (3 x for 10min). Mean fluorescence intensity was measured over the whole slice based on fluorescence images obtained from the fluorescence microscope 2.

2.2.5 HCL treatment and coating of cover-slips

Coverslips were cooked in 80 % EtOH +HCL for 15 min. Afterwards, coverslips were wash twice in 80 % EtOH followed by a washing step in 99 % EtOH. Dried coverslips were separated and placed in the centre of a 24 well plate. After at least 2 h incubation in PLL-coating solution at 37 °C, each well was washed 4 times with PBS. In each washing step, cover slips were lifted with a 10 µL pipette tip.

2.2.6 A2B5 cell culture

Single cell suspensions were obtained from cerebellar and cortical brain structures of P1-P3 C57BL/6 wildtype and *Tg(tetO-shRNA:kdm1a)* mice using the neuronal tissue dissociation kit. Mice were decapitated, meninges were removed, brain tissues dissected and further processed as suggested by the manufacturer's protocol. A2B5+ cells were isolated from single cell suspensions using the anti-A2B5 MicroBeads and LS MACS columns. For the *Tg(tetO-shRNA:kdm1a)* derived cultures, isolation were done separately for each pup as crossing of heterozygous *Tg(tetO-shRNA:kdm1a)* and C57BL/6 yielded a mixed population of *Tg(-/-)* and *Tg(+/-)* individuals whose identity was not known by the time of isolation. Genotyping has been done subsequently as described. A2B5+ cells were cultivated in differentiation medium. Medium was exchanged to 2/3 every second day. Experiments were done within passage 0 to passage 1. Cells were passaged using 25 µL Accutase per cm^2. For differentiation experiments, cells were plated at 25.000 cells per cm^2 on PLL coated petri dishes and PLL coated HCL-treated cover-slips respectively. After at least 2 days of cultivation in proliferation medium, differentiation was induced by the addition of differentiation medium for the indicated time. Differentiation medium was exchanged every 2 days. For inhibitor treatments, A2B5+ cells were exposed to 10 µM bizine and 1 µM SP2509 respectively prior to induction of differentiation. The endogenous *kdm1a* shRNA was induced by the addition of 1µg/mL doxycycline 3 days before induction of differentiation.

2.2.7 Cell line culture and inhibitor treatments

MCF-7 and SN4741were cultivated in media as indicated at 37 °C and 5 % CO_2. Media were changed every 2 to 3 days. For splitting, cells were washed once with PBS and incubated with trypsin at 25 µL per cm^2 for 1-2 min. The reaction was stopped by adding an excess of medium containing 10 %FCS. MCF-7 cells were split to a ratio of 1 to 10 and SN4741 of 1 to 20.

2.2.8 Cerebellar organotypic slice cultures

Slice cultures were obtain from 3 to 4 days old pups derived from C57BL/6 or *Tg(plp:GFP)* strains. Cerebella with attached hindbrain were dissected and cut into

350 µm sagittal sections using a Mcilwain tissue chopper. Slices were dissociated in dissecting medium (4 °C) and transferred to washing medium for at least 15 min at 4 °C. Up to 4 slices were transferred a Millicell Cell Culture Insert and cultivated for 3 days in OSC medium with or without horse serum for 3 days at 37 °C and 5 % CO_2. Afterwards, temperature was reduced to 33°C until the end of the experiment. Medium was changed every second day. For inhibitor treatments, 2 consecutive slices were separated and subjected to 10 µM bizine and DMSO treatment respectively. A 100 mM bizine stock solution was prepared in DMSO. OSCs were established in cooperation with Dr. Klaudia Lepka.

2.2.9 CellTiter-Blue® cell viability assay

A2B5+ OPCs were plated at 25.000 cells per cm^2 and treated with the indicated inhibitor concentrations for 24 h or the corresponding volume of DMSO. The amount of DMSO was adjusted to the highest inhibitor concentration. The assay was performed according to the manufacturer's instruction with the exception that new medium was added along with the substrate. Fluorescence was measured at 590 nm after excitation at 560 nm using the Tecan Genios Pro.

2.2.10 RNA isolation and qRT-PCR

RNA was isolated using the GeneJET RNA Purification Kit according to manufacturer's protocol. RNA content and purity were analyzed using a Nanodrop 2000 spectrophotometer. The cDNA was synthesized using the cDNA Reverse Transcription by following the manufacturer's instructions using the Biometra TGradient Thermocycler (10 min at 25 °C, 45 min at 48 °C and 5 min at 95 °C). For the qRT-PCR reaction, Power SYBR™ Green PCR master mix or Taqman Master Mix was used with the corresponding primer pairs. The qRT-PCR program was set up as follows: 2 min at 50 °C, 10 min at 95 °C, 40 cycles of 15 sec at 95 °C and 1 min at 60 °C. For reactions with power SYBRGeen, a dissociation curve was implemented at the end of the program ranging from 65 °C to 95 °C. Fold induction values were calculated in triplicates, based on the ΔCT validation procedure and normalized to GAPDH levels as internal control.

2.2.11 Mouse genotyping

Tail biopsies were incubated in 500 µL tail lysis buffer supplemented with 10 µL ProteinaseK overnight at 56 °C. Reaction mix was centrifuged at 18.000 g for 10 min and 1 µL subjected to the PCR reaction. Using the GoTaq® DNA Polymerase according to the manufactures protocol. The PCR program was set up as follows: 3 min at 95 °C followed by 40 cycles of 30 sec at 95 °C, 30 sec at 65 °C and 45 sec at 72 °C. PCR reaction was loaded on a 1.2 % agarose Tris-borate-EDTA gel containing ethidium bromide.

The *Tg(+/-)* yielded a 381 bp fragment and wildtype specific 700 bp fragment. *Tg(-/-)* were identified by the absence of the 381 bp fragment.

2.2.12 Electroporation

MCF-7 cells were harvested by trypsinization, washed once with PBS and 3.5 x 10^6 cells resuspended in 600 µL electroporation buffer containing 15 µg siRNA. Cells were immediately transferred to a electroporation cuvette and electroporated at 190 V, 500 Ω and 1000 µF and immediately resuspended in 600 µM FCS and cultivated in 1:5 conditioned medium. Conditions for electroporation were optimized using a pCMV- LifeAct-mCherry.

2.2.13 Immunoblot analysis

Cells pellets were lysed in RIPA Lysis and Extraction Buffer supplemented with PhosSTOP™ and cOmplete™, Mini, EDTA-free Protease Inhibitor Cocktail for 10 min at RT. All following steps were performed at 4 °C. Lysates were sonicated with 3 pulses using a Bandelin Sonopuls UW 2070 set to 6 cycles and 10 % power. Sonicated lysates were clarified at 18,000 g for 20 min. For quantification of the protein concentration, the bicinchoninic acid assay (BCA assay) was used according to the manufacturer's protocol using the Tecan Genios Pro. Samples were prepared with Protein Sample Loading Buffer (4x), boiled for 5 min and if not stated otherwise, supplemented with 100 mM DTT. Samples containing up to 10 µg protein were loaded on a 15-well Any kD™ Mini-PROTEAN® TGX™ Precast Protein gel and separated by SDS-PAGE. Using the Trans-Blot® Turbo™ Transfer System and the default mixed-KD blotting program (1.3 A, 25 V, 7 min), proteins were blotted onto

Trans-Blot® Turbo™ Mini PVDF. Membranes were blocked with 5 % BSA in PBS containing PBS-T for 2 h at RT. Blocked membranes were incubated overnight at 4°C with the primary antibody diluted in blocking buffer as depicted in table. After 3 washing steps (10 mL PBS-T, 10 min), the membranes were incubated with the IRD conjugated secondary antibody. Membranes were washed 3 times and stained bands detected with Odyssey Infrared Imaging System. Optical band densities were determined using the Image Studio™ Lite software. Band intensities were normalized to β-actin.

2.2.14 Silver gel staining

Samples were separated by SDS page. Gel was fixated for at least 15 min in SG buffer A and transferred to SG buffer B for 30 min. The gel was rehydrated by washing 3 times for 10 min in distilled water and subsequently stained with 6 mM silver nitrate in distilled water for up to 30 min. Stained gel was briefly washed with water and then with 236 mM sodium carbonate in water. The gel was subjected to the developer solution containing 236 mM sodium carbonate and 0.01 % (v/v) formaldehyde for 1 to 7 min. The reaction was finally quenched with 50 mM EDTA for 20 min followed by a washing step in water.

2.2.15 Co-Immunoprecipitiation

2.2.16 Antibody crosslinking

Dynabeads were wash 3 time in PBS and incubated with 2.5 µL LSD1 antibody or normal rabbit IgG per 25 µL Dynabeads per co-IP in PBS-T (0.02 %) for 30 min at RT under rotary agitation using the HulaMixer™. Beads were washed 3 times with PBS and 2 times with 0.2 M triethanolamine and subsequently crosslinked with 20 mM dimethyl pimelimidate dihydrochloride in 0.2 M TEA overnight at 4°C. Crosslinking reaction was quenched with 50 mM Tris (pH 7.5) at RT for 15 min. Afterwards, beads were washed 2 times with 0.1 % BSA in PBS-T. Non-crosslinked antibody were eluted in 2 washing steps with 0.1 citrate pH 2-3 followed by 2 washing steps with 0.1 % BSA in PBS-T. Labeled beads were transferred in PBS to new protein LoBind tubes.

2.2.16.1 Co-IP in A2B5+ mouse OPCs

Adherent cells were scraped in 500 µL PBS and centrifuged for 5 min at 350 g. Cell pellets were resuspended in 6 packed cell volumes (PCV) of native lysis buffer (~100 µL) and incubated for 30 min at RT under rotary agitation. Samples were carefully resuspended every 10 min using a 200 µL pipette tip set to 80 µL. After 30 min supernatants containing cytosolic and a first portion soluble nuclear proteins were removed and stored on ice. The remaining pellet mainly containing the histone fraction, associated proteins and soluble were resuspended in 100 µL native lysis buffer and placed on ice for 10 min. The lysates were left on ice for 10 min and sonified again under the same conditions. Lysates were centrifuged for 5 min at 18.000 g 4°C and pooled with the first fraction. For quantification of the protein concentration, the bicinchoninic acid assay (BCA assay) was used according to the manufacturer's protocol using the Tecan Genios Pro. Different amounts of protein were subjected to the antibody crosslinked Dynabeads™ Protein G (IgG 1 mg, Proliferation 1 mg and Differentiation 0.75 mg with 5 replicates each). Lysates were incubated with the Dynabeads overnight and after 3 washing steps in PBS transferred to a new 1.5 mL Eppendorf Safe-Lock tube. Bound proteins were eluted with 1x elution buffer for 10 min at 37 °C at 600 rpm using the shaking incubator.

2.2.16.2 Redox co-IP

Adherent SN4741 cells treated with 15 µM bizine or DMSO for 24 h were washed briefly with PBS containing 10 mM NEM and subsequently scraped in PBS containing 100 mM NEM. Pellets were lysed in 6x PCV of native lysis buffer supplemented with 100 mM NEM and incubated on ice for 30 min. Lysates were resuspended every 10 min and subsequently sonified with 5 pulses using a Bandelin Sonopuls UW 2070 set to 6 cycles and 15 % power. Excessive NEM was removed by size exclusion chromatography using the P6 matrix. Protein amount in the purified lysates was estimated by bicinchoninic acid assay (BCA assay) according to the manufacturer's protocol using the Tecan Genios Pro and 1 mg total protein added to the antibody crosslinked Dynabeads™ Protein G (n=5). Elution was carried out as described in Co-IP in A2B5+ mouse OPCs.

Immunoprecipitated proteins were stacked in by SDS-PAGE (approximately 5 mm running distance). After silver gel staining, the protein containing bands were cut

out of the gel and protein reduced with 10 mM DTT in 50 mM ammonium acetate aqueous solution for 45 min at 56°C. Thiols were then alkylated with 55 mM iodoacetaminde in 50 mM ammonium acetate for 30 min at RT.
Proteins were further processed and analyzed by mass spectrometry as previously described (Poschmann et al., 2014).

2.2.16.3 MS-coupled BIAM switch assay

Trichloric acid (TCA) was directly added to the adherent cells to precipitate proteins and preserve their redox state. Pellets were washed in 10 % and 5 % TCA and resuspended in NEM-DAB buffer for 1 h at RT and 850 rpm using the shaking incubator. Proteins were precipitated in ice-cold acetone, collected by centrifugation, washed with acetone and resolubilizated in DTT-DAB buffer for 5 minutes at RT in the dark followed by the addition of BIAM-DAB. After 1 h incubation at RT and 850 rpm, proteins were precipitated with ice-cold acetone overnight at -20 °C. The pellet was washed and resuspended in BIAM-IP buffer and 900 µg of proteins affinity purified using agarose streptavidin beads overnight at 4°C using the HulaMixer™ Sample Mixer according to the manufacturer's instructions for the spin-down method. Bound proteins were eluted in BIAM-IP elution buffer at 95°C for 5 min. Sample were diluted with 25 mM Tris/HCl, pH 8.5, 10 % acetonitrile to obtain a final GdmCl concentration of 0.6 M. Proteins were processed and analyzed by mass spectrometry as previously described by Dr. Ilka Wittig (Functional Proteomics, Faculty of Medicine, Goethe University Frankfurt) (Löwe et al., 2019). In brief, proteins were digested with 1 µg trypsin (sequencing grade) overnight at 37°C under gentle agitation. Digestion was stopped by adding 0.5 % TCA. Solubilized peptides were subjected to liquid chromatography / mass spectrometry (LC/MS) on Thermo Scientific™ Q Exactive Plus equipped with an ultra-high-performance liquid chromatography unit (Thermo Scientific Dionex Ultimate 3000) and a Nanospray Flex Ion-Source (Thermo Scientific). These experiments have been done together with Dr. Ilka Wittig, Dr. Juliana Heidler and Jana Meisterknecht in Frankfurt (Goethe-Universität Fachbereich MedizinFunktionelle Proteomics)

2.2.17 Cy-5 Maleimide labeling

TCA precipitated pellets were resuspended in NEM-DAB buffer for 1 h at 850 rpm using the shaking incubator to block free thiols. Alkylated lysates were precipitated and pellet washed 3 times in ice-cold acetone. Pellets were resuspended in resolubilization buffer, reduced with 500 µM DTT and boiled at 95 °C for 5 min. Reduced thiols were labeled with Cy5 maleimide for 1 h in the dark. After adding elution buffer, 1µg protein was loaded onto a SDS-gel and in-gel fluorescence scanned with the Typhoon™ Imager.

2.2.18 *In situ* labeling of sulfenic acids

Living cells were exposed to 5 mM dimedone for 30 min briefly washed with 100 mM NEM in PBS and immediately precipitated with TCA. Pellets were washed 3 times in ice-cold acetone and resuspended in resolubilization buffer containing 100 mM NEM. Protein concentration was determined by the BCA assay according to the manufacturer's protocol using the Tecan Genios Pro and 30 µg subjected to SDS-page. Dimedone was labeled with a custom-made polyclonal dimedone antibody.

2.2.19 Crosslinking and H_2O_2 incubation

Cells were scraped in PBS and pelleted at 350 g for 5 min. For H_2O_2 incubation, they were resuspended in PBS containing the indicated concentrations of H_2O_2. Cell pellet was lysed in 6 PCV native lysis buffer containing 100 mM NEM and processed as previously described in the redox co-IP.

For crosslinking experiments, cells were resuspended in PBS containing either 2.5 mM EGS or DSS and incubated for 30 min at RT. The reaction was quenched by adding 50 mM Tris-HCL for 15 min. Cell pellet was lysed in 6 PCV native lysis buffer containing 100 mM NEM and processed as previously described in the redox co-IP.

2.2.20 Bioinformatics

2.2.20.1 Subcellular localization

All proteins that were significantly less oxidized upon LSD1 knockout or inhibition were clustered to their subcellular localization using the `SubCell BarCode´ database

and the implemented `multi protein localization´ tool set to MCF-7 cell line (Orre et al., 2019).The ribosomal/nucleosol fraction (N1) was only clustered to the nucleus, when clustered as nuclear according to UniProt terms (UniProt: a worldwide hub of protein knowledge, 2019).

2.2.20.2 Molceular function

All nuclear targets were clustered to their Gene Ontology term `molecular function´ (GO:MF) using the ShinyGO v0.61 Gene Onotology enrichment tool with a 0.5 p-value cutoff (Ge et al., 2018). Considered were the ten most significant terms

2.2.20.3 Complex enrichment analysis

The Corum database includes 4274 mammalian protein complexes that were experimentally verified (Giurgiu et al., 2019). The `g:Profiler´ was used to perform enrichment analysis in the Corum database (Raudvere et al., 2019).

2.2.20.4 Protein-protein interaction

Only the nuclear targets found in the redoxome analysis upon knockout were searched in the STRING database using their UniProt identifier (Szklarczyk et al., 2015). Only results based on experimental evidence and databases with high confidence (≥ 0.07) were considered. The data was visualized using Cytoscape (Shannon et al., 2003). The interactome was then clustered to their molecular function with the ClusterONE plugin (Nepusz et al., 2012).

3 Results

3.1 LSD1 in oligodendrocyte development

Although the histone methylation pattern during OL development is subjected to extensive changes, no particular histone demethylase has been described in this context so far. LSD1 is expressed in OPCs and could potentially regulate different steps of differentiation.

3.1.1 Zebrafish

3.1.1.1 Establishment of the zebrafish model

Knockout of LSD1 in mice causes early embryonic lethality around embryonic day 7.5 corresponding to 10 hpf in zebrafish development (Zhu et al., 2014). Therefore, general development needs to be critical reviewed in the zebrafish embryonic model in order to specifically study the development of OLs. To begin the investigation in zebrafish, 1-cell staged eggs were injected with a translation blocking antisense morpholino (MO) targeting *kdm1a* messenger ribonucleic acid (mRNA). LSD1 knockdown did not cause increased mortality compared to a control mismatch morpholino (CTRL MO) or the uninjected (UI) control group. On the first glance, LSD1 morphants exhibited no obvious developmental abnormalities, except for a pericardial edema and a reduction in the number of circulating blood cells (**Figure 7** A).

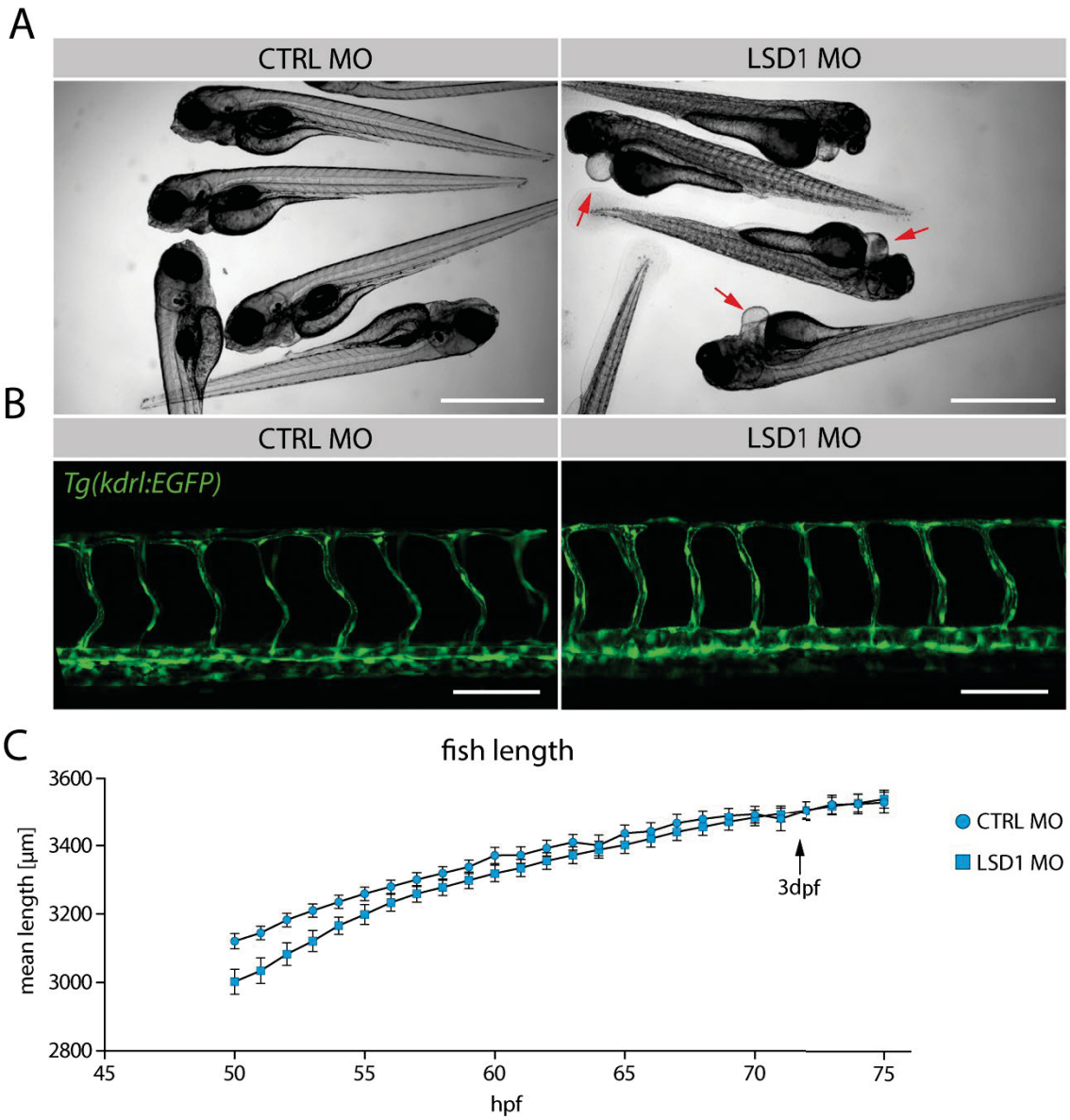

Figure 7 | LSD1 knockdown larvae developed a pericardial edema and an initial delay in length growth but no vascular defects

(A) Bright field images of 3 dpf larvae with control MO (left) vs. LSD1 MO (right). Pericardial edemata developed upon LSD1 knockdown are depicted with red arrows. Scale bars represent 1 mm. (B) Representative confocal images of maximum intensity z-projections show lateral views of *Tg(kdrl:EGFP)*. No differences in the development of the vasculature were observed at 2 dpf in 2 independent experiments with 2 fish each. Scale bars represent 50 µm. (C) Time-lapse measurement of the length growth. Bright-field images for length measurement were acquired from anesthetized fish every hour using the EnSight™ multimode plate reader. Data was obtained from a single injection with 25-26 larvae per condition shown as mean ±SEM. Black arrow depicts the earliest time point of subsequent investigations on OL development (3 dpf).

A pericardial edema typically manifests as consequence of cardiac and/or vascular defects. The development of the vasculature however, is a prerequisite for OPC migration and differentiation as it serves as a physicochemical scaffold (Tsai et al., 2016). Fortunately, the vasculature developed properly upon LSD1 knockdown as

suggested by the *Tg(kdrl:EGFP)*, a transgenic zebrafish line with a EGFP expressed under the regulatory elements of the vasculature-specific *kdrl* gene (**Figure 7** B).

For quantitative analysis of OL differentiation, OLs within 4 hemisegments of the spinal cord were counted. Differences in the overall length of the fish could lead to misinterpretation of absolute cell numbers. Therefore, the fish length was measured over time. An early delay in length growth persisting until 2.5 dpf was observed (**Figure 7** C). As quantitative analyses were carried out at 3 dpf and 5 dpf respectively, it could be excluded that difference in spinal cord length might influence the determination of absolute cell numbers.

A general issue of the MO technique are off-target effects causing phenotypes not related to the function of LSD1. A well-known effect is the non-specific activation of tumor suppressor P53 and subsequent induction of apoptosis (Gerety and Wilkinson, 2011). To address this issue, paraffin section of 3 dpf zebrafish were prepared. Sections were immunostained against cleaved caspase 3 and counterstained with haematoxylin. Under the experimental conditions used in this study, no abnormal induction of apoptosis was suggested by this preliminary staining (**Figure 8**, n=1).

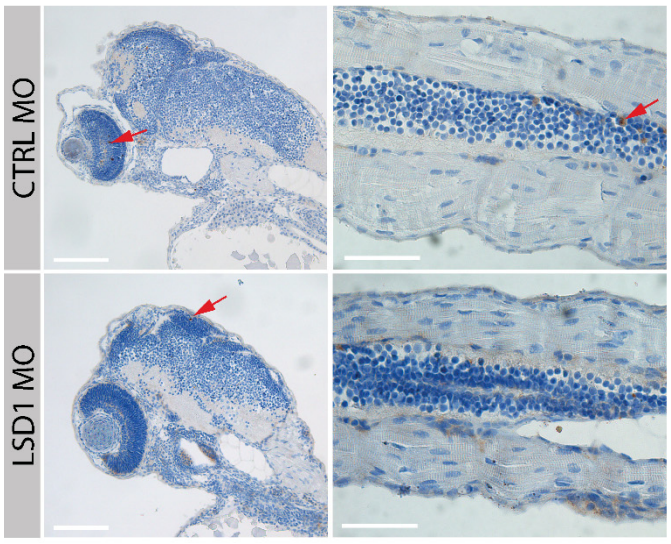

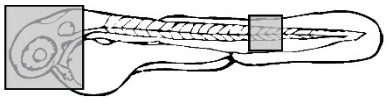

Figure 8 | No abnormal apoptosis was observed by anti-cleaved caspase 3 staining
Sagittal paraffin sections of 3 dpf larvae. Shown are LSD1 morphants (bottom) and larvae injected with a control mismatch MO (top). Arrows indicate cells labeled with anti-cleaved caspase 3. No difference could be observed based on the present experiment (n=1). Nuclei were counterstained with haematoxylin. Scale bars represent 200 µm. Immunostainings were done by Dr. Anna Japp (University Bonn).

Taken together, a so far unpublished LSD1 MO has been established. A previously described phenotype on the hematopoietic system was confirmed (Takeuchi et al., 2015). Furthermore, a developmental delay in length growth has been identified that was not expected to interfere with the analysis carried out in the following.

3.1.1.2 Establishment of a formaldehyde sensor *in vivo*

It has long been appreciated that repressive or activating function of LSD1 are conveyed by its enzymatic activity. In fact, non-enzymatic functions of LSD1 seem to exist and are subject of ongoing research (Maiques-Diaz et al., 2018). Therefore, LSD1 activity should be considered as an independent parameter beyond protein and transcript levels. In cell lysates, demethylase activity can be quantified by e.g. a reaction of fluorogens with the demethylation by-products. Recently, much effort has been devoted to develop fluorescent sensors applicable in living cells. To monitor demethylase activity even in a whole organism, is highly desirable and has not been achieved so far. FAP-1 is a formaldehyde-specific sensor designed to monitor formaldehyde in living cells (kindly provided by Thomas F. Brewer and Christopher J. Chang, UC Berkeley, Dept. of Chemistry, USA) (Brewer and Chang, 2015). FAP-1 exhibits a 2-aza-cope reactivity and is weakly fluorescent in its unreacted state. Upon reaction with formaldehyde, a 2-aza cope rearrangement renders the molecule about 8-fold more fluorescent (λ_{ex} = 645 nm, λ_{em} 655 and 750 nm). To get a first impression of the FAP-1 turn-on response *in vivo*, small droplets of FAP-1 (5 mM stock) were injected intracranial in 3 dpf larvae. At 2 h after injections, a fluorescence signal could be detected around the site of injection (**Figure 9**, top).

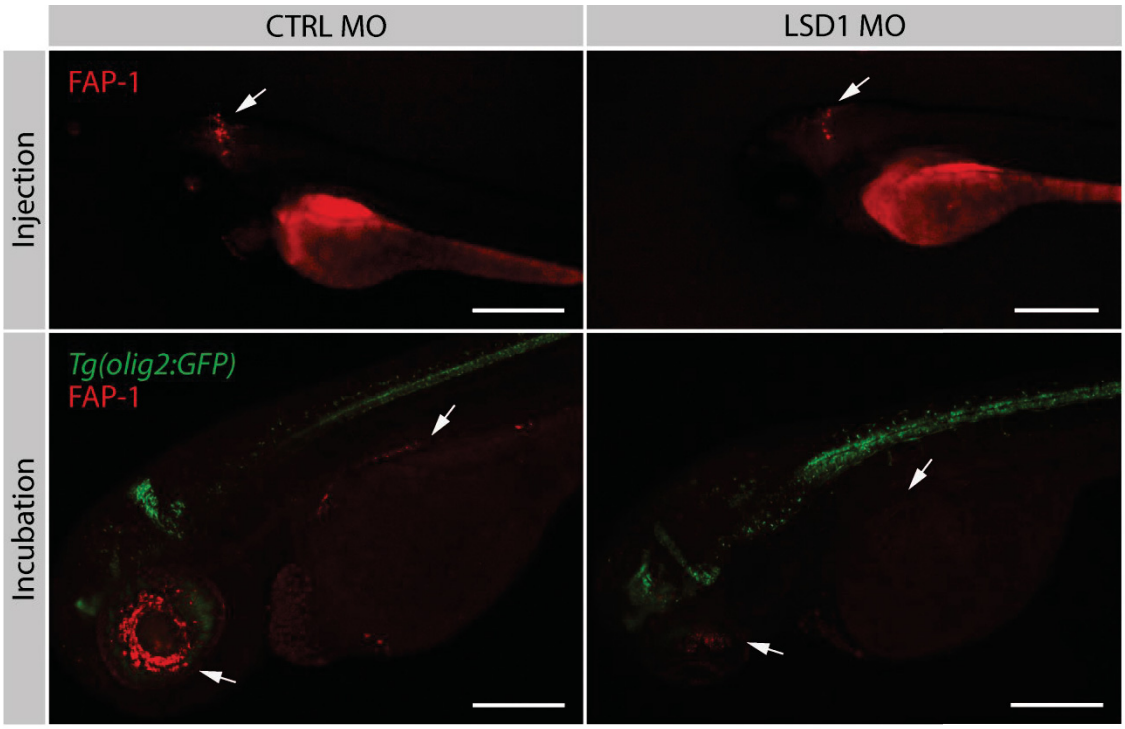

Figure 9 | *In vivo* detection of endogenous formaldehyde by FAP-1

Microinjection and incubation of 3 dpf zebrafish larvae with FAP-1 revealed a qualitative difference in the turn-on response of FAP-1 in control MO larvae (left) vs. LSD1 MO larvae (right). (Top) Intracranial injection of wildtype larvae with FAP-1. Shown are representative images acquired from a fluorescence microscope 2 h after injection (6-7 fish in total). Scale bars represent 500 µm. (Bottom) *Tg(olig2:GFP)* larvae were incubated for 20 h with 12.5 µM FAP-1. Maximum intensity z-projections of representative images obtained from a confocal microscope (5 fish in total). Scale bars represent 250 µm and arrows depict sites of FAP-1 turn-on responses.

Intriguingly, a qualitative difference in the signal between the LSD1 MO group (7 fish) and CTRL MO group (6 fish) was observed. Delivery of the probe via intracranial injection is an invasive approach and reproducibility in respect to the distribution of the probe and the final concentration, hampered by the injection procedure. The zebrafish is known to efficiently absorb low molecular weight compounds over the skin from the surrounding water. Therefore, zebrafish larvae were incubated with different concentrations of FAP-1 for 3 and 20 hours, respectively (**Figure 9**, bottom). It appeared that FAP-1 was not absorbed over the skin but rather accumulated in the eye. Again, a turn-on response could be observed in CTRL MO that was drastically reduced in larvae with decreased LSD1 level (5 larvae per condition). In addition, the probe did not cause any toxicity as assessed by the fish survival indicating its applicability *in vivo*.

Here, for the first time, the production of endogenous formaldehyde was visualized *in vivo* using a first-generation fluorescence-based sensor originally designed for cell

culture experiments. LSD1 appears to be the major source of formaldehyde as the MO-based knockdown decreased the signal in all labeled structures. The integration of FAP-1 in the following studies would require a uniform distribution in the CNS. However, uptake kinetics or conditions need to be improved for this purpose. Nevertheless, with this new technique, decreased LSD1 activity upon MO injection was confirmed.

3.1.1.3 LSD1 is essential for OL lineage commitment in the spinal cord

The *Tg(olig2:GFP)* fish drives the expression of cytosolic green fluorescent protein (GFP) under the *olig2* promotor and marks OPCs, OLs, descendent motor neurons and interneurons in the developing spinal cord (Shin et al., 2003). OPC specification is completed at 24 hpf and becomes visible in a bright GFP signal throughout the pMN domain. No obvious difference could be observed during this stage (**Figure 10** B).

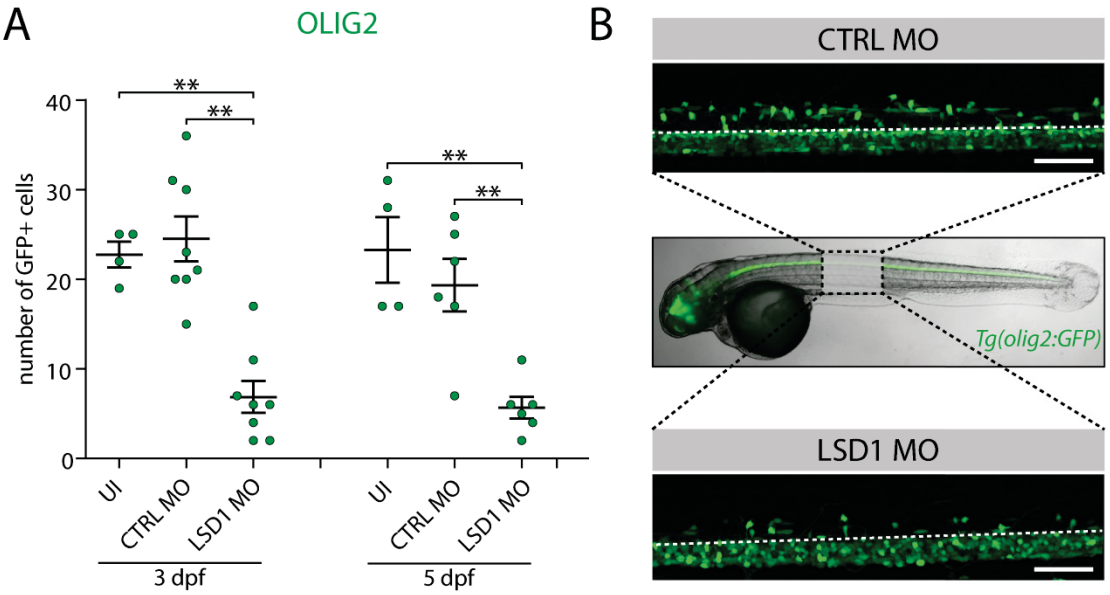

Figure 10 | LSD1 knockdown reduced the number of dorsal OLs in the zebrafish spinal cord

(A) Quantification of dorsal migrated GFP+ cells within 4 spinal hemisegments of the *Tg(olig2:GFP)*. GFP+ cells no longer associated with the ventral pMN domain were considered as dorsal migrating cells (above the white dashed shown line shown in B). Each dot represents 1 fish, shown with mean and ±SEM. Summary of 3 independent experiments. Mann-Whitney U-test: **p<0.01 (B) Representative lateral views of maximum intensity z-projections acquired from a two-photon light sheet microscope; CTRL MO (top) vs. LSD1 MO (bottom) at 5 dpf. Overlay of fluorescence and bright field images of a 3 dpf UI larvae acquired from a fluorescence microscope (middle). Scale bars represent 50 µm.

At 2.5 dpf OPCs give rise to OLs that still express OLIG2 but can be distinguish from OPCs as they migrate dorsally, away from the pMN domain. By counting the total cell number of dorsal positioned GFP positive (GFP+) cells in the living zebrafish, the extent of OL differentiation can be quantified. Knockdown of LSD1 reduced the number of dorsal migrated OLs by 70 % at 3 dpf and 75 % at 5 dpf (**Figure 10** A). This indicates that LSD1 is necessary for the differentiation of OPCs to OLs. Next, the small molecule inhibitor SP2509 was employed to substantiate the observed effects (Fiskus et al., 2014). Prolonged exposure to 2.5 µM SP2509 was well tolerated as assessed by the survival rate. In contrast to the MO treatment, no change in the length growth was observed (**Figure 11** A). Here, a novel automated algorithm for counting dorsal migrated GFP+ cells in the *Tg(olig2:GFP)* was used. Images were continuously acquired with an EnSight™ multimode plate reader over a time course of 25 h, starting from 50 hpf until 75 hpf. (**Figure 11** B). This approach allows a time-resolved high-throughput screen of OL differentiation in the spinal cord of anesthetized zebrafish. Although not as pronounced, zebrafish larvae that were continuously exposed to SP2509 had less OLs in the spinal cord at every time point analyzed (**Figure 11** B). To validate the applicability of the algorithm, LSD1 morphants were subjected to the high-throughput screen as a positive control. The result obtained from manual analysis using images derived from the two-photon light sheet microscope (**Figure 10** A) could be confirmed with the automated algorithm (**Figure 11** B).

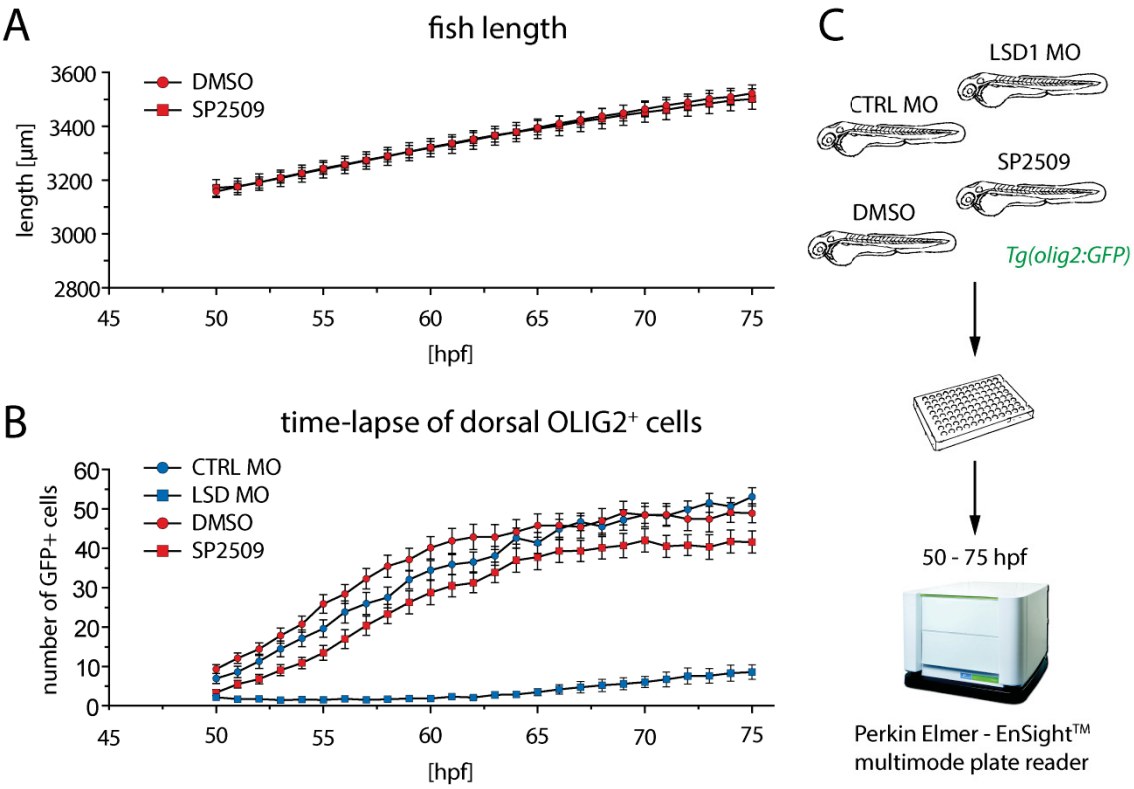

Figure 11 | Pharmacological inhibition of LSD1 reduced the number of dorsal OLs in the zebrafish spinal cord

High-throughput analysis of dorsal migrated GFP+ cells in the *Tg(olig2:GFP)* line through an automated counting algorithm using the EnSight™ multimode plate reader. (A) Overall lengths of anesthetized larvae were measured every hour based on brightfield images acquired from the EnSight™ multimode plate reader. Mean values of 25-26 fish obtained from a single injection shown as mean ±SEM. (B) Time-lapse of dorsal migrated GFP+ cells. Each dot shows the mean value of 25-26 fish obtained from a single injection or incubation experiment, respectively. The automated algorithm distinguishes between dorsal positioned GFP+ cells from ventral residing GFP+ cells. (C) 2.5 µM SP2509 was added to the fish water right after eggs were laid. After 8 h the embryos were de-chorinated and further incubated with SP2509. Right before the start of the time-lapse, the larvae were anesthetized and each fish positioned in a well of a 96-well plate containing 100 µL Danieau (1x) supplemented with anaesthetic and 2.5 µM SP2509 or DMSO. Dorsal GFP+ cells in the whole spinal cord were automatically counted every hour.

3.1.1.4 LSD1 regulates final differentiation of OLs in the spinal cord

Given that less premature OLs arrived in the dorsal spinal cord, it was expected that less OLs mature to myelinating OLs and subsequently myelination defects become visible. To verify this assumption, LSD1 was knocked down in the *Tg(cldnk:EGFP)* line. The *cldnk* gene encodes for claudin k (CLDK), a zebrafish-specific myelin protein suitable for identifying mature OLs (Ye et al., 2009; Münzel et al., 2012). Indeed, a significant reduction in the number of mature OLs was observed along the dorso-ventral axis (**Figure 12** A - dorsal; B - ventral). The relative number of dorsal and ventral CLDK-positive OLs was reduced by 65 % and 20 %, respectively. This

demonstrates the considerable biological significance of LSD1-mediated demethylation during OL differentiation in the zebrafish spinal cord.

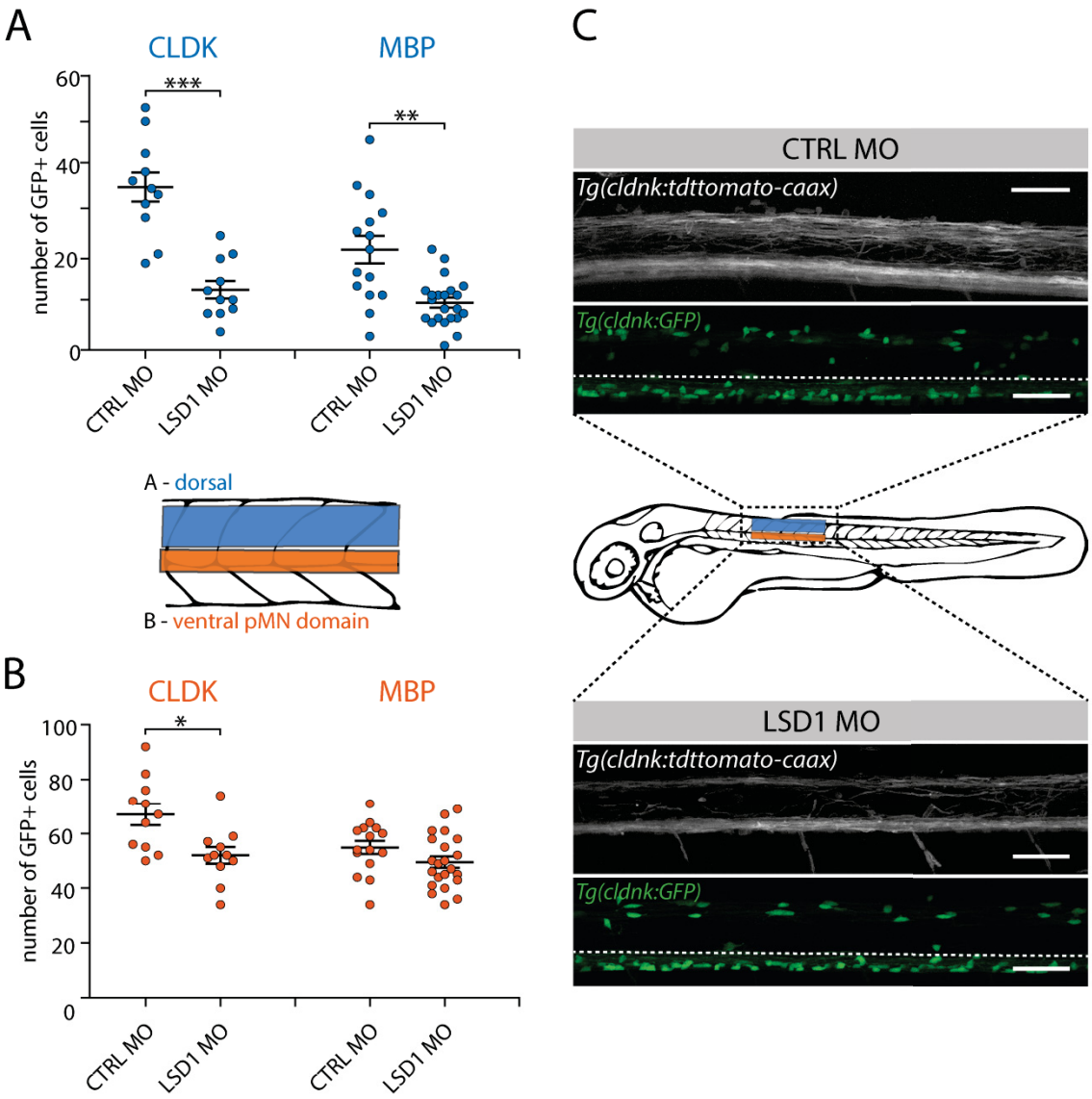

Figure 12 | LSD1 knockdown impaired OL differentiation and myelination in the zebrafish spinal cord

Number of GFP+ cells within 4 spinal hemisegments in *Tg(cldnk:GFP)* and *Tg(mbp:GFP)* 5 dpf larvae in (A) the dorsal spinal cord (depicted in blue) and (B) ventral pMN domain (depicted in orange). Live-cell images acquired from a two-photon point scanning microscope. Each dot represents 1 fish, shown with mean and ±SEM. Summary of 4 independent experiments. Mann-Whitney U-test: *p<0.05; **p<0.01; ***p<0.001. (C) Representative lateral views of maximum intensity z-projections of *Tg(cldnk:GFP)* and *Tg(cldnk:tdttomato-caax)*. GFP+ cells no longer associated with the ventral pMN domain were considered as dorsal migrating cells (above the white dashed line). CTRL MO (top) vs. LSD1 MO (bottom) larvae at 5 dpf. Scale bars: 500 µm.

To confirm these findings, the *Tg(mbp:EGFP)* line was used. The *Tg(mbp:EGFP)* line expresses enhanced green fluorescent protein (EGFP) under the regulatory elements of the myelin basic protein (MBP), which is an integral component of the myelin sheath and a well-accepted marker for mature OLs in both, zebrafish and

rodents (Almeida et al., 2011). Again, the number of dorsal OLs was significantly reduced, as 55 % fewer cells were positive for EGFP. The pool of ventral residing OLs however, was constant. Only a tendency to a reduction became apparent. To address the question whether the observed effects on differentiation impacts on functional myelination as well, a transgenic *cldnk* reporter line was used that expresses a membrane bound tdTomato (*Tg(cldnk:tdTomato-CAAX)*). At first glance, the myelin sheath was severely affected throughout the spinal cord in both, the ventral and dorsal domains (**Figure 12** C).

3.1.1.5 LSD1 is not essential for neurogenesis in the zebrafish spinal cord

The fact that OLs differentiation is literally abolished in the LSD1 MO group raises the question whether OPC differentiate at all. OPCs give first rise to motor neurons before they produce OLs. On the molecular level, MN specification becomes evident by a specific expression profile of motor neuron homeodomain containing transcription factors (Tanabe et al., 1998). Here, a transgenic enhancer trap line with a trapping construct inserted near the coding region of the *mnx2b* gene was used (Asakawa et al., 2012). The *mnx2b* gene encodes for the motor neuron and pancreas homeobox 2b (MNR2B) protein which is expressed in spinal and abducens MNs. The *Tg(mnx2b:GFP)* line shows a GFP signal in the somata of MNs and their axonal projections (**Figure 13** A).

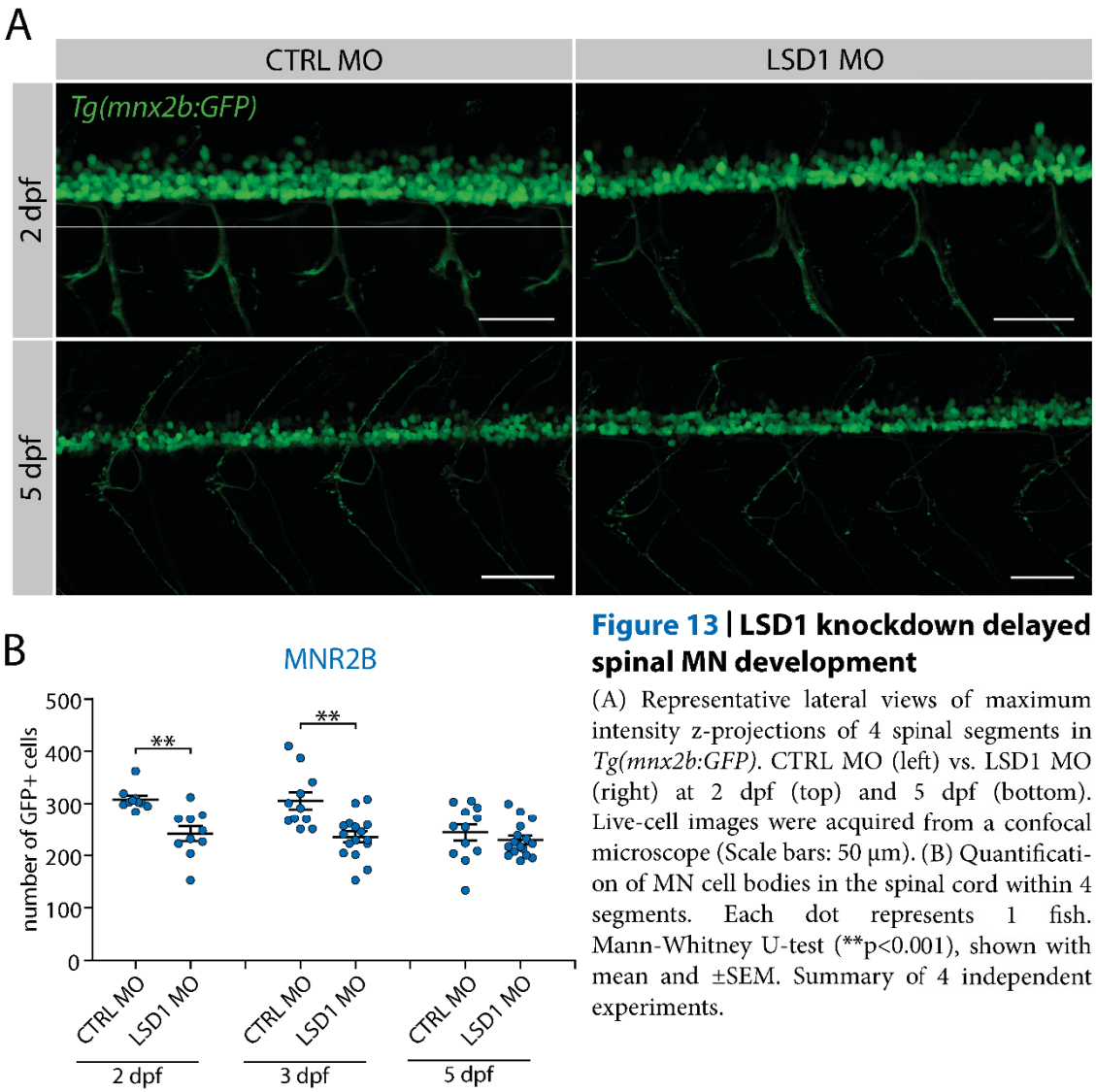

Figure 13 | LSD1 knockdown delayed spinal MN development

(A) Representative lateral views of maximum intensity z-projections of 4 spinal segments in *Tg(mnx2b:GFP)*. CTRL MO (left) vs. LSD1 MO (right) at 2 dpf (top) and 5 dpf (bottom). Live-cell images were acquired from a confocal microscope (Scale bars: 50 µm). (B) Quantification of MN cell bodies in the spinal cord within 4 segments. Each dot represents 1 fish. Mann-Whitney U-test (**p<0.001), shown with mean and ±SEM. Summary of 4 independent experiments.

The somata are evenly distributed throughout the pMN domain while their axons descend in bundles towards the peripheral muscle fibers. MNs were quantified by counting their cell bodies within 4 hemisgemts. At 2 and 3 dpf the number of *mnx2b* expressing neurons was significantly reduced by 21 %, while the difference could no longer be recognized by 5 dpf (**Figure 13** B). This observation suggested that the knockdown rather delayed the development of MN than impacted on the general decision whether OPCs become MNs.

To investigate whether OPCs fail to exit the cell cycle and persist as proliferating progenitors, an anti-PCNA staining was performed in paraffin sections of 3 dpf larvae. According to this preliminary investigation (n=1, 3 fish), the proportion of PCNA+ cells in the spinal cord is increased (**Figure 14**). Additional replicates are

needed to further support the notion that LSD1 knockdown leads to increased proliferation in the spinal cord.

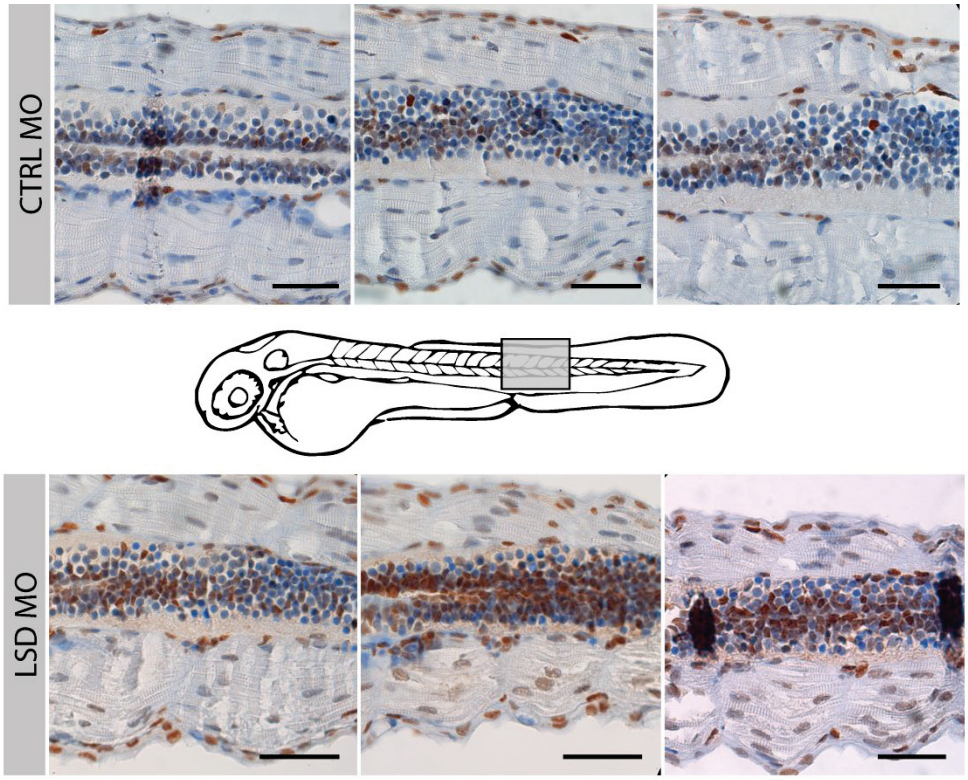

Figure 14 | Anti-PCNA staining suggested an increased proportion of proliferating cells in the spinal cord of 3 dpf LSD1 morphants
Images show saggital paraffin sections of 3 dpf larvae immunostained against PCNA. Nuclei were counterstained with haematoxylin. Shown are spinal sections from 3 fish obtained from a single injection. Scale bars represent 500 µm. Stainings were done in cooperation with Dr. Anna Japp (University Bonn).

The establishment of a functional neuronal network is a prerequisite for oligodendrogliosis, not only because neurons are the actual structures to be myelinated. Neurons provide a plethora of extrinsic cues that attract pre-myelinating OLs and orchestrate their terminal differentiation (He et al., 1996; Stevens et al., 2002). As already shown, the knockdown of LSD1 influenced the development of MNs but not to the same extent as shown for OLs. This observation suggested the need for further investigations. To provide a global overview of the neuronal network, antibodies against acetylated α-tubulin and the synaptic vesicle glycoprotein 2 (SV2) were used for whole mount stainings in 3 dpf larvae. Assuming that there is a causative relationship between the defect in oligodendrocyte differentiation and neurogenesis, it seemed reasonable to consider only those fishes for staining that obviously had fewer oligodendrocytes in the spinal cord. Whole

mount stainings were therefore done in the the *Tg(olig2:EGFP)* line. No obvious differences could be observed according to 8 whole mount stainings from 2 independent experiments (**Figure 15**).

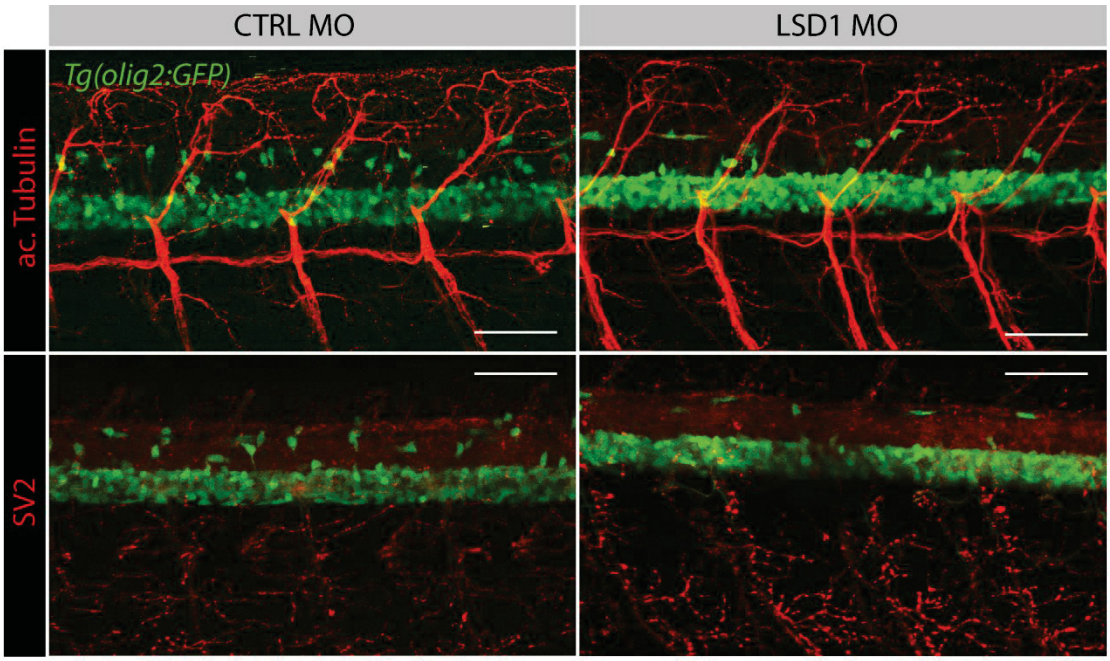

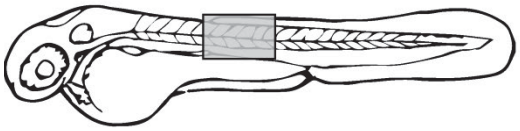

Figure 15 | SV2 and acylated tubulin whole mount stainings suggested no servere defects in neurogenesis in the zebrafish spinal cord upon LSD1 knockdown

Representative lateral views of 3 dpf *Tg(olig2:GFP)* spinal cord sections stained for acetylated tubulin (top) and SV2 (bottom). Shown are images of CTRL MO larvae (left) versus LSD1 MO larvae (right) obtained from a two-photon point scanning microscope. No obvious difference could be observed in 8 whole mount stainings obtained from 2 independent experiments. Scale bars represent 50 µm.

Although Schwann cells rather than OLs are responsible for myelination of neurons of the peripheral nervous system (PNS), development of the PNS was investigated as well.

Here, the production of neurogenin 1 (NGN1) positive dorsal root ganglion neurons (DRGNs) was followed. DRGNs are neurons of the PNS that convey sensory stimuli into the CNS. The analysis of DRGN development was rather randomly chosen to investigate the development of a representative neuronal cell type of the PNS. DRGNs arise from neural crest cells (NCC), a multipotent non-epithelial cell

population that appears in the periphery of the dorsal neural tube. NCCs give rise to neuronal and glial fated cells of the PNS, as well as multiple non-neural cells. The number of DRGNs anterior to the NCC stream was reduced by 30 % as evinced from the *Tg(neurog1:EGFP)* reporter line (**Figure 16**) (Blader et al., 2003).

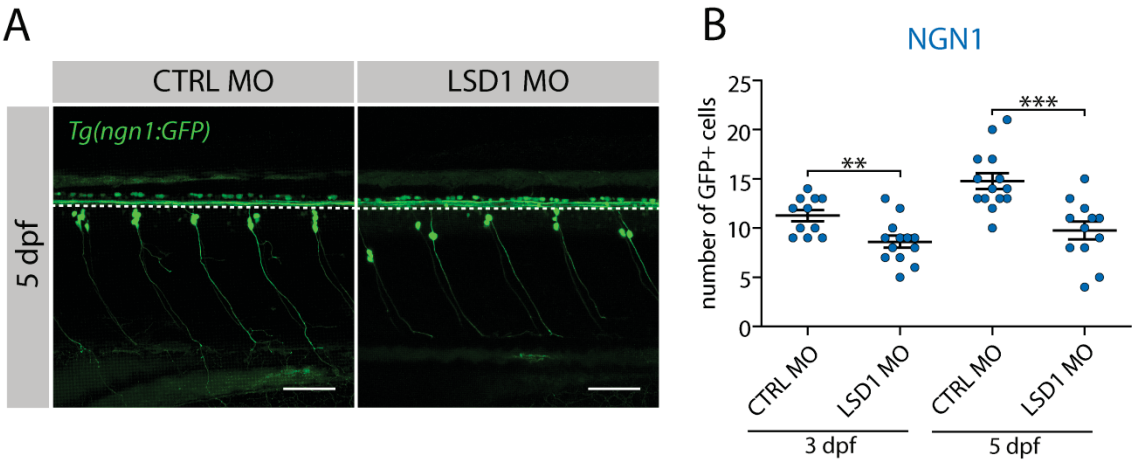

Figure 16 | LSD1 knockdown in zebrafish impaired the development of DRGNs

(A) Representative lateral views of maximum intensity z-projections of the *Tg(ngn1:GFP)* line. Shown are confocal images at 5 dpf. Scale bars represent 50 µm. (B) The number of GFP+ cells within 4 spinal hemisegments in *Tg(ngn1:GFP)* LSD1 was estimated at 3 dpf and 5 dpf. Each dot represents 1 fish. Statistical significance was determined by the Mann-Whitney U-test (**p<0.01; ***p<0.001), shown with mean and ±SEM. Summary of 3 independent experiments.

To confirm that this observation was not just due to a developmental delay similar to MN differentiation, DRGs were again examined at 5 dpf. The number of DRGNs was still reduced by 33 % compared to the CTRL MO group indicating that LSD1 specifically drives the specification of DRGNs.

These data revealed that LSD1 controls the generation of some neuronal subtypes. However, in conclusion, fundamental developmental defects, comparable to those observed during OL development and myelination, did not occur during neurogenesis upon LSD1 knockdown.

3.1.2 Mouse

LSD1 is expressed in OPCs *in vivo*, as shown by anti-LSD1 and -PDGFRα immunostainings in coronal brain sections of postnatal day 10 C57BL/6J mice (**Figure 17**).

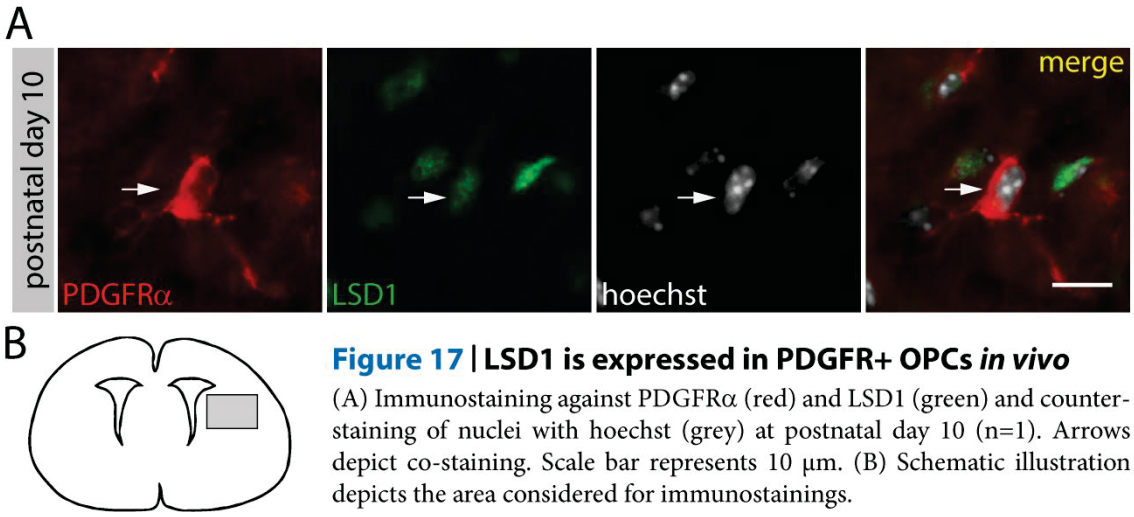

Figure 17 | LSD1 is expressed in PDGFR+ OPCs *in vivo*
(A) Immunostaining against PDGFRα (red) and LSD1 (green) and counter-staining of nuclei with hoechst (grey) at postnatal day 10 (n=1). Arrows depict co-staining. Scale bar represents 10 µm. (B) Schematic illustration depicts the area considered for immunostainings.

3.1.2.1 LSD1 regulates the transcriptional program in mouse-derived OPCs

To investigate if LSD1 specifically drives the intrinsic transcriptional program of OPCs, glial restricted progenitor cells were isolated from the brain of postnatal day 3-4 young mice. Using immunolabeled magnetic beads, targeting the OPC-specific ganglioside A2B5, a glial restricted progenitor pool was isolated from the mouse telencephalon and cerebellum. In the presence of the mitogens fibroblast growth factor (FGF) and platelet-derived growth factor (PDGF), A2B5+ OPCs proliferate and retain their characteristic bipolar to multipolar morphology. The A2B5+ OPC pool was isolated from a transgenic mouse harboring a tetracycline-controlled `tet-on´ short hairpin ribonucleic acid (shRNA) expression construct. The tet repressor (tetR) constitutively blocks the expression of the *kdm1a* shRNA until it is eliminated from the promoter by the addition of doxycycline (DOX) (**Figure 18** A) (Zhu et al., 2014; Sprüssel et al., 2012).

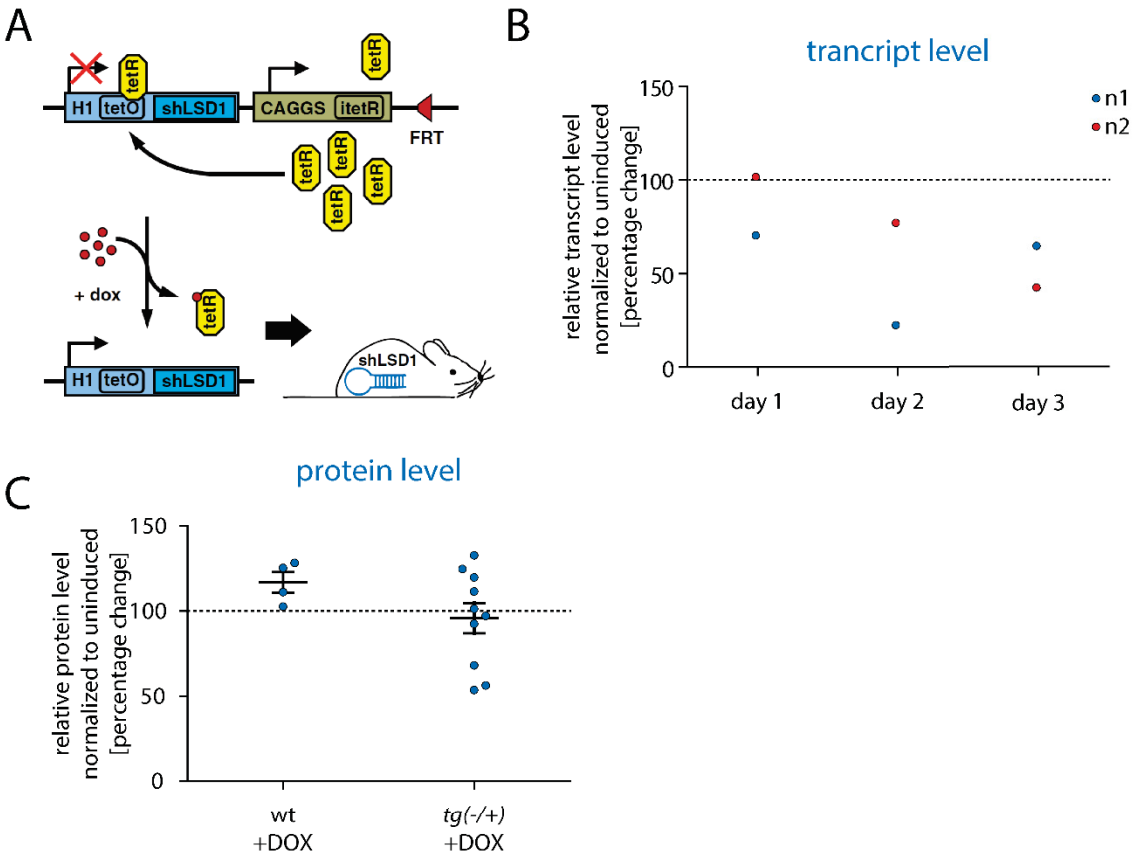

Figure 18 | Conditional LSD1 knockdown *in vitro*

(A) Schematic drawing of the TET-ON system used to induce the *kdm1a*-specific shRNA *in vivo* (Sprüssel et al 2012). The tetR repressor blocks the expression of the *kdm1a*-specific shRNA until it is eliminated from the promotor in the presence of doxycycline (DOX) . A2B5+ OPCs were isolated from heterozygous pups harboring the endogenous *kdm1a* shRNA expression construct (Tg(+/-)) or wildtype pups (wt) at postnatal day 3. (B) qPCR analysis of the remaining *kdm1a* mRNA level in DOX-induced proliferating A2B5+ OPCs isolated from Tg(-/+). OPCs were treated with 1 µg/mL DOX and normalized to the untreated Tg(-/+) (CTRL). The CTRL was set to 100 % depicted with a dashed line. (C) Immunoblot analysis of the LSD1 protein level after 5 days of differentiation. OPCs were treated with DOX for 3 days under proliferating conditions and subsequently differentiated in the presence of DOX for 5 days. Optical band densities were normalized to actin and the normalized LSD1 levels in untreated cells. Each dot represents an independent isolation obtained from a single pup (3 breedings in total).

The knockdown of LSD1 can be induced by the addition of DOX to the cell culture medium as previously described (Sprüssel et al., 2012). The induction of the endogenous shRNA in proliferating OPCs induced a mild knockdown over 3 days as evinced by qPCR analysis (**Figure 18** B). The remaining *kdm1a* transcript levels in 2 biological replicates were reduced at day 3 to 43 % and 65 %, respectively. Next, A2B5+ OPCs were again exposed to DOX for 3 days and then differentiated for 5 days in the presence of DOX. After 5 days, the LSD1 protein levels were quantified by immunoblot analysis (**Figure 18** C). Surprisingly, in wildtype OPCs, the LSD1 protein levels tend to be increased when compared to uninduced wildtype control. This

indicates that DOX per se could exert unwanted side-effects that lead to direct or indirect induction of LSD1. Only tendencies to a reduction of the LSD1 protein levels became evident in DOX-induced cultures of OPCs harbouring the shRNA expression construct (Tg(-/+)) when compared to the uninduced Tg(-/+).

To analyze the effect of the shRNA induction by DOX on lineage specific protein expression, MBP and GFAP protein levels were quantified by immunoblot analysis. While lysates of induced Tg(-/+) cells showed a reduction of MBP levels by 75 %, the GFAP protein levels, considered as a marker for astrocytes, were not affected (**Figure 19**).

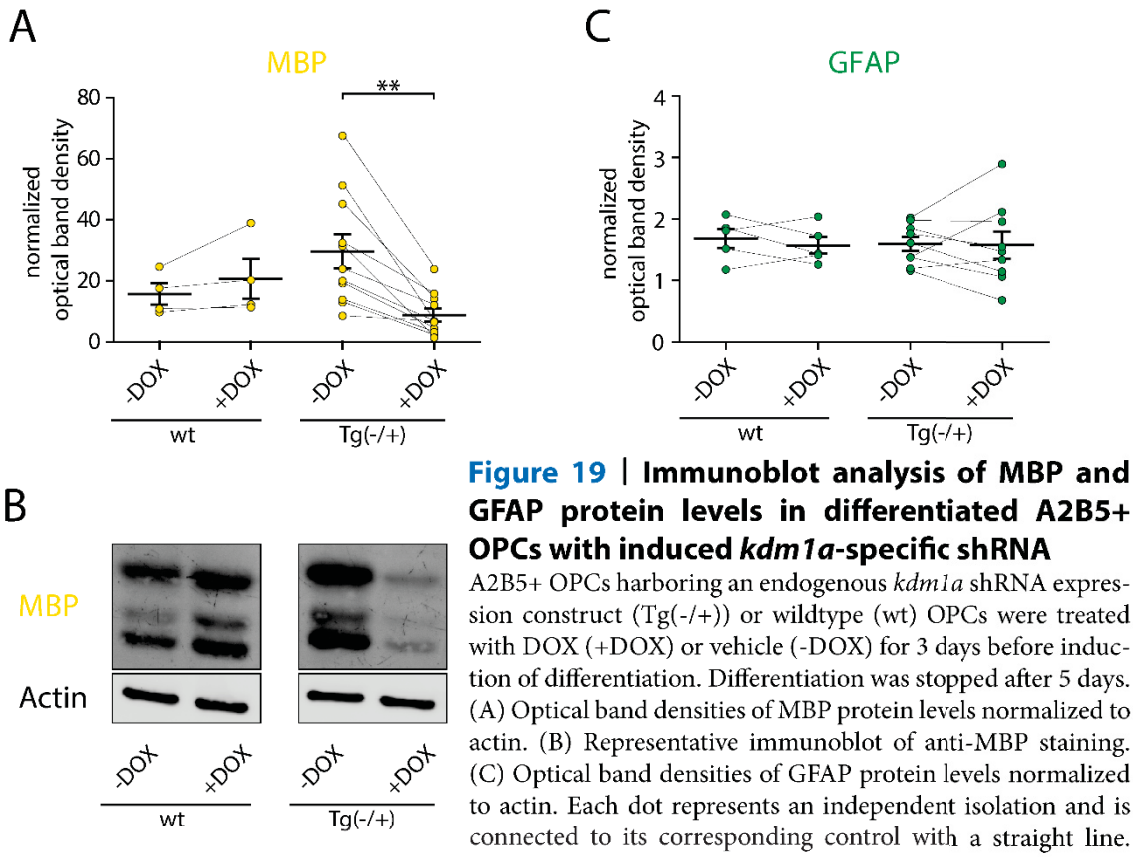

Figure 19 | Immunoblot analysis of MBP and GFAP protein levels in differentiated A2B5+ OPCs with induced *kdm1a*-specific shRNA

A2B5+ OPCs harboring an endogenous *kdm1a* shRNA expression construct (Tg(-/+)) or wildtype (wt) OPCs were treated with DOX (+DOX) or vehicle (-DOX) for 3 days before induction of differentiation. Differentiation was stopped after 5 days. (A) Optical band densities of MBP protein levels normalized to actin. (B) Representative immunoblot of anti-MBP staining. (C) Optical band densities of GFAP protein levels normalized to actin. Each dot represents an independent isolation and is connected to its corresponding control with a straight line. (Shown with mean ± SEM; Mann-Whitney U-test: **p<0.005; n=7-11; 3 breedings in total)

To corroborate whether the decreased MBP levels resulted from a relative reduction in the number of OLs, immunocytochemistry (ICC) stainings against MBP and the OL specific 2′, 3′-cyclic nucleotide-3′-phosphodiesterase (CNPase) were performed. Indeed, the relative number of mature OLs was reduced by about 60 % upon induction with DOX (**Figure 20**).

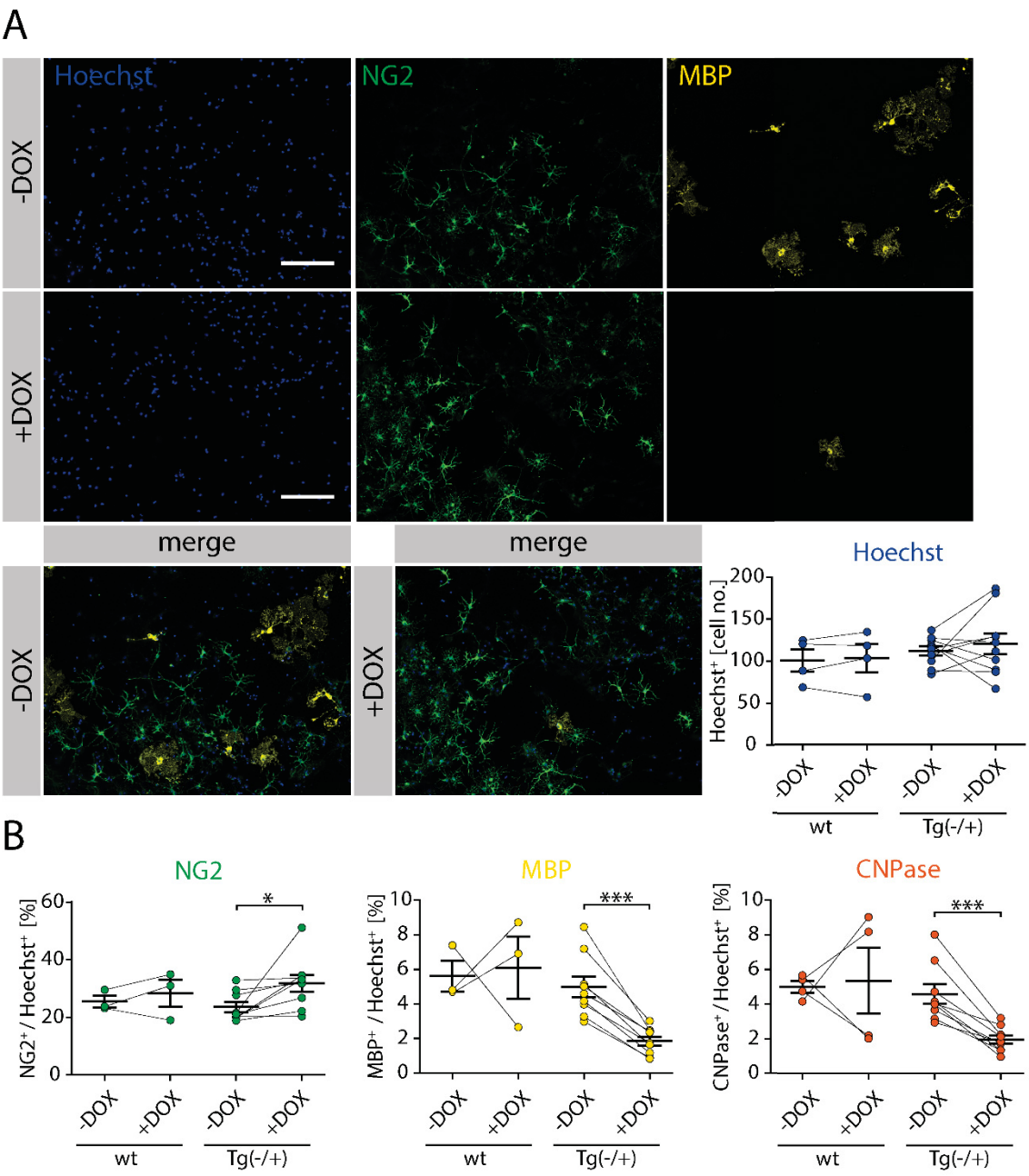

Figure 20 | Decreased LSD1 transcript levels reduced the relative number of OLs in differentiated A2B5+ OPCs

ICC stainings against myelin- and progenitor-specific marker proteins. A2B5+ OPCs harboring an endogenous *kdm1a* shRNA expression construct (Tg(-/+)) or wildtype (wt) OPCs were treated with DOX (+DOX) or vehicle (-DOX) for 3 days before induction of differentiation. Differentiation was stopped after 5 days. (A) Representative images of anti-MBP, anti-NG2 and nuclei counterstaining with Hoechst. Scale bars represent 15 µm. (B) Quantification of NG2, -MBP, -CNPase positive cells. Positive cells were normalized to the total cell number (Hoechst). Each dot represents an independent isolation obtained from a single pup and is connected to its corresponding control with a straight line (Mean ± SEM; Mann-Whitney U-test: *p<0.05 and ***p<0.0001; n=7, 3 breedings in total).

Importantly, it could be shown that differentiation of OPCs was arrested in pre-myelinating stage, as suggested by an increased proportion of cells, positive for the progenitor specific NG2.

To further characterize the immature phenotype, the population of O4+ cells was quantified by ICC (**Figure 21** A).

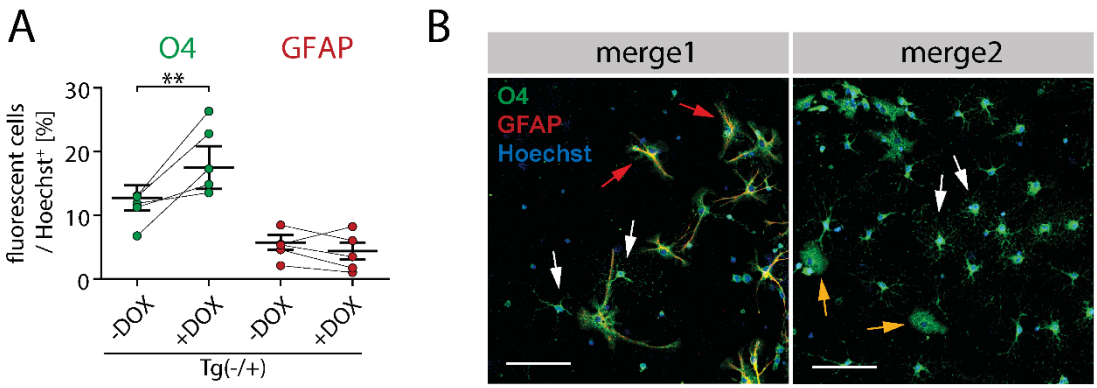

Figure 21 | ICC stainings against preOL-specific O4 and astrocyte-specific GFAP in differentiated A2B5+ OPCs with induced *kdm1a*-specific shRNA

A2B5+ OPCs harboring an endogenous *kdm1a* shRNA expression construct (Tg(-/+)) were treated with DOX (+DOX) or vehicle (-DOX) for 3 days before induction of differentiation. Differentiation was stopped after 5 days. (A) The relative number of O4+ preOL with an O4 like phenotype and GFAP+ cells. Each dot represents an independent isolation of cells obtained from a single pup and is connected to its corresponding control with a straight line (Mann-Whitney U-test:**p<0.01; n=5 shown with mean ± SEM; 3 breedings in total). (B) Two representative images depicting the premyelinating O4+ phenotype (white arrows) considered for quantification. The GFAP+/O4+ population (red arrows) was considered as GFAP fraction. Cells positive for O4, but with no premyelinating phenotype (orange arrows) were not considered for quantification. Scale bars represent 10 µM.

It is suggested that O4 immunoreactivity identifies a pre-myelinating stage that is more advanced compared to NG2+ progenitor cells (Reynolds and Hardy, 1997). Intriguingly, staining revealed a mixed population with dissimilar morphologies. A subpopulation with a premyelinating phenotype could be clearly identified and was considered for quantification (**Figure 21** B, white arrows). The remaining proportion of O4+ cells was highly heterogeneous and could be roughly divided into rounded cells (**Figure 21** B, orange arrows) and cells with astrocyte-like phenotypes (**Figure 21** B, red arrows). The O4+ cells that were considered for quantification were increased upon induction of the shRNA by about 40 %. The O4+ cells that exhibit an astrocyte-like shape showed in fact a weak immunoreactivity against GFAP as well (GFAP+/O4+). Noteworthy, a GFAP+/O4- population could not be identified as all GFAP+ cells were also positive for O4. No difference in the amount of GFAP+/O4+ was observed when LSD1 transcript levels were reduced prior to the induction of differentiation. It should be noted in conclusion, that due to the heterogeneity of the putative O4+ pool, the true identity remains to be defined.

Due to the uncertainty regarding the knockdown efficiency, pharmacological inhibitors were employed to inhibit the catalytic activity of LSD1. LSD1 resides in multifunctional protein complexes harboring a variety of other chromatin and DNA modifying factors. Thus, this approach further allowed distinguishing between a putative role of LSD1 as a scaffolding protein and its demethylase activity.

To test the applicability of different LSD1 inhibitors, the phenelzine and tranylcypromine derivates, bizine and ORY-1001 were tested for possible cytotoxicity in primary cells. Additionally, SP2509 that had been used in the zebrafish experiments before was tested as well. None of these compounds exerted any cytotoxic effects, even in concentrations way beyond working concentrations commonly applied in cancer cell lines e.g. around 10 µM for bizine and nanomolar concentrations for SP2509 and ORY-1001 (**Figure 22**) (Fiskus et al., 2014; Prusevich et al., 2014; Maes et al., 2018).

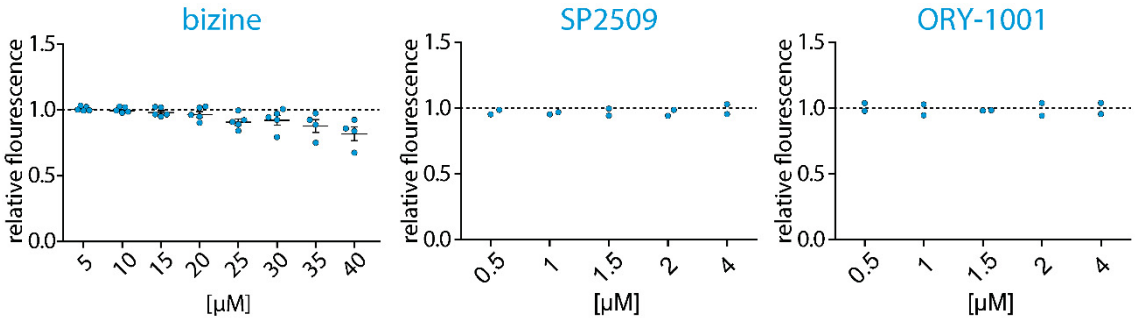

Figure 22 | Small molecule inhibitors targeting LSD1 were well tolerated in high doses in A2B5+ OPCs

A2B5+ OPCs were treated with indicated concentrations of bizine, SP2509 and ORY-1001 for 24 h under proliferating conditions. Resazurin turnover was measured using the `Cell Titer-Blue® Cell Viability Assay´. Effects of bizine treatment shown with mean ± SEM (n=4-5). Each dot represents an independent isolation and breeding.

For further studies, bizine in a working concentration of 10 µM was chosen. This inhibitor is suggested for application in neurodegenerative diseases and has particular low toxicity in other neural cell cultures (Prusevich et al., 2014). In addition, SP2509 with working concentration of 1 µM, as this small molecule inhibitor functions distinct from MAO derivates as revealed by a molecular docking simulation (Sorna et al., 2013). Moreover, SP2509 phenocopied the knockdown of LSD1 in zebrafish without causing noticeable side effects.

Upon inhibition with bizine, clear tendencies to reduced MBP protein levels and myelin-specific transcript levels could be shown by immunoblot analysis (**Figure 23** A) and quantitative real-time polymerase chain reaction (qRT-PCR) (**Figure 23** B).

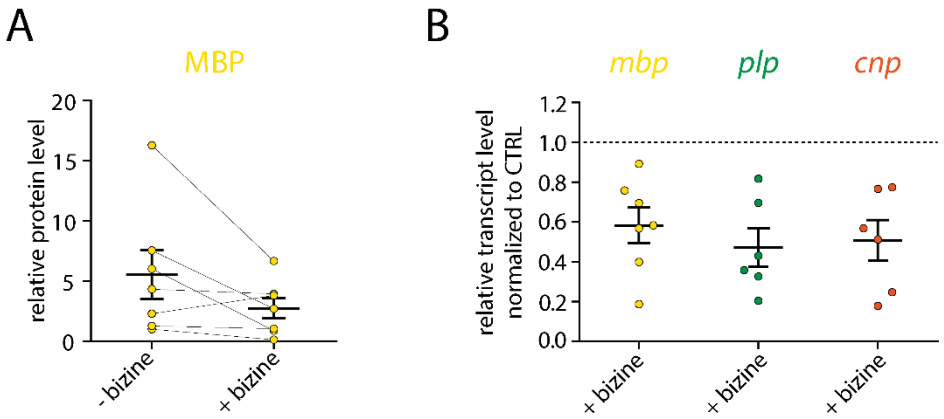

Figure 23 | Pharmacological inhibition with bizine reduced myelin-specific transcript and protein levels

A2B5+ OPCs were exposed to 10 µM bizine for 24 h under proliferating conditions, before induction of differentiation in the presence of bizine. (A) Densitometric analysis of immunoblots against MBP in lysates 5 days after induction of differentiation. Values are normalized to actin. Dots connected with a straight line indicate linked values within one experiment. (B) qRT-PCR analysis of myelin-specific transcript levels after 3 days of differentiation. Values are normalized to GAPDH and to the control (CTRL). Each dot represents an independent isolation. Values shown with mean ± SEM.

In addition, bizine reduced the relative number of mature OLs by about 50 % while a clear tendency to an increase in the relative number of NG2+ progenitors became evident (**Figure 24**).

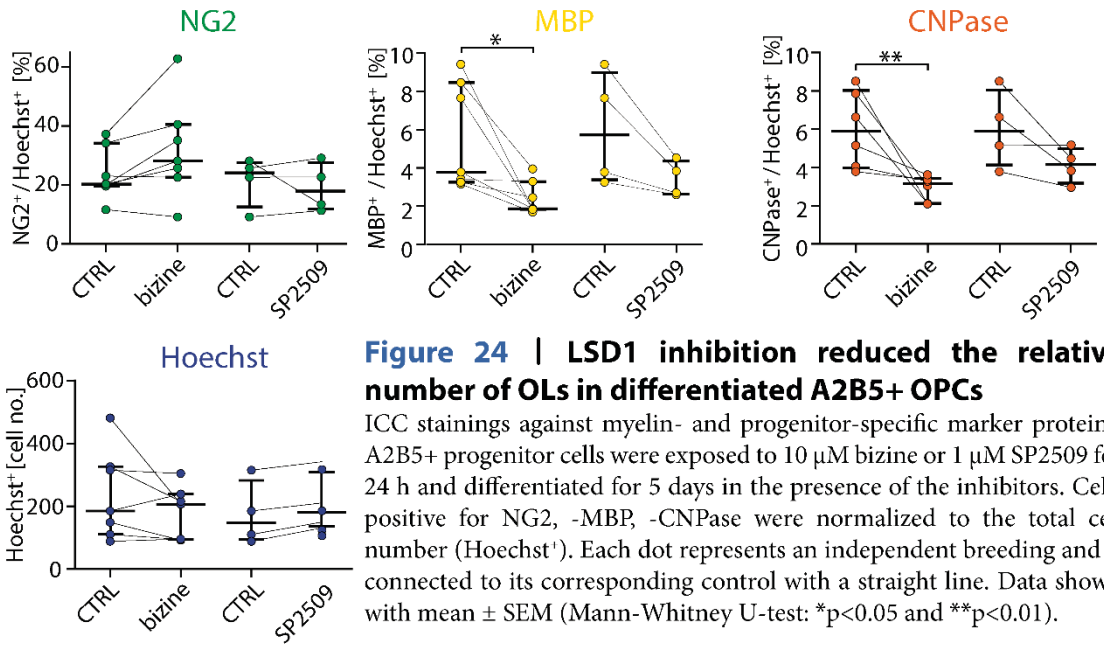

Figure 24 | LSD1 inhibition reduced the relative number of OLs in differentiated A2B5+ OPCs

ICC stainings against myelin- and progenitor-specific marker proteins. A2B5+ progenitor cells were exposed to 10 µM bizine or 1 µM SP2509 for 24 h and differentiated for 5 days in the presence of the inhibitors. Cells positive for NG2, -MBP, -CNPase were normalized to the total cell number (Hoechst⁺). Each dot represents an independent breeding and is connected to its corresponding control with a straight line. Data shown with mean ± SEM (Mann-Whitney U-test: *p<0.05 and **p<0.01).

A clear tendency to a reduced number of OLs could be confirmed using SP2509, but more replicate would have been necessary for final confirmation. Thus, by employing two different pharmacological inhibitors, the observed effects from the experiments of the shRNA induction could be corroborated.

3.1.2.2 Establishment of OSC to study myelination *ex vivo*

Cerebellar OSCs offer a powerful tool to study differentiation of OPCs in an environment closer to the *in vivo* situation. When isolated from postnatal staged mice, neurons e.g. purkinje cells are fully developed and the cerebellum is invaded by OPCs that are about to differentiate. Differentiation and myelination take place with high spatial and temporal precision *in vivo*. *Ex vivo*, in OSCs, the timing can be different and needs to be defined for the given cultivation conditions. Horse serum is frequently used in OSC experiments within the first 3 days as it provides a cocktail of grow factors beneficial for cell survival. However, its composition is not well defined and adds an unpredictable factor to the experiment. To establish ideal cultivation conditions and to define the timeframe of analysis, OSCs were prepared from a *Tg(plp:EGFP)* reporter mice (Sobottka et al., 2011). The *Tg(plp:EGFP)* reporter mouse allows real-time analysis of myelination and circumvents the problem of postfixation analysis. No difference in the kinetics and extent of myelination could be observed when OSCs were kept in serum containing medium compared to a previously described serum-free formulation for postnatal

hippocampal slice cultures (Neurobasal-A™, B-27™ Supplement, 2mM GlutaMAX™, 0.5% glucose; **Figure 25**) (Liu et al., 2017).

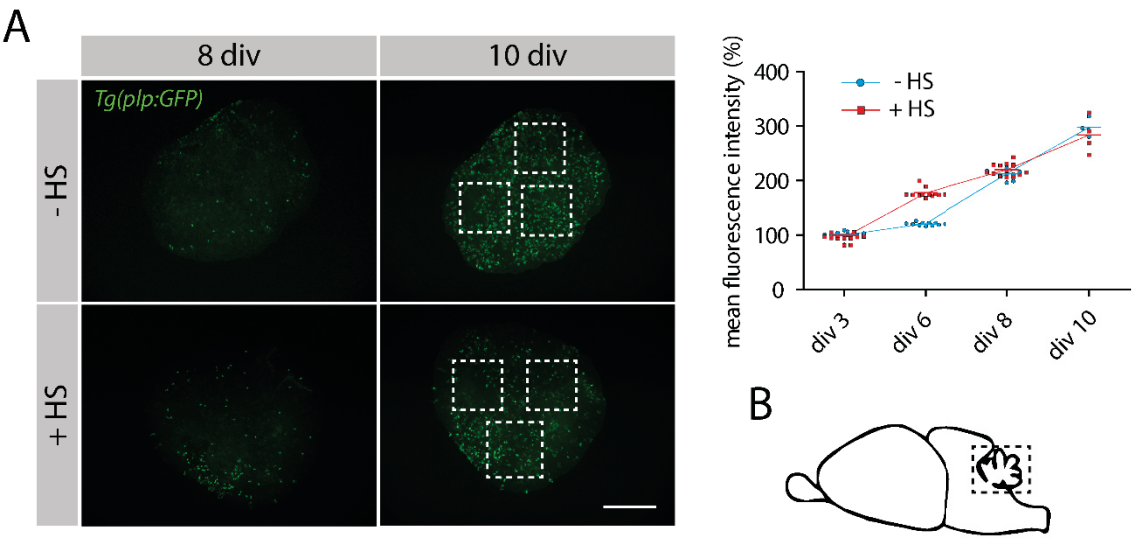

Figure 25 | Establishment of serum-free culturing conditions for cerebellar OSCs

Slices were obtained from postnatal day 4 *Tg(plp:GFP)* mice. For comparison, two adjacent slices were either maintained under serum free (-HS) or serum containing (+HS) conditions. (A, left) Representative images of myelinating slices. Squares with dashed lines, exemplarily shown for 10 div, mark the area considered for quantification. (A, right) Mean fluorescence intensity was quantified with `Fiji Is Just ImageJ´ and normalized to the mean fluorescence intensity of 3 div slices. Each dot represents a separate slice obtained from 3 independent breedings. Scale bar represents 1 mm. (B) Schematic illustration of the cerebellum. Cultures were prepared from 350 µM sagittal slices.

By day 7 *in vitro* (div) a considerable EGFP signal has been observed. Prolonged cultivation leads to excessive production of mature OLs which renders quantification in a 3-dimensional system difficult and error prone. Since bizine reflected the phenotype of the shRNA in the cell culture experiments, it was again used as a tool to modulate LSD1 activity in OSCs. When applied in the same concentration that has been used in cell culture experiments, bizine did not exert any toxicity as suggested by propidium iodide (PI) stainings (**Figure 26**).

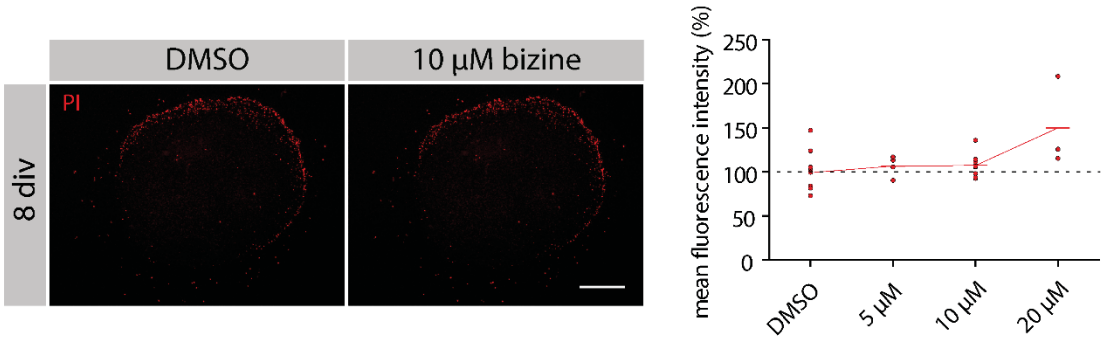

Figure 26 | Bizine showed no toxicity in cerebellar slice cultures

Two adjacent slices obtained from postnatal day 4 wildtype mice were treated with the indicated bizine concentrations or DMSO, respectively. (Left) Representative images of OSCs kept for 8 div in the presence of bizine or DMSO. Scale bar represents 1 mm. (Right) Quantification of mean fluorescence intensity triggered by PI/DNA intercalation in OSCs 8 div. Fluorescence intensity was quantified with `Fiji Is Just ImageJ´ and normalized to slices treated with DMSO. Each dot represents a separate slice obtained from 3 independent breedings.

3.1.2.3 LSD1 activity is necessary for OL differentiation in OSCs

After having established the OSC model to study OPC differentiation *ex vivo*, 2 adjacent slices were treated with bizine and DMSO, respectively. Immunoblot analysis of a pooled fraction of 6 slices already suggested that the development of OLs was impaired upon treatment with bizine within a single experiment (**Figure 27** C). Next, the number of differentiated OLs was determined by counting MBP+/OLIG2+ cells within 4 fields of views and normalized to the number of OLIG2+ cells (**Figure 27** B & D, OLs). To determine the absolute number of undifferentiated OPCs, OLIG2+/MBP- cells were counted (**Figure 27** D, OPCs). The experiments in OSCs confirmed the previous observations: the relative number of OLs was reduced by 45 % while clear tendencies to an enriched OPC pool were obvious.

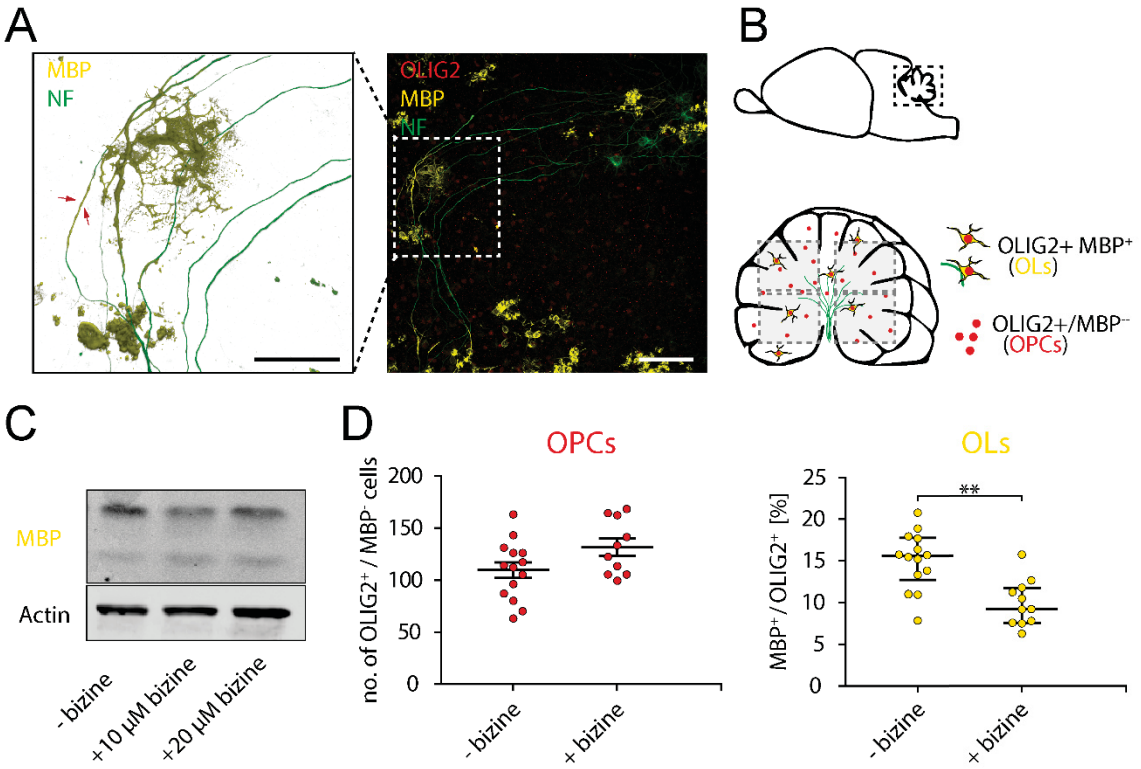

Figure 27 | Pharmalogical inhibition of LSD1 impaired OL differentiation in OSCs

For each experiment 2 adjacent slices of postnatal day 3 mice were separated, treated either with 10 µM bizine or DMSO for 7 div. (A) Representative confocal images of maximum intensity z-projections. Scale bars represent 100 µm. Red arrows (left) depict myelinated axons, indicating that functional myelination proceeds *ex vivo* in OSCs. (B) Positive cells were counted within 4 fields of view. MBP+/ OLIG2+ cells were considered as OLs and OLIG2+/MBP- cells as OPCs. (C) Immunoblot of MBP with 2 different concentrations of bizine (n=1). (D) Quantification of positive cells. Each dot represents a separate slice obtained from an individual pup out of 4 independent breedings shown with mean and ±SEM (Mann-Whitney U-test: **p<0.01; n=11-14)

3.1.2.4 The zinc finger protein ZFP516 recruits LSD1 during differentiation

LSD1 itself cannot bind to DNA. Thus, it depends on co-regulators that guide LSD1 to its targets genes. In order to identify and define regulatory complexes in proliferating OPCs and after initiation of differentiation, a co-immunoprecipitation (co-IP) of endogenous LSD1 with subsequent mass spectrometry analysis was performed. Toward this goal, LSD1 complexes were enriched from proliferating OPCs and OPCs subjected to differentiating stimuli for 24 h. A multitude of proteins were significantly enriched over the immunoglobulin G (IgG) control in both conditions (**Appendix**, Table 13-15). Proteins that are directly or indirectly involved in transcriptional regulation according their Gene Ontology term (GO-term) are shown here (**Figure 28** A, dark grey and red dots). From co-IP experiments it is not possible distinguish between direct or indirect interaction.

Furthermore, individual complexes cannot be distinguished from each other. Thus, it seemed reasonable to consider only those interacting partners for further discussion that have been previously identified by thorough biochemical characterization in neural and non-neural cells (**Figure 28** A, red dots). Although these information stem from other tissues and cells, it provides a rational basis to speculate about the particular compositions of LSD1 complexes here.

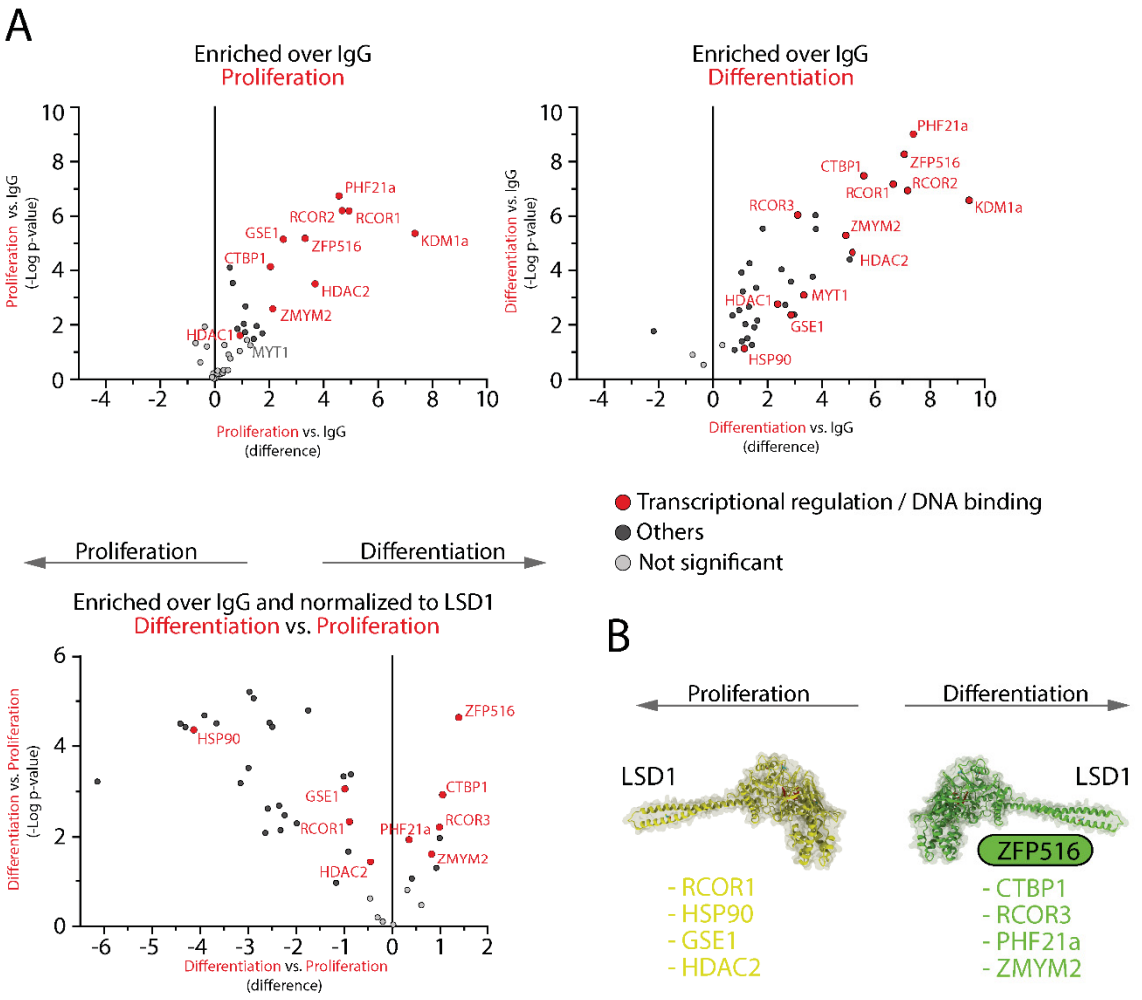

Figure 28 | LSD1 is recruited by ZFP516 in A2B5+ OPCs upon initiation of differentiation

LSD1 containing complexes were enriched by co-IP from endogenous LSD1 in proliferating A2B5+ OPCs or A2B5+ OPCs subjected differentiation stimuli for 24 h. (A) Mass spectometry analysis of enriched proteins under proliferating (top, left) or differentiating conditions (top, right; n=5). Shown are interacting proteins involved in transcriptional regulation according to GO term molecular function clustering. LSD1 interacting factors that have been previously described with experimental evidence are shown in red with protein name. Differentially bound proteins are shown (bottom, left). (B) Schematic illustration of factors that are specifically enriched under proliferating or differentiating conditions. The most highly enriched protein (ZFP516) is highlighted in green (PDB entry: 2H94)

The spectrum of interacting proteins under proliferating and differentiating conditions was similar at first glance. RCOR3, the molecular chaperon HSP90 and the myelin transcription factor 1 (MYT1) were identified solely upon induction of differentiation.

The overall aim was to identify differences in the binding of proteins. However, differences were not obvious here. A reasonably workaround strategy was to calculate the differences of enrichment between both conditions (**Figure 28** A - red dots; bottom). This approach unraveled whether components were recruited or were about to dissociate from LSD1 upon induction of differentiation. In this regard, a considerable enrichment of the zinc finger protein 516 (ZFP516) became evident. This observation led to the assumption that ZFP516 is an essential co-regulator for LSD1 during OL lineage commitment. Two independent studies point to the functional relevance of LSD1/ZFP516 interaction. During brown adipogenesis, ZFP516 is recruited together with LSD1to the promoter of the uncoupling protein 1 to erase the repressive H3K9 mark and promote development of brown fat cells *in vitro* and *in vivo* (Sambeat et al., 2016). In human breast cancer, ZFP516 recruits the repressive C-terminal-binding protein 1 (CTBP1)/LSD1 complex to the promotor of the epidermal growth factor receptor (EGFR), to erase the activating H3K4 mark (Li et al., 2017). Of note, CTBP1 was found to be differentially enriched as well.

To summarize the findings, the global knockdown of LSD1 in the developing zebrafish impaired OL differentiation. In primary cells and OSC experiments, it could be shown that OLs fail to differentiate and OPCs are arrested in the progenitor state. The analysis of the LSD1 interactome revealed that LSD1 exerts at least in part its function as a transcriptional regulator by engaging with the co-regulators CTBP1 and ZFP516.

3.2 LSD1 and its potential role in redox signaling

LSD1 produces H_2O_2 as a by-product of the demethylation reaction. The fate of H_2O_2 is largely unexplored and could potentially serve as a second messenger in redox signaling.

3.2.1 Pharmacological inhibition with bizine stabilizes the COREST/HDAC complex

As outlined in the introduction part (chapter 1.2.1), there are two ways how LSD1 could oxidize a target protein. Either directly or by a peroxiredoxin-dependent redox relay. In both cases, it can be assumed that transient or stable interaction with the redox target is necessary. The oxidized target can in theory either remain in contact with LSD1 or becomes released upon oxidation in the following termed as `oxidation and release´ mechanism. Thus, binding patterns or the redox state of binding partners are expected to change upon inhibition. To address this hypothesis, an enrichment of LSD1 interacting proteins in dependence of its activity appeared to be a reasonable approach. To provide information about the redox state of the interacting proteins an alkylation step would be necessary to irreversibly block reduced thiols and prevent unwanted oxidation upon cell lysis. As this step may cause detrimental effects during immunoaffinity purification, a redox-sensitive co-IP was established here. In brief, native lysates were prepared in the presence of N-ethylmaleimide (NEM) to block all reduced thiols. Purified lysates were subjected to co-IPs with two different commercially available antibodies. The co-IP efficiency was assessed by silver gel staining and revealed that NEM reduces the efficiency of the co-IP but still allows enrichment to a considerable extent (**Figure 29** B).

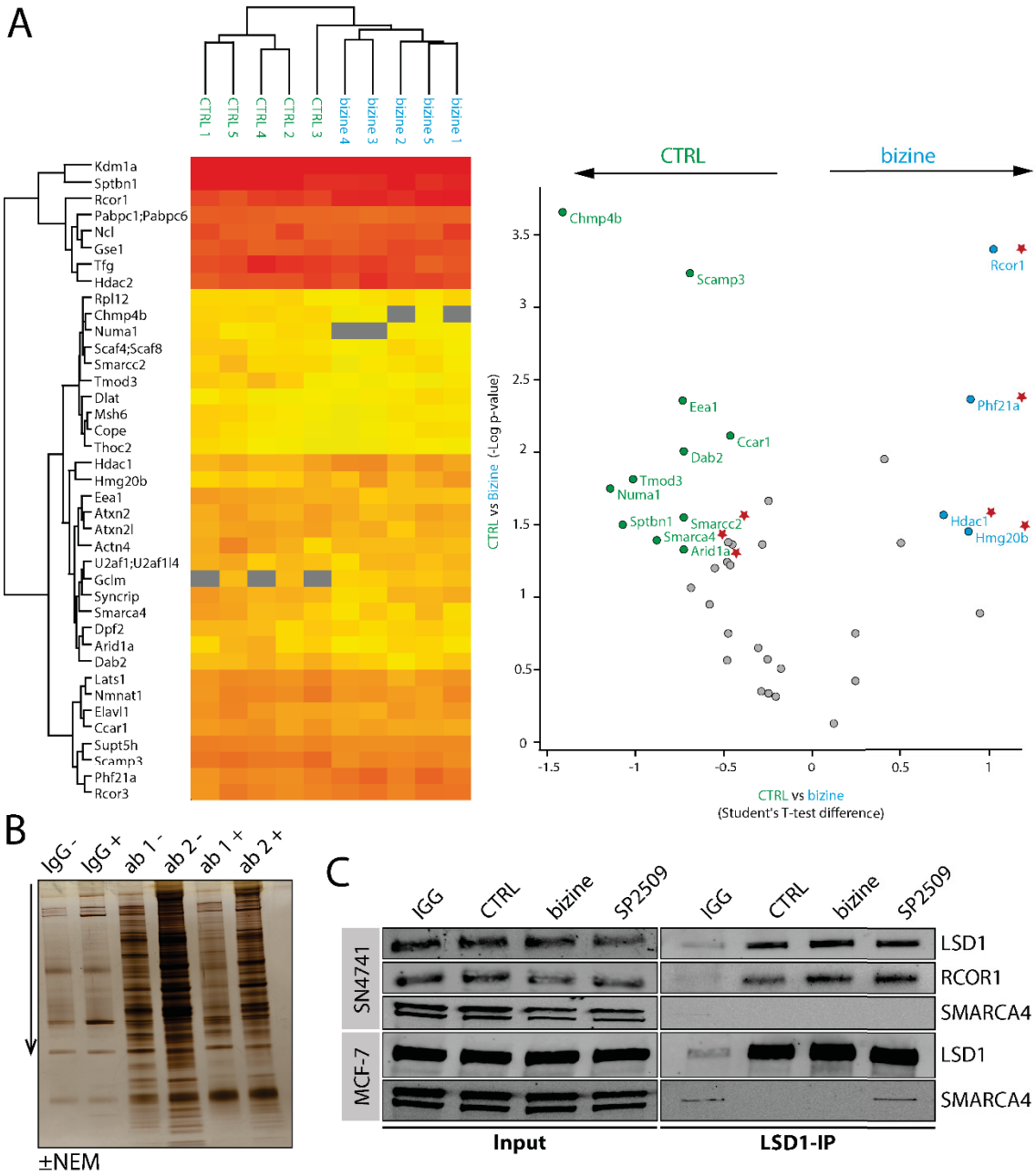

Figure 29 | LSD1 changed its interactome in an activity-dependent manner

(A) Mass spectometry analysis of co-immunoprecipitated LSD1 interacting proteins in SN4741 (n=5). SN4741 cells were treated with 15 µM bizine (bizine) or DMSO (CTRL) for 24 h. Cells were washed with 100 mM NEM in PBS and lysed in native lysis buffer containing 100 mM NEM. Lysates were purified by size-exclusion chromatography to remove excessive NEM and subsequently subjected to co-IP overnight. Heat map (left) shows significant enrichment over IgG control samples. Volcano plot (right) shows differentiatlly enriched proteins normalized to LSD1 (unpaired Student´s t-test; *p<0.05). Red asterisks depict LSD1 interacting partners that potentially reside within one complex. (B) Silver gel analysis of co-IPs with two different commercial antibodies (ab 1: Cell Signaling; ab 2: Abcam) against endogenous LSD1 in the presence or absence of 100 mM N-ethylmaleimide (±NEM). Ab 2 was used for the main experiment. (C) Immunoblot analysis of co-immunoprecipitated proteins from SN4741 and MCF-7 cells treated with 15 µM bizine and 1 µM SP2509 for 24 h, respectively.

For the main experiment, a substantia nigra derived mouse neuronal progenitor cell line (SN4741) was treated with or without 10 µM bizine for 24 h. SN4741 cells

acquired early characteristics of dopaminergic neurons and are immortalized by SV40 large T antigen insertion (Son et al., 1999). To distinguish between oxidized and reduced thiols during mass spectrometry analysis, co-IP eluates were reduced with DTT and subsequently alkylated with iodacetamide leading to carbamidomethylation of previously oxidized thiols. Due to their characteristic mass shift, both alkylation agents (NEM and iodacetamid) can be easily distinguished by mass spectrometry.

The co-IP revealed that LSD1 associates with SMARCA4, SMARCC2 and ARID1a. These are components of SWI/SNF chromatin remodeler complexes, whose interaction has not been described so far (**Figure 29** A, **Appendix** Table 18). Treatment with bizine attenuated these interactions and favored the engagement with components of the COREST repressor complex, which includes HDAC1, PHF21a, HMGB20b and RCOR1. This observation indicates that the complex assembly and disassembly is driven by the LSD1 activity. Immunoblot analysis of the co-IP eluate could not conclusively corroborate the finding that bizine-dependent inhibition stabilizes the interaction with RCOR1, as it was not obviously more enriched in the elution fraction (**Figure 29** C). Treatment with SP2509 did not corroborate the effect as well. In addition, the interaction of LSD1 with SMARCA4 could not be validated by immunoblot analysis at all. Usually overexpression of tagged protein variants is employed to efficiently enrich proteins for the identification of novel interaction partners. To circumvent artificial overexpression, the co-IP was again performed in a breast cancer cell line that endogenously overexpresses LSD1. In MCF-7 cells, SMARCA4 was slightly enriched in the SP2509 treated samples and in the IgG control but surprisingly not in the untreated, nor in the bizine treated cells. Although it could not be clearly shown by immunoblot analysis, inhibition of LSD1 undisputable resulted in a change of the interactome. Higher doses of bizine could help to demonstrate the stabilization of the COREST complex upon inhibition more clearly. To test if any protein bound to LSD1, is differentially oxidized, the interactome in both treated and untreated samples was screened for redox modifications. No NEM-labeled or iodacetamide-labeled peptides were enriched to a considerable amount as such quantification by mass spectometry would have been possible. This suggests that co-IPs from endogenous proteins are not a suitable approach to investigate this hypothesis.

3.2.2 LSD1 oxidizes itself and presumably forms an activity dependent oligomer

Probably because the enrichment of LSD1 was most prominent, several cysteines with oxidative modifications could reliable be identified with a considerable intensity on LSD1 itself. It could be shown that cysteine 491 (C491), C600, C618, C623 and C665 were oxidized in the untreated samples (**Figure 30** A & C). Treatment with bizine significantly reduced the oxidation of these cysteines indicating that LSD1 acts as a redox sensor probably controlled by its own activity. Indeed, it has been previously suggested that C600 can form an oxidation dependent intramolecular disulfide bridge with C618 (Ricq et al., 2016). The formation of the C600-C618 disulfide bridge reversibly inhibits the demethylase activity.

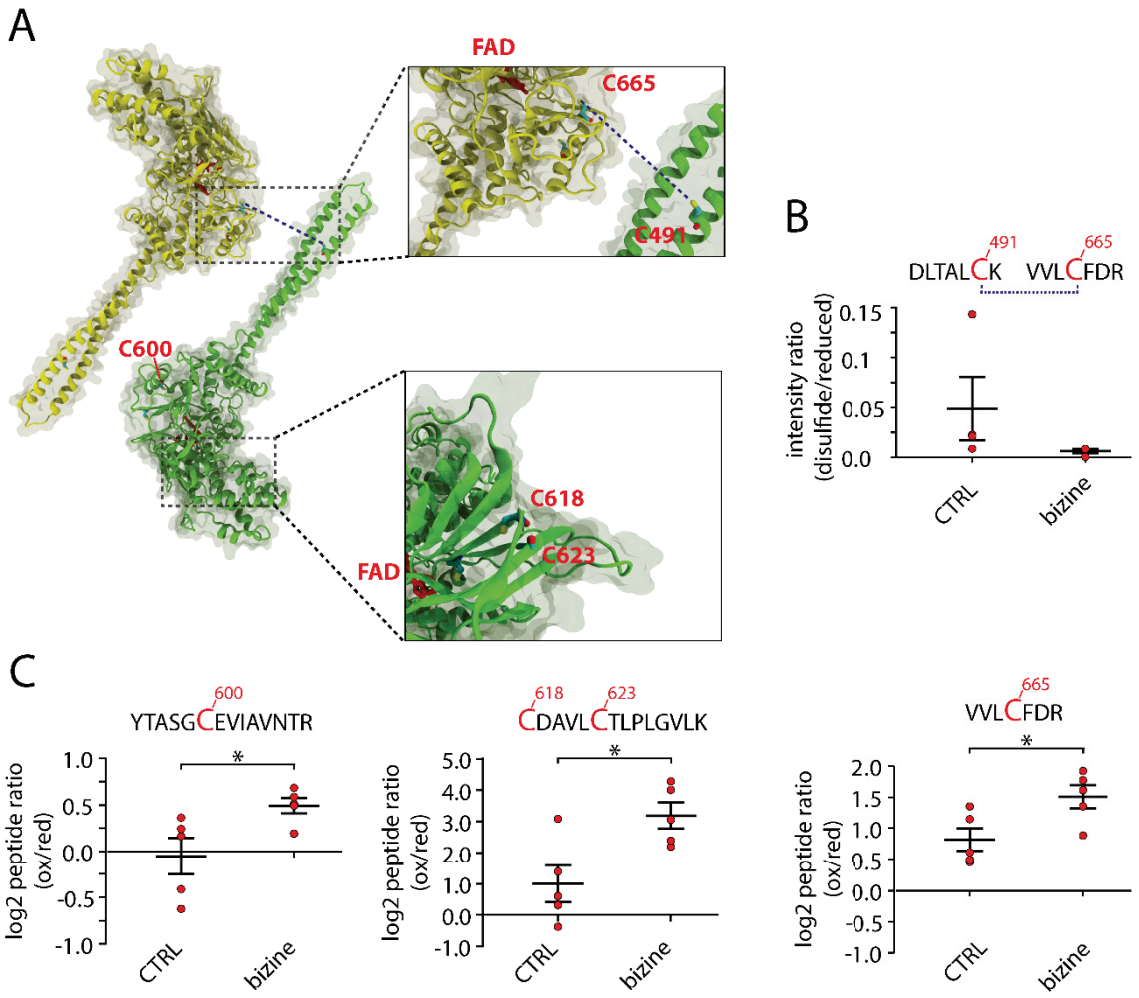

Figure 30 | Mass spectrometry analysis identified oxidized LSD1 peptides and a disulfide linkage in SN4741 cells

Endogenous LSD1 was enriched from NEM-alkylated SN4741 lysates by immunoprecipitation and subjected to mass spectometry analysis (CTRL vs. bizine). (A) Crystal structures depicting oxidized thiols, disulfide linkages, the flavin (FAD) and the hypothesized LSD1 homodimer. (B) Intensity ratios of the detected disulfide peptide (indicated above) and the NEM-alkylated VVLC(665)FDR peptide (reduced). Statistical significance was not calculated as only 4 replicates could be considered for quantification. (C) Log 2 of ratios of peak intensities of carbamidomethylated thiols (oxidized; ox) to NEM-alkylated thiols (reduced; red). Identified peptides indicated above. Each dot represents an independent biological and technical replicate (n=5). Statistical significance was determined by an unpaired t-test, shown with mean ±SEM (*p<0.05).

Mass spectrometry analysis proposed that C665-C491 form a disulfide bridge (**Figure 30** B). The formation of an intramolecular C665-C491 bridge appears to be highly unlikely due to the long distance. Inevitably, this leads to the assumption that LSD1 could form a dimer or oligomer, stabilized at least in part via an intermolecular C665-C491 disulfide bridge (**Figure 30** A).

Attempts to confirm the dimeric form by immunoblot analysis failed even with the addition of exogenous H_2O_2 in both, SN4741 and MCF-7 cells (**Figure 31**, left).

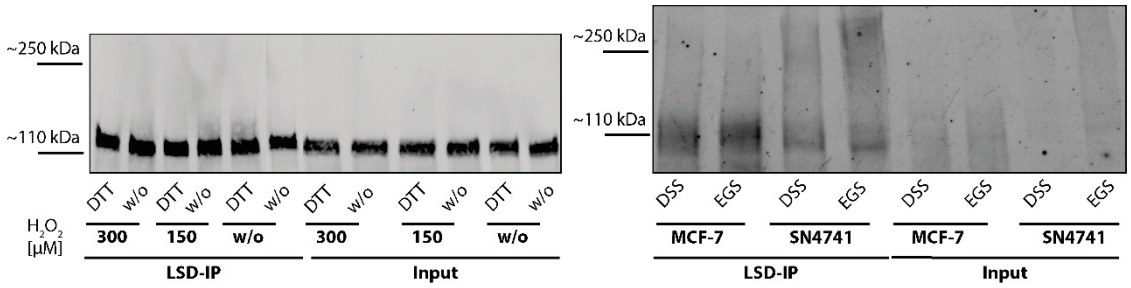

Figure 31 | Immunoblot analysis of LSD1 immunoprecipitated after chemical cross-linking and H_2O_2 incubation

SN4741 cells were incubated with indicated concentrations of H_2O_2 prior to LSD1 immunoprecipitation. Eluates were separated by SDS-PAGE and analyzed by immunoblot (left, n=1). Untreated MCF-7 and SN4741 cells were subjected to chemical crosslinking with EGS and DSS. Subsequently, LSD1 was immunoprecipitated and analyzed by immunoblot (right, n=1).

Disuccinimidyl suberate (DSS) and ethylene glycol bis(succinimidyl succinate) (EGS) are amine-reactive cell permeable crosslinker used to stabilized labile and transient protein interactions in living cells. To stabilize a putative LSD1 homodimer or any oligomeric form, MCF-7 and SN4741 cells were crosslinked with EGS and DSS. Crosslinked lysates were purified and LSD1 subsequently enriched by immunoaffinity purification. Again, no evidence for the existence of a dimer could be provided (**Figure 31**, right). Thus, vigorous attempts to proof the existence of a LSD1 dimer or an oligomeric structure failed with the experimental approach chosen here (e.g. denaturing conditions). In summary, inhibition with bizine changes the pattern of interacting proteins. This observation is accompanied with oxidative modifications of LSD1 which in part have been described to inhibit its own activity and might lead to structural changes as suggested by the data provided here (Ricq et al., 2016). Whether LSD1 regulates the redox state of its binding partners remains elusive from the co-IP.

Based to the present analysis, LSD1 mainly persists in its oxidized form in SN4741. This raises issues regarding the activity level of LSD1 in this particular cell line, as oxidation of C600 and C618 abolishes LSD1 activity. Due to this uncertainty, further studies were carried out only in the human estrogen responsive MCF-7 breast cancer cell line. In MCF-7 cells, LSD1 activity and H_2O_2 production is necessary to drive the expression of estrogen responsive genes (Perillo et al., 2008). Furthermore, LSD1 is overexpressed in breast cancer cells which could in theory increase the probability to detect redox targets.

3.2.3 LSD1 elicited global changes in the cellular redoxome

Considering the findings obtained from the co-IP, it seemed reasonable to choose an unbiased experimental approach that is independent of LSD1 interaction. This allowed also employing a knockout strategy for the following investigation. To knockout LSD1, MCF-7 cells were electroporated with a *kdm1a* specific small interfering RNA (siRNA). Knockout efficiency was confirmed by immunoblot analysis and appeared to be sufficient by day 3 (**Figure 32**).

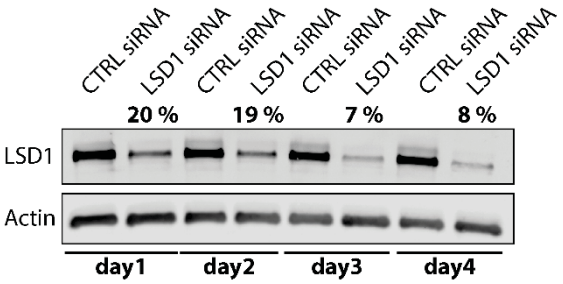

Figure 32 | LSD1 was efficiently knocked out in MCF-7 cells
The electroporation of MCF-7 was optimized and seemed to be most efficient at 190 V, 500 Ω and 1000 µF. Immunoblot analysis of LSD1 protein level over a period of 4 days (n=1). Remaining LSD1 protein level are estimated by densitometric analysis, normalized to actin and to the CTRL siRNA.

Bizine and SP2509 treatments were chosen as additional conditions for several reasons. The application of pharmacological inhibitors allows for the detection of early time points. Due to their high affinity, inhibition of LSD1 activity by small chemical compounds starts abruptly and mainly depends on their specific uptake kinetics. In case of bizine, robust inhibition is achieved after 6 h (Prusevich et al., 2014). The knockout on the other hand, only continuously lowers LSD1 protein level. Since LSD1 is overexpressed in MCF-7 cells, it could potentially elicit global changes in the redoxome. To follow this hypothesis, thiols were irreversibly alkylated with NEM followed by the treatment with DTT to reduce oxidized cysteine side chains. Previously oxidized cysteines were then labeled with the thiol reactive Cyanin-5-maleimid (CY5-M) and the lysates subsequently subjected to sodium dodecyl sulfate polyacrylamide gel electrophoresis (SDS PAGE). The intensity of the in-gel fluorescence emitted by CY5-M is proportional to the extent of protein oxidation. Treatment with bizine and SP2509 reduce the fluorescence signal after 5 h, 24 h and 48 h treatment indicating massive effects on the redoxome (**Figure 33**).

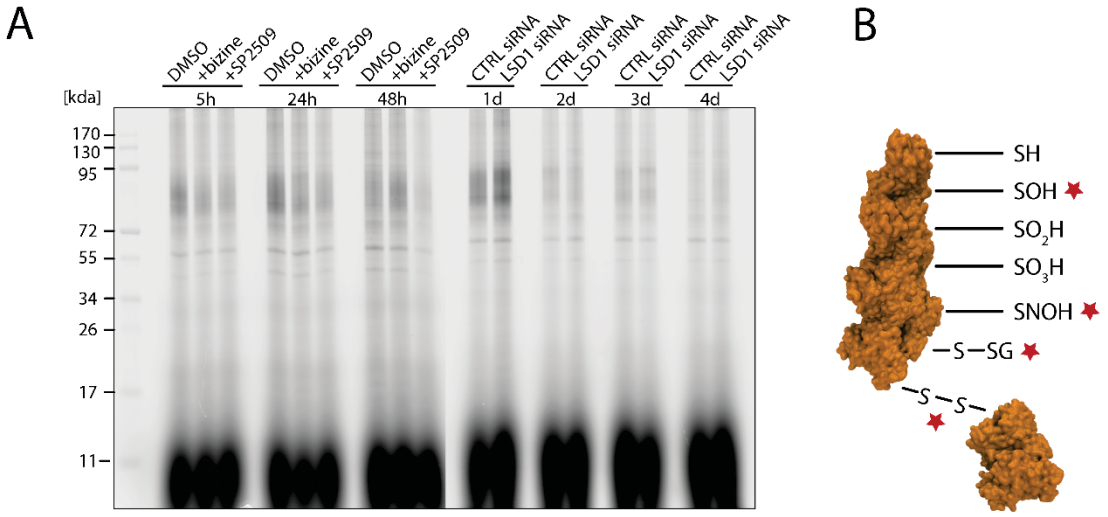

Figure 33 | Knockout or inhibition of LSD1 reduced the level of oxidized cysteines
MCF-7 cells were treated with 15 µM bizine or 1 µM SP2509 for the indicated time or subjected to a LSD1 knockout. Lysates were alkylated with NEM and reduced by DTT. Previously oxidized cysteines were then labeled with Cy5-maleimide (CY5-M). (A) Image of in-gel fluorescence produced by the thiol-reactive CY5-M (n=1). (B) Oxidative cysteine modifications detected by this method are indicated with red asterisks.

With the knockout of LSD1, a reduction of the signal became evident not before day 3. These observations indicated a causative relation between decreased LSD1 protein level or activity and cysteine oxidation.

To further investigate the type of cysteine oxidation, MCF-7 cells were incubated with dimedone. Dimedone is a cell-permeable probe that specifically binds to sulfenic acids *in situ* (Poole et al., 2005). This is of particular interest as sulfenic acids are transient intermediates that appear to be the origin for many redox modifications, e.g. disulfide bond formation. Due to their remarkable reactivity *in situ* labeling is necessary. Intriguingly, the detection of sulfenylated thiols by a dimedone-specific antibody revealed a global reduction starting from 24 h after addition of inhibitors and not before day 3 in the knockout samples (**Figure 34**).

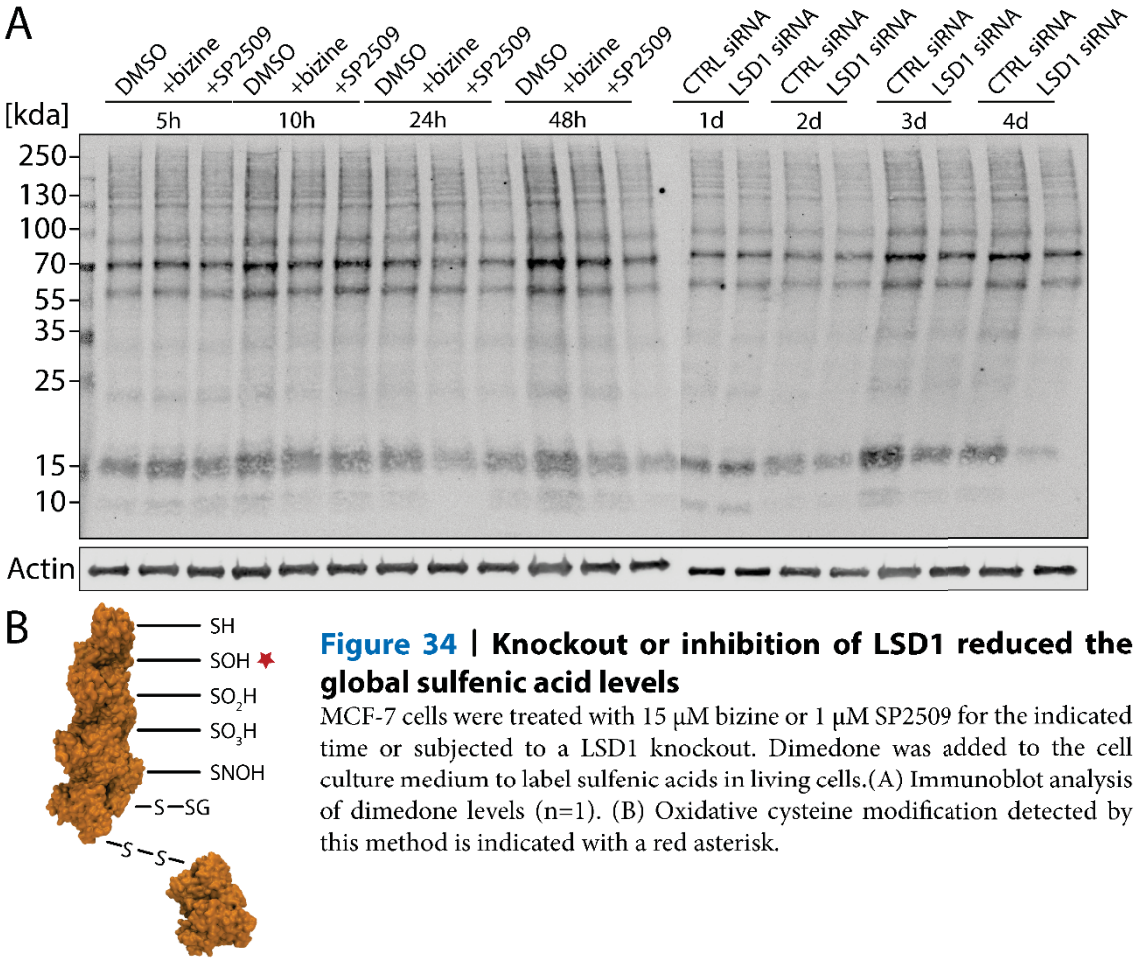

Figure 34 | Knockout or inhibition of LSD1 reduced the global sulfenic acid levels

MCF-7 cells were treated with 15 µM bizine or 1 µM SP2509 for the indicated time or subjected to a LSD1 knockout. Dimedone was added to the cell culture medium to label sulfenic acids in living cells.(A) Immunoblot analysis of dimedone levels (n=1). (B) Oxidative cysteine modification detected by this method is indicated with a red asterisk.

Sulfenic acids are prone to further react with free thiols. Glutathione is highly abundant and contains a free thiol that can readily form a mixed disulfide with sulfenic acids (gluathionylation). Although knockout and inhibition elicited obvious changes on sulfenic acid levels, the glutathionylation pattern of the proteome appear not to be changed to the similar extent as evinced by immunoblot analysis using an antibody against glutathionylated proteins (**Figure 35**).

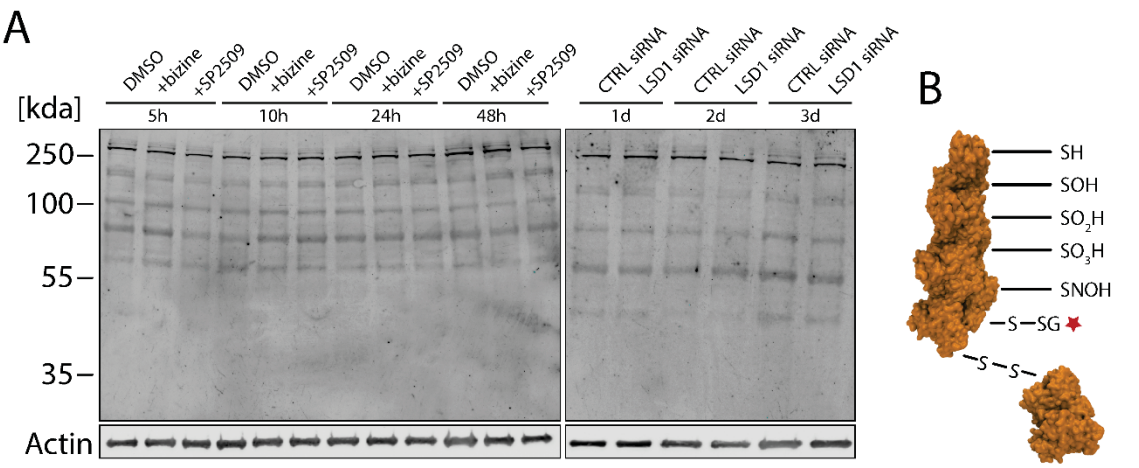

Figure 35 | Glutathionylation levels were not affected upon knockout or inhibition of LSD1 in MCF-7 cells

MCF-7 cells were treated with 15 µM bizine or 1 µM SP2509 for the indicated time or subjected to a LSD1 knockout. All thiols were alkylated with NEM prior to SDS-PAGE. (A) Immunoblot analysis of glutathionylated proteins (n=1). (B) Cysteine redox state detected by this method is indicated with a red asterisk.

3.2.4 LSD1 regulates the redox state of numerous nuclear proteins

As LSD1 knockout and inhibition had widespread effects on the redox state of many proteins, it was reasonable to further elucidate the underlying details. The biotinylated iodoacetamide (BIAM) switch assay coupled to mass spectrometry is a straightforward technique to identify differentially oxidized proteins (Löwe et al., 2019). Compared to co-IPs it offers an untargeted approach to analyse the redoxome over the full cellular proteome. The BIAM switch assay is based on 2 consecutive alkylation steps, followed by immunoaffinity enrichment and subsequent analysis via mass spectrometry (**Figure 36**).

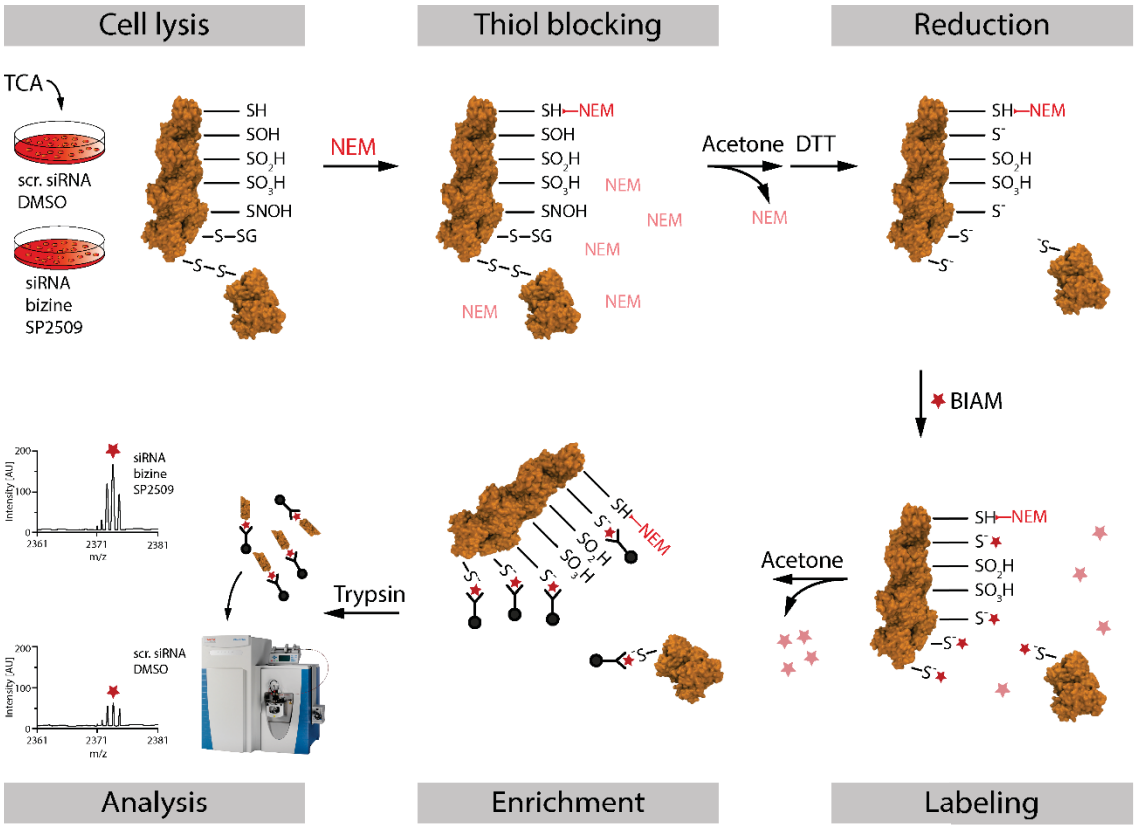

Figure 36 | BIAM switch assay coupled to mass spectometry
Workflow of the biotinylated iodoacetamide - (BIAM) switch assay coupled to mass spectrometry. MCF-7 cells are lysed and proteins precipitated using TCA (Cell lysis). Resolubilization in the presence of NEM blocks all reduced thiols and is followed by acetone precipitation to remove the excess of NEM (Thiol blocking). Subsequently, sulfenic acids, disulfides and nitrosylated thiols are reduced by DTT. These cysteines, formerly oxidized, are then labeled with BIAM (Labeling). Sulfinic and sulfonic acids are not reducible by DTT and will therefore not be labeled with BIAM. All formerly oxidized proteins that were labeled with BIAM can be enriched by affinity purification (Enrichment). After trypsin digestion of the enriched proteins, differentially oxidized targets are identified after mass spectometry analysis based on differences in the intensities (Analysis). Figure adapted from (Löwe et al., 2019).

In brief, proteins are precipitated directly from living cells by trichloroacetic acid (TCA) to preserve their redox signature. Reduced cysteines are then irreversible alkylated by NEM, followed by the complete reduction of the oxidized cysteine pool. All previously oxidized cysteines are now accessible for labeling with BIAM and can be enriched by streptavidin-coupled beads prior to mass spectometry analysis. The degree of enrichment of a target protein is proportional to the extent of oxidation of its cysteine residues. Of note, overoxidized sulfinic and sulfonic acids cannot be reduced by DTT and thus, will not be labeled by BIAM. This has to be considered and will again be addressed in the discussion part. The analyzed datasets contain proteins from all organelles (**Appendix**, Table 19-21). With LSD1 being a nuclear protein, it is feasible to assume that potential redox targets are located in the

nucleus. Still LSD1-derived redox equivalents could in theory be shuttled to the cytosol via peroxiredoxins to achieve inter-organelle target oxidation. However as this can be considered as a rather rare event, it was reasonable to reduce the dataset to the nuclear compartment comprising potential targets with high confidence. Subcellular location of proteins is usually determined based GO-terms and UniProt annotations. These databases, however, do not distinguish between cell types. Thus, the subcellular localization was clustered based on a MCF-7 specific database (Orre et al., 2019). As this database does not further distinguish between ribosomal and nucleoplasm located proteins, all ribosomal proteins were therefore only classified as nuclear when annotated according to UniProt (UniProt: a worldwide hub of protein knowledge, 2019). For all following investigation, only nuclear proteins that were significantly less oxidized were considered. It should still be considered that LSD1 is essential for many cellular functions. Therefore, the list of differently oxidized proteins contains firstly possible LSD1 redox targets and secondly, proteins that change their redox status due to secondary effects. Secondary effects could affect proteins of every compartment and may change the redox state in either direction (more oxidized and less oxidized). Direct oxidation would be expected to occur mainly in the nucleus. Two observations foster the notion that LSD1 indeed oxidizes numerous proteins. First, with 40 % (knockout), 47 % (bizine) and 50 % (SP2509), the majority of proteins that were identified as less oxidized were allocated to the nucleus (**Figure 37** A - red dots; right half of the volcano plots).

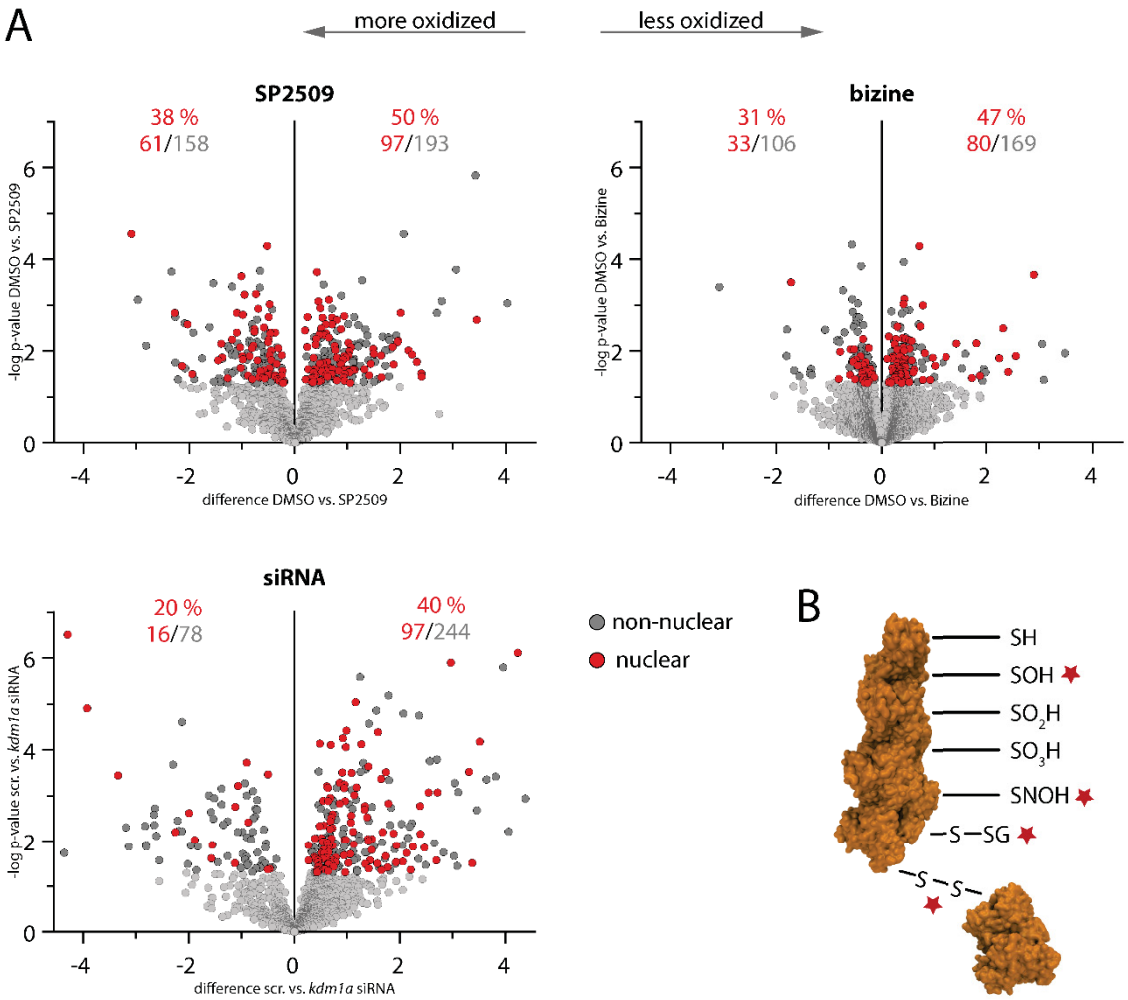

Figure 37 | Mass spectometry-coupled BIAM switch assay identified numerous potential LSD1 redox targets

MCF-7 were treated with 15 µM bizine, 1 µM SP2509 for 24 hours or electroporated with *kdm1a* specific siRNA 3 days before analysis. Whole cell protein was subjected to the BIAM-switch assay and analyzed by mass spectometry. (A) Volcano plots of differentially oxidized proteins. Significant changed proteins are represented as dark grey dots, as red dots when localized in the nucleus and non-significant changed proteins as light grey dots (p-value < 0.05, n=6). Nuclear localization was determined according to uniprot terms and `www.subcellularbarcode.de´ (Orre et al. 2019). (B) Schematic representation of cysteine redox states. Proteins enrichment is proportional to the particular oxidation states marked with red asterisks.

Second, the majority of all proteins that significantly changed their redox state (either more or less oxidized), was less oxidized upon knockout or inhibition (knockout: 86 %; bizine: 70 %; SP2509: 61 %). The comparison of the targets found in all 3 analyses revealed that only 7 % of the SP2509 dependent targets and 13 % of the bizine dependent targets overlap with the knockout.

Clustering of the potential targets to their molecular function using ShineyGO v0.61 Ontology Enrichment Analysis tool revealed that the majority is involved in RNA

processing and metabolism, transcriptional regulation and chromatin remodeling (**Figure 38**) (Ge et al., 2018).

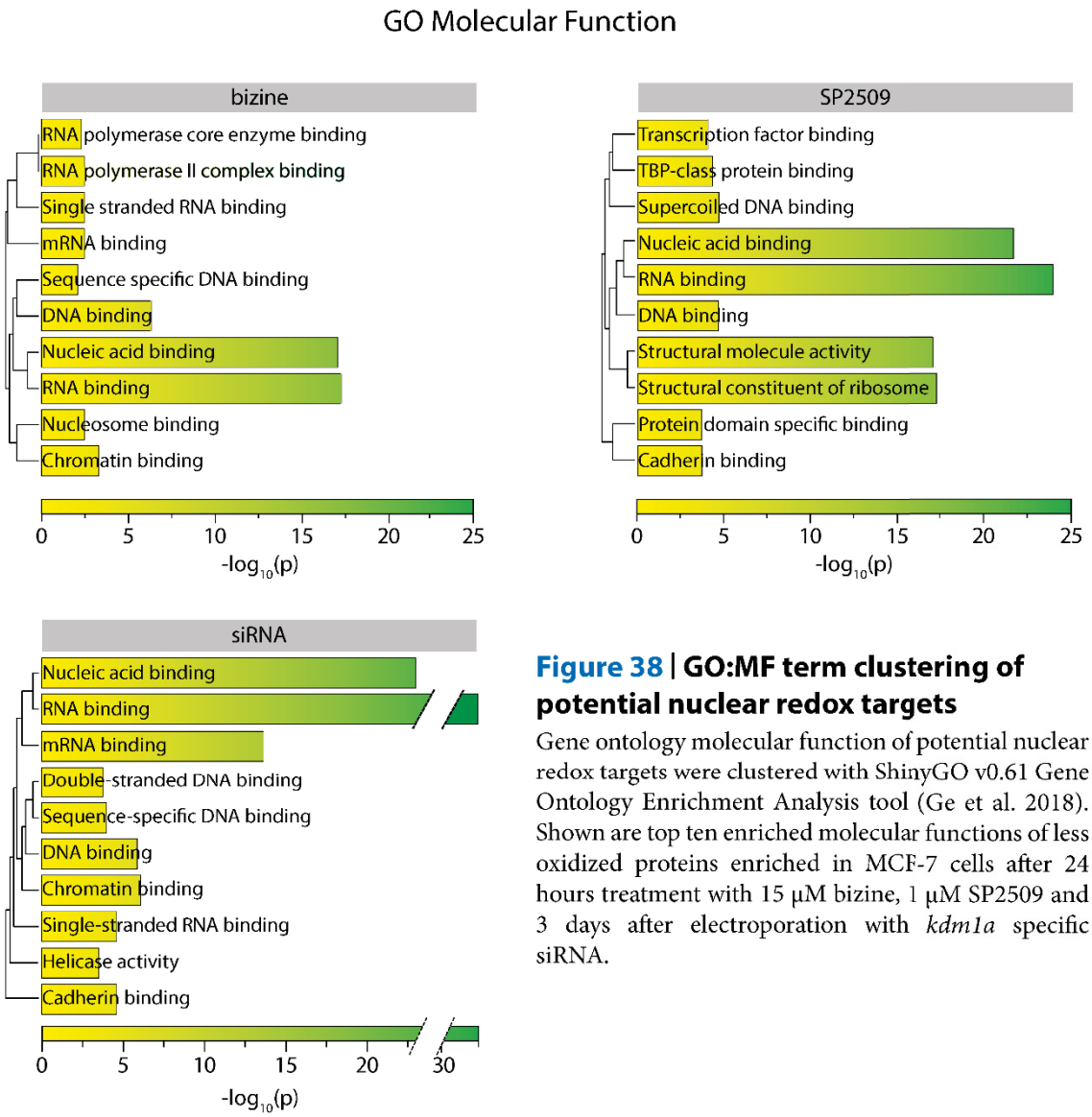

Figure 38 | GO:MF term clustering of potential nuclear redox targets

Gene ontology molecular function of potential nuclear redox targets were clustered with ShinyGO v0.61 Gene Ontology Enrichment Analysis tool (Ge et al. 2018). Shown are top ten enriched molecular functions of less oxidized proteins enriched in MCF-7 cells after 24 hours treatment with 15 µM bizine, 1 µM SP2509 and 3 days after electroporation with *kdm1a* specific siRNA.

This indicates that LSD1 indeed oxidizes its local surrounding and may adopt novel functions in RNA processing by oxidation.

3.2.5 The majority of the redox targets are physically associated

As learnt from the redox co-IP in SN4741, inhibition of LSD1 activity enriches the HDAC1/COREST complex. This indicates that whole complexes could be subjected to LSD1-dependent redox regulation leading to a functional change or disassembly thereof.

To follow this idea, all LSD1 targets were analyzed for their enrichment in complexes. The CORUM database is a manually curated repository of experimentally identified complexes (Giurgiu et al., 2019). Using g:Profiler, the CORUM database was searched for significant enrichment in known protein complexes (Raudvere et al., 2019). Intriguingly, many targets clustered in experimentally verified complexes. Thus, LSD1 could indeed be responsible for regulating complex integrity and function through the oxidation of several complex components (**Figure 39**).

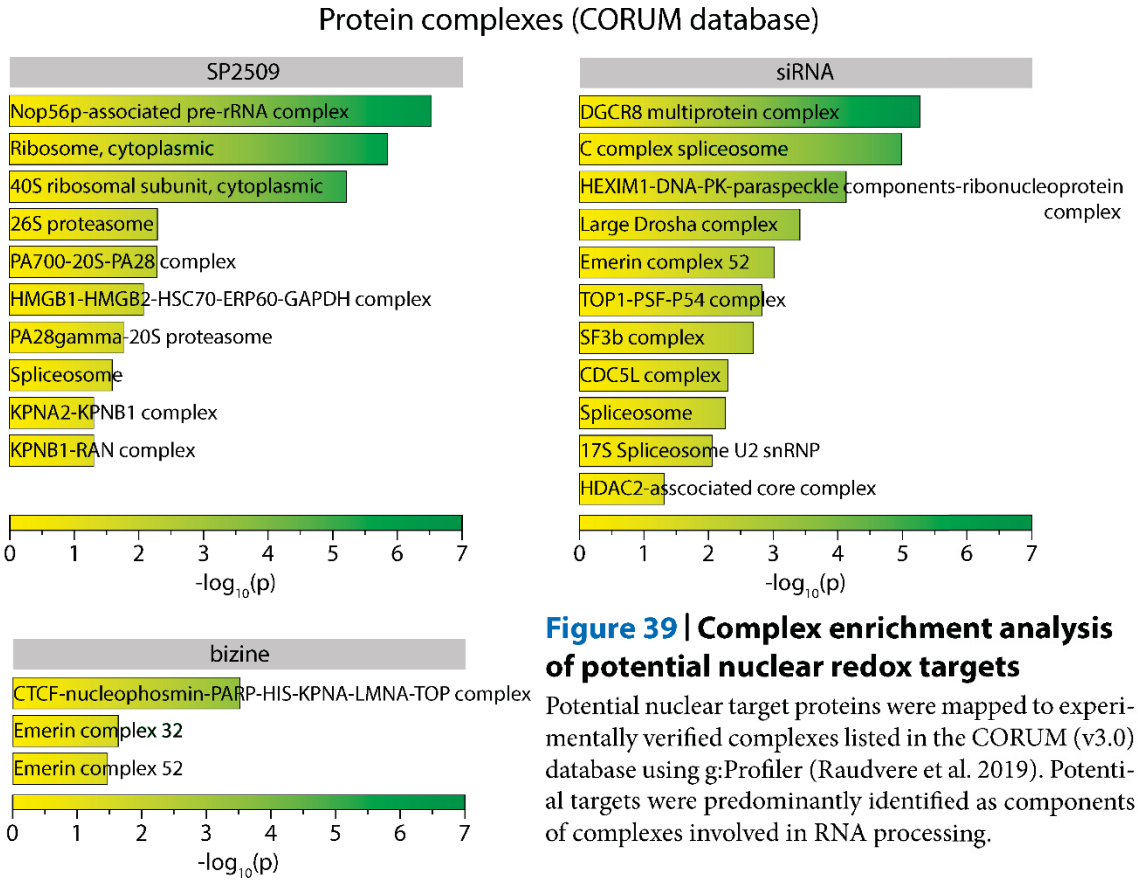

Figure 39 | Complex enrichment analysis of potential nuclear redox targets

Potential nuclear target proteins were mapped to experimentally verified complexes listed in the CORUM (v3.0) database using g:Profiler (Raudvere et al. 2019). Potential targets were predominantly identified as components of complexes involved in RNA processing.

To provide a global view of interaction, targets obtained after knockout were queried from the STRING protein database using high confidence (0.7) settings, experimental evidence and databases (Szklarczyk et al., 2015).

The retrieved interactome was visualized using Cytoscape and again clustered according to their go terms using the ClusterONE add-on 1.0 (Shannon et al., 2003; Nepusz et al., 2012). The global perspective provided here, illustrates that the majority of targets are functionally and physically connected (**Figure 40**).

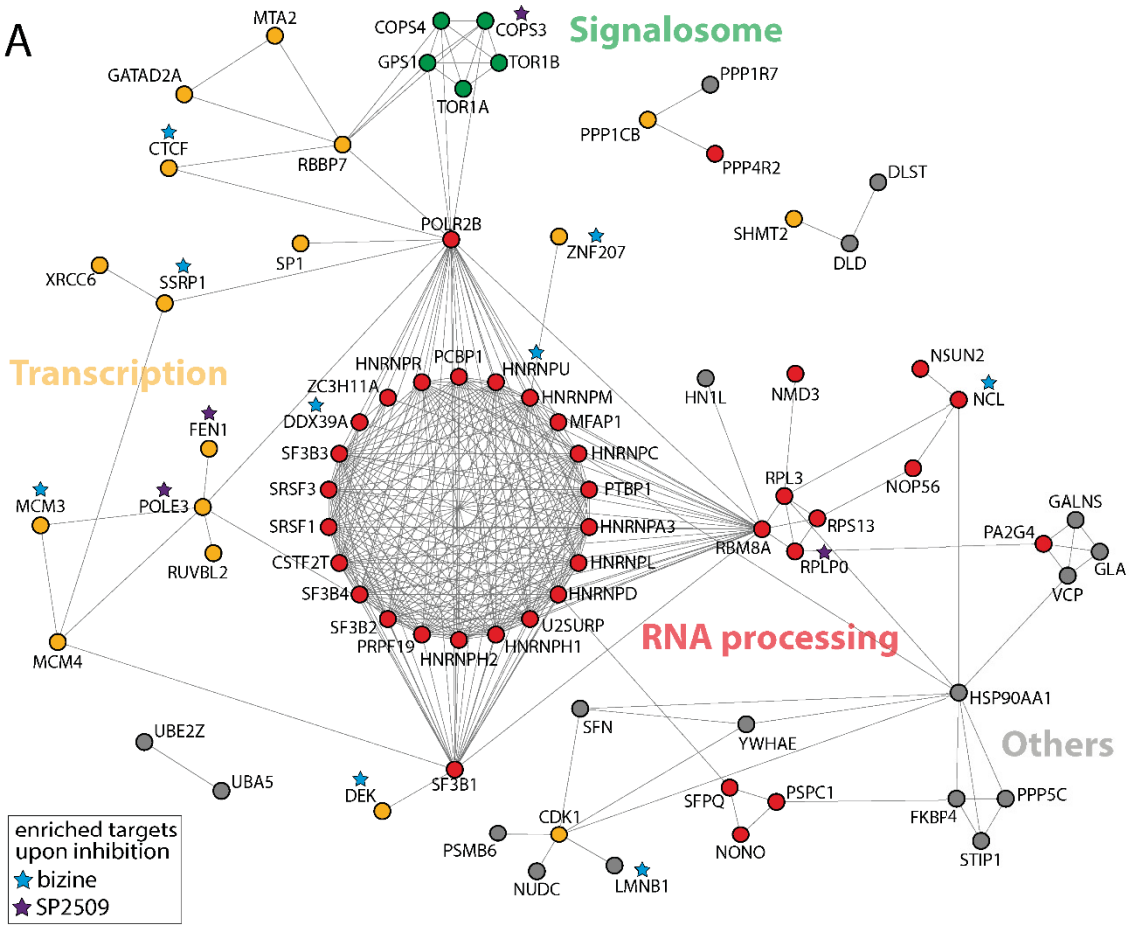

Figure 40 | Protein interactions of potential nuclear redox targets identified upon LSD1 knockout

(A) Nuclear targets enriched after LSD1 knockout were considered for analysis. The network was generated using the STRING database version 11 based on experimental evidence and databases with high confidence interaction score (≥ 0.7) (Szklarczyk et al. 2015). The network was visualized with Cytoscape 3.7.2 using the ClusterONE add-on version 1.0 (Shannon et al. 2003; Nepusz et al. 2012). The majority of potential redox targets are involved in transcription (yellow dots), RNA processing (red dots) and signalosome (green dots) according to molecular function GO terms. Proteins not clustered in these functional groups are shown as grey dots (others). (B) Nuclear targets with no evidence for interaction are shown (bottom left, `no direct interaction´). Proteins identified in BIAM switch assays upon pharmacological inhibition are marked as overlapping targets with blue asterisks (bizine) or purple asterisks (SP2509). The majority of the targets are predicted to act in a functionally connected network.

Consistently with the previously used clustering algorithm (ShineyGO v0.61), the majority of targets clustered to RNA processing and transcription regulation. The transcriptional repressor, transcription factor 25 (TCF25), was the only target identified in all analysis. Although an unbiased approach was chosen here, with metastasis-associated protein 2 (MTA2), GATA zinc finger domain containing 2A

(GATAD2A) and retinoblastoma binding protein 7 (RBBP7) 3 core components of the nucleosome remodeling and deacetylase complex (NuRD) complex, were found as possible targets. This complex is filed as `HDAC2 associated core complex´ in the CORUM database (**Figure 39** A, siRNA). The NuRD complex is a multifunctional machinery that links nucleosome remodeling to histone deacetylase and demethylation activities and functions during both, development and tumorigenesis (Fujita et al., 2003; Kim et al., 2008). LSD1 is an integral component of the NuRD complex as it has been shown in breast cancer *in vitro* and *in vivo* (Wang et al., 2009b). The components MTA2, GATAD2A and RBBP7 found here are the core components and function to maintain complex integrity. Additionally, they recruit factors that convey remodeling, deacetylation and demethylation activities.

3.2.6 Numerous redox targets interact with LSD1

Given that known interacting partners are among the redox targets, it seemed reasonable to again perform a co-IP with inhibited and non-inhibited LSD1 activity in order to test the hypothesis of an `oxidation and release´ mechanism (**Figure 41** B). This time, the alkylation reagent NEM was omitted in the Co-IP, since the sole purpose of this preliminary experiment (n=1) was to obtain indications for interaction and activity dependent changes. Many targets were found to interact with LSD1 (**Figure 41** A). Nucleolin (NCL), heterogeneous nuclear ribonucleoprotein K (HNRNPK) and heat shock protein HSP 90-alpha (HSP90AA1) were more than twofold enriched upon inhibiton of LSD1 activity. This observation indicates that these candidates might interact with LSD1 and become released upon oxidation. In addition, all interacting proteins identified in the previously performed co-IP in proliferating A2B5+ OPCs were compared with the redoxome analysis. Only a few proteins, mainly involved in RNA processing, were found to change their redox state.in MCF-7 cells and interact in A2B5+ OPCs.

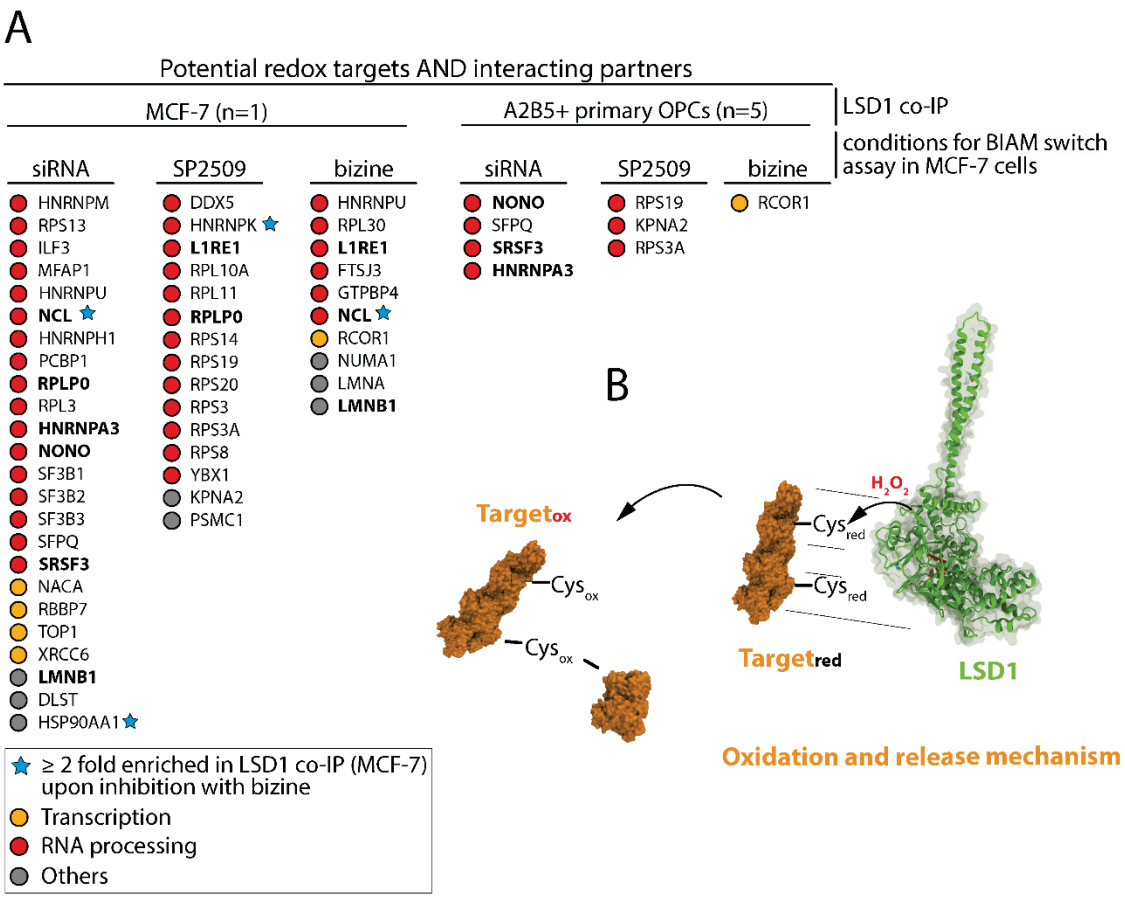

Figure 41 | Numerous potential redox targets were identified as interacting partners

List of proteins identified as both, `less oxidized´ in BIAM switch assays upon LSD1 knockout or inhibition (bizine or SP2509) and identified here as interacting partners by co-IP coupled to mass spectrometry analysis. Potential redox targets identified in more than one condition for the BIAM switch assay are depicted in bold letters (overlapping targets). Proteins involved in transcription are shown as yellow dots and as red dots when involved in RNA processing according to molecular function GO terms. Proteins not clustered in these functional groups are shown as grey dots (others). (A, left) MCF-7 cells were incubated with 15 µM bizine for 24 h and subjected to co-IP coupled to mass spectometry (n=1). Blue asterisks mark targets that were more than two fold enriched as interacting partners upon 24 h treatment with 15 µM bizine in MCF-7 (n=1). (A, right) The same comparison with all identified interacting partners in proliferating A2B5+ primary mouse OPCs (n=5, no bizine treatment). (B) Illustrated is the hypothesized `interaction and release´ mechanism. According to this hypothesis, a target protein interacts with LSD1 and is released in an activity-dependent manner. This hypothesis has been examined here by co-IP combined with pharmacological inhibition of LSD1 activity. (LSD1 PDB entry: 2H94).

As previously described, LSD1 interacts with the NuRD complex as RBBP7 could be identified in the co-IP in MCF-7 cells. Of note, in this preliminary experiment RBBP7 enrichment did not change upon inhibition indicating that oxidation of the NuRD complex could rather have consequences for recruitment stabilization of additional factors than triggering complex disassembly. Under the assumption of an `oxidation and release´ mechanism, nucleolin (NCL) seems to be a promising candidate. The preliminary co-IP indicated that LSD1 may interact with NCL. Interaction was

strongly enhanced when LSD1 was inhibited (~3 fold enriched). NCL is involved in RNA processing and harbours only a single cysteine in one of its RNA binding domains (C543).

3.2.7 The protein levels of several targets are directly or indirectly regulated by LSD1

LSD1 is a transcriptional regulator and modulation of its protein level or activity results in a change of the proteome triggering a change in many cellular functions. All targets enriched here harbor a redox-sensitive cysteine, otherwise they would not have been enriched (**Figure 36**). However, changes in the level of enriched proteins due to transcriptional regulation directly or indirectly mediated by LSD1, could lead to false readouts. Although oxidation of regulated proteins is still possible, their detection and quantification are challenging. To provide insights into the regulation of the protein levels, the full proteome in the same samples have been analyzed by mass spectrometry upon knockout. The proteome analysis identified ~2000 proteins (**Appendix**, Table 22). Of the 127 redox targets, 86 could be identified in the proteome analysis. Of these 86 targets, 28 were significantly downregulated, with CHMP4B only one protein upregulated and 56 not changed (**Figure 42**).

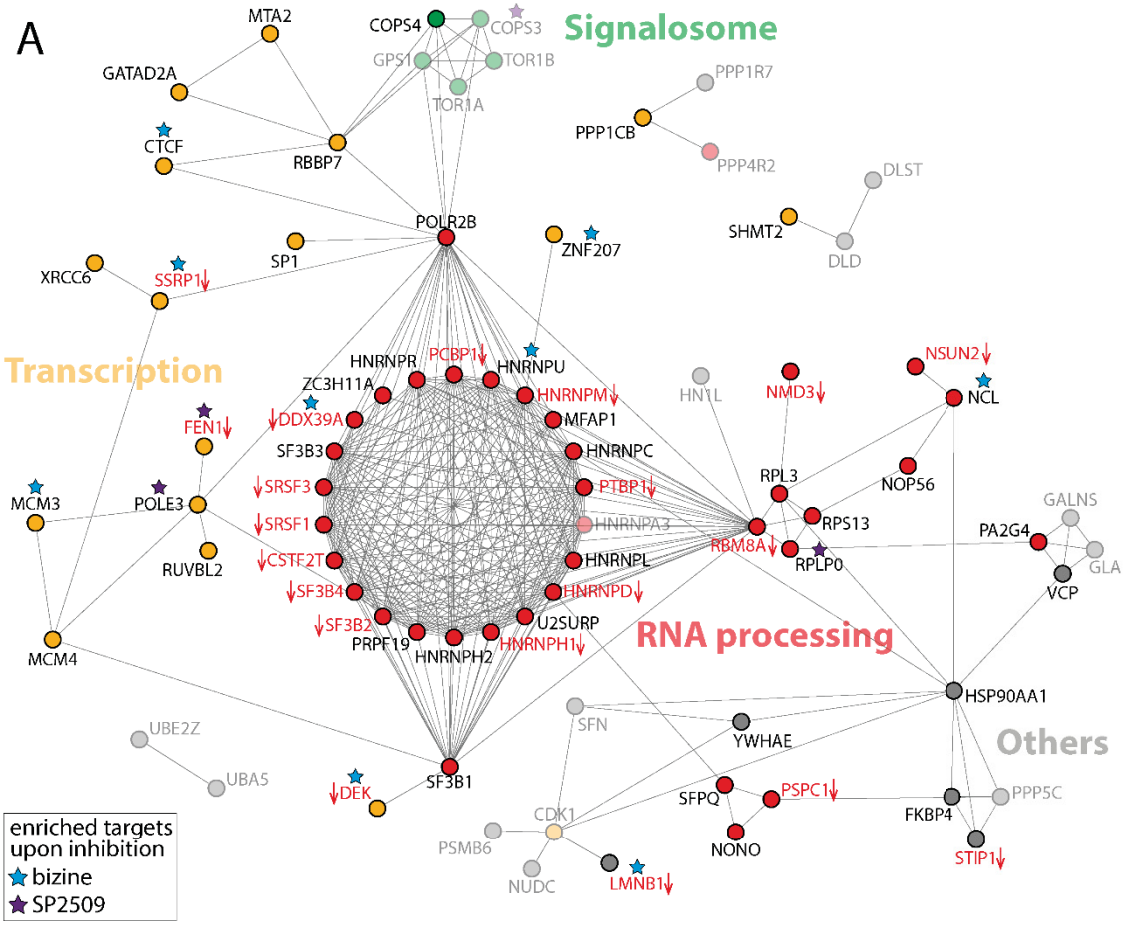

Figure 42 | Protein interactions of potential nuclear redox targets identified upon LSD1 knockout normalized to the full proteome analysis

(A) Nuclear targets enriched after LSD1 knockout were considered for analysis. The network was generated using the STRING database version 11 based on experimental evidence and databases with high confidence interaction score (≥0.7) (Szklarczyk et al. 2015). All targets that are reduced on the protein level according to the full proteom analysis are indicated in red letters and in green when upregulated (p-value < 0.05). All target proteins not found in the proteom analysis are shown with reduced opacity. The network was visualized with Cytoscape 3.7.2 using the ClusterONE add-on version 1.0 (Shannon et al. 2003; Nepusz et al. 2012). The majority of potential redox targets are involved in transcription (yellow dots), RNA processing (red dots) and signalosome (green dots) according to molecular function GO terms. Proteins not clustered in these functional groups are shown as grey dots (others). (B) Nuclear targets with no evidence for interaction are shown (bottom left, `no direct interaction´). Proteins identified in BIAM switch assays upon pharmacological inhibition are marked as overlapping targets with blue asterisks (bizine) or purple asterisks (SP2509).

Thus, based on the present proteome data, 56 nuclear redox targets can be considered for validation.

In conclusion, an untargeted approach to enrich differentially oxidized proteins lead to the identification of numerous proteins that may represent novel redox targets.

3.2.8 Investigation of a PRX2 redox relay for LSD1-derived H_2O_2

The NuRD complex has been thoroughly biochemically characterized, but the presence of a peroxiredoxin could not be shown so far. Therefore, one could assume that in this particular case LSD1 directly oxidizes its core-components due to the short distances to other complex components. Yet, a peroxiredoxin-mediated redox relay cannot be excluded in this case or in general. All peroxiredoxins were found in the present redoxome analysis, but only PRX2 and PRX3 were found to be significantly less oxidized upon knockout. This indicates that LSD1-derived H_2O_2 is conveyed via the peroxiredoxin system, possibly to redox targets found in the present redoxome analysis. Both peroxiredoxins were not clustered as nuclear proteins according to the clustering procedure performed in the study. Whereas PRX3 is well described as a mitochondrial peroxiredoxin, the subcellular localization of PRX2 is ambiguous. In fact, it has been described as a nuclear protein in several cancer cell lines and to function in a redox relay with the transcriptional regulator STAT3 (Shiota et al., 2011; Sobotta et al., 2015). PRX2 usually forms a dimer and each dimer possesses 2 cysteines that serve as redox sensors (**Figure 43** B, "PRX$_{red}$").

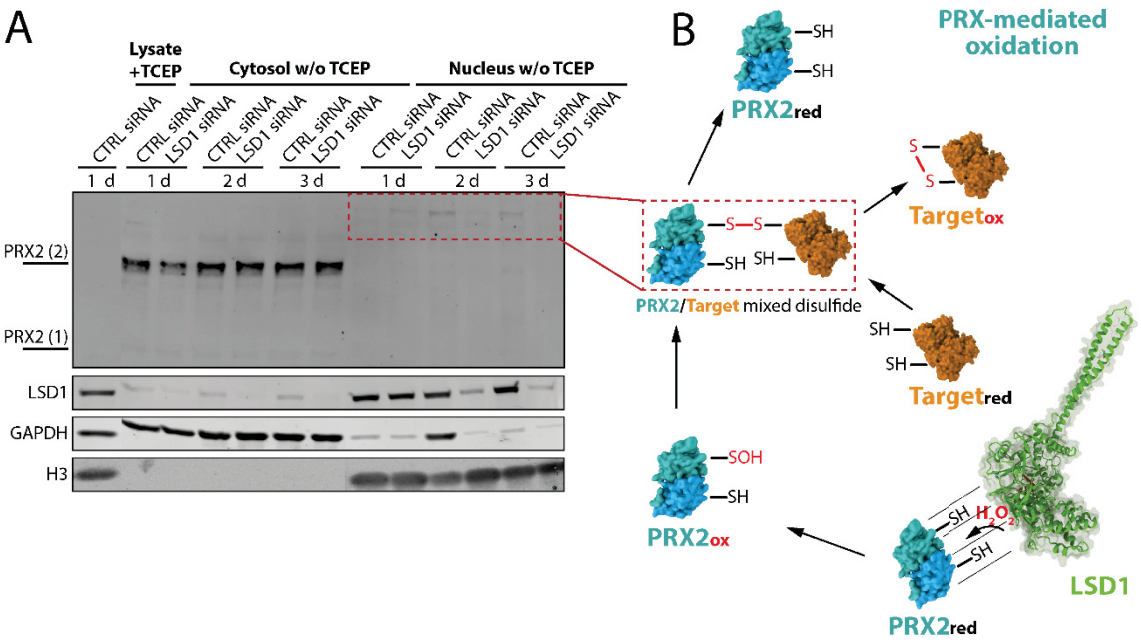

Figure 43 | Indications for the existence of PRX2 disulfide exchange intermediates
MCF-7 cells subjected to a LSD1 knockout for up to 3 days. The organelle fraction was separated from the cytosolic fraction. (A) Representative immunoblot staining against PRX2 in fractionated MCF-7 lysates (n=4). Purity of the cytosolic fraction was assessed by anti-GAPDH staining and the nuclear fraction by anti-histone 3 (H3) staining. The knockout was confirmed by anti-LSD1 staining. Whole cell lysate of the `day 1 CTRL siRNA´ sample was reduced with TCEP as a control. The PRX2 dimer is labeled as PRX2 (2) and the putative monomer as PRX2 (1). Red dashed lines highlight possible PRX2/Target mixed disulfide as part of a putative LSD1-induced PRX2 redox relay. (B) Possible mechanism of the hypothesized LSD1/PRX2/Target redox relay. The peroxidatic cysteine reacts with the LSD1 derived H2O2 to form a sulfenic acid (PRX2ox). Instead of forming an interdimeric disulfide with the opposing monomer (not shown here), it forms a mixed disulfide with the target protein (PRX2/Target mixed disulfide; red dashed line). Upon disulfide exchange, the target protein is released and possibly forms a intramolecular disulfide bond (exemplarily shown here; Targetox) or a intermolecular or mixed disulfide bond (LSD1, PRX2 PDB entry: 2H94, 5IJT). The experiment was conducted by Jan Schmitz and supervised by Thomas Hildebrandt.

The peroxidatic cysteine accepts the redox equivalent and immediately forms an intersubunit disulfide with the resolving cysteine of the opposing monomer. The disulfide is reduced by e.g. thioredoxin resulting in an efficient detoxification of H_2O_2. If the redox equivalent is transferred to a redox target, it forms a disulfide with the respective protein and not with the opposing monomer (**Figure 43** B, "PRX2/Target mixed disulfide"). Subsequently, the oxidized target is released, resulting in a disulfide exchange. In the resulting situation, the redox equivalent is transferred to the redox target and not fed into the thioredoxin system. Toward the goal of providing evidence for a LSD1/PRX2 redox relay, the cytosolic fraction was separated from the organelle fraction and subjected to a non-reducing SDS-PAGE (**Figure 43** A). A digitonin-based fractionation protocol was set up leading to

efficient separation of the organelle fraction in the presence of NEM to prevent artificial oxidation during lysis. There were only minor cytosolic impurities as suggested by immunoblot analysis of glyceraldehyde 3-phosphate dehydrogenase (GAPDH) protein level. First it could be shown that the PRX2 dimer is not present in the nucleus but in the cytosol (**Figure 43** A, "PRX2 (2)"). This challenges its ability to accept LSD1-derived redox equivalents from the nucleus. Noteworthy, the PRX2 monomer was not detectable with this antibody under the present experimental conditions. Even after addition of the reducing agent TCEP, which disrupted the dimer as expected, no monomeric PRX2 could be detected (**Figure 43** A, see lane "Lysate + TCEP"). However, higher molecular weight bands around 60 kDa were detected in the nuclear fraction and could be interpreted as mixed disulfides between oxidized PRX2 dimers and a redox target (**Figure 43** A, "red dashed rectangle"). This is supported by the following: first, the band intensity is directly proportional to the LSD1 protein level and second, not detectable under reducing conditions. In conclusion, the immunoblot analysis neither proved nor disproved that PRX2 conveys LSD1-derived redox equivalents to a target protein. Instead, arguments for both scenarios were provided. The cytosolic localization of the dimer suggested that PRX2 is not present in the nucleus. However, the monomeric form of PRX2 was not detectable. Still the starting point of the redox relay could be the monomeric form that is upon oxidation either translocated or forms a mixed disulfide with the target as suggested here by the higher molecular weight bands.

To summarize these findings, LSD1 regulates the redox state of numerous proteins. The majority could be allocated to the nucleus and several known LSD1 interactors could be identified. This strongly indicates that LSD1 links epigenetics to nuclear redox signaling and thereby broadening its regulatory function to a yet unknown extent.

4 Discussion

The overall aims of this study were, first, to investigate the role of LSD1during OPC differentiation and second, to unravel a potential function of LSD1 in redox signaling.

Key findings of this present study are that the extent of OL differentiation and subsequent myelination in zebrafish are severely diminished upon global knockdown using an antisense MO. Consistently, in primary murine cell cultures and OSCs, it became evident that LSD1 specifically regulates the intrinsic transcriptional program during the transition of OPCs to OLs. During this stage, LSD1 and CTBP1 are recruited by ZFP516 indicating a crucial function of these components during induction of differentiation.

The second key finding of this study is that the H_2O_2 produced along with the demethylation reaction has a highly significant role in regulating the nuclear redoxome. LSD1 is auto-oxidized in an activity-dependent manner at several cysteines, while two of them seem to form a long-range disulfide bond, indicating significant changes in the structural parameters induced by its own activity. Moreover, knockout or inhibition with two different pharmacological inhibitors changes the redox state of numerous nuclear proteins. Indications were provided, that LSD1 oxidizes its targets by direct oxidation and via a PRX2-mediated thiol switch.

4.1 LSD1 in oligodendrocyte development

Although LSD1 is highly conserved between vertebrates and mammals, the translation between rodents and zebrafish is not always guaranteed (Shi et al., 2004). Indeed, the germline knockout of LSD1 in zebrafish does not result in embryonic lethality as observed in mice. LSD1 null mutants survive up to 10 dpf, which is far beyond the embryonic stage. This observation could be due to the maternal expression of *kdm1a* mRNA in zebrafish (Takeuchi et al., 2015). Differences exist also in the process of myelination, although the zebrafish is a well-accepted model and the majority of genes involved in myelination are conserved between lower vertebrates and mammals. CLDK is a zebrafish specific component of the myelin sheet and does not exist in mammalian species. Vice versa, PDGFRα is

not expressed in zebrafish OPCs (Park et al., 2002). In the present study, no early lethality could be observed although the MO used in this study also targets maternal transcripts. Most probably this due to the mild knockdown typically induced MOs. Even though LSD1 morphants survive, it remains elusive whether stem cells properly develop into progenitor and differentiated cell types when LSD1 is knocked down in the whole organism. OPCs are descendants form ESC and NSCs in which demethylation mediated by LSD1 is a significant event in rodents and human cells (Wang et al., 2014; Yokoyama et al., 2008; Whyte et al., 2012; Han et al., 2014). Thus, one of the key questions ultimately arising from the experimental approach chosen here is whether the extent of OPC specification is diminished due to developmental defects already occurring in ESCs or during the specification of NSCs and OPCs. A reduction in the number of OPCs alone could be causative for a reduced number of OLs and would impede the intended investigation of the role of LSD1 during the transition of OPCs to OLs. OPCs reside in the ventral pMN domain, while they migrate dorsally once committed to the OL lineage. At first glance, no obvious difference became evident from the GFP signal in the *Tg(olig2:GFP)* line in the pMN domain. Nevertheless, drawing the conclusion that the OPC pool is not affected remains somewhat speculative here. For quantification of ventral residing OPCs, it would be necessary to clearly identify single GFP+ cells. However, the high density of progenitor cells in the pMN domain render it practically impossible to count single cells. Apart from those technical issues, quantification of OLIG2+ OPCs would be only possible in a very narrow time window. MNs and OLs express OLIG2 as well and arise about 4 h after OPCs are specified around 28 hpf (Ravanelli and Appel, 2015). The cell bodies of OLIG2+ MN co-reside in the pMN domain and cannot be distinguished from OLIG2+ OPCs. Additionally, within the above-mentioned time window LSD1 morphants exhibit a developmental delay as suggested by a shorter body length and an initially reduced number of MNs. This makes it difficult, if not impossible, to compare the extent of OPCs specification during this stage based on the expression of the common marker OLIG2. As already mentioned, PDGFRα is absent in zebrafish OPCs and NG2 expression is not detectable before 5 dpf (Ravanelli et al., 2018). Thus, due to technical limitations and the lack of suitable markers, the extent of OPCs specification could not be conclusively assessed.

Given that LSD1 could be responsible to repress genes involved in final maturation e.g. *mbp* and *plp*, its knockdown would lead to precocious differentiation before premature OLs could migrate to their designated location. Most likely this would increase the proportion of apoptotic cells, which however was not observed here. To further investigate whether OPCs prematurely develop, the *Tg(nkx2.2a:GFP)* line would allow for the identification of early OLs as NKX2A is expressed immediately upon initial commitment.

Of note, the PCNA stainings in the zebrafish spinal cord suggested that OPCs fail to exit the cell cycle and differentiate into OLs. This indicates that LSD1 functions first of all as a repressor for progenitor specific genes as it has been previously described in hematopoietic stem cells (Kerenyi et al., 2013). Still the true identity of PCNA+ cells identified in the paraffin sections is ambiguous and should be confirmed by cell specific analysis, e.g. by employing the bromodeoxyuridine (BrdU) incorporation technique in the *Tg(olig2:GFP)* line.

As mentioned before, several studies in mice have shown that LSD1-dependent transcriptional regulation is necessary for NCS maintenance, development of neurons as well as maintenance of cell functions in adult neurons. Since the neuronal network is the actual substrate for OLs, it is of vital importance to investigate if and how LSD1 knockdown impacts on neurogenesis. Surprisingly, even in morphants with a strong reduction in the number of dorsal migrating OLIG2+ cells, the neuronal network developed properly as suggested by the whole mount stainings. Although delayed in development, MNs were fully established at 5 dpf. The delay in MN development indicates that back-up mechanisms could exist that compensate for the loss of LSD1, if LSD1 is involved in MN differentiation at all. This provides further ground to assume that LSD1 is not essential for CNS neurogenesis in the zebrafish spinal cord, but for the development of OLs. Still some neuronal subtypes might be affected as suggested by the reduced number of DRGNs. The NCC-derived DRGNs are part of the PNS. NCCs are generated when epithelial cells delaminate from the dorsal neural tube. The process when cells lose their epithelial characteristics and acquire the ability to migrate is termed epithelial-mesenchymal transition (EMT). EMT is an important process during many steps of embryogenesis and regeneration and mirrors in part during metastasis of epithelial cancer types. Two possible explanations for the reduced number of DRGNs arise from studies in mice and breast

cancer models. First, LSD1 occupies the *neurog1* promotor in mouse ESCs upon initiation of neural differentiation (Han et al., 2014). This suggests that LSD1 could be directly involved in establishing NGN1 dependent DRGN identity. Second, from epithelial cancers it is known that LSD1 initiates the EMT specific transcriptional program to promote metastasis (Boulding et al., 2018). The LSD1 knockdown could therefore prevent EMT-driven delamination of NCCs during development, leading to a reduced number of DRGNs. It was beyond scope of this study to dissect the role of LSD1 during DRGN development. However, the observation exemplifies the presumptive complexity how LSD1 directly or indirectly regulates cell differentiation *in vivo*.

In summary, it could be shown that neurogenesis in the CNS spinal cord does not necessarily require LSD1. More transgenic lines would be necessary to investigate neurogenesis in the spinal cord in detail.

Apart from cell fates, LSD1 regulates many cellular functions of differentiated cells (Christopher et al., 2017; Wang et al., 2014; Sakamoto et al., 2015). This is of particular importance during OL development *in vivo* as dorsal migration is not only orchestrated by OPC intrinsic transcriptional regulation. Extrinsic signals such as BMP and WNT signals secreted from the roof plate and SHH signals secreted from the ventral notch cord are essentially involved in the spatiotemporal regulation of OL generation. It is still unclear at this point if the observed effect is due to OPC intrinsic regulation or due to functional changes in cells that establish the extrinsic signaling pattern. To pursue this approach in further depth, pharmacological inhibitors could be employed that interfere with e.g. SHH and NOTCH morphogen production. However, the objective of this study was to investigate cell intrinsic mechanisms. Thus, it would be highly desirable to apply a photo-inducible MO. A photo-inducible MO is a MO that is bound to an inhibitory light-sensitive fragment. Upon illumination at 365 nm, the fragments is cleaved and the MO activated (Tomasini et al., 2009). This mechanism provides full spatiotemporal control over the knockdown. A more practicable approach could involve the application of a splice blocking MO which only targets newly synthesized mRNA and not maternal inherited transcripts. Maternal transcripts could help to overcome the preceding phases of development before OL differentiation starts. This approach would

require more detailed investigation on the distribution of maternal transcripts upon application of a splice blocking morpholino.

To learn if LSD1 regulates the OPC intrinsic program, further investigations were carried out in murine A2B5+ OPCs enriched from postnatal mouse brains. The pool of A2B5+ glial restricted progenitor cells isolated here are prone to differentiate into astrocytes or OLs. Upon induction of differentiation, cells neither differentiated to astrocytes nor to OLs. This raises the question about the cellular fate of OPCs with reduced LSD1 activity or decreased transcript levels *in vitro*. The relative number of NG2+ OPCs was significantly higher than in the wildtype culture indicating that the induction of the endogenous shRNA with DOX stabilizes the progenitor specific transcriptional program. In theory, OPCs that do not differentiate would undergo apoptosis as the intrinsic program prevents differentiation but at the same time cells are forced to differentiate by exposure to pro-differentiating stimuli. This question has not been addressed so far.

Nevertheless, doubts remain about the effects observed upon induction with the endogenous shRNA. The observed reduction of the transcript level corresponds approximately to those observed *in vivo* upon administration of DOX to the drinking water (Sprüssel et al., 2012). On the protein level however, LSD1 seems not to be significantly downregulated in every biological replicate in postmitotic OLs. Nevertheless, each experiment uniformly showed a reduced number of mature OLs. One explanation for this could be that quantitative analysis from immunoblots is not suitable for detecting the rather mild knockdown. Massive secondary effects are also imaginable, which, however, would question the applicability of this system in general. In brief, the overexpression of a shRNA requires further downstream processing events involving the specific activity of e.g. the endoribonuclease dicer and the ribonuclease drosha. The processing machinery could reach its capacity limit and other endogenous regulatory microRNAs might be inadequately processed. To exclude such side effects, a transgenic mouse with an inducible non-targeting shRNA would be necessary. Still the observed effects could be corroborated with the pharmacological inhibitor bizine in OSCs and thus, not only in cell culture but also in a different model. Although the experiments involving pharmacological inhibitors have not finally eliminated all remaining uncertainties,

it strongly supports the hypothesis that LSD1 is essential for the differentiation of OPC.

It was not scope of this study to investigate the potential application of LSD1 inhibitors for treatment of neurodegenerative disease. However, LSD1 is suggested as a target for treatment of neurodegenerative diseases as such it is worth commenting on possible direct neurobiological effects triggered by LSD1 inhibition based on the present findings. The dual LSD1/MAO-B inhibitor ORY-2001 (vafidemstat) has entered phase II clinical trial for treatment of MS and Alzheimer's disease (Clinical Trials Register EudraCT 2017-002838-23EU) due to its beneficial outcome in an animal model of MS, experimental autoimmune encephalomyelitis (EAE) model (ACTRIMS 2018 - Posters, 2018). This is attributed to the immunomodulatory effects as suggested by reduced lymphocyte egress and infiltration. Based on the data provided here, it is strongly suggested to consider neurobiological effects as well. OPCs respond to demyelinating insults by extensive proliferation and expansion to give rise to a reasonable amount of premyelinating OLs (Levine and Reynolds, 1999). According to the present data, inhibition of LSD1 activity could lead to an increased enrichment of the endogenous OPC pool during this stage. Given the inhibitory breaks on OPC differentiation would be released in appropriate time, transient inhibition of LSD1 could paradoxically enhance remyelination and prevent neuronal loss due to an OPCs intrinsic mechanism in addition to the reported immunomodulatory effects.

To begin the investigation on the molecular function of LSD1, a co-IP analysis was performed. It remains a technical challenge to enrich LSD1 complexes using an endogenous approach in primary cells due to the cellular heterogeneity and the limited number of cells. In return, this approach provides a more realistic view of the composition of LSD1 complexes than obtained from overexpressed and tagged LSD1 variants in cell lines. The differentially enriched proteins, ZFP516, CTBP1 and RCOR3 were significantly recruited to LSD1 24 h after induction of differentiation.

The function of ZFP516 as a recruiter of LSD1 containing complexes has been demonstrated before. In breast cancer cells, ZFP516 is responsible for guiding the LSD1/CTBP1/COREST complex to the promotor of the epidermal growth factor receptor (EGFR) to repress its transcription by H3K4 demethylation (Li et al., 2017). In murine brown adipose tissue (BAT), it has been shown that ZFP516 recruits LSD1

to the promotor of genes involved in BAT development and homeostasis (Sambeat et al., 2016). In the latter case, ZFP516 acts as a transcriptional activator as it enables LSD1 to convey its function as a H3K9 demethylase. Given that ZFP516 and CTBP1 are both recruited to LSD1 upon induction of differentiation, the complex could be crucial for OL development. In view of these studies, it is unclear whether ZFP516/CTBP1/LSD1 acts as a transcriptional repressor of e.g. cell cycle inhibitors or as an activator of genes involved in OL maturation.
Here, it could be shown for the first time that OPC differentiation and myelination require LSD1-mediated transcriptional regulation.

4.1.1 LSD1 in Oligodendrocyte development - Outlook

Primary cells are known to be difficult to transfect. Attempts to transfect the A2B5+ OPCs by using lipid-based delivery systems were not successful. It is essential to confirm the observed effects with another knockdown experiment, by using e.g. a lentivirus-based approach. If the effect can be confirmed, there would be sufficient justification to continue the investigation in a murine model *in vivo*. Only an OPC/OL-specific knockdown for LSD1 would be a reasonable approach. In particular, a conditional knockdown can be achieved by breeding a mutant mouse harboring a floxed *kdm1a* with a *cspg4* specific or *Pdgfr* specific cre recombinase strain (Wang et al., 2007; Roesch et al., 2008; Minocha et al., 2015). Furthermore, it would be desirable to further develop the project based on the obtained co-IP data. In particular, to test the significance of the interaction, it would be feasible to knock down ZFP516 and CTBP1 together with LSD1 or alone in differentiating OPCs. Co-stainings of these components in postnatal brain slices would help to indicate the biological significance of the interaction.
The identification of the transcriptional targets of LSD1 would require a chromatin-immunoprecipitation with subsequent DNA sequencing (CHIP-seq) against LSD1 and preferentially ZFP516 and CTBP as well.

4.2 LSD1 and its potential role in redox signaling

The function of LSD1-derived H_2O_2 is currently unclear. There is every reason to believe that H_2O_2 is functionally relevant. Otherwise it is hard to understand why

the flavo-dependent H_2O_2 producing LSD1 still exists although elaborate detoxification is required in contrast to the jumonji-C (JmjC) domain-containing demethylases. In fact, the JmjC demethylases are able to demethylate all methylation states. Thus, in theory, they have been able to replace the function of LSD1. In the present study an untargeted and targeted approach was chosen to provide indications for LSD1-dependent protein oxidation and its possible consequences. From both perspectives, strong indications for LSD1-mediated redox signaling events could be provided. By co-IP it could be shown that LSD1 is oxidized at multiple cysteines in an activity-dependent manner. LSD1 could serve as a redox sensor as some of these cysteines are relevant for its demethylase activity (Ricq et al., 2016). Although evidence for the existence of a LSD1 oligomeric structure was provided by mass spectrometry, the validation by non-reducing SDS-PAGE was not successful. Assuming that an oligomeric form of LSD1 indeed exists, one has to consider that an antibody-based detection of a LSD1 oligomer under denaturing conditions is technically not possible. Thus, native conditions provided by either native gel electrophoresis or size-exclusion chromatography could circumvent possible detrimental effects of denaturing agents. At this stage it would be, first of all, reasonable to provide a biochemical proof for the existence of an oligomer. This could be achieved by taking a simplified approach using recombinant LSD1 and exogenous H_2O_2. Although it could not conclusively be shown that LSD1 adopts an oligomeric structure, it is clear that self-oxidation changes its structural parameters and activity.

In addition to these findings, inhibition of LSD1 activity with bizine resulted in a reproducible enrichment of the LSD1/COREST complex. Non-inhibited LSD1 rather associates with other factors e.g. SWI/SNF chromatin remodelers. Assuming that this observation was not due to a bizine-specific effect but indeed related to the LSD1 activity, one could conclude that the demethylation reaction serves as a release signal for the complex at the same time. A release mechanism for the LSD1/COREST complex induced by an intrinsic signal arising from the actual demethylation reaction would provide an elegant and direct mechanism for complex disassembly which is in general believed to be driven indirectly by posttranslational modifications (Han et al., 2014; Peng et al., 2017). The observed cysteine oxidation in LSD1 could be causative for the disassembly. They would

change the physiochemical properties of LSD1 and ultimately its specific binding affinities to interacting partners. Thus, it fosters LSD1 to engage with other components that favor the oxidized state e.g. SWI/SNF chromatin remodelers. This mechanism would set a molecular threshold for immediate reassembly of the LSD1/COREST complex that favors the reduced LSD1 variant according to the present data. This threshold would need to be overcome by the specific activity of a reductase. Intriguingly, using an intermediate trapping approach for the disulfide reductase thioredoxin 1 (TRX1), LSD1 could be identified as a substrate for TRX1 in HELA cells (unpublished data from our group). This provides additional evidence that LSD1 is subjected to reversible and physiological relevant redox modifications. At this stage, it was unclear whether only LSD1 was oxidized or interacting partners as well, because the co-IP was not suitable to obtain information about the redox state of interacting partners. Binding of a target in its oxidized and reduced state in an adequate amount would be a prerequisite to identify differentially oxidized interactors. Based on the observations here, an `oxidation and release´ mechanism seems to be likely. Thus, even if a target protein in its reduced state would be sufficiently enriched as such reliable identification of peptides with oxidized cysteines would have been possible, information about the redox state of the unbound target protein is lost. A reversal IP of the unbound fraction against the protein of interest could in principle solve this question. But considering that the `oxidation and release´ mechanism could also occur based on a transient `touch and go´ interaction, it was necessary to continue with an untargeted approach.

Oxidative modifications of epigenetic factors and transcriptional regulators have been previously shown. These comprise HDACs, p53, NF-κB, SP1 and many more (Meyer et al., 1993; Morel and Barouki, 1999). In case of HDAC2, a redox-dependent release from the chromatin was observed indicating, that histone-bound complexes could indeed disassemble due to oxidation (Nott et al., 2008). As already suggested by immunoblot analysis, proteins are less decorated with sulfenic acids upon knockout and inhibition with 2 different pharmacological inhibitors. Thus, it was not surprising to see that a huge proportion of proteins were differentially oxidized according to the BIAM switch analysis. Almost half of the differentially oxidized proteins could be clustered as nuclear proteins although the complete cellular redoxome was analyzed. This strongly suggested that LSD1 changes the local redox

environment of the nucleus. Indications could be provided that whole LSD1-containing complexes are oxidized by LSD1. This could be shown e.g. for core components of the NURD complex (GATAD2A, RBBP7 and MTA2) and give every reason to assume that other LSD1-containing complexes are subjected to oxidative modification as well e.g. the COREST complex in SN4741. Intriguingly, also GATAD2A, RBBP7 and MTA2 were identified as TRX1 substrates using theTRX1-trapping mutant in HELA cells. Many other targets, e.g. the previously mentioned SP1 and NCL, were found as substrates for TRX1 in HELA cells as well.

A set of proteins were detected as seemingly more oxidized in the BIAM switch assay, which contradicts the hypothesis. The observation may not necessarily be wrong considering that substantial secondary effects could interfere with the investigation of direct effects. It is equally likely that the BIAM switch assay leads to a false-positive detection of more oxidized proteins. In brief, a major drawback of the BIAM switch technique is that reduction by DTT is necessary to enable BIAM labeling and subsequent enrichment (**Figure 35**). The degree of enrichment is proportional to the degree of oxidation and differentially oxidized proteins are identified based on significant differences. Overoxidized variants comprising sulfinic and sulfonic acids cannot be reduced by DTT and are not enriched although being oxidized. These states are therefore not distinguishably from thiols that become alkylated in the first step to avoid enrichment. Now assuming the scenario that LSD1 is responsible for the overoxidation of a protein, the LSD1 knockout or inhibition would lower the oxidation state of the cysteine, but not necessarily to the fully reduced thiol. Residual LSD1 activity could still facilitate `normal´ (DTT reducible) oxidation. In this particular situation, the target protein becomes misleadingly enriched upon LSD1 knockout or inhibition and not in the control. Therefore, it should always be considered that those proteins that were detected as more oxidized could in theory be targets for LSD1-dependent overoxidation.

Scaffolding functions of LSD1 are subject of ongoing research (Lan et al., 2019). Using the full knockout, LSD1 containing complexes might disassemble and as a consequence thereof, components are exposed to a new microenvironment with different physicochemical properties which per se could change the redox state of a particular protein. To address this issue, pharmacological inhibitors were employed. In this context it should be considered that binding of small molecules do

not guarantee complex integrity (Fiskus et al., 2014). Instead of using pharmacological inhibitors, the application of an inducible system driving the expression of a previously published inactive LSD1 mutant variant would be a highly desirable tool for future investigations (Lee et al., 2005). As evidenced by immunoblot analysis of *in situ* labeled sulfenic acids, obvious differences arose 10 h after addition of the inhibitors. The knockout exerts global effects 3 days post-electroporation, soon after LSD1 protein levels were significantly decreased. The comparison between inhibitor treatments and knockout when considering a single time point for analysis are limited to the different kinetics of H_2O_2 reduction. Out of all potential nuclear redox targets found in the analysis upon inhibition with bizine and SP2509, 13 % and 7 % respectively, overlap with the knockout targets. The degree of overlaps appeared to be relatively small. However, the spectrum and degree of overlap most likely change in dependency of the concentration, and more importantly, incubation time. Therefore, the rather low number of common targets at the time of analysis does not necessarily mean that these inhibitors do not properly target LSD1 activity. Again, it was not purpose of this study to investigate the function of LSD1 inhibitors. However, additional information revealed by the present study are so far unrecognized redox-dependent off-target effects of inhibitors. It would be a possible scenario that low molecular weight compounds indirectly or directly change the functionality of other proteins in a redox-dependent manner, non-related to LSD1-dependent oxidation. This could also affect proteins in organelles in which LSD1 is not present. Considering the ongoing discussion about specificity and off-target effects of small molecules, this would introduce a new aspect to this issue and propose a concrete approach for analysis.

It remained open whether LSD1 needs the specificity and reactivity of PRX2 to deploy its redox equivalents to target proteins. Indications for the existence of LSD1-dependent PRX2-linked mixed disulfides were provided by immunoblot analysis. In addition, the redoxome analysis demonstrated that PRX2 is significantly less oxidized upon LSD1 knockout. Thus, more detailed investigations in this direction would be desirable. In particular, the overall aim at this stage is to provide a mechanistic proof that PRX2 forms a mixed disulfide with targets found in the redoxome analysis. This could be achieved by addition of exogenous H_2O_2 and subsequent analysis of the mixed conjugates by mass spectrometry. The

involvement of PRX2 in this process would be a desirable scenario concerning the technical realization of further studies. The redox cascade (LSD1/PRX2/Target) could be easily disrupted by a knockout of PRX2, while the LSD1 protein level, its complex integrity and function as a transcriptional regulator remain unchanged.

In the scenario of direct oxidation mediated by LSD1, it will be difficult to provide definitive evidence. LSD1 activity would need to be modulated in order to study target oxidation. The major challenge when modulating LSD1 activity would be to decouple the function of LSD1 as a redox regulator from its function as a transcriptional regulator. While LSD1 oxidizes a target protein, it changes the transcriptional program of the cell by histone demethylation at the same time. This became not only evident in the proteome analysis carried out here, but was also extensively investigated specifically in breast cancer models elsewhere (Boulding et al., 2018). It will lead to a variety of functional changes, the cause of which is difficult to attribute to either oxidation or transcriptional regulation. The intervention in the histone code, as achieved by the knockout of LSD1, triggers not only changes in the cellular functions, but also affects the overall DNA/histone structure. With LSD1 functioning as a transcriptional repressor and activator, specific regulatory elements of the DNA change their accessibility. This fact is of particular importance, when redox regulated DNA binding proteins, e.g. the transcription factor SP1, are considered for functional validation. DNA binding analysis would be an obvious approach to further investigate the functional consequences of SP1 oxidation as it has been previously shown that oxidative modification changes its DNA binding abilities (Ammendola et al., 1994). However, these investigations would be biased as the knockout potentially changes the amount of accessible SP1 consensus motifs. Changes in the availability of SP1 binding sites will per se impact on the pattern and degree of SP1 binding that does not reflect oxidation-driven processes but is rather forced by a change in the availability of SP1 attracting DNA motifs. This is comparable to an enzyme activity assay performed with different amounts of substrate.

Intriguingly, SP1 becomes increasingly methylated when LSD1 levels are decreased, indicating that it could serve as a novel non-histone substrate for LSD1 (Chuang et al., 2011). This observation is accompanied with a decrease in the DNA binding ability. The particular case of SP1, shows how complex intertwining regulatory

mechanisms can create a situation in which an oxidation-based mechanism can hardly be assigned to a function.

So far LSD1 has been recognized as transcriptional regulator acting on the histone level. In addition, numerous non-histone substrates were identified indicating its role in regulating non-histone protein function and stability as well. The present study has brought light to a completely new and innovative aspect of LSD1-dependent regulation, involving the by-product H_2O_2.

4.2.1 LSD1 and its potential role in redox signaling – Outlook

At present, numerous potential LSD1 targets are subjected to validation.

Obviously Considering the difficulties described above, no general guideline for validation can be provided. Obviously, validation has to be adapted to the particular target. In case of SP1, this might involve a recombinant protein-based assay.

Toward the goal of identifying the complete thiol switch, trapping experiments in MCF-7 cells and SN4741 should be performed. These experiments do not only provide evidence that the targets considered here are indeed reversibly redox regulated. In addition, they support the present observation as the trapping experiments rely on a different principle of enrichment.

Still the main challenge in the future will be to demonstrate the biological significance of LSD1-dependent target oxidation. In this regard, it will be of vital importance to decouple LSD1-dependent demethylation and transcriptional regulation from oxidation. In theory, a fusion construct of LSD1 with catalase could enable H_2O_2 detoxification, while transcriptional regulation is still active. However, this would most likely affect the interaction with many targets per se.

5 References

(2018). ACTRIMS 2018 - Posters. Multiple sclerosis (Houndmills, Basingstoke, England) *24*, 11-117.

Almeida, R.G., Czopka, T., ffrench-Constant, C., and Lyons, D.A. (2011). Individual axons regulate the myelinating potential of single oligodendrocytes in vivo. Development *138*, 4443-4450.

Ammendola, R., Mesuraca, M., Russo, T., and Cimino, F. (1994). The DNA-binding efficiency of Sp1 is affected by redox changes. European Journal of Biochemistry *225*, 483-489.

Andrés, M.E., Burger, C., Peral-Rubio, M.J., Battaglioli, E., Anderson, M.E., Grimes, J., Dallman, J., Ballas, N., and Mandel, G. (1999). CoREST: A functional corepressor required for regulation of neural-specific gene expression. PNAS *96*, 9873-9878.

Arnér, E.S.J., and Holmgren, A. (2000). Physiological functions of thioredoxin and thioredoxin reductase. European Journal of Biochemistry *267*, 6102-6109.

Asakawa, K., Higashijima, S.-i., and Kawakami, K. (2012). An mnr2b/hlxb9lb enhancer trap line that labels spinal and abducens motor neurons in zebrafish. Developmental Dynamics *241*, 327-332.

Baracskay, K.L., Kidd, G.J., Miller, R.H., and Trapp, B.D. (2007). NG2-positive cells generate A2B5-positive oligodendrocyte precursor cells. Glia *55*, 1001-1010.

Becker, P.B., and Hörz, W. (2002). ATP-dependent nucleosome remodeling. Annual review of biochemistry *71*, 247-273.

Biteau, B., Labarre, J., and Toledano, M.B. (2003). ATP-dependent reduction of cysteine–sulphinic acid by S. cerevisiae sulphiredoxin. Nature *425*, 980-984.

Blader, P., Plessy, C., and Strähle, U. (2003). Multiple regulatory elements with spatially and temporally distinct activities control neurogenin1 expression in primary neurons of the zebrafish embryo. Mechanisms of Development *120*, 211-218.

Boulding, T., McCuaig, R.D., Tan, A., Hardy, K., Wu, F., Dunn, J., Kalimutho, M., Sutton, C.R., Forwood, J.K., and Bert, A.G., et al. (2018) LSD1 activation promotes inducible EMT programs and modulates the tumour microenvironment in breast cancer. Sci Rep *8*, 1-18.

Bradl, M., and Lassmann, H. (2010). Oligodendrocytes: biology and pathology. Acta Neuropathol *119*, 37-53.

Bräutigam, L., Jensen, L.D.E., Poschmann, G., Nyström, S., Bannenberg, S., Dreij, K., Lepka, K., Prozorovski, T., Montano, S.J., and Aktas, O., et al. (2013). Glutaredoxin regulates vascular development by reversible glutathionylation of sirtuin 1. Proceedings of the National Academy of Sciences of the United States of America *110*, 20057-20062.

Brewer, T.F., and Chang, C.J. (2015). An Aza-Cope Reactivity-Based Fluorescent Probe for Imaging Formaldehyde in Living Cells. Journal of the American Chemical Society *137*, 10886-10889.

Britsch, S., Goerich, D.E., Riethmacher, D., Peirano, R.I., Rossner, M., Nave, K.-A., Birchmeier, C., and Wegner, M. (2001). The transcription factor Sox10 is a key regulator of peripheral glial development. Genes Dev. *15*, 66-78.

Cai, J., Qi, Y., Hu, X., Tan, M., Liu, Z., Zhang, J., Li, Q., Sander, M., and Qiu, M. (2005). Generation of Oligodendrocyte Precursor Cells from Mouse Dorsal Spinal Cord Independent of Nkx6 Regulation and Shh Signaling. Neuron *45*, 41-53.

Christopher, M.A., Myrick, D.A., Barwick, B.G., Engstrom, A.K., Porter-Stransky, K.A., Boss, J.M., Weinshenker, D., Levey, A.I., and Katz, D.J. (2017) LSD1 protects against hippocampal and cortical neurodegeneration. Nat Commun *8*, 1-13.

Chuang, J.-Y., Chang, W.-C., and Hung, J.-J. (2011). Hydrogen peroxide induces Sp1 methylation and thereby suppresses cyclin B1 via recruitment of Suv39H1 and HDAC1 in cancer cells. Free Radical Biology and Medicine *51*, 2309-2318.

Clark, D.J., and Kimura, T. (1990). Electrostatic mechanism of chromatin folding. Journal of Molecular Biology *211*, 883-896.

Clarke, L.E., Young, K.M., Hamilton, N.B., Li, H., Richardson, W.D., and Attwell, D. (2012). Properties and Fate of Oligodendrocyte Progenitor Cells in the Corpus Callosum, Motor Cortex, and Piriform Cortex of the Mouse. J. Neurosci. *32*, 8173-8185.

Cox, A.G., Peskin, A.V., Paton, L.N., Winterbourn, C.C., and Hampton, M.B. (2009). Redox potential and peroxide reactivity of human peroxiredoxin 3. Biochemistry *48*, 6495-6501.

Culhane, J.C., and Cole, P.A. (2007). LSD1 and The Chemistry of Histone Demethylation. Current opinion in chemical biology *11*, 561-568.

Dimou, L., and Gallo, V. (2015). NG2-glia and their functions in the central nervous system. Glia *63*, 1429-1451.

Doyle, K., and Fitzpatrick, F.A. (2010). Redox signaling, alkylation (carbonylation) of conserved cysteines inactivates class I histone deacetylases 1, 2, and 3 and antagonizes their transcriptional repressor function. The Journal of biological chemistry *285*, 17417-17424.

Emery, B., and Lu, Q.R. (2015). Transcriptional and Epigenetic Regulation of Oligodendrocyte Development and Myelination in the Central Nervous System. Cold Spring Harbor Perspectives in Biology *7*.

Fancy, S.P.J., Zhao, C., and Franklin, R.J.M. (2004). Increased expression of Nkx2.2 and Olig2 identifies reactive oligodendrocyte progenitor cells responding to demyelination in the adult CNS. Molecular and cellular neurosciences *27*, 247-254.

Fields, R.D. (2015). A new mechanism of nervous system plasticity: activity-dependent myelination. Nat Rev Neurosci *16*, 756-767.

Fiskus, W., Sharma, S., Shah, B., Portier, B.P., Devaraj, S.G.T., Liu, K., Iyer, S.P., Bearss, D., and Bhalla, K.N. (2014). Highly effective combination of LSD1 (KDM1A) antagonist and pan-histone deacetylase inhibitor against human AML cells. Leukemia *28*, 2155-2164.

Forneris, F., Binda, C., Dall'Aglio, A., Fraaije, M.W., Battaglioli, E., and Mattevi, A. (2006). A Highly Specific Mechanism of Histone H3-K4 Recognition by Histone Demethylase LSD1. J. Biol. Chem. *281*, 35289-35295.

Fujita, N., Jaye, D.L., Kajita, M., Geigerman, C., Moreno, C.S., and Wade, P.A. (2003). MTA3, a Mi-2/NuRD Complex Subunit, Regulates an Invasive Growth Pathway in Breast Cancer. Cell *113*, 207-219.

Gähwiler, B.H., Capogna, M., Debanne, D., McKinney, R.A., and Thompson, S.M. (1997). Organotypic slice cultures: a technique has come of age. Trends in Neurosciences *20*, 471-477.

Ge, S.X., Jung, D., and Yao, R. (2018). ShinyGO: a graphical gene-set enrichment tool for animals and plants. Bioinformatics.

Gerety, S.S., and Wilkinson, D.G. (2011). Morpholino artifacts provide pitfalls and reveal a novel role for pro-apoptotic genes in hindbrain boundary development. Developmental Biology *350*, 279-289.

Giurgiu, M., Reinhard, J., Brauner, B., Dunger-Kaltenbach, I., Fobo, G., Frishman, G., Montrone, C., and Ruepp, A. (2019). CORUM: the comprehensive resource of mammalian protein complexes—2019. Nucleic Acids Res *47*, D559-D563.

Hajihosseini, M., Tham, T.N., and Dubois-Dalcq, M. (1996). Origin of Oligodendrocytes within the Human Spinal Cord. J. Neurosci. *16*, 7981-7994.

Han, X., Gui, B., Xiong, C., Zhao, L., Liang, J., Sun, L., Yang, X., Yu, W., Si, W., and Yan, R., et al. (2014). Destabilizing LSD1 by Jade-2 Promotes Neurogenesis: An Antibraking System in Neural Development. Molecular Cell *55*, 482-494.

Hara, M.R., Agrawal, N., Kim, S.F., Cascio, M.B., Fujimuro, M., Ozeki, Y., Takahashi, M., Cheah, J.H., Tankou, S.K., and Hester, L.D., et al. (2005). S -nitrosylated GAPDH initiates apoptotic cell death by nuclear translocation following Siah1 binding. Nat Cell Biol *7*, 665-674.

He, D., Marie, C., Zhao, C., Kim, B., Wang, J., Deng, Y., Clavairoly, A., Frah, M., Wang, H., and He, X., et al. (2016). Chd7 cooperates with Sox10 and regulates the onset of CNS myelination and remyelination. Nat Neurosci *19*, 678-689.

He, M., Howe, D.G., and McCarthy, K.D. (1996). Oligodendroglial Signal Transduction Systems Are Regulated by Neuronal Contact. Journal of Neurochemistry *67*, 1491-1499.

Heide, H., Bleier, L., Steger, M., Ackermann, J., Dröse, S., Schwamb, B., Zörnig, M., Reichert, A.S., Koch, I., and Wittig, I., et al. (2012). Complexome Profiling Identifies TMEM126B as a Component of the Mitochondrial Complex I Assembly Complex. Cell Metabolism *16*, 538-549.

Howe, K., Clark, M.D., Torroja, C.F., Torrance, J., Berthelot, C., Muffato, M., Collins, J.E., Humphray, S., McLaren, K., and Matthews, L., et al. (2013). The zebrafish reference genome sequence and its relationship to the human genome. Nature *496*, 498-503.

Huang, J., Sengupta, R., Espejo, A.B., Lee, M.G., Dorsey, J.A., Richter, M., Opravil, S., Shiekhattar, R., Bedford, M.T., and Jenuwein, T., et al. (2007). p53 is regulated by the lysine demethylase LSD1. Nature *449*, 105-108.

Jackson, E.L., Garcia-Verdugo, J.M., Gil-Perotin, S., Roy, M., Quinones-Hinojosa, A., VandenBerg, S., and Alvarez-Buylla, A. (2006). PDGFRα-Positive B Cells Are Neural Stem Cells in the Adult SVZ that Form Glioma-like Growths in Response to Increased PDGF Signaling. Neuron *51*, 187-199.

Jenuwein, T., and Allis, C.D. (2001). Translating the Histone Code. Science *293*, 1074-1080.

Jeserich, G., Klempahn, K., and Pfeiffer, M. (2008). Features and Functions of Oligodendrocytes and Myelin Proteins of Lower Vertebrate Species. J Mol Neurosci *35*, 117-126.

Kerenyi, M.A., Shao, Z., Hsu, Y.-J., Guo, G., Luc, S., O'Brien, K., Fujiwara, Y., Peng, C., Nguyen, M., and Orkin, S.H. (2013). Histone demethylase Lsd1 represses hematopoietic stem and progenitor cell signatures during blood cell maturation. eLife *2*, e00633.

Kessaris, N., Fogarty, M., Iannarelli, P., Grist, M., Wegner, M., and Richardson, W.D. (2006). Competing waves of oligodendrocytes in the forebrain and postnatal elimination of an embryonic lineage. Nat Neurosci *9*, 173-179.

Kim, J., Chu, J., Shen, X., Wang, J., and Orkin, S.H. (2008). An extended transcriptional network for pluripotency of embryonic stem cells. Cell *132*.

Kragten, E., Lalande, I., Zimmermann, K., Roggo, S., Schindler, P., Muller, D., van Oostrum, J., Waldmeier, P., and Furst, P. (1998). Glyceraldehyde-3-phosphate dehydrogenase, the putative target of the antiapoptotic compounds CGP 3466 and R-(-)-deprenyl. The Journal of biological chemistry *273*, 5821-5828.

Lan, H., Tan, M., Zhang, Q., Yang, F., Wang, S., Li, H., Xiong, X., and Sun, Y. (2019). LSD1 destabilizes FBXW7 and abrogates FBXW7 functions independent of its demethylase activity. Proceedings of the National Academy of Sciences of the United States of America *116*, 12311-12320.

Lee, K.J., and Jessell, T.M. (1999). The specification of dorsal cell fates in the vertebrate central nervous system. Annual review of neuroscience *22*, 261-294.

Lee, M.G., Wynder, C., Cooch, N., and Shiekhattar, R. (2005a). An essential role for CoREST in nucleosomal histone 3 lysine 4 demethylation. Nature *437*, 432-435.

Lee, M.G., Wynder, C., Cooch, N., and Shiekhattar, R. (2005b). An essential role for CoREST in nucleosomal histone 3 lysine 4 demethylation. Nature *437*, 432-435.

Lee, S.-K., Lee, B., Ruiz, E.C., and Pfaff, S.L. (2005c). Olig2 and Ngn2 function in opposition to modulate gene expression in motor neuron progenitor cells. Genes & Development *19*, 282-294.

Levine, J.M., and Reynolds, R. (1999). Activation and Proliferation of Endogenous Oligodendrocyte Precursor Cells during Ethidium Bromide-Induced Demyelination. Experimental Neurology *160*, 333-347.

Li, L., Liu, X., He, L., Yang, J., Pei, F., Li, W., Liu, S., Chen, Z., Xie, G., and Xu, B., et al. (2017) ZNF516 suppresses EGFR by targeting the CtBP/LSD1/CoREST complex to chromatin. Nat Commun *8*, 1-17.

Lieschke, G.J., and Currie, P.D. (2007). Animal models of human disease: zebrafish swim into view. Nat Rev Genet *8*, 353-367.

Liu, J., Magri, L., Zhang, F., Marsh, N.O., Albrecht, S., Huynh, J.L., Kaur, J., Kuhlmann, T., Zhang, W., and Slesinger, P.A., et al. (2015). Chromatin Landscape Defined by Repressive Histone Methylation during Oligodendrocyte Differentiation. J. Neurosci. *35*, 352-365.

Liu, J., Saponjian, Y., Mahoney, M.M., Staley, K.J., and Berdichevsky, Y. (2017). Epileptogenesis in organotypic hippocampal cultures has limited dependence on culture medium composition. PloS one *12*, e0172677.

Löwe, O., Rezende, F., Heidler, J., Wittig, I., Helfinger, V., Brandes, R.P., and Schröder, K. (2019). BIAM switch assay coupled to mass spectrometry identifies novel redox targets of NADPH oxidase 4. Redox Biology *21*, 101125.

Lu, Q.R., Sun, T., Zhu, Z., Ma, N., Garcia, M., Stiles, C.D., and Rowitch, D.H. (2002). Common Developmental Requirement for Olig Function Indicates a Motor Neuron/Oligodendrocyte Connection. Cell *109*, 75-86.

Lu, Q.R., Yuk, D.-i., Alberta, J.A., Zhu, Z., Pawlitzky, I., Chan, J., McMahon, A.P., Stiles, C.D., and Rowitch, D.H. (2000). Sonic Hedgehog–Regulated Oligodendrocyte Lineage Genes Encoding bHLH Proteins in the Mammalian Central Nervous System. Neuron *25*, 317-329.

Lupo, G., Harris, W.A., and Lewis, K.E. (2006). Mechanisms of ventral patterning in the vertebrate nervous system. Nat Rev Neurosci *7*, 103-114.

Maes, T., Mascaró, C., Tirapu, I., Estiarte, A., Ciceri, F., Lunardi, S., Guibourt, N., Perdones, A., Lufino, M.M.P., and Somervaille, T.C.P., et al. (2018). ORY-1001, a Potent and Selective Covalent KDM1A Inhibitor, for the Treatment of Acute Leukemia. Cancer cell *33*, 495-511.e12.

Maiques-Diaz, A., Spencer, G.J., Lynch, J.T., Ciceri, F., Williams, E.L., Amaral, F.M.R., Wiseman, D.H., Harris, W.J., Li, Y., and Sahoo, S., et al. (2018). Enhancer Activation by Pharmacologic Displacement of LSD1 from GFI1 Induces Differentiation in Acute Myeloid Leukemia. Cell Reports *22*, 3641-3659.

Manta, B., Hugo, M., Ortiz, C., Ferrer-Sueta, G., Trujillo, M., and Denicola, A. (2009). The peroxidase and peroxynitrite reductase activity of human erythrocyte peroxiredoxin 2. Archives of Biochemistry and Biophysics *484*, 146-154.

Marie, C., Clavairoly, A., Frah, M., Hmidan, H., Yan, J., Zhao, C., van Steenwinckel, J., Daveau, R., Zalc, B., and Hassan, B., et al. (2018). Oligodendrocyte precursor survival and differentiation requires chromatin remodeling by Chd7 and Chd8. PNAS *115*, E8246-E8255.

Marin-Husstege, M., Muggironi, M., Liu, A., and Casaccia-Bonnefil, P. (2002). Histone Deacetylase Activity Is Necessary for Oligodendrocyte Lineage Progression. J. Neurosci. *22*, 10333-10345.

Masahira, N., Takebayashi, H., Ono, K., Watanabe, K., Ding, L., Furusho, M., Ogawa, Y., Nabeshima, Y.-i., Alvarez-Buylla, A., and Shimizu, K., et al. (2006). Olig2-positive progenitors in the embryonic spinal cord give rise not only to motoneurons and oligodendrocytes, but also to a subset of astrocytes and ependymal cells. Developmental Biology *293*, 358-369.

Metzger, E., Wissmann, M., Yin, N., Müller, J.M., Schneider, R., Peters, Antoine H. F. M., Günther, T., Buettner, R., and Schüle, R. (2005). LSD1 demethylates repressive

histone marks to promote androgen-receptor-dependent transcription. Nature *437*, 436-439.

Meyer, M., Schreck, R., and Baeuerle, P.A. (1993). H2O2 and antioxidants have opposite effects on activation of NF-kappa B and AP-1 in intact cells: AP-1 as secondary antioxidant-responsive factor. The EMBO Journal *12*, 2005-2015.

Minocha, S., Valloton, D., Brunet, I., Eichmann, A., Hornung, J.-P., and Lebrand, C. (2015). NG2 glia are required for vessel network formation during embryonic development. eLife *4*.

Morel, Y., and Barouki, R. (1999). Repression of gene expression by oxidative stress. Biochemical Journal *342*, 481-496.

Münzel, E.J., Schaefer, K., Obirei, B., Kremmer, E., Burton, E.A., Kuscha, V., Becker, C.G., Brösamle, C., Williams, A., and Becker, T. (2012). Claudin k is specifically expressed in cells that form myelin during development of the nervous system and regeneration of the optic nerve in adult zebrafish. Glia *60*, 253-270.

Nepusz, T., Yu, H., and Paccanaro, A. (2012). Detecting overlapping protein complexes in protein-protein interaction networks. Nat Methods *9*, 471-472.

Nielsen, J.A., Hudson, L.D., and Armstrong, R.C. (2002). Nuclear organization in differentiating oligodendrocytes. Journal of Cell Science *115*, 4071-4079.

Nishiyama, A., Komitova, M., Suzuki, R., and Zhu, X. (2009). Polydendrocytes (NG2 cells): multifunctional cells with lineage plasticity. Nat Rev Neurosci *10*, 9-22.

Niwa, H., and Umehara, T. (2017). Structural insight into inhibitors of flavin adenine dinucleotide-dependent lysine demethylases. Epigenetics *12*, 340-352.

Nott, A., Watson, P.M., Robinson, J.D., Crepaldi, L., and Riccio, A. (2008). S - nitrosylation of histone deacetylase 2 induces chromatin remodelling in neurons. Nature *455*, 411-415.

Orre, L.M., Vesterlund, M., Pan, Y., Arslan, T., Zhu, Y., Fernandez Woodbridge, A., Frings, O., Fredlund, E., and Lehtiö, J. (2019). SubCellBarCode: Proteome-wide Mapping of Protein Localization and Relocalization. Molecular Cell *73*, 166-182.e7.

Park, H.-C., Mehta, A., Richardson, J.S., and Appel, B. (2002). olig2 Is Required for Zebrafish Primary Motor Neuron and Oligodendrocyte Development. Developmental Biology *248*, 356-368.

Park, H.-C., Shin, J., Roberts, R.K., and Appel, B. (2007). An olig2 reporter gene marks oligodendrocyte precursors in the postembryonic spinal cord of zebrafish. Developmental Dynamics *236*, 3402-3407.

Peng, B., Shi, R., Jiang, W., Ding, Y.-H., Dong, M.-Q., Zhu, W.-G., and Xu, X. (2017). Phosphorylation of LSD1 by PLK1 promotes its chromatin release during mitosis. Cell Biosci *7*, 1-7.

Perillo, B., Ombra, M.N., Bertoni, A., Cuozzo, C., Sacchetti, S., Sasso, A., Chiariotti, L., Malorni, A., Abbondanza, C., and Avvedimento, E.V. (2008). DNA Oxidation as Triggered by H3K9me2 Demethylation Drives Estrogen-Induced Gene Expression. Science *319*, 202-206.

Poole, L.B., Karplus, P.A., and Claiborne, A. (2004). Protein sulfenic acids in redox signaling. Annual review of pharmacology and toxicology *44*, 325-347.

Poole, L.B., Zeng, B.-B., Knaggs, S.A., Yakubu, M., and King, S.B. (2005). Synthesis of chemical probes to map sulfenic acid modifications on proteins. Bioconjugate chemistry *16*, 1624-1628.

Poschmann, G., Seyfarth, K., Besong Agbo, D., Klafki, H.-W., Rozman, J., Wurst, W., Wiltfang, J., Meyer, H.E., Klingenspor, M., and Stühler, K. (2014). High-fat diet induced isoform changes of the Parkinson's disease protein DJ-1. Journal of proteome research *13*, 2339-2351.

Preston, M.A., and Macklin, W.B. (2015). Zebrafish as a Model to Investigate CNS Myelination. Glia *63*, 177-193.

Pringle, N.P., and Richardson, W.D. (1993). A singularity of PDGF alpha-receptor expression in the dorsoventral axis of the neural tube may define the origin of the oligodendrocyte lineage. Development *117*, 525-533.

Prusevich, P., Kalin, J.H., Ming, S.A., Basso, M., Givens, J., Li, X., Hu, J., Taylor, M.S., Cieniewicz, A.M., and Hsiao, P.-Y., et al. (2014). A selective phenelzine analogue inhibitor of histone demethylase LSD1. ACS chemical biology *9*, 1284-1293.

Raudvere, U., Kolberg, L., Kuzmin, I., Arak, T., Adler, P., Peterson, H., and Vilo, J. (2019). g:Profiler: a web server for functional enrichment analysis and conversions of gene lists (2019 update). Nucleic Acids Res *47*, W191-W198.

Ravanelli, A.M., and Appel, B. (2015). Motor neurons and oligodendrocytes arise from distinct cell lineages by progenitor recruitment. Genes Dev. *29*, 2504-2515.

Ravanelli, A.M., Kearns, C.A., Powers, R.K., Wang, Y., Hines, J.H., Donaldson, M.J., and Appel, B. (2018). Sequential specification of oligodendrocyte lineage cells by distinct levels of Hedgehog and Notch signaling. Developmental Biology *444*, 93-106.

Reynolds, R., and Hardy, R. (1997). Oligodendroglial progenitors labeled with the O4 antibody persist in the adult rat cerebral cortex in vivo. Journal of Neuroscience Research *47*, 455-470.

Ricq, E.L., Hooker, J.M., and Haggarty, S.J. (2016). Activity-dependent Regulation of Histone Lysine Demethylase KDM1A by a Putative Thiol/Disulfide Switch*. The Journal of biological chemistry *291*, 24756-24767.

Roesch, K., Jadhav, A.P., Trimarchi, J.M., Stadler, M.B., Roska, B., Sun, B.B., and Cepko, C.L. (2008). The transcriptome of retinal Müller glial cells. Journal of Comparative Neurology *509*, 225-238.

Sakamoto, A., Hino, S., Nagaoka, K., Anan, K., Takase, R., Matsumori, H., Ojima, H., Kanai, Y., Arita, K., and Nakao, M. (2015). Lysine Demethylase LSD1 Coordinates Glycolytic and Mitochondrial Metabolism in Hepatocellular Carcinoma Cells. Cancer Res *75*, 1445-1456.

Sambeat, A., Gulyaeva, O., Dempersmier, J., Tharp, K.M., Stahl, A., Paul, S.M., and Sul, H.S. (2016). LSD1 Interacts with Zfp516 to Promote UCP1 Transcription and Brown Fat Program. Cell Reports *15*, 2536-2549.

Schmidt, D.M.Z., and McCafferty, D.G. (2007). trans-2-Phenylcyclopropylamine is a mechanism-based inactivator of the histone demethylase LSD1. Biochemistry *46*, 4408-4416.

Shannon, P., Markiel, A., Ozier, O., Baliga, N.S., Wang, J.T., Ramage, D., Amin, N., Schwikowski, B., and Ideker, T. (2003). Cytoscape: A Software Environment for Integrated Models of Biomolecular Interaction Networks. Genome Res. *13*, 2498-2504.

Shi, Y., Lan, F., Matson, C., Mulligan, P., Whetstine, J.R., Cole, P.A., Casero, R.A., and Shi, Y. (2004). Histone Demethylation Mediated by the Nuclear Amine Oxidase Homolog LSD1. Cell *119*, 941-953.

Shin, J., Park, H.-C., Topczewska, J.M., Mawdsley, D.J., and Appel, B. (2003). Neural cell fate analysis in zebrafish using olig2 BAC transgenics. Methods Cell Sci *25*, 7-14.

Sobottka, B., Ziegler, U., Kaech, A., Becher, B., and Goebels, N. (2011). CNS live imaging reveals a new mechanism of myelination: The liquid croissant model. Glia *59*, 1841-1849.

Son, J.H., Chun, H.S., Joh, T.H., Cho, S., Conti, B., and Lee, J.W. (1999). Neuroprotection and Neuronal Differentiation Studies Using Substantia Nigra Dopaminergic Cells Derived from Transgenic Mouse Embryos. J. Neurosci. *19*, 10-20.

Sorna, V., Theisen, E.R., Stephens, B., Warner, S.L., Bearss, D.J., Vankayalapati, H., and Sharma, S. (2013). High-throughput virtual screening identifies novel N'-(1-phenylethylidene)-benzohydrazides as potent, specific, and reversible LSD1 inhibitors. Journal of medicinal chemistry *56*, 9496-9508.

Spitzer, S.O., Sitnikov, S., Kamen, Y., Evans, K.A., Kronenberg-Versteeg, D., Dietmann, S., Faria, O. de, Agathou, S., and Káradóttir, R.T. (2019). Oligodendrocyte Progenitor Cells Become Regionally Diverse and Heterogeneous with Age. Neuron *101*, 459-471.e5.

Sprüssel, A., Schulte, J.H., Weber, S., Necke, M., Händschke, K., Thor, T., Pajtler, K.W., Schramm, A., König, K., and Diehl, L., et al. (2012). Lysine-specific demethylase 1 restricts hematopoietic progenitor proliferation and is essential for terminal differentiation. Leukemia *26*, 2039-2051.

Stevens, B., Porta, S., Haak, L.L., Gallo, V., and Fields, R.D. (2002). Adenosine: A Neuron-Glial Transmitter Promoting Myelination in the CNS in Response to Action Potentials. Neuron *36*, 855-868.

Stöcker, S., Maurer, M., Ruppert, T., and Dick, T.P. (2018). A role for 2-Cys peroxiredoxins in facilitating cytosolic protein thiol oxidation. Nature chemical biology *14*, 148-155.

Strathmann, F.G., Wang, X., and Mayer-Pröschel, M. (2007). Identification of two novel glial-restricted cell populations in the embryonic telencephalon arising from unique origins. BMC developmental biology *7*, 33.

Suuronen, T., Kolehmainen, P., and Salminen, A. (2000). Protective effect of l-Deprenyl against apoptosis induced by okadaic acid in cultured neuronal cells. Biochemical Pharmacology *59*, 1589-1595.

Swiss, V.A., Nguyen, T., Dugas, J., Ibrahim, A., Barres, B., Androulakis, I.P., and Casaccia, P. (2011). Identification of a Gene Regulatory Network Necessary for the Initiation of Oligodendrocyte Differentiation. PLOS ONE *6*, e18088.

Szklarczyk, D., Franceschini, A., Wyder, S., Forslund, K., Heller, D., Huerta-Cepas, J., Simonovic, M., Roth, A., Santos, A., and Tsafou, K.P., et al. (2015). STRING v10:

protein–protein interaction networks, integrated over the tree of life. Nucleic Acids Res *43*, D447-D452.

Takeuchi, M., Fuse, Y., Watanabe, M., Andrea, C.-S., Takeuchi, M., Nakajima, H., Ohashi, K., Kaneko, H., Kobayashi-Osaki, M., and Yamamoto, M., et al. (2015). LSD1/KDM1A promotes hematopoietic commitment of hemangioblasts through downregulation of Etv2. PNAS *112*, 13922-13927.

Tanabe, Y., William, C., and Jessell, T.M. (1998). Specification of Motor Neuron Identity by the MNR2 Homeodomain Protein. Cell *95*, 67-80.

Tatton, W.G., and Chalmers-Redman, R.M. (1996). Modulation of gene expression rather than monoamine oxidase inhibition: (-)-deprenyl-related compounds in controlling neurodegeneration. Neurology *47*, S171-83.

Tekki-Kessaris, N., Woodruff, R., Hall, A.C., Gaffield, W., Kimura, S., Stiles, C.D., Rowitch, D.H., and Richardson, W.D. (2001). Hedgehog-dependent oligodendrocyte lineage specification in the telencephalon. Development *128*, 2545-2554.

Timsit, S., Martinez, S., Allinquant, B., Peyron, F., Puelles, L., and Zalc, B. (1995). Oligodendrocytes originate in a restricted zone of the embryonic ventral neural tube defined by DM-20 mRNA expression. J. Neurosci. *15*, 1012-1024.

Tsai, H.-H., Niu, J., Munji, R., Davalos, D., Chang, J., Zhang, H., Tien, A.-C., Kuo, C.J., Chan, J.R., and Daneman, R., et al. (2016). Oligodendrocyte precursors migrate along vasculature in the developing nervous system. Science *351*, 379-384.

(2019). UniProt: a worldwide hub of protein knowledge. Nucleic Acids Res *47*, D506-D515.

van der Reest, J., Lilla, S., Zheng, L., Zanivan, S., and Gottlieb, E. (2018). Proteome-wide analysis of cysteine oxidation reveals metabolic sensitivity to redox stress. Nat Commun *9*, 1-16.

van Tilborg, E., Theije, Caroline G. M. de, van Hal, M., Wagenaar, N., Vries, L.S.d., Benders, M.J., Rowitch, D.H., and Nijboer, C.H. (2018). Origin and dynamics of oligodendrocytes in the developing brain: Implications for perinatal white matter injury. Glia *66*, 221-238.

Velu, C.S., Niture, S.K., Doneanu, C.E., Pattabiraman, N., and Srivenugopal, K.S. (2007). Human p53 is Inhibited by Glutathionylation of Cysteines Present in the Proximal DNA-Binding Domain During Oxidative Stress†. Biochemistry *46*, 7765-7780.

Wang, J., Scully, K., Zhu, X., Cai, L., Zhang, J., Prefontaine, G.G., Krones, A., Ohgi, K.A., Zhu, P., and Garcia-Bassets, I., et al. (2007). Opposing LSD1 complexes function in developmental gene activation and repression programmes. Nature *446*, 882-887.

Wang, Y., Wu, Q., Yang, P., Wang, C., Liu, J., Ding, W., Liu, W., Bai, Y., Yang, Y., and Wang, H., et al. (2016) LSD1 co-repressor Rcor2 orchestrates neurogenesis in the developing mouse brain. Nat Commun *7*, 1-14.

Wang, Y., Zhang, H., Chen, Y., Sun, Y., Yang, F., Yu, W., Liang, J., Sun, L., Yang, X., and Shi, L., et al. (2009). LSD1 Is a Subunit of the NuRD Complex and Targets the Metastasis Programs in Breast Cancer. Cell *138*, 660-672.

Wegner, M. (2008). A Matter of Identity: Transcriptional Control in Oligodendrocytes. J Mol Neurosci *35*, 3-12.

Whyte, W.A., Bilodeau, S., Orlando, D.A., Hoke, H.A., Frampton, G.M., Foster, C.T., Cowley, S.M., and Young, R.A. (2012). Enhancer decommissioning by LSD1 during embryonic stem cell differentiation. Nature *482*, 221-225.

Wu, Z., Connolly, J., and Biggar, K.K. (2017). Beyond histones - the expanding roles of protein lysine methylation. The FEBS journal *284*, 2732-2744.

Ye, F., Chen, Y., Hoang, T., Montgomery, R.L., Zhao, X.-h., Bu, H., Hu, T., Taketo, M.M., van Es, J.H., and Clevers, H., et al. (2009). HDAC1 and HDAC2 Regulate Oligodendrocyte Differentiation By Disrupting β-Catenin-TCF Interaction. Nature neuroscience *12*, 829-838.

Yokoyama, A., Takezawa, S., Schüle, R., Kitagawa, H., and Kato, S. (2008). Transrepressive Function of TLX Requires the Histone Demethylase LSD1. Molecular and Cellular Biology *28*, 3995-4003.

Yu, Y., Chen, Y., Kim, B., Wang, H., Zhao, C., He, X., Liu, L., Liu, W., Wu, L.M.N., and Mao, M., et al. (2013). Olig2 Targets Chromatin Remodelers to Enhancers to Initiate Oligodendrocyte Differentiation. Cell *152*, 248-261.

Zhu, D., Hölz, S., Metzger, E., Pavlovic, M., Jandausch, A., Jilg, C., Galgoczy, P., Herz, C., Moser, M., and Metzger, D., et al. (2014) Lysine-specific demethylase 1 regulates differentiation onset and migration of trophoblast stem cells. Nat Commun *5*, 1-14.

6 Appendix

Table 13: LSD1 co-IP in proliferating A2B5+ OPCs – all identified proteins normalized to IgG

Uniprot ID	Gene name	Coverage [%]	Unique peptides	-log p-value Diff_Proli
Q9CYL5	*Glipr2*	31.2	3	7.78013
P97351	*Rps3a*	58	16	6.36593
P84104	*Srsf3; Gm12355*	21.3	3	6.05733
Q9R0H0	*Acox1*	13.3	5	5.41038
Q8CBY8	*Dctn4*	11.6	4	5.15012
Q61655	*Ddx19a; Ddx19b*	10.5	2	5.06314
E9Q9B7	*Kidins220*	3.2	4	5.04387
P23116	*Eif3a*	2.5	2	4.9951
Q9DB20	*Atp5o*	62	12	4.8999
Q68FG2	*Sptbn2*	4.4	4	4.828
Q8C2Q3	*Rbm14*	25.1	10	4.79263
P50149	*Gnai1*	32.8	3	4.72357
Q9WVJ2	*Psmd13*	6.9	2	4.64636
Q7TSH3	*Znf516*	15.3	13	4.63534
P25206	*Mcm3*	4.1	2	4.52073
Q9CXS4	*Cenpv*	24.6	3	4.50578
Q80Z24	*Negr1*	14.9	3	4.44797
Q03265	*Atp5a1*	54.6	32	4.44538
Q9DCT2	*Ndufs3*	9.9	2	4.44344
Q9Z0N1	*Eif2s3x*	10.2	3	4.43218
Q9CX86	*Hnrnpa0*	23.3	4	4.42995
P26516	*Psmd7*	8.7	2	4.38573
P07901	*Hsp90aa1*	14.1	3	4.36129
P30999	*Ctnnd1*	6.9	3	4.32739
Q8VDN2	*Atp1a1*	14.5	5	4.32
P15116	*Cdh2*	5.2	2	4.31348
P63038	*Hspd1*	42.2	17	4.27735
Q8BHC4	*Dcakd*	24.2	4	4.09952
Q8BG95	*Ppp1r12b*	5.9	3	4.05773
P05480	*Src*	10.8	3	4.03938
Q9CPQ3	*Tomm22*	32.4	2	4.00025
Q8VHM5	*Hnrnpr*	9.7	2	3.99648
P47738	*Aldh2*	13.5	2	3.92566
O54931	*Pakap; Akap2*	3.5	2	3.87238
Q9CZ13	*Uqcrc1*	6.9	2	3.81675
Q8BU30	*Iars*	4	3	3.76797
Q8BFR5	*Tufm*	14.4	4	3.76576
Q8C845	*Efhd2*	58.3	13	3.76261
P61027	*Rab10*	11.5	2	3.74554

Q6PIE5	*Atp1a2; Atp1a3*	19.5	8	3.68273
Q8CGB3	*Uaca*	1.9	2	3.67429
Q7TPR4	*Actn1*	15.1	3	3.65041
Q8JZK9	*Hmgcs1*	13.5	4	3.64291
Q80U35	*Arhgef17*	5.7	6	3.62574
Q99JR1	*Sfxn1*	22.4	4	3.61014
Q8HW98	*Iglon5*	5.7	2	3.57693
P63325	*Rps10*	29.1	4	3.54949
P61164	*Actr1a; Actr1b*	19.7	4	3.5483
Q6P4T2	*Snrnp200*	2.3	4	3.52015
Q9D1I6	*Mrpl14*	20	2	3.49981
Q68FL6	*Mars*	6.7	3	3.39494
P38647	*Hspa9*	31.7	20	3.38426
Q8R0X7	*Sgpl1*	8.8	3	3.38341
Q3UDD3	*Poldip3*	23.1	6	3.33588
Q920L1	*Fads1*	22.3	2	3.30667
P84228	*H3f3a; Hist1h3b; Hist1h3a; H3f3c*	36.3	9	3.22105
P63037	*Dnaja1*	17.4	4	3.18994
P45591	*Cfl2*	33.7	2	3.15004
Q8CDN6	*Txnl1*	10	2	3.13495
Q3U3C9	*Gse1*	6	5	3.062
Q8VEM8	*Slc25a3*	18.2	4	3.05316
P54071	*Idh2*	18.7	2	3.03508
O88712	*Ctbp1*	17.5	6	2.93407
Q6P6M7	*Sepsecs*	3.6	2	2.79867
Q6P9Q6	*Fkbp15*	13.7	10	2.75554
Q9EP89	*Lactb*	7.4	4	2.73238
Q03173	*Enah*	19	10	2.71485
Q9EPU0	*Upf1*	5	4	2.69277
Q8BGS1	*Epb41l5*	8.1	3	2.66987
O88685	*Psmc3*	10.8	2	2.64394
Q6AXB7	*Fmr1*	13.8	5	2.64236
Q9JKF1	*Iqgap1*	4.9	5	2.62552
Q641P0	*Actr3b*	23.9	3	2.55861
Q8CFE3	*Rcor1*	40.8	9	2.33888
Q9JJW6	*Alyref; Alyref2*	31.4	6	2.30229
Q6PGA0	*Rcor3*	13.1	3	2.21627
Q99KI0	*Aco2*	7.3	3	2.17192
P62320	*Snrpd3*	12.7	2	2.15499
P43277	*Hist1h1d*	27.1	2	2.09296
Q91VA7	*Idh3b*	12.8	3	2.09262
Q61666	*Hira*	3.3	2	1.97934
Q6ZPK0	*Phf21a*	38.1	17	1.94008
Q8BJA3	*Hmbox1*	11.3	3	1.67826
Q9CU65	*Zmym2*	5.9	6	1.6223

P70288	*Hdac2*	21.3	4	1.43029
P08775	*Polr2a*	4.5	6	1.29116
Q76KF0	*Sema6d*	10.5	7	1.27677
Q569Z6	*Thrap3*	13.7	11	1.0584
Q9Z275	*Rlbp1*	12	2	1.05442
Q8CFI7	*Polr2b*	6	5	0.963159

Table 14: LSD1 co-IP in A2B5+ OPCs after 24 h of differentiation – all identified proteins normalized to IgG

Uniprot ID	Gene name	Coverage [%]	Unique peptides	- log p value Diff_IGG
Q6ZPK0	*Phf21a*	38.1	17	9.01432
P14115	*Rpl27a*	23.6	4	8.37572
G3X9J0	*Sipa1l3*	19.3	22	8.35782
Q9JHU4	*Dync1h1*	11.3	36	8.30565
Q7TSH3	*Znf516*	15.3	13	8.27184
Q9QXS1	*Plec*	12.1	37	8.23296
Q8BVU0	*Lrch3*	31.8	18	7.84446
P70429	*Enah*	19	10	7.82601
O88712	*Ctbp1*	17.5	6	7.47703
P70248	*Myo1e*	10.2	9	7.43433
Q80X90	*Flnb*	11.5	16	7.27117
Q9JJ28	*Flii*	23.1	21	7.23692
Q8CFE3	*Rcor1*	40.8	9	7.16694
Q5SXA5	*Tom1l2*	42.2	13	6.97918
P19096	*Fasn*	14.7	23	6.97691
Q6P9Q6	*Fkbp15*	13.7	10	6.96969
Q8C796	*Rcor2*	27.9	10	6.94158
P63038	*Hspd1*	42.2	17	6.78761
Q5PR69	*C530008M17Rik; Kiaa1211*	20.2	18	6.74445
Q9WTI7	*Myo1c*	21.1	17	6.69979
P68040	*Gnb2l1*	37.9	8	6.64447
Q6ZQ88	*Kdm1a*	52.2	38	6.5805
Q9Z1G4	*Atp6v0a1*	12.9	8	6.57419
Q60930	*Vdac2*	59.3	15	6.5071
P39447	*Tjp1*	20.8	28	6.47151
P62852	*Rps25*	32.3	4	6.45493
Q8BGH2	*Samm50*	24.7	11	6.37239
Q04447	*Ckb*	31	11	6.37066
P51880	*Fabp7*	72	9	6.36976
Q9JHJ0	*Tmod3*	31.5	9	6.32843
Q2KN98	*Specc1l*	7.2	6	6.22074
Q9D8E6	*Rpl4*	40.1	19	6.17204

Q91Z25	*Arpc1b*	41.8	11	6.12598
Q3UDC3	*Tom1*	36.2	12	6.05074
P61161	*Actr2*	39.8	19	6.04101
Q6PGA0	*Rcor3*	13.1	3	6.03815
Q569Z6	*Thrap3*	13.7	11	6.02504
Q91YR1	*Twf1*	38.9	12	5.95928
P62264	*Rps14*	41.7	9	5.86669
P60710	*Actb*	89.1	4	5.8566
Q80TE4	*Sipa1l2*	14.3	14	5.81126
Q9JM76	*Arpc3*	52.2	9	5.7744
Q9D898	*Arpc5l*	54.9	6	5.76617
Q02053	*Uba1*	21.4	13	5.73738
Q9JMH9	*Myo18a*	36	65	5.73222
Q6P6M7	*Sepsecs*	3.6	2	5.69652
Q62261	*Sptbn1*	14.9	24	5.61929
Q6DFV3	*Arhgap21*	11.5	13	5.58603
Q9WTM5	*Ruvbl2*	16.8	6	5.57483
P62702	*Rps4x; Gm15013*	43.3	11	5.55441
Q8BG81	*Poldip3*	23.1	6	5.53889
Q61584	*Fxr1*	14.1	5	5.52196
Q76KF0	*Sema6d*	10.5	7	5.35536
P13595	*Ncam1*	34.8	15	5.32705
Q8BTM8	*Flna*	12.5	19	5.2928
Q9CU65	*Zmym2*	5.9	6	5.28575
Q3UH68	*Limch1*	24.9	23	5.25702
Q9DBR7	*Ppp1r12a*	28.3	23	5.23027
P55096	*Abcd3*	25.5	12	5.22755
Q5SVJ1	*Camk2b*	22.1	6	5.17843
Q61553	*Fscn1*	43.8	16	5.16811
Q9JL26	*Fmnl2*	22.4	22	5.12167
P17426	*Ap2a1*	17.7	8	5.11124
Q8CAQ8	*Immt*	50.2	30	5.10027
Q6ZWY3	*Rps27l; Rps27*	25.6	2	5.04251
Q8CH77	*Nav1*	20.4	30	5.01868
Q921L6	*Cttn*	25.1	10	4.98846
Q80UE4	*Epb4.1l2; Epb41l2*	13.1	6	4.98717
Q9D0R8	*Lsm12*	15.4	2	4.9367
O88990		32.2	1	4.90789
Q8VEM8	*Slc25a3*	18.2	4	4.87294
P60867	*Rps20*	41.2	6	4.85518
P21107	*Tpm3*	30.8	2	4.84549
P80315	*Cct4*	36.4	14	4.82912
B9EJ86	*Osbpl8*	11.6	7	4.77717
P45591	*Cfl2*	33.7	2	4.77262
Q8C845	*Efhd2*	58.3	13	4.7241

P59999	*Arpc4*	64.9	16	4.70153
P70288	*Hdac2*	21.3	4	4.66056
P23242	*Gja1*	29.3	9	4.60044
Q7TQD7	*Myo1b*	46.6	50	4.58614
E9Q447	*Sptan1*	20.6	41	4.56414
P63276	*Rps17*	46.7	5	4.5609
P47757	*Capzb*	80.9	7	4.52656
Q9CZU6	*Cs; Csl*	9.5	4	4.48775
P68033	*Actc1; Actg2; Acta1; Acta2*	55.4	5	4.48734
P14131	*Rps16*	51.4	10	4.48588
P47738	*Aldh2*	13.5	2	4.4852
P58252	*Eef2*	29.3	17	4.47594
F2Z471	*Vdac1*	70.5	2	4.46569
P08775	*Polr2a*	4.5	6	4.40603
Q9Z0U1	*Tjp2*	17.9	12	4.38221
P62880	*Gnb2*	63.8	7	4.36177
P47754	*Capza2*	76.9	15	4.35068
P11499	*Hsp90ab1*	37	16	4.26217
P38647	*Hspa9*	31.7	20	4.26035
P14869	*Rplp0*	43.8	12	4.25115
P62245	*Rps15a*	55.4	8	4.245
Q9CRB9	*Chchd3*	37.4	7	4.22493
Q99KP6	*Prpf19*	22.4	7	4.21782
P52480	*Pkm*	19.8	6	4.20974
P80314	*Cct2*	23	8	4.20043
Q3U0I3	*Cct3*	10.5	5	4.1995
Q9R0Q6	*Arpc1a*	53	14	4.10363
Q8BH44	*Coro2b*	56.5	29	4.08267
P62631	*Eef1a1*	49.4	27	4.07733
Q02248	*Ctnnb1*	20.2	11	4.07638
Q60790	*Rasa3*	29	17	4.07302
Q8BP43	*Tpm1*	31.9	6	4.05216
O08638	*Myh11*	12.7	3	4.04676
Q8BJA3	*Hmbox1*	11.3	3	4.03354
Q6R891	*Ppp1r9b*	37.3	24	3.99409
O88569	*Hnrnpa2b1*	32.9	8	3.92488
Q8C2Q3	*Rbm14*	25.1	10	3.92032
Q5SXY1	*Specc1*	32	28	3.84772
P60766	*Cdc42*	32.5	4	3.83469
P51150	*Rab7a*	30	5	3.82775
P12960	*Cntn1*	41.9	31	3.79274
Q99JY9	*Actr3*	66.5	23	3.79065
Q6PFF0	*Scaf4*	3.9	3	3.77051
Q6PIE5	*Atp1a2; Atp1a3*	19.5	8	3.71613
Q9Z329	*Itpr2*	8.2	15	3.7132
P53026	*Rpl10a*	29.5	6	3.62827

Q8BP67	*Rpl24*	22.3	5	3.615
Q8VDR9	*Dock7*	40.8	74	3.60347
Q8K019	*Bclaf1*	5.3	3	3.58567
P86048	*Rpl10; Rpl10l*	37.8	6	3.57052
P54071	*Idh2*	18.7	2	3.53114
Q9DB20	*Atp5o*	62	12	3.52344
Q68FD5	*Cltc*	30.6	45	3.51461
P97351	*Rps3a*	58	16	3.49202
Q99104	*Myo5a*	51.5	102	3.49179
Q8VD75	*Hip1*	9.8	7	3.46559
Q9DAY9	*Npm1*	13.6	3	3.46355
Q4VBF8	*Sipa1l1*	10.2	10	3.44826
Q9CZ13	*Uqcrc1*	6.9	2	3.41658
Q3UMG5	*Lrch2*	17.6	14	3.37704
P84099	*Rpl19*	22.2	5	3.36055
P43277	*Hist1h1d*	27.1	2	3.35887
P63087	*Ppp1cc*	61.9	1	3.32657
P62830	*Rpl23*	47.1	8	3.3224
P62281	*Rps11*	66.5	11	3.31311
Q9DCL9	*Paics*	17.2	6	3.30422
Q60605	*Myl6*	67.1	6	3.29592
Q9JKK7	*Tmod2*	38.5	14	3.28892
P25206	*Mcm3*	4.1	2	3.23103
Q8VDD5	*Myh9*	77.3	185	3.2277
Q9CVB6	*Arpc2*	55.7	15	3.20561
P68372	*Tubb4b*	76.9	2	3.17006
P62874	*Gnb1*	70.6	9	3.16625
Q03265	*Atp5a1*	54.6	32	3.14347
P62137	*Ppp1ca*	66.7	7	3.1335
Q9CXW4	*Rpl11*	45.5	9	3.11138
Q8CFC2	*Myt1*	8	4	3.09485
P62717	*Rpl18a*	41.5	7	3.07475
Q9WUM4	*Coro1c*	47.9	19	3.04647
Q61390	*Cct6a*	23.4	9	3.03879
Q8CGP4	*Hist1h2aa; H2afj; Hist3h2a; Hist1h2ah; Hist1h2ak; Hist1h2af; Hist2h2aa1; Hist2h2ac*	37.3	5	3.02791
P47753	*Capza1*	61.5	10	3.01816
Q9QXS6	*Dbn1*	42.8	1	3.01372
Q9CYL5	*Glipr2*	31.2	3	3.01307
Q9D4J1	*Efhd1*	37.9	8	3.01233
Q9CPQ3	*Tomm22*	32.4	2	3.0087
P17742	*Ppia*	36.6	5	2.9868
E9Q175	*Myo6*	65.7	1	2.98096

Q80Z24	*Negr1*	14.9	3	2.96198
Q8CDN6	*Txnl1*	10	2	2.94664
Q6P5H2	*Nes*	9.7	12	2.92602
Q61879	*Myh10*	75.7	169	2.90802
Q8VDN2	*Atp1a1*	14.5	5	2.89408
Q3THE2	*Myl12b*	50	1	2.87166
P80316	*Cct5*	11.5	5	2.83553
Q8BMS1	*Hadha*	25.4	14	2.82875
Q8K4L2	*Svil*	34.9	52	2.80864
P62082	*Rps7*	34.5	7	2.80517
Q8CBY8	*Dctn4*	11.6	4	2.80065
P60843	*Eif4a1; Eif4a2*	30	7	2.78114
Q9JIK5	*Ddx21*	25.1	14	2.76467
O09106	*Hdac1*	18.3	3	2.76003
Q9Z2X1	*Hnrnpf*	26.3	7	2.75876
P51863	*Atp6v0d1*	20.5	6	2.72813
Q8CFI7	*Polr2b*	6	5	2.72692
P62908	*Rps3*	69.5	17	2.72391
Q920L1	*Fads1*	22.3	2	2.68792
Q8HW98	*Iglon5*	5.7	2	2.67632
Q91VA7	*Idh3b*	12.8	3	2.66209
Q9JJW6	*Alyref; Alyref2*	31.4	6	2.65942
Q9CZM2	*Rpl15*	11.3	3	2.65158
P62141	*Ppp1cb*	55.7	6	2.64839
Q3TLP8	*Rac1; Rac3*	38.9	8	2.63077
Q5SWZ5	*Mprip*	19.5	3	2.61709
Q921R2	*Rps13*	45.7	8	2.61179
P62806	*Hist1h4a*	65	12	2.59742
P08113	*Hsp90b1*	12.5	6	2.59481
P42932	*Cct8*	17.2	7	2.59424
Q9DC51	*Gnai3*	37.3	7	2.54967
F6Q2E3	*Psmc3*	10.8	2	2.54283
Q61655	*Ddx19a; Ddx19b*	10.5	2	2.53898
P41105	*Rpl28*	56.9	10	2.52921
P80313	*Cct7*	20	6	2.51414
Q9ERG0	*Lima1*	47.7	38	2.51069
P11983	*Tcp1*	15.3	7	2.48333
Q99KI0	*Aco2*	7.3	3	2.48204
Q9CQM8	*Rpl21*	27.5	3	2.47424
P61164	*Actr1a; Actr1b*	19.7	4	2.46596
P62889	*Rpl30*	43.5	5	2.46179
P18760	*Cfl1*	62	7	2.41684
Q6AXB7	*Fmr1*	13.8	5	2.41561
Q7TPR4	*Actn1*	15.1	3	2.39535
P05214	*Tuba1a; Tuba3a*	63.9	1	2.39031

P61358	*Rpl27*	41.9	5	2.38389
Q61666	*Hira*	3.3	2	2.37119
Q3U3C9	*Gse1*	6	5	2.36429
P99024	*Tubb5*	78.8	6	2.36071
O70503	*Hsd17b12*	31.7	6	2.35901
Q922Q8	*Lrrc59*	27.7	6	2.3577
P63037	*Dnaja1*	17.4	4	2.34519
P08752	*Gnai2*	61.1	14	2.30564
P84104	*Srsf3; Gm12355*	21.3	3	2.26593
Q8BH59	*Slc25a12*	23	8	2.26392
Q8CGB3	*Uaca*	1.9	2	2.26113
Q641P0	*Actr3b*	23.9	3	2.25874
P14206	*Rpsa*	37.3	7	2.24817
P62267	*Rps23*	41.3	6	2.19857
P14148	*Rpl7*	35.2	11	2.19572
Q9CPQ1	*Cox6c*	26.3	2	2.16321
Q8BQ30	*Ppp1r18*	23.9	9	2.16275
Q50HX3	*Rab14*	33.5	5	2.16231
Q6P4T2	*Snrnp200*	2.3	4	2.15937
P27659	*Rpl3*	29.3	11	2.15631
Q9R0P5	*Dstn*	20.6	2	2.15607
Q791V5	*Mtch2*	34.7	8	2.13279
Q3TF41	*Nap1l1*	15.5	3	2.1312
P18872	*Gnao1*	39.3	11	2.12932
Q9DBG3	*Ap2b1*	9.5	7	2.11604
Q9EP89	*Lactb*	7.4	4	2.11288
Q7TPV4	*Mybbp1a*	17.2	14	2.10808
Q8C5G6	*Tollip*	37.7	5	2.0771
Q8BHC4	*Dcakd*	24.2	4	2.0693
Q8BU30	*Iars*	4	3	2.0411
Q9EPU0	*Upf1*	5	4	2.01867
P05480	*Src*	10.8	3	2.00958
Q8VHM5	*Hnrnpr*	9.7	2	2.00211
P39688	*Fyn*	25.7	8	1.98935
Q99JY8	*Ppap2b*	26.3	7	1.96312
Q6ZWN5	*Rps9*	30.4	9	1.95487
P62242	*Rps8*	60.1	10	1.93895
Q8BGN3	*Enpp6*	27.3	11	1.93671
A2AI08	*Tprn*	13	6	1.92524
P62918	*Rpl8*	33.9	10	1.91957
P62320	*Snrpd3*	12.7	2	1.90891
P12970	*Rpl7a*	29.3	8	1.89338
Q9DAS9	*Gng12*	63.1	5	1.88679
P26516	*Psmd7*	8.7	2	1.86352
P19253	*Rpl13a*	42.4	9	1.84866
Q5EBP8	*Hnrnpa1*	22	8	1.84247

P63094	*Gnas*	31	9	1.82993
Q8BTI8	*Srrm2*	2.9	5	1.78558
P62814	*Atp6v1b2*	13.5	5	1.77645
P20152	*Vim*	82.2	50	1.76909
P84244	*H3f3a; Hist1h3b; Hist1h3a; H3f3c*	36.3	9	1.76408
Q6URW6	*Myh14*	43.1	66	1.75635
P14685	*Psmd3*	12.5	6	1.74443
Q91V55	*Rps5*	53.4	10	1.71456
O54931	*Pakap; Akap2*	3.5	2	1.68349
P35979	*Rpl12*	38.8	6	1.66599
P62900	*Rpl31*	33.6	4	1.65426
Q60931	*Vdac3*	65	15	1.64956
Q8BG95	*Ppp1r12b*	5.9	3	1.60958
Q64331	*Myo6*	65.9	1	1.59807
O55142	*Rpl35a*	22.7	3	1.59202
P30999	*Ctnnd1*	6.9	3	1.56592
Q9R0H0	*Acox1*	13.3	5	1.55724
P60335	*Pcbp1*	26.7	4	1.53854
E9Q9B7	*Kidins220*	3.2	4	1.53624
Q9D1I6	*Mrpl14*	20	2	1.53349
P23116	*Eif3a*	2.5	2	1.53201
Q76MZ3	*Ppp2r1a; Ppp2r1b*	16.8	6	1.53197
P25444	*Rps2*	51.5	18	1.52805
P35279	*Rab6a; Rab6b; Rab39a*	17.8	4	1.52471
Q9QZQ8	*H2afy*	16.7	3	1.51254
Q9JKF1	*Iqgap1*	4.9	5	1.50333
Q9DCT2	*Ndufs3*	9.9	2	1.46249
P60122	*Ruvbl1*	13.2	4	1.4599
Q68FG2	*Sptbn2*	4.4	4	1.44478
P62754	*Rps6*	31.3	7	1.43061
P50516	*Atp6v1a*	26.9	10	1.42925
Q8R0X7	*Sgpl1*	8.8	3	1.42627
Q8CBB6	*Hist1h2bf; Hist1h2br; Hist1h2bp; Hist1h2ba; Hist3h2ba; Hist3h2bb*	77.8	0	1.42506
P70168	*Kpnb1*	3.4	2	1.42081
Q68FL6	*Mars*	6.7	3	1.40168
Q9CXS4	*Cenpv*	24.6	3	1.39897
Q8BG33	*Ntm*	20.3	5	1.3952
P19783	*Cox4i1*	31.4	4	1.39114
Q9Z275	*Rlbp1*	12	2	1.3776

P32883	*Kras; Hras; Nras*	36	6	1.37203
Q8BGJ5	*Ptbp1*	27.8	9	1.37119
P63260	*Actg1*	89.1	3	1.36868
Q9CR57	*Rpl14*	30.9	7	1.32014
P62983	*Rps27a; Gm8797; Uba52; Kxd1; Ubc; Ubb*	50.6	10	1.31679
P00405	*Mtco2*	23.3	4	1.31661
P62492	*Rab11b; Rab11a*	30.9	5	1.30227
Q60932	*Vdac1*	74.7	5	1.28711
P47911	*Rpl6*	39.9	13	1.28113
Q9CWF2	*Tubb2b*	78.7	2	1.27206
Q9CX86	*Hnrnpa0*	23.3	4	1.2619
Q8JZK9	*Hmgcs1*	13.5	4	1.22225
Q99JR1	*Sfxn1*	22.4	4	1.20391
P15116	*Cdh2*	5.2	2	1.1962
P61027	*Rab10*	11.5	2	1.18886
Q6ZWV7	*Rpl35*	22	3	1.17932
Q8BFR5	*Tufm*	14.4	4	1.15116
Q9WVJ2	*Psmd13*	6.9	2	1.15082
Q61820	*Ran; 1700009N14Rik*	27.3	5	1.14852
Q8BGS1	*Epb41l5*	8.1	3	1.14598
Q80U35	*Arhgef17*	5.7	6	1.14314
P35980	*Rpl18*	43.4	9	1.13722
Q9CPP0	*Npm3*	17.7	2	1.13045
P07901	*Hsp90aa1*	14.1	3	1.13035
Q61753	*Phgdh*	31.1	12	1.1065
Q3TYE5	*Lsamp*	37.6	11	1.09902
H3BJD6	*Ppp1r9a*	25.1	3	1.08866
Q9Z0N1	*Eif2s3x*	10.2	3	1.08038
Q61382	*Traf4*	15.7	5	1.06564
P20612	*Gnai1*	32.8	3	1.05496
P62259	*Ywhae*	24.3	4	1.01919
P63325	*Rps10*	29.1	4	1.00781

Table 15: LSD1 co-IP in A2B5+ cells – difference proliferating A2B5+ OPCs to A2B5+ OPCs after 24 h differentiation normalized to IgG and LSD1

Uniprot ID	Gene name	Coverage [%]	Unique peptides	-log p value
Q6ZPK0	*Phf21a*	38.1	17	6.73516
Q8C796	*Rcor2*	27.9	10	6.19772

Q8CFE3	*Rcor1*	40.8	9	6.18532
Q6ZQ88	*Kdm1a*	52.2	38	5.36124
Q7TSH3	*Znf516*	15.3	13	5.17896
Q3U3C9	*Gse1*	6	5	5.14754
Q03173	*Enah*	19	10	4.79652
Q76KF0	*Sema6d*	10.5	7	4.2376
O88712	*Ctbp1*	17.5	6	4.135
Q8VIJ6	*Sfpq*	29.8	15	4.10584
Q6P9Q6	*Fkbp15*	13.7	10	3.75897
Q99K48	*Nono*	22.6	7	3.54016
P70288	*Hdac2*	21.3	4	3.50008
P97820	*Map4k4*	6.2	4	3.39847
Q99PL5	*Rrbp1*	6.5	6	3.0182
Q9CZX8	*Rps19*	31	5	2.82185
Q61584	*Fxr1*	14.1	5	2.67945
P84104	*Srsf3; Gm12355*	21.3	3	2.65472
Q9CU65	*Zmym2*	5.9	6	2.58945
Q8C845	*Efhd2*	58.3	13	2.45429
P35922	*Fmr1*	13.8	5	2.43247
P97351	*Rps3a*	58	16	2.36496
Q9CYL5	*Glipr2*	31.2	3	2.29731
Q91ZU6	*Dst*	1.7	8	2.09614
Q8BJA3	*Hmbox1*	11.3	3	2.03575
P30999	*Ctnnd1*	6.9	3	1.96587
Q99JI6	*Rap1b; Rap1a*	34.2	4	1.96434
P08775	*Polr2a*	4.5	6	1.95111
P52293	*Kpna2*	10	3	1.85418
Q80Z24	*Negr1*	14.9	3	1.8225
Q8BG05	*Hnrnpa3; Gm6793*	17.3	3	1.73004
P62046	*Lrch1*	11.3	4	1.70848
Q9CX86	*Hnrnpa0*	23.3	4	1.68613
Q9CPW4	*Arpc5*	41.7	4	1.63847
O09106	*Hdac1*	18.3	3	1.60907
Q7TMM9	*Tubb2a*	69.9	1	1.55459
F8WI35	*H3f3a; Hist1h3b; Hist1h3a; H3f3c*	36.3	9	1.47781

Table 16: LSD1 redox co-IP in SN4741 cells – CTRL normalized to IgG

Uniprot ID	Gene name	Coverage [%]	Unique peptides	-log p value
Q542G9	*Anxa2*	33	9	2.60063
E9QAQ7	*Arid1a*	2.5	3	2.81506
Q925I1	*Atad3; Atad3a*	9.1	4	1.9837
O70305	*Atxn2*	8.6	8	3.02446
Q3TGG2	*Atxn2l*	8	6	1.95953
Q9CQC6	*Bzw1*	14.9	5	3.32151
Q8CH18	*Ccar1*	7.8	7	2.20816
Q9D8B3	*Chmp4b*	11.2	2	2.33456
Q9DCN2	*Cyb5r3*	26.5	6	2.36531
Q9DCE6	*Dab2*	7.9	5	5.01332
Q61103	*Dpf2*	13.6	4	3.20783
E9Q557	*Dsp*	2.6	6	3.40534
Q8BL66	*Eea1*	8.8	9	2.95842
Q8JZQ9	*Eif3b*	38.2	23	2.17735
Q7TPD1	*Fbxo11*	15.3	1	5.21395
Q3U3C9	*Gse1*	28.2	23	3.74523
Q58E49	*Hdac1; Gm10093*	17.6	2	2.90546
P70288	*Hdac2*	32.6	6	2.93117
P43274	*Hist1h1e*	22.4	2	2.63115
Q05DT2	*Hmg20b*	32.1	6	2.00376
P38647	*Hspa9*	25.2	12	1.85448
P63038	*Hspd1*	22.7	7	2.54685
Q02257	*Jup*	7.9	4	4.91298
Q6ZQ88	*Kdm1a*	60.4	43	4.52756
Q8BYR2	*Lats1*	8.9	8	5.02365
P14873	*Map1b; Map1a*	1.1	2	2.55685
Q91W39	*Ncoa5*	10.7	5	4.02693
Q3V449	*Nmnat1*	22.8	6	5.60503
E9Q7G0	*Numa1*	3.9	6	2.26325
Q60597	*Ogdh*	2.6	2	1.89789
P29341	*Pabpc1; Pabpc6*	28	12	2.95551
Q6ZPK0	*Phf21a*	26	13	3.57964
Q8CFE3	*Rcor1*	56.5	14	8.1675
Q6PGA0	*Rcor3*	37.7	12	4.62766
Q91YQ5	*Rpn1*	27.8	12	2.78752
Q6PFF0	*Scaf4; Scaf8*	2.3	2	4.37761
Q3UXS0	*Scamp3*	28.6	5	6.21613
Q3TKT4	*Smarca4*	7.6	9	3.84923
Q3UID0	*Smarcc2*	4	2	3.68369
Q9CSN1	*Snw1*	13.4	5	4.36044

Q62261	*Sptbn1*	46.7	94	2.01238
Q8BTI8	*Srrm2*	11.9	24	1.92727
O55201	*Supt5h*	14.3	11	3.74333
Q7TMK9	*Syncrip*	19	5	1.89925
Q9Z1A1	*Tfg*	43.6	14	4.19223
Q9JHJ0	*Tmod3*	23.3	5	2.01298

Table 17: LSD1 redox co-IP in SN4741 cells – Bizine normalized to IgG

Uniprot ID	Gene name	Coverage [%]	Unique peptides	-log p value
Q3ULT2	*Actn4*	23.9	8	2.89176
Q5FWB7	*Aldoa; Aldoart1*	60.4	15	2.47764
Q542G9	*Anxa2*	33	9	2.50839
E9QAQ7	*Arid1a*	2.5	3	3.29174
E9QM77	*Atxn2*	8.6	8	3.45866
Q9CQC6	*Bzw1*	14.9	5	2.1593
Q8CH18	*Ccar1*	7.8	7	2.25643
F6YFR7	*Cope*	30.8	3	2.22934
E9QL31	*Dab2*	7.9	5	4.23772
Q3U1J4	*Ddb1*	17.6	17	2.2137
Q8BMF4	*Dlat*	8.7	4	2.6956
Q61103	*Dpf2*	13.6	4	3.53017
E9Q557	*Dsp*	2.6	6	4.89137
Q8BL66	*Eea1*	8.8	9	2.56682
P58252	*Eef2*	58.5	42	2.9231
P70372	*Elavl1*	26.1	7	2.18483
Q7TPD1	*Fbxo11*	15.3	1	3.43631
Q4FJZ6	*Gclm*	13.1	3	2.43781
Q3U3C9	*Gse1*	28.2	23	4.2386
Q58E49	*Hdac1; Gm10093*	17.6	2	3.66061
P70288	*Hdac2*	32.6	6	3.64243
Q8C3I8	*Hgh1*	12.5	3	2.4721
P43274	*Hist1h1e*	22.4	2	2.17411
Q05DT2	*Hmg20b*	32.1	6	3.18528
Q80Y52	*Hsp90aa1*	44.6	17	2.36122
Q3UAD6	*Hsp90b1*	15.6	6	2.43163
Q02257	*Jup*	7.9	4	2.24099
Q6ZQ88	*Kdm1a*	60.4	43	4.70341
Q8BYR2	*Lats1*	8.9	8	4.80025
P08249	*Mdh2*	24.9	6	2.37134
P54276	*Msh6*	5	5	2.34346
Q922D8	*Mthfd1*	18.8	13	2.34275
P09405	*Ncl*	27.4	19	2.31487
Q91W39	*Ncoa5*	10.7	5	4.59819

Q3V449	*Nmnat1*	22.8	6	6.09664
Q6PIP5	*Nudcd1*	34.5	14	2.30995
Q60597	*Ogdh*	2.6	2	2.11941
P09103	*P4hb*	14.3	5	2.72855
P29341	*Pabpc1; Pabpc6*	28	12	3.21521
Q6ZPK0	*Phf21a*	26	13	4.38673
Q8CFE3	*Rcor1*	56.5	14	9.35263
Q6PGA0	*Rcor3*	37.7	12	5.41407
Q5BLK0	*Rpl12*	35.8	4	2.60297
Q6PFF0	*Scaf4; Scaf8*	2.3	2	4.13218
Q3UXS0	*Scamp3*	28.6	5	6.21765
Q8K2B3	*Sdha*	7.1	4	2.11997
Q3TKT4	*Smarca4*	7.6	9	2.95616
Q3UID0	*Smarcc2*	4	2	3.42769
Q9CSN1	*Snw1*	13.4	5	4.3022
O55201	*Supt5h*	14.3	11	3.97236
Q9Z1A1	*Tfg*	43.6	14	4.16549
E9Q5E2	*Thoc2*	5.1	7	3.61128
Q14C24	*U2af1; U2af1l4*	14.6	4	2.39416
Q02053	*Uba1*	30.8	21	3.46335
P63101	*Ywhaz*	33.1	3	2.4295

Table 18: LSD1 redox co-IP in SN4741 cells – Difference bizine to CTRL normalized to IGG and LSD1

Uniprot ID	Gene name	t-test Difference bizine_CTRL
Q8CFE3	*Rcor1*	1.01
Q6ZPK0	*Phf21a*	0.88
Q05DT2	*Hmg20b*	0.87
Q58E49	*Hdac1; Gm10093*	0.73
Q8CH18	*Ccar1*	-0.47
Q3UXS0	*Scamp3*	-0.70
Q6PDG5	*Smarcc2*	-0.74
E9QAQ7	*Arid1a*	-0.74
P98078	*Dab2*	-0.74
Q8BL66	*Eea1*	-0.74
Q3TKT4	*Smarca4*	-0.89
Q9JHJ0	*Tmod3*	-1.03
Q62261	*Sptbn1*	-1.09
F6ZQA3	*Numa1*	-1.16
Q9D8B3	*Chmp4b*	-1.43

Table 19: BIAM switch assay coupled to mass spectometry – differentially oxidized proteins upon LSD1 knockout

UniProt ID	Gene name	Coverage [%]	Unique peptides	Fold oxidized siRNA_CTRL	-log p value
P60981	*Dstn*	25.2	2	-20.79	2.933
Q13228	*Selenbp1*	10.8	4	-18.75	6.112
Q8NF37	*Lpcat1*	6.4	1	-16.62	2.205
P13995	*Mthfd2*	5	1	-15.46	5.795
O75063	*Fam20b*	2.4	1	-14.07	3.413
Q6PK18	*Ogfod3*	4.4	1	-12.48	3.347
P53582	*Metap1*	2.8	1	-11.4	4.175
Q15738	*Nsdhl*	5.9	1	-10.98	2.676
O14656	*Tor1a*	3.9	2	-10.32	1.504
Q9NXW2	*Dnajb12*	18.5	4	-9.92	3.513
O00217	*Ndufs8*	10.9	1	-8.59	3.072
Q15008	*Psmd6*	19.4	2	-8.5	1.445
P32322	*Pycr1*	6.2	1	-8.2	3.269
P82650	*Mrps22*	7.3	1	-8.15	1.654
Q15435	*Ppp1r7*	6.6	1	-7.79	5.899
P46778	*Rpl21*	11.2	1	-7.1	1.739
Q9UNS2	*Cops3*	6.4	2	-6.55	3.061
Q9UJU6	*Dbnl*	15.6	1	-6.49	3.784
Q9Y237	*Pin4*	15.4	1	-6.43	1.567
Q9UGT4	*Susd2*	7.2	3	-6.27	1.946
Q9BQE4	*Vimp*	7.2	1	-5.91	3.75
Q8NE71	*Abcf1*	1.8	1	-5.83	3.059
P61165	*Tmem258*	16.3	1	-5.61	1.461
Q96D46	*Nmd3*	9.6	3	-5.51	1.848
Q15393	*Sf3b3*	1.2	1	-5.21	2.151
P08047	*Sp1*	9.3	1	-5.2	2.761
Q13617	*Cul2*	2.2	1	-5.14	4.741
P34932	*Hspa4*	3.7	2	-5.09	1.595
Q13283	*G3bp1*	8.8	2	-4.74	1.868
Q13445	*Tmed1*	14.6	1	-4.66	2.385
Q9Y266	*Nudc*	7.6	2	-4.6	1.359
Q15056	*Eif4h*	16.9	2	-4.55	2.311
Q9H4M9	*Ehd1*	4.9	1	-4.45	2.071
Q9Y5X3	*Snx5*	51.6	1	-4.43	2.064
Q9H832	*Ube2z*	4.2	1	-4.36	1.731
P00918	*Ca2*	15.8	4	-4.19	4.787
Q08945	*Ssrp1*	2	1	-4.14	1.538
P51148	*Rab5c*	6.5	1	-4.13	1.903
Q96NB2	*Sfxn2*	20.9	1	-4.08	2.372

Q969G3	*Smarce1*	15.3	2	-3.82	1.892
P55795	*Hnrnph2*	18.7	2	-3.8	1.525
Q712K3	*Ube2r2*	7.6	2	-3.75	1.49
P23434	*Gcsh*	20	1	-3.73	1.81
Q8TEX9	*Ipo4*	18.8	1	-3.67	2.164
Q6P587	*Fahd1*	7.1	1	-3.55	2.729
Q7Z4W1	*Dcxr*	21.5	4	-3.5	1.347
Q15363	*Tmed2*	43.1	2	-3.5	2.348
Q96RQ3	*Mccc1*	8.5	4	-3.46	3.331
Q6UXD5	*Sez6l2*	5.3	1	-3.44	5.181
Q15046	*Kars*	8.5	5	-3.43	2.82
P11387	*Top1*	3.4	2	-3.39	1.417
P53041	*Ppp5c*	6.5	2	-3.33	3.505
P34059	*Galns*	5.9	1	-3.31	1.657
A4D1S0	*Klrg2*	2.7	1	-3.28	1.605
Q99497	*Park7*	39.2	5	-3.19	2.195
Q07812	*Bax*	24	3	-3.16	1.967
P33991	*Mcm4*	3.2	2	-3.13	1.351
O15042	*U2surp*	16.8	1	-3.11	3.359
Q9HD45	*Tm9sf3*	10.3	1	-3.02	1.419
Q16576	*Rbbp7*	9.6	3	-3	4.382
Q6UWU4	*C6orf89*	8.9	2	-2.97	1.497
P07919	*Uqcrh; Uqcrhl*	74.7	7	-2.93	4.855
Q96NT5	*Slc46a1*	2.6	1	-2.85	1.889
O96005	*Clptm1*	2.4	2	-2.77	2.74
P39023	*Rpl3*	13.1	4	-2.76	2.039
Q9BZF1	*Osbpl8*	23.7	1	-2.75	1.798
Q9NPD8	*Ube2t*	8.6	1	-2.7	1.565
P17568	*Ndufb7*	24.1	3	-2.68	1.987
P50395	*Gdi2*	19.6	3	-2.66	4.57
Q13148	*Tardbp*	6.5	1	-2.65	1.389
P12277	*Ckb*	8.6	1	-2.65	2.435
P35659	*Dek*	8.3	1	-2.64	1.995
Q96HQ2	*Cdkn2aipnl*	15.5	1	-2.64	3.634
P30876	*Polr2b*	1.2	1	-2.62	2.037
Q9BT78	*Cops4*	7.3	1	-2.59	2.522
P06865	*Hexa*	7.1	4	-2.57	1.742
Q13740	*Alcam*	18.2	8	-2.56	3.573
Q92616	*Gcn1l1*	0.4	1	-2.53	1.741
Q13435	*Sf3b2*	8.5	3	-2.53	1.492
O94776	*Mta2*	1.5	1	-2.52	2.765
P49711	*Ctcf*	3	2	-2.51	2.689
Q16775	*Hagh*	64.1	3	-2.47	3.709
Q02790	*Fkbp4*	38.6	14	-2.41	4.122
P55789	*Gfer*	33.9	2	-2.39	3.511
P21926	*Cd9*	15.1	3	-2.37	5.585

Q13641	*Tpbg*	6.9	3	-2.34	2.001
Q96A59	*Marveld3*	5	1	-2.33	2.109
E9PKU7	*Ganab*	19.5	1	-2.28	1.324
P21912	*Sdhb*	17.1	2	-2.27	1.358
P09960	*Lta4h*	2.1	1	-2.27	1.608
P62277	*Rps13*	10.3	1	-2.26	3.17
P49588	*Aars*	11.6	7	-2.24	2.91
Q8WXF1	*Pspc1*	16.6	8	-2.23	5.04
Q9H0H5	*Racgap1*	10.9	2	-2.2	3.008
Q9P0I2	*Emc3*	7.3	1	-2.18	1.57
Q14118	*Dag1*	9.5	6	-2.17	1.925
Q9NRF9	*Pole3*	10.9	1	-2.16	2.199
Q5JU69	*Tor2a*	5	1	-2.16	1.761
Q15149	*Plec*	2.1	7	-2.15	2.711
Q96CN7	*Isoc1*	15.4	2	-2.12	3.118
P34897	*Shmt2*	19	8	-2.11	3.495
Q9Y5S9	*Rbm8a*	17.2	2	-2.11	2.553
O43670	*Znf207*	3.8	1	-2.1	2.405
P35813	*Ppm1a*	8.6	2	-2.08	1.704
Q9Y3A6	*Tmed5*	5.2	1	-2.06	1.701
Q14247	*Cttn*	23.1	8	-2.05	2.814
Q9NY27	*Ppp4r2*	7	1	-2.03	1.512
Q9P2E9	*Rrbp1*	4.9	2	-2.03	1.967
P06280	*Gla*	19.1	6	-1.98	4.418
Q9UMS4	*Prpf19*	31.1	1	-1.96	4.053
Q9H1E3	*Nucks1*	7.4	1	-1.96	2.02
P18031	*Ptpn1*	10.1	3	-1.95	1.684
Q8WWM7	*Atxn2l*	2.9	2	-1.94	2.874
P14866	*Hnrnpl*	28.5	7	-1.94	1.305
Q9H444	*Chmp4b*	21.4	4	-1.93	2.022
P36957	*Dlst*	5.7	2	-1.93	3.239
P61604	*Hspe1*	55.9	5	-1.92	1.88
P17050	*Naga*	2.7	1	-1.92	3.161
Q9Y230	*Ruvbl2*	23.5	8	-1.91	1.682
O43615	*Timm44*	9.5	1	-1.91	2.271
P62873	*Gnb1*	16.8	2	-1.89	1.71
Q9BV57	*Adi1*	7.8	1	-1.89	4.252
Q13438	*Os9*	14.7	7	-1.88	2.16
P20700	*Lmnb1*	39.9	18	-1.88	3.499
P06493	*Cdc2; Cdk1*	17.2	4	-1.82	2.82
P54578	*Usp14*	11.3	4	-1.81	1.728
Q15427	*Sf3b4*	10.8	3	-1.81	3.281
O14618	*Ccs*	29.4	1	-1.8	1.443
P30084	*Echs1*	36.2	7	-1.76	1.416
O43175	*Phgdh*	15.9	6	-1.74	3.169
Q9Y678	*Copg1*	7	4	-1.74	1.481

P31930	*Uqcrc1*	9.4	3	-1.73	2.466
Q07955	*Srsf1*	21.3	4	-1.72	1.631
P61006	*Rab8a*	21.7	3	-1.72	1.402
Q15904	*Atp6ap1*	16.4	3	-1.72	1.941
P62140	*Ppp1cb*	32	2	-1.72	1.528
Q92896	*Glg1*	9.4	9	-1.71	2.577
P35606	*Copb2*	3.5	2	-1.68	1.778
O15305	*Pmm2*	12.3	1	-1.67	1.658
Q6NUK1	*Slc25a24*	7.3	3	-1.67	2.783
P31947	*Sfn*	49.6	8	-1.67	1.426
P20645	*M6pr*	28.5	7	-1.66	2.878
Q86YP4	*Gatad2a; Gatad2b*	3.6	2	-1.65	2.585
P51991	*Hnrnpa3*	37.8	13	-1.65	1.897
Q16740	*Clpp*	25.8	2	-1.65	1.308
P39748	*Fen1*	10.3	3	-1.65	2.282
Q99623	*Phb2*	13.8	4	-1.64	1.565
P09669	*Cox6c*	25.3	2	-1.63	2.011
O75477	*Erlin1*	16.5	5	-1.63	1.593
Q13263	*Trim28*	18.7	9	-1.63	2.511
Q9BQ70	*Tcf25*	17.1	2	-1.62	2.052
P05198	*Eif2s1*	23.2	5	-1.62	2.925
Q8NBJ5	*Colgalt1*	2.4	1	-1.62	1.417
Q9H0L4	*Cstf2t*	5.7	1	-1.61	4.102
P28838	*Lap3*	11.9	4	-1.61	1.803
Q9P0L0	*Vapa*	32.1	6	-1.6	2.426
P62258	*Ywhae*	43.1	13	-1.6	2.26
P31943	*Hnrnph1*	30.3	5	-1.6	2.943
O60568	*Plod3*	14.9	9	-1.6	1.984
O43390	*Hnrnpr*	4.1	1	-1.6	1.518
P13498	*Cyba*	15.9	1	-1.59	2.06
P50990	*Cct8*	23.7	11	-1.58	2.162
P47985	*Uqcrfs1; Uqcrfs1p1*	34.7	10	-1.58	1.784
Q99832	*Cct7*	23.8	10	-1.58	1.817
Q99714	*Hsd17b10*	23	4	-1.58	2.12
Q02818	*Nucb1*	9.8	4	-1.57	1.742
Q9NT62	*Atg3*	16.2	6	-1.57	1.823
Q3LXA3	*Dak; Tkfc*	10.1	4	-1.57	2.039
O75533	*Sf3b1*	2	2	-1.56	1.48
P52272	*Hnrnpm*	30.3	17	-1.56	1.896
Q9NXG6	*P4htm*	6.2	2	-1.56	2.046
P28072	*Psmb6*	8.8	2	-1.56	1.74
Q14103	*Hnrnpd*	14.4	2	-1.56	1.493
P47756	*Capzb*	11.9	3	-1.56	2.532
P19338	*Ncl*	23.1	16	-1.56	2.874
Q00839	*Hnrnpu*	21.8	13	-1.56	1.33

Q96PK6	*Rbm14*	4.6	3	-1.56	1.813
O14657	*Tor1b*	7.1	3	-1.55	3.165
Q9UHL4	*Dpp7*	12.8	5	-1.55	1.517
Q15233	*Nono*	38.2	13	-1.54	1.957
O15394	*Ncam2*	8.3	5	-1.53	2.623
Q7KZF4	*Snd1*	4.8	3	-1.53	1.615
Q9NR28	*Diablo*	7.5	1	-1.53	3.199
Q9GZM5	*Yipf3*	14.5	2	-1.53	1.635
P40227	*Cct6a*	28.1	11	-1.52	2.085
Q12906	*Ilf3*	19.4	12	-1.51	1.62
P27824	*Canx*	17.1	9	-1.5	1.621
Q9BV40	*Vamp8*	38	3	-1.5	1.64
P15311	*Ezr*	18.1	8	-1.5	1.857
Q9UG63	*Abcf2*	5	1	-1.5	1.393
Q08J23	*Nsun2*	8.1	4	-1.49	1.372
Q9H0X4	*Itfg3*	24.5	2	-1.49	1.516
P45974	*Usp5*	6.8	4	-1.49	1.525
P09622	*Dld*	19.8	6	-1.49	1.367
P0DMV9	*Hspa1b; Hspa1a*	29.9	7	-1.48	1.824
P17987	*Tcp1*	31.8	10	-1.47	1.581
Q9UBV2	*Sel1l*	10.4	1	-1.47	1.328
Q92841	*Ddx17*	14	4	-1.47	1.98
O75152	*Zc3h11a*	4.3	1	-1.47	1.719
P23588	*Eif4b*	9.4	3	-1.47	1.918
P07910	*Hnrnpc*	34.7	9	-1.47	1.803
P23246	*Sfpq*	15.6	6	-1.47	2.337
Q13098	*Gps1*	24.1	1	-1.46	2.879
P31948	*Stip1*	43.3	19	-1.45	1.603
P60842	*Eif4a1*	26.1	6	-1.45	1.386
Q9NRP2	*Cmc2*	21.8	2	-1.44	1.652
P12956	*Xrcc6*	25.8	11	-1.44	1.977
P62879	*Gnb2; Gnb4*	11.8	2	-1.44	1.516
P30048	*Prdx3*	9.8	2	-1.44	1.79
P00367	*Glud1*	29.4	11	-1.44	1.879
P32119	*Prdx2*	38.9	11	-1.44	1.666
P25205	*Mcm3*	9.3	5	-1.43	1.73
Q8WW12	*Pcnp*	10.1	1	-1.43	2.058
P12830	*Cdh1*	14.4	10	-1.42	1.598
O94905	*Erlin2*	24.2	6	-1.42	1.44
Q9HCN8	*Sdf2l1*	43.9	4	-1.42	2.71
Q9H910	*Hn1l*	51.7	6	-1.4	4.135
P11441	*Ubl4a*	10	2	-1.39	2.329
Q9Y4L1	*Hyou1*	11	6	-1.38	1.443
P00374	*Dhfr*	8.6	1	-1.38	3.518
Q12792	*Twf1*	4	2	-1.37	2.793
Q9HC38	*Glod4*	8.8	2	-1.37	1.68

Q9GZZ9	*Uba5*	30.2	6	-1.37	1.349
Q15365	*Pcbp1*	43.3	6	-1.37	1.326
P55072	*Vcp*	36.7	25	-1.36	1.57
P07900	*Hsp90aa1*	37.6	17	-1.36	1.517
P26599	*Ptbp1*	9	4	-1.36	1.419
Q9UQ80	*Pa2g4*	26.6	10	-1.35	1.303
Q13765	*Naca*	35.3	4	-1.34	1.352
O75874	*Idh1*	26.3	7	-1.34	2.053
P22695	*Uqcrc2*	7.3	2	-1.32	1.577
Q9UBS4	*Dnajb11*	27.4	11	-1.31	1.579
P49368	*Cct3*	34.2	13	-1.31	1.51
P15559	*Nqo1*	15.8	3	-1.31	1.302
O00567	*Nop56*	5.4	2	-1.31	1.6
O00148	*Ddx39a; Ddx39b*	13.1	1	-1.31	2.052
P07996	*Thbs1*	3.9	1	-1.3	1.666
P05388	*Rplp0; Rplp0p6*	17	4	-1.3	1.634
O00170	*Aip*	8.8	2	-1.3	1.848
P07108	*Dbi*	37.9	3	-1.26	1.737
O75347	*Tbca*	69	6	-1.25	1.761
O95994	*Agr2*	48.6	7	-1.22	1.56
P55081	*Mfap1*	4.6	1	-1.2	1.568
P84103	*Srsf3*	40	2	-1.2	1.901
Q9NUQ9	*Fam49b*	10.8	3	1.27	1.598
Q96BM9	*Arl8a*	7.5	1	1.33	1.407
P11413	*G6pd*	27	14	1.38	1.401
Q00688	*Fkbp3*	9.4	2	1.38	1.381
P04792	*Hspb1*	61	11	1.41	3.457
P60866	*Rps20*	25.2	2	1.42	1.369
P04632	*Capns1*	18	4	1.45	1.946
Q9NR12	*Pdlim7*	2.4	1	1.46	1.845
P30511	*Hla-F*	9.9	1	1.47	1.496
P37802	*Tagln2*	57.3	10	1.49	2.245
P60903	*S100a10*	14.4	2	1.52	1.561
Q6ZVM7	*Tom1l2*	11.8	3	1.57	1.399
P10321	*Hla-C*	22.8	0	1.58	1.425
P63173	*Rpl38*	37.5	2	1.63	1.733
Q96HE7	*Ero1l*	26.5	10	1.63	2.892
P35080	*Pfn2*	17.6	2	1.63	2.689
Q8N129	*Cnpy4*	50.8	5	1.66	1.392
P04439	*Hla-A*	42.8	4	1.66	2.708
P12429	*Anxa3*	26	8	1.68	2.533
P25325	*Mpst*	21.9	4	1.71	2.49
P62942	*Fkbp12-Exin; Fkbp1a*	35.1	1	1.72	3.092
Q96G23	*Cers2*	17.2	2	1.73	2.199
Q5UCC4	*Emc10*	7.3	2	1.74	1.311
P63313	*Tmsb10*	68.2	3	1.76	2.022

P31949	*S100a11*	38.1	4	1.84	2.406
Q9H061	*Tmem126a*	10.5	2	1.84	1.5
O43278	*Spint1*	10	2	1.86	1.458
P25815	*S100p*	17.9	2	1.87	3.712
Q9Y6N5	*Sqrdl*	24.4	8	1.87	2.994
Q969W9	*Pmepa1*	5.8	1	1.88	2.078
Q14126	*Dsg2*	5.4	4	1.88	1.648
Q9BTY2	*Fuca2*	4.5	2	1.91	1.572
O00469	*Plod2*	3.7	2	1.92	3.267
Q9NYP7	*Elovl5*	5	1	1.97	1.706
O43291	*Spint2*	12.9	2	1.98	2.194
P12532	*Ckmt1b; Ckmt1a*	20.2	1	2.02	1.398
Q15942	*Zyx*	6.5	2	2.09	3.205
O00391	*Qsox1*	11.5	6	2.11	2.192
Q9UK76	*Hn1*	16.1	1	2.17	2.75
P49903	*Sephs1*	3.8	1	2.18	1.502
P60983	*Gmfb*	42.7	5	2.41	2.429
P14550	*Akr1a1*	6.8	1	2.41	1.659
P62495	*Etf1*	15.8	1	2.55	2.351
P08648	*Itga5*	2.8	2	2.6	2.797
P68133	*Acta1; Actc1; Actg2; Acta2*	32.9	4	2.61	3.142
Q13586	*Stim1*	4	1	2.73	1.529
Q16698	*Decr1*	3.3	1	2.87	2.935
P09496	*Clta*	7.7	2	2.9	2.488
P21291	*Csrp1*	50.8	6	2.94	1.91
Q31612	*Hla-B*	16	0	2.98	1.61
F6VZ39	*Rbm38*	8.9	1	3	2.628
P35237	*Serpinb6*	22.6	6	3.08	2.997
P19174	*Plcg1*	1.4	1	3.55	1.872
Q96NY8	*Pvrl4*	5.7	2	3.62	1.355
P04083	*Anxa1*	7.8	1	3.71	2.022
O43760	*Syngr2*	15.4	1	3.9	1.891
Q9NQ88	*Tigar*	6.3	1	3.99	2.609
P48960	*Cd97; Adgre2; Emr2*	2.9	2	4.05	1.483
Q9NX62	*Impad1*	31.7	1	4.37	4.602
Q10589	*Bst2*	5.6	1	4.4	2.211
Q9Y653	*Adgrg1; Gpr56*	15.2	2	4.56	2.22
P49458	*Srp9*	16.7	1	4.65	2.446
O43761	*Syngr3*	6.6	1	4.78	2.196
Q99439	*Cnn2*	33.5	5	4.93	3.677
Q8N6H7	*Arfgap2*	4	1	5.92	1.567
Q9Y240	*Clec11a*	3.4	1	6.13	2.11
P61769	*B2m*	11.3	1	6.26	2.713
Q8WTV0	*Scarb1*	2.5	1	6.31	2.349
O75083	*Wdr1*	9	2	6.32	2.577

P12109	*Col6a1*	2.7	2	6.99	1.864
Q9Y3C8	*Ufc1*	16.2	3	7	1.912
Q01581	*Hmgcs1*	5.8	1	7.11	2.327
P05976; P08590	*Myl1; Myl3*	8.2	1	8.82	1.867
P09497	*Cltb*	15.7	4	9.14	2.299
P62316	*Snrpd2*	12.8	1	10.15	3.437
Q92876	*Klk6*	13.1	2	15.26	4.904
P07711	*Ctsl*	8.4	2	19.66	6.512
Q86XT9	*Tmem219*	5.6	1	20.55	1.726

Table 20: BIAM switch assay coupled to mass spectometry – differentially oxidized proteins upon bizine treatment

UniProt ID	Gene name	Coverage [%]	Unique peptides	Fold oxidized bizine_CTRL	-log p value
P27338	*Maob*	3.3	1	-103.79	6.007
P35030	*Prss3*	7.3	1	-11.13	1.953
Q04941	*Plp2*	8.6	1	-8.43	1.368
Q9Y4G6	*Tln2*	1	1	-8.27	2.15
O00505	*Kpna3*	4	2	-7.41	3.663
Q9NYB9	*Abi2*	14.2	4	-5.86	1.887
P61956	*Sumo2*	27.4	2	-5.31	1.539
Q9UFW8	*Cggbp1*	16.8	3	-4.97	2.49
Q13595	*Tra2a*	14.5	4	-4.72	1.839
P33908	*Man1a1*	3.1	1	-3.94	1.533
Q96L92	*Snx27*	6.3	2	-3.86	1.601
H0Y5N9	*Col12a1*	1.5	1	-3.8	1.342
O14929	*Hat1*	7.4	2	-3.68	1.459
Q9UMY1	*Nol7*	7.4	1	-3.51	2.164
H3BU16	*Hn1l*	73.7	11	-3.45	1.61
Q96KC8	*Dnajc1*	4.3	2	-3.31	1.405
Q14534	*Sqle*	2.4	1	-3.03	1.939
Q8N766	*Emc1*	3.2	2	-2.91	1.617
Q6PL18	*Atad2*	3	2	-2.69	2.157
Q86U44	*Mettl3*	10.1	2	-2.35	1.87
Q8IUD2	*Erc1*	3.6	2	-2.26	1.751
Q92747	*Arpc1a*	2.7	1	-2.02	1.677
P48147	*Prep*	3.8	2	-2	1.433
P04818	*Tyms*	4.2	1	-1.95	1.855
Q969S3	*Znf622*	7.1	2	-1.89	1.371
Q9Y3L5	*Rap2c*	10.3	1	-1.8	1.849
P62888	*Rpl30*	48.2	4	-1.76	1.957
P61421	*Atp6v0d1*	16.8	3	-1.72	1.622
Q96T88	*Uhrf1*	6.9	4	-1.72	2.999
P41743	*Prkci*	8.6	3	-1.71	1.375

Q9NP58	*Abcb6*	6.7	2	-1.69	2.084
P52735	*Vav2*	4.8	4	-1.69	1.753
Q9NV56	*Mrgbp*	12.3	3	-1.66	2.54
Q00534	*Cdk6*	7.1	2	-1.64	4.292
Q96RQ3	*Mccc1*	20.2	8	-1.62	2.584
Q8NHS0	*Dnajb6*	9.2	2	-1.6	1.332
B1AK87	*Capzb*	65	16	-1.54	2.097
Q9UGU5	*Hmgxb4*	6	1	-1.53	1.593
P46977	*Stt3a*	5.7	3	-1.51	1.71
O43324	*Eef1e1*	7.3	1	-1.51	1.539
Q712K3	*Ube2r2*	2.9	1	-1.51	2.09
P35580	*Myh10*	5.4	9	-1.49	1.774
O15514	*Polr2d*	25	2	-1.48	2.22
Q86TU7	*Setd3*	5.9	2	-1.48	1.797
P61225	*Rap2b*	7.7	2	-1.48	2.179
O43776	*Nars*	17.7	6	-1.48	1.509
O95470	*Sgpl1*	11.4	4	-1.46	1.699
Q96G23	*Cers2*	7	1	-1.45	1.935
Q9UNL2	*Ssr3*	8	1	-1.45	2.166
P49711	*Ctcf*	8.5	5	-1.44	2.053
Q86UP2	*Ktn1*	8.5	9	-1.43	2.897
P42285	*Skiv2l2*	2.7	2	-1.43	1.321
Q9UMR2	*Ddx19a*	15.2	6	-1.43	2.242
P68366	*Tuba4a*	50.9	21	-1.43	1.744
P62241	*Rps8*	36.7	10	-1.41	1.678
P45880	*Vdac2*	31.6	6	-1.41	1.391
Q9UMS0	*Nfu1*	15	2	-1.4	1.427
Q969H8	*Mydgf*	48.8	4	-1.39	1.553
Q9NWV4	*C1orf123*	36.9	4	-1.39	1.567
Q9BZE4	*Gtpbp4*	6.8	3	-1.39	1.397
Q08945	*Ssrp1*	10.3	5	-1.37	1.822
Q8TAQ2	*Smarcc2*	5.9	5	-1.37	1.504
Q15286	*Rab35*	6.5	1	-1.37	1.473
Q13523	*Prpf4b*	8.4	7	-1.37	2.271
Q14C86	*Gapvd1*	1.8	2	-1.37	1.359
Q9Y606	*Pus1*	11.8	4	-1.36	1.648
Q8TCU6	*Prex1*	11.5	13	-1.36	2.297
P11279	*Lamp1*	6.2	3	-1.36	1.409
P13693	*Tpt1*	52.9	11	-1.35	2.249
Q5SXM8	*Dnlz*	27.5	2	-1.35	2.885
O14681	*Ei24*	92.9	2	-1.35	3.138
Q99543	*Dnajc2*	12.4	6	-1.34	1.735
P36873	*Ppp1cc*	28	8	-1.34	1.361
Q96N66	*Mboat7*	9.5	3	-1.34	1.417
Q9BXY0	*Mak16*	6	1	-1.34	1.812
P15941	*Muc1*	15.8	3	-1.33	2.007

P55011	*Slc12a2*	9.3	6	-1.33	3.944
Q12972	*Ppp1r8*	9.1	2	-1.33	2.072
Q99757	*Txn2*	73.4	2	-1.33	1.38
Q9HB71	*Cacybp*	45.2	11	-1.33	3.028
Q8IZP0	*Abi1*	12.2	3	-1.33	1.659
Q9H147	*Dnttip1*	23.4	5	-1.33	1.67
P24593	*Igfbp5*	16.9	7	-1.32	1.536
Q9NQX5	*Npdc1*	8.9	3	-1.32	1.432
P25205	*Mcm3*	14.6	11	-1.32	2.284
O00193	*C11orf58*	29.3	2	-1.32	1.48
P63272	*Supt4h1*	23.8	1	-1.32	1.331
H7BZJ3	*Pdia3*	58.5	11	-1.32	1.725
P46060	*Rangap1*	15.5	6	-1.32	1.337
Q3YEC7	*Rabl6*	5.6	2	-1.31	1.574
Q9H2H8	*Ppil3*	35.7	3	-1.31	1.35
Q9Y2U8	*Lemd3*	7.8	5	-1.3	1.355
Q6ZVM7	*Tom1l2*	32.7	9	-1.3	2.82
P10909	*Clu*	21.2	7	-1.3	1.302
P63208	*Skp1*	57.7	6	-1.3	1.36
O75223	*Ggct*	28.7	7	-1.29	2.09
P51571	*Ssr4*	27.2	5	-1.29	2.097
O94905	*Erlin2*	29.2	9	-1.29	1.539
Q9BZF1	*Osbpl8*	23.7	1	-1.29	1.526
P09972	*Aldoc*	22.8	10	-1.28	1.372
P18583	*Son*	2.3	3	-1.28	1.426
Q6P1J9	*Cdc73*	4	2	-1.28	1.502
Q92990	*Glmn*	1.9	1	-1.28	1.767
Q8N6H7	*Arfgap2*	47.5	13	-1.28	1.927
Q8WW12	*Pcnp*	29.8	5	-1.28	1.611
Q9BV36	*Mlph*	21.5	12	-1.28	2.501
Q15004	*Kiaa0101*	21.7	2	-1.28	1.489
P51572	*Bcap31*	38.2	15	-1.28	1.849
Q13740	*Alcam*	33.8	17	-1.27	2.527
O00762	*Ube2c*	24	4	-1.27	1.388
Q9BWQ6	*Yipf2*	15.6	1	-1.27	1.393
Q99961	*Sh3gl1*	24.2	8	-1.27	1.821
Q9UN81	*L1re1*	40.8	11	-1.27	1.877
P51149	*Rab7a*	35.3	8	-1.27	1.46
Q1L5Z9	*Lonrf2*	2.4	1	-1.27	1.49
Q14696	*Mesdc2*	26.5	6	-1.26	1.766
P49755	*Tmed10*	50.7	22	-1.26	1.922
Q15005	*Spcs2*	38.2	5	-1.26	1.658
Q9UKL0	*Rcor1*	10.1	4	-1.26	1.539
O14828	*Scamp3*	22.2	6	-1.26	1.695
P35659	*Dek*	18.1	6	-1.25	1.545
O75534	*Csde1*	14.9	11	-1.25	1.338

Q08379	*Golga2*	8.3	7	-1.25	1.49
P05023	*Atp1a1*	34.8	34	-1.25	2.095
A0A0B4J220	*C11orf98*	34.1	4	-1.25	1.436
O43852	*Calu*	49.8	10	-1.25	1.64
Q13347	*Eif3i*	36.9	11	-1.24	1.453
Q92805	*Golga1*	7.8	4	-1.23	1.933
O00148	*Ddx39a*	32.6	9	-1.23	1.746
Q3KQU3	*Map7d1*	2	1	-1.23	2.532
P33316	*Dut*	56.9	7	-1.22	1.364
P20700	*Lmnb1*	70.3	54	-1.22	2.034
Q9P2E9	*Rrbp1*	24.8	27	-1.22	1.435
Q14974	*Kpnb1*	12.6	11	-1.21	1.666
Q13242	*Srsf9*	38	11	-1.21	1.478
O00487	*Psmd14*	32.9	5	-1.21	1.644
Q969G3	*Smarce1*	17.3	6	-1.21	1.553
Q9GZZ1	*Naa50*	53.1	3	-1.2	1.47
Q14444	*Caprin1*	19.9	12	-1.2	2.26
P09874	*Parp1*	16.4	14	-1.2	1.441
Q8N335	*Gpd1l*	25.4	8	-1.2	1.547
Q9BQ70	*Tcf25*	12.9	6	-1.2	1.449
Q14258	*Trim25*	21	10	-1.2	1.385
Q13409	*Dync1i2*	12.4	4	-1.2	1.586
P61106	*Rab14*	42.3	6	-1.19	1.36
Q14165	*Mlec*	11.5	2	-1.19	1.352
Q9UPT8	*Zc3h4*	8.4	4	-1.18	1.42
Q15691	*Mapre1*	53	10	-1.18	1.715
P35998	*Psmc2*	53.8	21	-1.18	2.578
Q00839	*Hnrnpu*	37.7	31	-1.18	2.15
Q6P996	*Pdxdc1*	21.3	12	-1.18	2.216
P13798	*Apeh*	25	4	-1.17	1.306
P04843	*Rpn1*	43.7	24	-1.17	1.733
Q8WVV4	*Pof1b*	28	11	-1.16	1.417
Q8IY81	*Ftsj3*	14.8	9	-1.16	1.564
Q9BY42	*Rtfdc1*	21.4	8	-1.16	1.88
Q9NY33	*Dpp3*	23.7	11	-1.15	1.44
P05198	*Eif2s1*	56.8	17	-1.15	1.988
O15355	*Ppm1g*	39.2	13	-1.15	1.634
O43670	*Znf207*	5.5	3	-1.14	1.84
P19338	*Ncl*	45.2	41	-1.13	1.351
Q07065	*Ckap4*	65.8	37	-1.13	2.865
Q14980	*Numa1*	19.9	31	-1.13	1.307
Q16543	*Cdc37*	47.9	19	-1.13	1.977
P00918	*Ca2*	66.9	20	-1.12	1.399
P49591	*Sars*	30	19	-1.1	1.335
P02545	*Lmna*	78.6	75	-1.1	2.32
Q13263	*Trim28*	50.7	30	-1.09	1.318

Q14320	*Fam50a*	20.4	7	-1.08	1.834
P20933	*Aga*	22.8	6	1.1	1.381
Q99848	*Ebna1bp2*	26	8	1.11	1.428
P36578	*Rpl4*	47.8	25	1.13	1.659
Q15181	*Ppa1*	63.3	12	1.13	1.467
P15586	*Gns*	17.7	7	1.13	1.488
P23284	*Ppib*	56	16	1.14	1.608
P21333	*Flna*	56.8	127	1.14	1.686
P09429	*Hmgb1*	60.9	19	1.15	1.482
P51688	*Sgsh*	12	5	1.15	1.478
Q15365	*Pcbp1*	80.1	19	1.16	1.612
P19388	*Polr2e*	31.3	4	1.17	1.615
O96000	*Ndufb10*	47.7	11	1.17	1.651
O15231	*Znf185*	43.7	21	1.19	2.066
Q7Z6Z7	*Huwe1*	2.7	6	1.19	1.346
P47224	*Rabif*	22	2	1.19	1.504
P54578	*Usp14*	48.8	16	1.19	1.48
Q9UMY4	*Snx12*	68	10	1.19	1.577
O43252	*Papss1*	18.8	8	1.19	1.415
O43837	*Idh3b*	34.5	5	1.2	1.868
P04080	*Cstb*	79.6	6	1.2	1.552
P48047	*Atp5o*	64.3	14	1.2	1.553
P10619	*Ctsa*	8.9	4	1.2	1.328
Q53HV7	*Smug1*	7.5	1	1.21	1.304
Q8NFV4	*Abhd11*	64.8	15	1.21	1.839
P53004	*Blvra*	16.9	4	1.21	1.897
Q9HCU4	*Celsr2*	12.3	21	1.22	1.319
P11908	*Prps2; Prps1*	18.6	4	1.22	1.41
Q6NUK1	*Slc25a24*	32.5	14	1.22	1.582
O00264	*Pgrmc1*	24.1	7	1.22	2.077
O43447	*Ppih*	40.1	5	1.23	1.364
O60869	*Edf1*	32.4	5	1.23	1.339
Q7Z4H3	*Hddc2*	42.6	6	1.24	1.379
P25787	*Psma2*	53.4	11	1.24	1.76
P62937	*Ppia*	86.1	17	1.24	1.7
Q9BV57	*Adi1*	50.8	7	1.24	1.575
P28331	*Ndufs1*	28.6	11	1.24	1.727
P30086	*Pebp1*	81.3	16	1.25	1.414
P53801	*Pttg1ip*	7.5	1	1.25	1.311
Q9HCH5	*Sytl2*	10.9	19	1.26	1.43
P34897	*Shmt2*	55.2	23	1.27	1.419
Q9BS40	*Lxn*	21.2	4	1.28	2.566
Q5BKX5	*C19orf54*	2.8	1	1.28	1.577
Q00577	*Pura*	14.6	3	1.28	1.691
Q9Y508	*Rnf114*	15.4	3	1.28	2.263
O43681	*Asna1*	22.1	7	1.28	1.372

Q13867	*Blmh*	12.3	2	1.29	1.44
Q5TFE4	*Nt5dc1*	26.4	7	1.29	1.591
Q92597	*Ndrg1*	15	5	1.29	1.493
Q9NZL9	*Mat2b*	14.7	4	1.29	1.382
P23771	*Gata3*	14.2	5	1.3	1.53
P18669	*Pgam1; Pgam4*	76.8	22	1.3	1.459
Q96SZ5	*Ado*	9.6	3	1.3	2.106
B1ANS9	*Wdr64*	1.8	2	1.3	1.81
Q15942	*Zyx*	32	14	1.31	1.694
P04632	*Capns1*	49.4	17	1.31	3.857
P82650	*Mrps22*	7.8	2	1.32	1.304
Q96GE9	*Tmem261*	32.8	1	1.32	1.92
P09382	*Lgals1*	65.9	6	1.32	1.998
Q495W5	*Fut11*	2	1	1.32	1.436
Q9BUH6	*C9orf142*	32.8	7	1.33	1.886
Q8WVM8	*Scfd1*	16.2	7	1.33	1.386
Q8IWL3	*Hscb*	12.6	2	1.35	2.735
P32322	*Pycr1*	23.5	7	1.36	1.744
Q9NR12	*Pdlim7*	26.7	8	1.36	1.402
P31937	*Hibadh*	47.6	11	1.36	1.632
Q99439	*Cnn2*	40.9	9	1.37	3.042
Q9H501	*Esf1*	1.6	1	1.37	1.687
Q9Y6M9	*Ndufb9*	34.5	5	1.37	2.423
P28676	*Gca*	13	2	1.39	2.735
P18564	*Itgb6*	1.3	1	1.4	2.649
Q8IYT4	*Katnal2*	9.4	1	1.4	1.986
P78406	*Rae1*	31	8	1.41	1.812
P30046	*Ddt; Ddtl*	44.1	4	1.41	1.975
Q13084	*Mrpl28*	21.9	4	1.42	2.59
Q9H8W5	*Trim45*	6.3	2	1.42	1.385
P08579	*Snrpb2*	16.9	3	1.44	2.04
Q8IWY4	*Scube2; Scube1; Scube3*	3	2	1.44	1.837
Q01995	*Tagln*	65.7	10	1.45	2.53
Q9Y3D2	*Msrb2*	11.5	2	1.45	1.682
Q9Y6H1	*Chchd2; Chchd2p9*	18.5	1	1.46	1.769
Q9ULF5	*Slc39a10*	14.3	2	1.46	2.857
P53634	*Ctsc*	4.9	1	1.47	1.809
O75828	*Cbr3*	25.6	7	1.47	3.132
Q8N2F6	*Armc10*	10.8	3	1.48	1.764
Q13011	*Ech1*	32.9	9	1.48	4.325
P51452	*Dusp3*	18.9	2	1.5	2.04
Q969T9	*Wbp2*	20.5	2	1.52	1.482
P61769	*B2m*	47.9	5	1.53	1.653
P62837	*Ube2d2*	42.9	4	1.63	2.407
P17900	*Gm2a*	16.1	3	1.67	3.323

O00410	*Ipo5*	35.1	2	1.73	1.982
Q9BVS5	*Trmt61b*	3.8	1	1.74	2.2
P18084	*Itgb5*	27.3	2	1.76	2.247
P05386	*Rplp1*	84.2	4	1.76	1.397
P12074	*Cox6a1*	26.6	1	1.8	2.23
Q9UL45	*Bloc1s6*	33.3	1	2.11	2.462
P28290	*Ssfa2*	1.2	1	2.51	1.475
P16219	*Acads*	3.2	1	2.53	1.607
M0QY43	*Myh14*	18.4	14	2.57	1.521
Q9Y6Y8	*Sec23ip*	3.3	1	2.95	1.459
Q96GS4	*C17orf59*	16.5	3	3.16	1.58
P08670	*Vim; Prph*	8.1	4	3.29	3.498
P63172	*Dynlt1*	23.9	1	3.48	2.473
Q8NFJ5	*Gprc5a*	13.7	2	3.5	1.896
P35754	*Glrx*	39.6	3	8.46	3.396
Q969Q0	*Rpl36a; Rpl36al; Rpl36a-Hnrnph2*	14.1	3	38.94	8.797

Table 21: BIAM switch assay coupled to mass spectometry – differentially oxidized proteins upon SP2509 treatment

UniProt ID	Gene name	Coverage [%]	Unique peptides	fold oxidized SP2509_CTRL	- log p value
Q15388	*Tomm20*	34.5	4	-16.32	3.04
P49721	*Psmb2*	26.9	3	-10.95	2.68
Q9P2B2	*Ptgfrn*	5.7	5	-10.81	5.83
Q13442	*Pdap1*	17.1	2	-8.36	3.78
Q08209	*Ppp3ca; Ppp3cb*	9.4	4	-6.92	3.09
P07741	*Aprt*	42.8	7	-6.50	2.83
P62308	*Snrpg; Snrpgp15*	20.3	2	-5.32	1.44
Q9GZZ1	*Naa50*	49.4	3	-5.27	1.51
P56537	*Eif6*	36.7	5	-5.01	1.76
Q99873	*Prmt1*	10.8	3	-4.69	1.92
Q15257	*PPP2R4; Dkfzp781m17165*	19.6	4	-4.48	2.01
Q8N983	*Mrpl43*	19.6	3	-4.19	4.56
P0DPB6	*Polr1d*	26.3	4	-4.03	2.83
Q8WXX5	*Dnajc9*	49.6	14	-4.00	2.22
Q01658	*Dr1*	23.9	4	-3.88	2.19
P12532	*Ckmt1a; Ckmt1b*	39.8	10	-3.85	2.34
P15941	*Muc1*	7.4	1	-3.80	1.71
P60866	*Rps20*	35.3	7	-3.69	2.09
P47813	*Eif1ax; Eif1ay*	41	6	-3.64	2.04
O00423	*Eml1*	30.6	2	-3.50	2.24
P02144	*Mb*	38.3	5	-3.49	1.45

P60953	*Cdc42*	41.4	8	-3.46	2.30
P53597	*Suclg1*	7.2	2	-3.43	1.68
P51149	*Rab7a*	61.8	13	-3.30	2.01
O95202	*Letm1*	13.7	9	-3.30	2.31
O75531	*Banf1*	59.6	6	-3.17	1.43
P49773	*Hint1*	70.6	7	-3.15	1.90
Q9NQX5	*Npdc1*	6.9	2	-3.11	1.38
P43487	*Ranbp1*	53.2	9	-2.96	1.76
Q15008	*Psmd6*	29.2	4	-2.89	1.33
Q9HAV7	*Grpel1*	62.7	11	-2.84	1.93
O00204	*Sult2b1*	11	3	-2.84	1.94
Q9H773	*Dctpp1*	42.9	5	-2.84	2.05
P36551	*Cpox*	9.7	1	-2.81	1.72
Q9UKD2	*Mrto4*	14.2	4	-2.72	1.47
O60763	*Uso1*	6.3	3	-2.68	1.80
Q9UHQ4	*Bcap29*	13.7	2	-2.66	2.34
O15305	*Pmm2*	30.1	8	-2.64	2.16
P63000	*Rac1; Rac2; Rac3*	22.9	4	-2.60	1.48
Q6EMK4	*Vasn*	6.7	3	-2.56	2.48
Q9Y3L3	*Sh3bp1*	4.1	2	-2.56	1.60
Q96EY8	*Mmab*	23.6	6	-2.54	1.33
Q9NXG6	*P4htm*	13.1	4	-2.49	3.54
Q15005	*Spcs2*	23.6	3	-2.48	1.68
P63208	*Skp1*	73	8	-2.46	2.18
Q16625	*Ocln*	9.4	3	-2.42	2.13
P13693	*Tpt1*	41.3	12	-2.38	2.10
Q9NUQ9	*Fam49b*	14.8	4	-2.38	2.57
Q9P289	*Stk26; Stk25*	16.6	3	-2.34	2.15
P62263	*Rps14*	41.7	9	-2.32	1.59
P16152	*Cbr1*	27.8	4	-2.31	2.74
P37108	*Srp14*	47	6	-2.31	1.61
P51572	*Bcap31*	39	22	-2.24	1.83
P55209	*Nap1l1*	41.8	4	-2.23	1.59
Q12765	*Scrn1*	13.3	5	-2.21	1.80
P15374	*Uchl3*	30.4	5	-2.19	1.75
P21912	*Sdhb*	15.7	4	-2.19	1.78
P28331	*Ndufs1*	8.8	4	-2.19	1.44
Q71DI3	*Hist2h3a*	47.8	1	-2.17	2.08
P09497	*Cltb*	30.1	9	-2.17	1.31
Q9NRF9	*Pole3*	20.4	2	-2.16	1.30
P08134	*Rhoc*	15.4	3	-2.16	1.99
P62241	*Rps8*	36.7	9	-2.15	1.53
Q9UN81	*L1re1*	20.1	7	-2.15	1.91
P62826	*Ran*	17.6	4	-2.13	2.18
P04632	*Capns1*	35.7	11	-2.10	2.59
P31949	*S100a11*	86.7	11	-2.10	1.90

P55317	*Foxa1*	3.6	1	-2.07	1.60
P63173	*Rpl38*	54.3	5	-2.06	1.53
Q9Y383	*Luc7l2*	32.7	12	-2.05	1.59
P25398	*Rps12*	59.8	9	-2.03	1.85
P10606	*Cox5b*	20.9	4	-2.03	1.86
P05455	*Ssb*	34.8	15	-2.02	1.50
Q9UN37	*Vps4a*	12.4	4	-2.02	1.98
Q9HB07	*C12orf10*	11.3	2	-2.01	1.35
O15347	*Hmgb3*	36.7	9	-1.99	1.89
P53990	*Ist1*	44.7	7	-1.98	2.76
P23193	*Tcea1*	39.5	9	-1.97	1.89
P0DMV9	*Hspa1b; Hspa1a*	60.7	19	-1.97	1.59
Q99848	*Ebna1bp2*	16.6	5	-1.93	1.59
P61247	*Rps3a*	62.1	23	-1.93	1.42
Q9HB71	*Cacybp*	50	13	-1.93	1.81
P31946	*Ywhab*	76.4	16	-1.92	1.86
P01034	*Cst3*	30.8	4	-1.92	3.21
Q5TEC6	*Hist2h3ps2*	24.3	2	-1.92	1.70
Q9H1E3	*Nucks1*	18.5	2	-1.91	2.48
O00231	*Psmd11*	29.4	12	-1.90	1.72
P08243	*Asns*	3.6	2	-1.90	1.57
Q99615	*Dnajc7*	13.4	5	-1.89	1.57
Q96JH7	*Vcpip1*	3.7	2	-1.88	1.43
P50502	*St13; St13p5; St13p4*	20.3	10	-1.85	1.45
Q96CN7	*Isoc1*	28.5	5	-1.85	1.43
Q96KP4	*Cndp2*	25.5	9	-1.84	2.16
P22061	*Pcmt1*	39.9	9	-1.83	2.44
P62136	*Ppp1ca*	26.1	3	-1.81	2.68
P07195	*Ldhb*	21.9	3	-1.79	1.60
P33316	*Dut*	42.6	5	-1.78	1.36
Q13641	*Tpbg*	9.3	4	-1.78	2.03
P02794	*Fth1*	21.6	3	-1.76	1.85
O14828	*Scamp3*	19.9	5	-1.76	1.85
P23528	*Cfl1*	92.8	16	-1.75	1.38
P52292	*Kpna2*	15.7	6	-1.74	2.02
P61981	*Ywhag*	67.2	14	-1.74	1.64
Q16698	*Decr1*	20.6	7	-1.74	1.38
Q15758	*Slc1a5*	12.9	7	-1.74	1.78
P05388	*Rplp0; Rplp0p6*	22.1	6	-1.74	2.11
P20290	*Btf3*	20.4	2	-1.73	1.79
P18206	*Vcl*	22.2	20	-1.72	2.18
P30084	*Echs1*	43.4	11	-1.71	1.59
P61289	*Psme3*	27.9	4	-1.70	1.61
O60701	*Ugdh*	44.5	16	-1.70	1.75
Q15006	*Emc2*	29.6	5	-1.69	2.73
P39019	*Rps19*	41.4	8	-1.69	2.58

O00264	*Pgrmc1*	15.9	5	-1.67	1.48
P19404	*Ndufv2*	21.4	4	-1.67	2.92
Q16651	*Prss8*	6.1	2	-1.67	2.20
O75223	*Ggct*	22.9	7	-1.65	1.85
P26583	*Hmgb2*	32.5	10	-1.65	1.50
P39748	*Fen1*	24.7	7	-1.64	1.63
Q13838	*Ddx39b*	32.5	5	-1.64	2.29
Q16543	*Cdc37*	47.9	19	-1.64	2.00
Q99613	*Eif3c; Eif3cl*	10.8	7	-1.64	3.12
Q13630	*Tsta3*	15.3	5	-1.63	1.49
O15355	*Ppm1g*	35.2	13	-1.63	1.44
P09429	*Hmgb1*	44.2	15	-1.62	1.76
Q8N335	*Gpd1l*	13.4	2	-1.62	1.41
P50395	*Gdi2*	34.8	10	-1.57	1.85
Q71UI9	*H2afv; H2afz*	47.5	4	-1.57	2.39
O95456	*Psmg1*	31.7	1	-1.57	1.41
O75844	*Zmpste24*	7.4	2	-1.55	1.47
P03372	*Esr1*	5.8	1	-1.54	1.56
P25786	*Psma1*	39.2	9	-1.53	2.58
P62913	*Rpl11*	29.8	6	-1.52	1.64
Q9Y4L1	*Hyou1*	28.1	16	-1.51	1.63
P52815	*Mrpl12*	7.5	3	-1.50	1.82
O00299	*Clic1*	46.5	9	-1.50	1.57
Q15904	*Atp6ap1*	16.4	3	-1.50	1.89
O43291	*Spint2*	28.2	5	-1.49	1.56
Q9BQ70	*Tcf25*	17.1	2	-1.48	2.35
P50213	*Idh3a*	26.3	8	-1.48	1.66
P49368	*Cct3*	52.2	21	-1.48	1.99
P09467	*Fbp1*	53.8	15	-1.48	1.68
P24534	*Eef1b2*	44	7	-1.48	2.34
P05556	*Itgb1*	15	10	-1.48	1.34
P35270	*Spr*	29.1	5	-1.46	3.45
Q02818	*Nucb1*	22.3	9	-1.46	1.41
P23396	*Rps3*	52.3	12	-1.46	1.58
O00193	*C11orf58; SMAP*	25.6	2	-1.44	1.74
Q99879	*Hist1h2bm*	72.2	1	-1.44	2.73
Q14974	*Kpnb1*	12.4	10	-1.43	1.55
P00918	*Ca2*	31.9	8	-1.42	1.47
P09496	*Clta*	11.5	5	-1.42	2.29
Q92598	*Hsph1*	24.9	18	-1.41	2.46
Q13404	*Ube2v1; Tmem189-Ube2v1*	45.6	2	-1.40	2.49
Q86VP6	*Cand1*	8.1	6	-1.39	1.35
P17844	*Ddx5*	27	14	-1.38	2.35
P05387	*Rplp2*	64.3	6	-1.36	1.36
Q01130	*Srsf2*	38.5	5	-1.35	2.94

P26196	*Ddx6*	13.5	3	-1.34	1.73
Q9Y4Z0	*Lsm4*	15.2	3	-1.33	1.34
Q9UHX1	*Puf60*	20.6	7	-1.32	2.35
P49023	*Pxn*	7.2	3	-1.29	1.48
P28066	*Psma5*	32.8	6	1.29	3.08
Q13347	*Eif3i*	26.8	7	1.34	1.32
O43399	*Tpd52l2*	23.9	7	1.35	1.42
Q15056	*Eif4h*	35.5	7	1.36	1.85
Q9NX40	*Ociad1*	33.5	6	1.37	2.13
P62906	*Rpl10a*	27.2	6	1.38	3.72
P67809	*Ybx1*	51.2	13	1.39	1.58
P46783	*Rps10*	38.8	7	1.39	2.26
O43768	*Ensa*	19.3	3	1.40	1.72
P35637	*Fus*	20.2	6	1.41	1.41
Q92841	*Ddx17*	20.9	8	1.41	2.14
P80303	*Nucb2; Hel-S-109; Nucb2*	36.4	13	1.41	1.47
P80723	*Basp1*	33.9	5	1.41	1.45
P17931	*Lgals3*	17.2	4	1.41	1.60
P01111	*Nras; Hras*	48.7	3	1.41	1.76
P35998	*Psmc2*	27.5	13	1.42	2.30
Q9Y3B9	*Rrp15*	4.6	1	1.43	1.33
Q15637	*Sf1*	14.2	7	1.43	1.85
P09012	*Snrpa*	14.2	2	1.47	1.53
Q01105	*Set; Setsip*	27.4	5	1.49	1.32
P11142	*Hspa8*	52.8	18	1.49	1.42
P42126	*Eci1; Dci*	13.6	4	1.49	1.70
P16403	*Hist1h1c; Hist1h1a*	31	3	1.50	1.32
P61978	*Hnrnpk*	57	8	1.50	1.40
P62191	*Psmc1*	36.4	18	1.52	1.60
P30044	*Prdx5*	49.1	10	1.53	1.39
P62333	*Psmc6*	27.5	10	1.54	2.74
Q9UNS2	*Cops3*	17.3	5	1.57	2.09
P37837	*Taldo1*	16.9	5	1.57	1.88
Q29RF7	*Pds5a*	3.9	3	1.58	1.38
P62805	*Hist1h4a*	64.1	10	1.59	2.45
P02545	*Lmna*	39.2	0	1.59	1.32
Q01813	*Pfkp*	5.2	4	1.59	1.35
Q15365	*Pcbp1*	50.8	8	1.59	1.30
P17980	*Psmc3*	47	14	1.60	1.57
P21333	*Flna*	33.3	3	1.62	1.91
P33991	*Mcm4*	9	6	1.63	1.46
Q9Y3I0	*Rtcb*	25.5	10	1.63	1.91
Q14203	*DCTN1; Dkfzp686e0752*	4.2	4	1.63	1.35
P35579	*Myh9*	29.5	44	1.64	1.63

P09651	*Hnrnpa1; Hnrnpa1l2*	48.2	18	1.65	1.35
Q8IZR5	*Cmtm4*	10	2	1.65	1.42
Q9BUF5	*Tubb6*	18.2	2	1.66	1.84
O00567	*Nop56*	6.6	4	1.67	2.06
E9PQ80	*Chmp4a*	4.7	1	1.67	1.38
Q07157	*Tjp1*	3.3	3	1.68	2.08
P22314	*Uba1*	33	26	1.68	1.72
Q96NB2	*Sfxn2*	8.1	2	1.69	1.40
Q15942	*Zyx*	20.5	9	1.69	1.47
P14618	*Pkm*	66.1	36	1.69	2.40
P52272	*Hnrnpm*	39.3	26	1.69	1.44
P00558	*Pgk1*	71.9	26	1.70	1.71
P33176	*Kif5b*	12.7	8	1.70	1.90
O75369	*Flnb*	9	14	1.72	2.91
Q15019	*Septin9*	26.2	5	1.73	2.00
Q93084	*Atp2a3*	5.7	2	1.73	2.01
P00367	*Glud1; Glud2*	24.9	11	1.74	1.34
P51991	*Hnrnpa3*	38.1	16	1.74	1.80
P08195	*Slc3a2*	20	11	1.74	1.56
Q9UM54	*Myo6*	4.5	4	1.75	2.40
Q8WWM7	*Atxn2l*	5.3	5	1.77	2.38
P18754	*Rcc1*	24.7	5	1.80	1.49
O14579	*Cope*	22.1	5	1.81	1.47
P30101	*Pdia3*	66.3	33	1.82	1.91
P38646	*Hspa9*	38.3	22	1.84	3.02
P22626	*Hnrnpa2b1*	47.6	22	1.87	1.62
P28074	*Psmb5*	9.9	2	1.87	2.74
P50454	*Serpinh1*	19.9	5	1.91	1.71
Q9ULV4	*Coro1c*	29.1	4	1.91	2.25
P07686	*Hexb*	41.1	14	1.93	1.39
Q32MZ4	*Lrrfip1*	5.6	4	1.94	2.19
Q9H3N1	*Tmx1*	19.6	5	1.96	1.94
Q92625	*Anks1a*	2.3	2	1.97	1.69
P61006	*Rab8a*	21.7	3	1.97	1.88
P06576	*Atp5b*	74.7	25	1.98	1.68
Q9Y230	*Ruvbl2*	21.4	8	1.99	1.48
P25705	*Atp5a1*	35.4	16	2.01	1.72
P09622	*Dld*	20.6	7	2.02	4.29
P12830	*Cdh1*	21	12	2.04	1.34
P40939	*Hadha*	14.9	8	2.11	1.54
Q96EY1	*Dnaja3*	15	5	2.11	1.51
Q8WW12	*Pcnp*	18.5	3	2.13	1.40
P14625	*Hsp90b1*	21.7	14	2.13	2.33
Q96HE7	*Ero1l*	32.7	7	2.15	1.97
O60506	*Syncrip*	15.1	6	2.17	1.58
P27695	*Apex1*	23.1	5	2.17	2.51

P04439	*Hla-A*	27.4	3	2.20	1.73
P23588	*Eif4b*	16.6	6	2.26	1.64
P68036	*Ube2l3*	69.5	14	2.27	1.42
P49755	*Tmed10*	45.7	13	2.28	1.73
Q01650	*Slc7a5*	6.7	3	2.28	1.82
P18124	*Rpl7*	28.6	8	2.28	2.11
P30085	*Cmpk1*	31.6	5	2.29	1.56
P00338	*Ldha*	31	8	2.31	3.75
P50552	*Vasp*	18.9	5	2.34	3.38
P62280	*Rps11*	21.2	3	2.39	1.72
O43670	*Znf207*	4.1	2	2.39	1.43
P84098	*Rpl19*	38.3	9	2.41	1.70
P61026	*Rab10*	17	2	2.41	1.41
Q14847	*Lasp1*	33	8	2.54	2.14
O60568	*Plod3*	18.4	11	2.58	1.76
P07237	*P4hb*	72.4	48	2.59	2.92
P54819	*Ak2*	66.9	16	2.61	1.80
Q9NRP2	*Cmc2*	21.8	2	2.68	2.69
Q9HCC0	*Mccc2*	6.2	3	2.69	2.20
P27816	*Map4*	6.4	7	2.70	1.55
P38606	*Atp6v1a*	7.1	4	2.74	1.52
P26373	*Rpl13*	19.9	6	2.88	1.30
Q9BS26	*Erp44*	45.6	18	2.88	1.68
P09874	*Parp1*	9.8	8	2.90	3.24
O94905	*Erlin2*	20.9	5	3.05	1.58
Q02809	*Plod1*	3.6	2	3.31	1.37
P61106	*Rab14*	20.9	3	3.35	2.09
O14618	*Ccs*	39.7	3	3.58	1.37
Q86X29	*Lsr*	14.5	7	3.74	1.66
P20700	*Lmnb1*	54.9	27	3.77	2.42
Q9NT62	*Atg3*	18.8	6	3.84	2.41
Q7Z7H5	*Tmed4*	18.9	3	3.88	1.48
P46013	*Mki67*	1.3	2	4.08	2.48
Q5RI15	*Cox20*	21.2	3	4.20	1.32
P30041	*Prdx6*	67.9	17	4.23	1.36
O43242	*Psmd3*	16.5	6	4.30	2.12
Q15738	*Nsdhl*	11.4	2	4.37	2.47
P07814	*Eprs*	5.2	7	4.64	1.37
O94766	*B3gat3*	6.9	2	4.80	2.58
Q15233	*Nono*	47.3	22	4.81	1.39
P35241	*Rdx*	23.8	8	4.83	2.17
Q15459	*Sf3a1*	3.9	4	5.01	2.06
P61254	*Rpl26; Rpl26l1*	33.8	2	7.02	1.45
P11387	*Top1*	7.2	5	7.86	1.89
P04843	*Rpn1*	21.7	10	8.53	2.23
Q15084	*Pdia6*	51.1	23	2.18	2.18

P51858	*Hdgf*	30.4	5	1.46	1.46
Q9HDC9	*Apmap*	31.7	8	1.81	1.81
P04181	*Oat*	6.2	2	1.95	1.95
P17568	*Ndufb7*	24.1	3	1.46	1.46
Q9UBS4	*Dnajb11*	30.7	12	1.89	1.89
P63279	*Ube2i*	21.9	3	3.23	3.23
Q9HCN8	*Sdf2l1*	53.4	6	1.51	1.51
P15311	*Ezr*	30.9	14	1.89	1.89
P13667	*Pdia4*	45.7	29	2.79	2.79
Q9UHD8	*Septin9*	21.2	10	1.62	1.62
Q14696	*Mesdc2*	12.4	3	1.82	1.82
P10599	*Txn*	31.4	5	1.89	1.89
O76021	*Rsl1d1*	11.2	3	3.63	3.63
O43390	*Hnrnpr*	14.2	4	1.63	1.63
P61088	*Ube2n*	71.7	9	2.08	2.08
O76024	*Wfs1*	8.1	6	2.17	2.17
O00515	*Lad1*	9.4	3	2.83	2.83
Q9UPT8	*Zc3h4*	6.6	3	2.40	2.40
P61086	*Ube2k*	36	7	1.91	1.91
Q9BVK6	*Tmed9*	31.1	9	1.99	1.99
Q15363	*Tmed2*	31.9	4	1.57	1.57
P26885	*Fkbp2*	33.8	4	2.25	2.25
P02786	*Tfrc*	12.5	7	3.40	3.40
Q14697	*Ganab*	30.6	4	1.94	1.94
O60749	*Snx2*	9.6	4	1.51	1.51
Q02878	*Rpl6*	13.5	5	1.92	1.92
Q13162	*Prdx4*	40.2	8	2.04	2.04
P27824	*Canx*	28.9	16	1.54	1.54
Q14247	*Cttn*	30.9	11	2.10	2.10
P19338	*Ncl*	30.6	22	1.41	1.41
P31146	*Coro1a*	6.1	2	1.30	1.30
Q92544	*Tm9sf4*	6.4	4	1.34	1.34
Q9Y697	*Nfs1*	16	4	1.86	1.86
Q969H8	*Mydgf*	38.1	3	1.83	1.83
P27797	*Calr*	60.2	15	2.16	2.16
P49257	*Lman1*	10.2	5	1.33	1.33
Q9Y6N5	*Sqrdl*	11.1	5	1.41	1.41
P35222	*Ctnnb1*	3.8	2	1.80	1.80
P20340	*Rab6a*	22.1	4	1.33	1.33
P13674	*P4ha1*	34.5	14	3.48	3.48
Q13438	*Os9*	18.6	9	2.52	2.52
O15460	*P4ha2*	9.7	4	1.84	1.84
Q07020	*Rpl18*	20	2	1.39	1.39
Q99470	*Sdf2*	18	2	2.40	2.40
Q03252	*Lmnb2*	9.4	3	1.50	1.50
Q96S66	*Clcc1*	12.7	4	2.58	2.58

P31350	*Rrm2*	6.1	3	1.62	1.62
O60361	*Nme2p1*	40.1	1	2.60	2.60
P08621	*Snrnp70*	11.7	5	1.67	1.67
P63010	*Ap2b1; Ap1b1*	2.7	2	1.38	1.38
P54578	*Usp14*	8.1	3	2.74	2.74
O75477	*Erlin1*	19.4	5	1.75	1.75
P38159	*Rbmx; Rbmxl1*	42.5	17	2.83	2.83
P39060	*Col18a1*	3.1	3	3.73	3.73
P50914	*Rpl14*	25	3	2.12	2.12
Q13509	*Tubb3*	33.6	3	3.12	3.12
Q92597	*Ndrg1*	10.9	3	4.56	4.56

Table 22: Proteome analysis – changed protein levels upon LSD1 knockout

UniProt ID	Gene name	Coverage [%]	Unique peptides	Fold changed siRNA_CTRL	-log p value
Q15465	*Shh*	13	3	-17.75	3.48
Q9BVK6	*Tmed9*	15.7	2	-15.93	5.50
O15551	*Cldn3*	6.4	1	-14.69	3.95
P52815	*Mrpl12*	2.5	1	-13.40	2.28
A0A1W2PQC2	*Hadh*	33.9	2	-10.28	3.08
P81274	*Gpsm2*	2.2	1	-8.99	5.88
Q9Y4P3	*Tbl2*	3.2	1	-7.13	1.65
P48431	*Sox2*	6.3	1	-6.66	2.40
O60341	*Kdm1a*	6.7	4	-6.23	2.31
Q96BT3	*Cenpt*	14	1	-5.14	2.03
Q7Z2W4	*Zc3hav1*	1.3	1	-4.81	1.32
P56385	*Atp5i*	34.8	2	-4.64	1.37
Q9GZN1	*Actr6*	5.1	1	-4.57	1.60
Q96RE7	*Nacc1*	8	3	-4.39	1.63
Q6N021	*Tet2*	1.9	1	-4.37	1.43
Q6ZSJ8	*C1orf122*	12.7	1	-4.23	1.49
Q9BQ75	*Cmss1*	3.6	1	-4.05	1.33
O60281	*Znf292*	0.8	1	-3.54	1.53
Q5T9B7	*Ak1*	27.5	1	-3.45	3.17
P48059	*Lims1*	5.7	1	-3.39	1.61
P56159	*Gfra1*	18.1	5	-3.26	2.60
Q3KR16	*Plekhg6*	3.4	1	-3.23	2.40
O15240	*Vgf*	14.3	6	-3.22	4.82
Q9H3P2	*Nelfa*	6.6	3	-3.19	1.33
Q14254	*Flot2*	18.9	7	-3.18	3.05
Q9H2F5	*Epc1*	2.9	1	-3.17	2.13
Q7L4I2	*Rsrc2*	5.1	2	-3.02	3.55
Q08J23	*Nsun2*	5.2	2	-3.01	1.87
Q5T8P6	*Rbm26*	3.7	2	-2.99	1.77

Q13526	*Pin1*	38.9	2	-2.94	2.59
Q9UKL0	*Rcor1*	26.8	6	-2.85	6.35
Q9BQ04	*Rbm4b; Rbm4*	27.3	1	-2.75	2.55
Q13207	*Tbx2*	7.9	5	-2.74	1.56
P28331	*Ndufs1*	7.4	2	-2.71	1.53
P34947	*Grk6; Grk5*	2.9	1	-2.70	1.64
Q8TD43	*Trpm4*	1.8	1	-2.70	1.97
Q9BRJ7	*Nudt16l1*	10.1	2	-2.68	1.90
Q6P1L8	*Mrpl14*	6.9	1	-2.62	1.73
Q9Y6X9	*Morc2*	12	1	-2.62	1.41
P78347	*Gtf2i*	41.5	33	-2.48	6.02
O15392	*Birc5*	9.9	1	-2.46	2.71
O75525	*Khdrbs3*	9.2	2	-2.45	1.53
Q9UN76	*Slc6a14*	2.2	1	-2.43	1.54
Q69YI7	*Naif1*	4	1	-2.42	1.85
O60306	*Aqr*	2.9	3	-2.41	1.36
O75955	*Flot1*	31.1	9	-2.41	3.01
Q16625	*Ocln*	16.3	5	-2.41	4.64
P26196	*Ddx6*	13.5	3	-2.41	2.17
Q9BYN8	*Mrps26*	8.8	1	-2.39	3.28
O43684	*Bub3*	15.8	3	-2.39	1.54
Q13111	*Chaf1a*	13.4	6	-2.37	3.71
Q9HC84	*Muc5b*	4.4	5	-2.37	3.71
Q9BW71	*Hirip3*	4.5	2	-2.36	3.54
Q9HCY8	*S100a14*	65.4	5	-2.35	3.39
P16455	*Mgmt*	11.6	2	-2.34	1.90
Q15599	*Slc9a3r2*	34.1	10	-2.33	8.56
P00338	*Ldha*	4.8	1	-2.29	3.03
Q6IAA8	*Lamtor1*	16.5	1	-2.26	2.07
Q9BXS6	*Nusap1*	5.4	2	-2.23	1.43
A0A1B0GW37		3.9	1	-2.21	3.78
P13984	*Gtf2f2*	20.5	4	-2.20	1.80
Q68DK7	*Msl1*	20.2	5	-2.18	2.82
Q96D46	*Nmd3*	7.2	2	-2.18	1.91
O95994	*Agr2*	65.1	10	-2.16	2.30
Q15366	*Pcbp2; Pcbp3*	31.6	4	-2.15	2.44
Q9NZI7	*Ubp1*	11.1	4	-2.14	2.66
P62873	*Gnb1*	12.1	2	-2.14	3.60
O95239	*Kif4a*	18.4	16	-2.12	5.18
P61165	*Tmem258*	16.3	1	-2.10	1.56
Q99583	*Mnt*	30.3	1	-2.08	1.39
Q6SPF0	*Samd1*	18.3	5	-2.08	4.95
Q02241	*Kif23*	22.2	16	-2.06	5.02
Q15147	*Plcb4*	2.1	2	-2.06	2.35
Q8WYB5	*Kat6b*	4.3	6	-2.06	3.17
Q01105	*Set; Setsip*	18	4	-2.05	1.74

Q15545	*Taf7*	11.5	3	-2.01	2.18
O43524	*Foxo3*	1.8	1	-2.01	1.74
Q13459	*Myo9b*	0.8	1	-2.00	2.15
Q14807	*Kif22*	4.7	2	-1.98	1.31
P29372	*Mpg*	28.2	5	-1.98	4.45
Q8IY57	*Yaf2*	15	1	-1.97	1.55
Q9BQ61	*C19orf43*	23.9	4	-1.95	5.09
Q9BU76	*Mmtag2*	15.2	3	-1.95	3.71
Q15911	*Zfhx3*	2.5	6	-1.94	1.31
Q01130	*Srsf2*	36.9	4	-1.93	3.02
P05204	*Hmgn2*	43.3	5	-1.92	2.56
O95347	*Smc2*	10.3	11	-1.91	3.35
Q14697	*Ganab*	7.4	5	-1.91	4.53
Q9NZ63	*C9orf78*	15.9	3	-1.91	2.96
P40199	*Ceacam6*	6.1	1	-1.87	1.94
P35269	*Gtf2f1*	18.8	6	-1.87	2.26
Q9Y237	*Pin4*	41.2	3	-1.86	1.74
Q9UNL4	*Ing4*	46.8	1	-1.86	1.59
Q96GY3	*Lin37*	12.6	2	-1.85	1.98
Q01664	*Tfap4*	26.9	6	-1.85	2.99
Q86UK7	*Znf598*	4.1	3	-1.84	2.37
Q9UIU6	*Six4*	5.9	1	-1.83	1.60
O15054	*Kdm6b*	15.1	20	-1.81	2.38
P51531	*Smarca2*	11.4	8	-1.80	1.83
Q9P2P1	*Nynrin*	0.9	1	-1.79	1.39
Q96DF8	*Dgcr14*	14.3	3	-1.79	4.57
Q8NDX6	*Znf740*	6.7	1	-1.79	2.88
P39748	*Fen1*	38.4	9	-1.79	2.82
Q9Y6X8	*Zhx2*	8.4	5	-1.78	2.37
F5H3C5	*Sod2*	37.8	3	-1.78	1.59
P36508	*Znf143; Znf76*	6.1	2	-1.78	3.56
Q01970	*Plcb3*	5.9	5	-1.78	2.83
Q9UHF7	*Trps1*	21.5	19	-1.78	4.56
Q8WUT1	*Poldip3*	21.4	1	-1.77	2.71
Q8WYH8	*Ing5*	40.1	3	-1.77	2.63
Q9Y3L3	*Sh3bp1*	5	2	-1.76	1.60
O14578	*Cit*	7.2	7	-1.76	2.50
P01861	*Ighg1; Ighg3; Ighg2; Ighg4*	5.1	2	-1.76	5.65
P15941	*Muc1*	23.2	4	-1.75	4.25
P23511	*Nfya*	12.1	2	-1.74	4.06
Q9NP97	*Dynlrb2; Dynlrb1*	22.5	1	-1.74	1.90
P12081	*Hars*	20.5	5	-1.73	5.26
Q86VE0	*Mypop*	5.8	1	-1.72	3.19
P13995	*Mthfd2*	10.4	2	-1.71	1.65
P53803	*Polr2k*	31	2	-1.71	2.75

Q9BWN1	*Prr14*	6.7	3	-1.71	2.75
P13631	*Rarg*	4.4	1	-1.70	1.82
Q8TBE0	*Bahd1*	2.1	1	-1.70	2.54
O95251	*Kat7*	12.4	6	-1.69	3.18
Q96KM6	*Znf512b*	19.1	11	-1.69	3.10
Q8IY18	*Smc5*	5.5	5	-1.68	2.83
Q5SZX6	*Cct3*	11.4	3	-1.68	1.64
Q5T7W0	*Znf618*	4.6	2	-1.68	2.12
P52701	*Msh6*	5.5	5	-1.67	2.13
P26583	*Hmgb2*	34.9	13	-1.67	3.71
P55347	*Pknox1*	4.7	1	-1.66	2.85
Q9Y2T7	*Ybx2*	16.5	2	-1.65	2.53
P11388	*Top2a*	22.8	22	-1.65	2.67
Q9UGY1	*Nol12*	10.7	2	-1.64	1.37
Q9NV56	*Mrgbp*	43.6	4	-1.64	2.49
Q9BRJ6	*C7orf50*	42.2	6	-1.63	3.26
Q01658	*Dr1*	42.6	4	-1.63	1.45
Q96T88	*Uhrf1*	27.5	18	-1.63	4.27
Q5T0W9	*Fam83b*	9	6	-1.63	1.88
Q4KMQ1	*Tprn*	23.8	13	-1.62	3.38
P53999	*Sub1*	42.5	8	-1.62	3.07
Q9H1E3	*Nucks1*	30.5	10	-1.62	3.79
O15347	*Hmgb3*	40.5	11	-1.62	2.27
Q71DI3	*Hist2h3a*	49.3	2	-1.62	1.67
Q49A26	*Glyr1*	14.5	5	-1.61	2.02
Q86UV5	*Usp48*	4.4	1	-1.61	1.54
Q8TA86	*Rp9*	6.8	1	-1.61	1.48
P62306	*Snrpf*	15.1	1	-1.61	3.86
Q9UFW8	*Cggbp1*	18	3	-1.60	4.81
Q96T60	*Pnkp*	10.7	4	-1.60	1.54
Q6PL18	*Atad2*	24.9	27	-1.60	5.03
Q9H0H5	*Racgap1*	24.7	9	-1.60	5.11
Q9NS69	*Tomm22*	14.8	1	-1.60	2.42
P61244	*Max*	31.9	4	-1.60	3.77
P30405	*Ppif*	19.3	2	-1.59	2.98
O60216	*Rad21*	24.7	15	-1.59	2.11
Q15269	*Pwp2*	8.7	4	-1.59	1.40
O43809	*Nudt21*	15.9	4	-1.59	3.45
Q03164	*Kmt2a*	1.6	5	-1.59	1.68
Q66K89	*E4f1*	7.2	1	-1.59	2.56
Q6UXN9	*Wdr82*	6.4	1	-1.58	1.78
Q92665	*Mrps31*	6.8	2	-1.58	1.84
Q9Y2S6	*Tma7*	18.8	2	-1.58	2.78
Q6KC79	*Nipbl*	8.8	17	-1.57	2.38
Q92945	*Khsrp*	41.2	24	-1.57	5.36
Q9NVU7	*Sdad1*	5.5	3	-1.57	2.79

Q9NUQ3	*Txlng*	7.6	3	-1.57	1.54
P12004	*Pcna*	29.1	5	-1.57	3.46
Q9BSC4	*Nol10*	8	4	-1.56	1.90
P46013	*Mki67*	49.4	142	-1.56	2.92
P30040	*Erp29*	22.2	4	-1.56	3.04
Q92769	*Hdac2*	8.8	1	-1.55	1.46
Q5QNZ2	*Atp5f1*	4.6	2	-1.55	4.34
Q92917	*Gpkow*	14.1	4	-1.55	1.45
Q9P275	*Usp36*	9.7	6	-1.55	2.05
Q15004	*Kiaa0101*	44	2	-1.55	1.43
Q9BY77	*Poldip3*	36.1	8	-1.55	4.07
Q9NZM1	*Myof*	8.3	13	-1.54	3.76
P41208	*Cetn2*	71.5	9	-1.54	3.36
Q9NPF5	*Dmap1*	24.2	9	-1.54	1.66
P20042	*Eif2s2*	39.3	16	-1.53	1.83
Q9Y446	*Pkp3*	21.1	11	-1.53	3.24
P23588	*Eif4b*	15.1	7	-1.53	3.28
Q5TZA2	*Crocc*	1.8	3	-1.53	2.72
Q9H0E9	*Brd8*	16.1	8	-1.52	2.70
O00159	*Myo1c*	12.7	10	-1.52	3.38
Q15542	*Taf5*	6.9	3	-1.52	2.77
Q12792	*Twf1*	15.4	3	-1.52	4.20
O15391	*Yy2*	6.5	2	-1.52	3.41
Q9HBM6	*Taf9b; Taf9*	11.2	3	-1.51	2.06
Q92879	*Celf1*	29.4	9	-1.51	1.94
Q96MF7	*Nsmce2*	35.3	5	-1.51	2.48
Q9BR76	*Coro1b*	21.7	7	-1.51	3.76
P25490	*Yy1*	20.5	5	-1.51	3.00
P45973	*Cbx5*	67.5	19	-1.50	3.64
Q9NWB6	*Arglu1*	5.9	2	-1.50	2.20
Q9NQS7	*Incenp*	14.3	10	-1.50	3.89
O75940	*Smndc1*	38.2	6	-1.50	1.97
Q8N3F8	*Micall1*	7	1	-1.49	1.40
Q96JM3	*Champ1*	32.8	22	-1.49	2.15
Q96FF9	*Cdca5*	32.6	6	-1.49	3.12
O75475	*Psip1*	41.5	20	-1.49	3.29
Q15388	*Tomm20*	22.8	2	-1.48	2.30
P52434	*Polr2h*	12.8	2	-1.48	2.28
Q9UQB8	*Baiap2*	8.7	4	-1.48	2.58
Q8NC51	*Serbp1*	26.7	10	-1.48	2.23
Q8TAD8	*Snip1*	3.3	1	-1.48	1.49
Q96NB3	*Znf830*	22.8	4	-1.48	1.63
P09429	*Hmgb1*	49.8	12	-1.48	1.96
P23193	*Tcea1*	51.2	12	-1.47	2.67
Q9NX63	*Chchd3*	28	7	-1.47	1.56
P35659	*Dek*	34.4	14	-1.47	3.99

Q6IQ32	*Adnp2*	2.8	2	-1.46	1.66
Q15365	*Pcbp1*	52	8	-1.46	2.55
P54727	*Rad23b*	26.7	9	-1.46	2.67
P50990	*Cct8*	6	3	-1.46	3.35
O60869	*Edf1*	41.2	9	-1.46	4.94
Q9UKF6	*Cpsf3*	7.7	3	-1.46	2.68
Q12788	*Tbl3*	14.2	5	-1.45	2.75
Q9NYH9	*Utp6*	9.7	6	-1.45	2.79
Q96E11	*Mrrf*	35.9	6	-1.45	1.48
Q96ES7	*Ccdc101*	14.3	2	-1.45	1.63
O60828	*Pqbp1*	36.2	5	-1.45	2.11
Q8TEM1	*Nup210*	8.2	11	-1.45	2.21
Q9NPA8	*Eny2*	36.6	3	-1.44	2.24
Q8NEJ9	*Ngdn*	27.9	7	-1.44	2.30
P31948	*Stip1*	14.9	8	-1.44	1.48
P18887	*Xrcc1*	6.5	3	-1.44	2.13
P26358	*Dnmt1*	11.4	15	-1.44	4.22
Q8IYB3	*Srrm1*	8.9	5	-1.44	2.77
P26641	*Eef1g*	19.2	8	-1.44	1.72
Q9P0T4	*Znf581*	6.1	1	-1.43	1.87
Q86XP3	*Ddx42*	17.8	9	-1.43	1.77
P39880	*Cux1*	34.1	19	-1.43	2.62
Q8WW12	*Pcnp*	23.6	4	-1.43	2.45
P62277	*Rps13*	24.5	5	-1.43	2.19
Q08378	*Golga3*	7.7	7	-1.43	1.74
Q00059	*Tfam*	42.3	14	-1.43	2.50
Q9BTC0	*Dido1*	13	19	-1.43	3.75
P22415	*Usf1*	18.4	4	-1.43	2.04
Q6ZRS2	*Srcap*	4.5	10	-1.43	1.95
P62854	*Rps26; Rps26p11*	20.9	2	-1.43	1.47
Q8WXX5	*Dnajc9*	46.2	12	-1.42	3.30
P60866	*Rps20*	47.9	6	-1.42	3.07
O75937	*Dnajc8*	50.2	11	-1.42	2.58
Q13151	*Hnrnpa0*	38.7	10	-1.42	2.50
P25208	*Nfyb*	31.4	5	-1.42	1.89
Q9UMN6	*Kmt2b*	1.7	3	-1.42	1.43
O00148	*Ddx39a*	32.3	5	-1.42	2.23
P61088	*Ube2n; Ube2nl*	17.1	2	-1.42	1.48
E9PKP7	*Ubtf*	38.7	1	-1.41	3.28
Q8ND56	*Lsm14a*	10	1	-1.41	1.97
Q96I24	*Fubp3*	56.8	23	-1.41	3.94
Q13243	*Srsf5*	25	5	-1.41	2.58
P17931	*Lgals3*	17.2	4	-1.41	2.46
Q5EBL8	*Pdzd11*	35.7	2	-1.41	2.03
Q15056	*Eif4h*	39.1	9	-1.40	1.33
Q7KZF4	*Snd1*	39.9	26	-1.40	2.53

H0Y2W2	*Atad3a*	15	0	-1.40	1.91
O75128	*Cobl*	3.2	2	-1.40	2.00
Q92925	*Smarcd2*	14.5	6	-1.40	2.25
P15311	*Ezr*	29.9	13	-1.40	1.78
P51858	*Hdgf*	47.9	12	-1.39	1.89
Q9H875	*Prkrip1*	15.2	2	-1.39	2.72
P23771	*Gata3*	17.8	6	-1.39	3.15
Q5TBP9	*Lsm14b*	21.4	3	-1.39	1.99
Q8WXF1	*Pspc1*	41.5	20	-1.39	3.29
Q15723	*Elf2*	15.9	2	-1.39	1.94
Q9HAF1	*Meaf6*	33.5	6	-1.39	2.89
P62847	*Rps24*	35.1	4	-1.38	1.98
Q15906	*Vps72*	19.8	5	-1.38	1.92
P28290	*Ssfa2*	10.7	9	-1.38	1.38
Q13442	*Pdap1*	42	13	-1.38	3.37
Q9NQG5	*Rprd1b*	28.5	7	-1.38	1.87
Q8NCN4	*Rnf169*	5.4	2	-1.38	1.31
O75151	*Phf2*	11	8	-1.38	2.47
Q08945	*Ssrp1*	23.8	18	-1.38	3.17
P55145	*Manf*	35.1	6	-1.38	1.78
Q15428	*Sf3a2*	17	6	-1.37	2.57
Q16629	*Srsf7*	30.7	3	-1.37	1.72
P13987	*Cd59*	11.1	1	-1.37	1.48
P52272	*Hnrnpm*	48.2	20	-1.36	3.13
F5H608	*Atp5h*	23	2	-1.36	2.16
P40429	*Rpl13a; Rpl13a*	29.6	7	-1.36	2.39
Q13416	*Orc2*	18	6	-1.36	1.47
Q8N6H7	*Arfgap2*	27.7	5	-1.36	1.36
A8MXP9	*Matr3*	40	1	-1.36	2.44
P62805	*Hist1h4a*	68.9	14	-1.36	2.61
Q8WVK2	*Snrnp27*	36.1	4	-1.36	1.94
Q15691	*Mapre1*	29.5	6	-1.36	1.33
Q9NS91	*Rad18*	2.6	1	-1.35	1.68
D6R9P3	*Hnrnpab*	38.6	4	-1.35	1.95
P68104	*Eef1a1; Eef1a1p5*	48.9	6	-1.35	1.50
Q9GZU8	*Fam192a*	15.6	1	-1.35	1.38
P19387	*Polr2c*	7.6	2	-1.35	1.64
Q13045	*Flii*	6.9	5	-1.35	1.33
Q9NPD3	*Exosc4*	9.8	3	-1.35	1.65
P62851	*Rps25*	24	3	-1.35	1.71
P26599	*Ptbp1*	53.4	18	-1.34	1.71
Q9P258	*Rcc2*	10.3	5	-1.34	2.07
Q9UIS9	*Mbd1*	15.7	6	-1.34	1.45
Q16630	*Cpsf6*	23.2	7	-1.34	1.94
Q8N684	*Cpsf7*	23.4	9	-1.34	2.14
O95926	*Syf2*	41.2	7	-1.34	2.07

P42166	*Tmpo*	57.2	20	-1.34	3.69
P78371	*Cct2*	18.3	6	-1.34	1.45
Q15427	*Sf3b4*	21.5	6	-1.34	1.58
Q02880	*Top2b*	30.4	32	-1.34	3.09
Q01085	*Tial1*	36	6	-1.34	1.36
Q9NUP9	*Lin7c*	31.5	5	-1.34	3.40
Q13247	*Srsf6*	25.3	7	-1.33	2.18
O75486	*Supt3h*	15.5	3	-1.33	1.42
O95696	*Brd1*	9.5	6	-1.33	2.00
O43583	*Denr*	52.5	9	-1.33	1.94
Q96AY3	*Fkbp10*	5	2	-1.33	1.57
Q9H0L4	*Cstf2t*	33.4	7	-1.33	2.46
P08670	*Vim*	53.8	20	-1.33	3.34
Q8IWZ8	*Sugp1*	11.2	5	-1.33	1.42
P26368	*U2af2*	43.4	12	-1.33	1.83
Q92785	*Dpf2*	25.7	7	-1.32	1.50
Q1KMD3	*Hnrnpul2; Hnrnpul2-Bscl2*	52.1	32	-1.32	2.33
Q13185	*Cbx3*	56.3	9	-1.32	1.90
Q92979	*Emg1*	14.8	3	-1.32	1.64
P62701	*Rps4x*	38.8	11	-1.32	1.67
P52435	*Polr2j; Polr2j3; Polr2j2*	50.4	4	-1.32	1.45
Q9UNP9	*Ppie*	41.2	9	-1.32	2.36
P84098	*Rpl19*	19.2	6	-1.32	2.45
Q29RF7	*Pds5a*	8	7	-1.32	2.30
Q9Y3C6	*Ppil1*	27.1	3	-1.32	1.88
Q9NTI5	*Pds5b*	8.9	6	-1.32	1.95
P04843	*Rpn1*	25.7	11	-1.32	2.61
P30101	*Pdia3*	24	8	-1.32	1.65
Q5SRQ3	*Csnk2b-Ly6g5b-1181; Csnk2b; Csnk2b-Ly6g5b--991*	18.4	3	-1.31	1.45
O15460	*P4ha2*	5.6	2	-1.31	1.35
P62081	*Rps7*	53.6	11	-1.31	1.58
P08579	*Snrpb2*	25.3	4	-1.31	3.19
P23396	*Rps3*	41.2	8	-1.31	1.66
Q99549	*Mphosph8*	23.3	13	-1.31	2.18
Q15637	*Sf1*	21	14	-1.31	1.83
Q86V81	*Alyref*	52.1	2	-1.31	1.83
O14979	*Hnrnpdl*	39.7	17	-1.31	1.90
Q9NSI2	*Fam207a*	30.4	5	-1.31	3.09
Q9Y4Y9	*Lsm5*	85.7	3	-1.31	2.75
Q8WWQ0	*Phip*	9.2	14	-1.31	2.06
Q7L014	*Ddx46*	25.9	1	-1.30	2.38
O15514	*Polr2d*	69	10	-1.30	1.59
Q9UIG0	*Baz1b*	19.4	24	-1.30	1.44

Q9NV31	*Imp3*	15.2	2	-1.30	1.46
P49848	*Taf6*	6.7	4	-1.30	1.82
P83916	*Cbx1*	58.4	9	-1.30	3.36
P16403	*Hist1h1c*	33.3	3	-1.30	2.31
O95758	*Ptbp3*	22.6	10	-1.30	2.92
Q7Z4V5	*Hdgfrp2*	11.2	8	-1.30	1.48
P62304	*Snrpe*	78.8	3	-1.30	1.65
O95400	*Cd2bp2*	51.3	12	-1.30	2.86
O75962	*Trio*	2	1	-1.30	1.92
P84103	*Srsf3*	37.8	6	-1.30	1.58
Q13838	*Ddx39b*	40.2	9	-1.30	1.76
P51398	*Dap3*	5	1	-1.30	2.05
Q15287	*Rnps1*	35.1	7	-1.30	1.34
P16401	*Hist1h1b*	33.2	14	-1.30	2.22
Q14103	*Hnrnpd*	34.1	11	-1.30	2.21
Q8IXM2	*C17orf49; BAP18; RNASEK-C17orf49*	40.8	5	-1.30	1.40
Q96A72	*Magohb*	60	1	-1.30	1.66
Q8WYP5	*Ahctf1*	13.1	18	-1.29	2.10
Q96T23	*Rsf1*	28.8	34	-1.29	3.35
Q14498	*Rbm39*	29.6	10	-1.29	2.72
Q9UHX1	*Puf60*	32.7	13	-1.29	2.43
Q9UPN4	*Cep131*	4.5	3	-1.29	1.54
P61978	*Hnrnpk*	63.3	6	-1.29	2.26
P98175	*Rbm10*	26.5	17	-1.29	2.50
Q15717	*Elavl1*	40.2	12	-1.29	2.68
P27695	*Apex1*	47.5	12	-1.28	1.79
P49916	*Lig3*	15.6	10	-1.28	2.29
P20700	*Lmnb1*	72.4	58	-1.28	3.11
Q12830	*Bptf*	9.3	19	-1.28	3.45
Q14839	*Chd4*	28.8	38	-1.27	1.38
Q96DI7	*Snrnp40*	12.3	2	-1.27	1.85
O43823	*Akap8*	26.6	13	-1.27	2.15
Q03188	*Cenpc*	16.1	10	-1.27	2.49
O43390	*Hnrnpr*	47.7	23	-1.27	3.02
P50402	*Emd*	37.8	9	-1.27	2.30
Q16778	*Hist2h2be; Hist1h2bj; Hist1h2bb; Hist1h2bo*	65.9	0	-1.27	1.44
Q07955	*Srsf1*	55.7	20	-1.27	2.20
P23284	*Ppib*	58.3	17	-1.27	3.50
P10412	*Hist1h1e*	32.9	3	-1.27	2.56
P38646	*Hspa9*	36.7	17	-1.26	2.13
H0YAE9	*Rnaset2*	5.4	1	-1.26	1.78
P38919	*Eif4a3*	45.3	14	-1.26	1.34
Q9Y5B6	*Paxbp1*	2	1	-1.26	1.54

Q13427	*Ppig*	15.5	12	-1.26	2.57
P35232	*Phb*	31.3	5	-1.26	1.46
Q96SB8	*Smc6*	11.6	9	-1.26	1.95
P62316	*Snrpd2*	65.3	13	-1.26	2.71
Q9BUQ8	*Ddx23*	35.9	30	-1.26	2.57
Q9UIF9	*Baz2a*	5.9	9	-1.26	1.86
P31942	*Hnrnph3*	47.7	13	-1.25	2.70
P09012	*Snrpa*	19.1	3	-1.25	1.71
P25705	*Atp5a1*	38.9	15	-1.25	2.71
P0DN76	*U2af1*	37.5	6	-1.25	1.81
Q08211	*Dhx9*	30.1	33	-1.25	1.40
Q96C57	*C12orf43*	34.8	4	-1.25	1.61
Q9H2K8	*Taok3*	25.3	18	-1.24	2.12
Q8TAT6	*Nploc4*	13.4	1	-1.24	1.45
P05114	*Hmgn1*	53	9	-1.24	3.09
Q9H0A0	*Nat10*	23.5	16	-1.24	1.36
Q13573	*Snw1*	48.3	26	-1.24	1.46
Q99986	*Vrk1*	38.4	10	-1.24	2.24
Q96HS1	*Pgam5*	12.5	3	-1.23	2.13
P35637	*Fus*	24.9	11	-1.23	2.18
Q14676	*Mdc1*	14.6	14	-1.23	1.39
Q9UN81	*L1re1*	33.7	12	-1.23	1.93
Q9NW64	*Rbm22*	35.5	10	-1.23	1.85
Q9H307	*Pnn*	36.1	31	-1.23	2.63
P41091	*Eif2s3; Eif2s3l*	34.1	10	-1.23	1.39
Q92797	*Sympk*	14.8	11	-1.23	1.50
Q9BVL2	*Nupl1*	9.3	4	-1.23	1.50
P22087	*Fbl*	25.9	10	-1.23	1.62
Q03252	*Lmnb2*	58.2	43	-1.22	2.67
O95777	*Lsm8*	71.9	5	-1.22	1.75
Q9Y2K7	*Kdm2a*	8.4	7	-1.22	2.84
Q9BZF9	*Uaca*	27.9	32	-1.22	1.67
Q8WZ42	*Ttn*	0.3	9	-1.22	1.32
Q5UIP0	*Rif1*	11.9	17	-1.22	1.67
O00541	*Pes1*	13.6	4	-1.22	1.41
Q9UQE7	*Smc3*	41.4	49	-1.22	2.58
O14686	*Kmt2d*	0.8	4	-1.22	1.67
Q15424	*Safb*	31.4	21	-1.21	2.24
Q9UKV3	*Acin1*	37.6	35	-1.21	2.34
Q9Y5S9	*Rbm8a*	58	10	-1.21	1.96
Q13435	*Sf3b2*	43.5	25	-1.21	2.17
Q96EU6	*Rrp36*	36.3	7	-1.21	1.65
P06400	*Rb1*	2.7	2	-1.21	1.58
Q9Y5B9	*Supt16h*	22.6	22	-1.21	2.60
P67809	*Ybx1*	44.1	6	-1.21	2.15
P22626	*Hnrnpa2b1*	76.8	37	-1.21	1.78

Q9NYB0	*Terf2ip*	29.8	5	-1.21	1.96
Q9BRD0	*Bud13*	3.7	2	-1.21	1.95
O43143	*Dhx15*	11.8	11	-1.21	1.45
O60506	*Syncrip*	58.9	34	-1.21	1.70
A0A0C4DG89	*Ddx46*	26	1	-1.21	2.67
Q99879	*Hist1h2bm*	65.9	1	-1.21	2.06
Q969G3	*Smarce1*	35.1	12	-1.20	1.82
Q02878	*Rpl6*	23.3	7	-1.20	1.79
P42167	*Tmpo*	52	2	-1.20	1.50
O95232	*Luc7l3*	24.5	11	-1.20	2.09
P27816	*Map4*	18.8	26	-1.20	1.41
P09874	*Parp1*	50.4	47	-1.20	1.80
O14776	*Tcerg1*	28.6	34	-1.20	1.94
P49458	*Srp9*	34.9	3	-1.19	1.40
P84090	*Erh*	55.8	7	-1.19	1.92
P16402	*Hist1h1d*	32.6	3	-1.19	1.36
Q9NYF8	*Bclaf1*	25.9	4	-1.19	1.78
Q07020	*Rpl18*	20.1	3	-1.19	1.33
P33240	*Cstf2*	40.6	10	-1.19	1.50
P43243	*Matr3*	39.4	1	-1.19	1.40
P50914	*Rpl14*	33.1	4	-1.19	2.02
Q14683	*Smc1a*	46.2	56	-1.18	2.20
O95785	*Wiz*	24.2	13	-1.18	1.60
P14859	*Pou2f1*	19.8	9	-1.18	1.48
Q9BWJ5	*Sf3b5*	64	4	-1.18	1.44
Q9Y3U8	*Rpl36*	26.7	6	-1.18	1.36
O60264	*Smarca5*	27.8	27	-1.17	2.50
P63162	*Snrpn; Snrpb*	27.8	5	-1.17	2.01
O94906	*Prpf6*	36.5	29	-1.17	1.48
P08621	*Snrnp70*	47.1	17	-1.16	2.17
Q13242	*Srsf9*	41.6	16	-1.16	1.48
P49756	*Rbm25*	29.2	22	-1.15	1.79
Q96JP5	*Zfp91-Cntf; Zfp91*	4.2	1	-1.15	1.60
P31943	*Hnrnph1*	57	15	-1.15	2.68
Q9Y383	*Luc7l2*	38.8	8	-1.15	1.70
Q96MU7	*Ythdc1*	8.7	6	-1.14	1.66
Q9BWF3	*Rbm4*	34.6	2	-1.14	2.89
Q6ISB3	*Grhl2*	42.9	18	-1.14	1.70
G3V4W0	*Hnrnpc*	71	4	-1.13	1.47
P38432	*Coil*	15.6	9	-1.13	1.46
O95478	*Nsa2*	21.2	5	-1.11	1.61
P62979	*Rps27a; Ubb; Ubc; Uba52*	59	10	-1.10	1.92
P17844	*Ddx5*	45.3	19	1.12	1.47
P46087	*Nop2*	25	18	1.12	1.57

O95425	*Svil*	9	14	1.13	1.32
Q9BPX5	*Arpc5l*	38.6	4	1.21	2.57
A0A0A0MRM8	*Myo6*	33.8	1	1.21	2.53
Q9H501	*Esf1*	12.8	13	1.21	1.61
O43719	*Htatsf1*	8.6	4	1.21	1.54
Q27J81	*Inf2*	18.3	7	1.22	1.33
O14974	*Ppp1r12a*	28.4	30	1.23	1.41
Q6PJG2	*Elmsan1*	22.6	17	1.23	1.61
D6R904	*Tpm3*	67.4	0	1.24	4.18
Q9P2M7	*Cgn*	49.3	53	1.27	2.37
Q2TB10	*Znf800*	7	1	1.27	2.34
Q5VZF2	*Mbll; Mbnl2; Mbnl1*	11	1	1.27	3.38
Q5T7V8	*Gorab*	9.4	2	1.27	1.79
P19105	*Myl12a; Myl12b; Myl9*	60.5	9	1.28	1.58
P60953	*Cdc42*	27.2	5	1.29	1.39
Q7Z7K6	*Cenpv*	9.8	2	1.30	1.32
Q5HYB6	*Dkfzp686j1372*	70.7	0	1.31	3.19
Q6NZY4	*Zcchc8*	15.1	6	1.32	1.47
Q9BUP0	*Efhd1*	55.2	15	1.33	3.51
Q92614	*Myo18a*	20.5	30	1.33	1.85
Q9Y657	*Spin1*	37.8	6	1.33	1.96
Q7Z406	*Myh14*	44.2	71	1.33	1.52
Q9P0M6	*H2afy2*	27.7	5	1.35	1.85
Q99733	*Nap1l4*	19.4	3	1.36	1.42
O75362	*Znf217*	23.2	17	1.38	2.54
Q1ED39	*Knop1*	36.9	12	1.38	1.58
Q9BV36	*Mlph*	32.2	9	1.39	2.48
P08238	*Hsp90ab1*	23.2	8	1.40	2.11
Q6NUQ4	*Tmem214*	5.1	3	1.40	1.41
Q9H0U9	*Tspyl1*	14.6	4	1.40	3.77
H7BYY1	*Tpm1*	81	0	1.40	2.81
P63261	*Actg1*	78.1	2	1.41	2.96
P63010	*Ap2b1*	2.8	1	1.45	3.37
M0QY43	*Myh14*	32.4	2	1.46	1.35
P05976	*Myl1; Myl3*	8.2	2	1.47	2.08
Q14966	*Znf638*	22.5	28	1.48	1.41
A8CG34	*Pom121c*	8.1	2	1.48	1.73
Q9C0C2	*Tnks1bp1*	4.7	4	1.49	1.42
Q9UL16	*Cfap45*	2.3	1	1.50	1.46
Q14247	*Cttn*	46.2	26	1.50	4.35
P63313	*Tmsb10*	63.6	3	1.51	1.58
P37802	*Tagln2*	42.8	7	1.53	1.59
P61158	*Actr3*	36.8	8	1.53	2.44
Q5T0I0	*Gsn*	41.5	2	1.54	2.17

Q8N884	*Mb21d1*	10	3	1.54	3.21
O43707	*Actn4*	68.6	44	1.55	3.49
P07951	*Tpm2*	32.4	0	1.57	3.11
P61218	*Polr2f*	26.5	1	1.58	1.42
Q14677	*Clint1*	10.9	4	1.58	2.56
O75369	*Flnb*	56.7	89	1.59	2.99
P17980	*Psmc3*	10.9	2	1.60	1.33
O15143	*Arpc1b*	21	6	1.61	3.86
Q96IZ0	*Pawr*	47.4	11	1.63	1.94
Q9H8G2	*Caap1*	6.6	2	1.64	1.52
Q9Y2X9	*Znf281*	2	1	1.64	1.58
P08195	*Slc3a2*	6.3	2	1.64	1.78
Q9H3U1	*Unc45a*	18.4	14	1.65	4.85
Q6ZVM7	*Tom1l2*	38.9	15	1.66	2.56
Q15758	*Slc1a5*	9.9	2	1.67	1.71
P17676	*Cebpb*	27.8	6	1.67	1.62
O95817	*Bag3*	32.2	11	1.67	2.16
O75190	*Dnajb6*	20.2	5	1.68	2.07
A0AV96	*Rbm47*	54.2	2	1.68	2.23
Q14651	*Pls1*	3.3	1	1.69	1.58
E7EX73	*Eif4g1*	7	7	1.70	2.09
Q01082	*Sptbn1*	53.7	108	1.70	5.26
Q13813	*Sptan1*	68.1	1	1.71	5.35
H0YL52	*Tpm1*	70.2	2	1.72	5.20
Q9UHG0	*Dcdc2*	12.2	3	1.73	1.87
Q8N8S7	*Enah*	13	4	1.74	1.86
Q9UQN3	*Chmp2b*	10.4	2	1.75	1.45
Q9Y3L5	*Rap2c*	10.3	1	1.75	2.68
Q9H444	*Chmp4b*	17.9	3	1.76	1.54
O15049	*N4bp3*	3.9	2	1.76	1.97
Q9H6W3	*No66*	22.9	10	1.78	2.51
P67936	*Tpm4*	76.6	16	1.78	7.04
Q9UHB6	*Lima1*	45.7	28	1.79	5.92
O00515	*Lad1*	42.4	21	1.81	3.49
P09496	*Clta*	10.9	4	1.82	2.70
P61160	*Actr2*	26.6	7	1.84	3.11
Q53SF7	*Cobll1*	4.5	3	1.85	1.48
Q8N594	*Mpnd*	13.2	1	1.87	1.53
Q5M775	*Specc1*	22.3	16	1.89	4.74
O15020	*Sptbn2*	31.8	48	1.90	3.74
P22314	*Uba1*	7	4	1.90	2.62
P31949	*S100a11*	36.2	3	1.91	2.51
P62328	*Tmsb4x*	86.4	5	1.92	4.45
Q8IVI9	*Nostrin*	14.7	1	1.94	3.00
P35998	*Psmc2*	6	2	1.99	1.45
P15408	*Fosl2*	29.7	5	2.00	5.05

Q9ULV4	*Coro1c*	25.7	6	2.02	3.26
Q7Z6I8	*C5orf24*	22.3	3	2.02	2.63
Q92610	*Znf592*	6.2	3	2.03	1.43
P12814	*Actn1*	51.1	22	2.03	4.31
O15145	*Arpc3*	20.8	3	2.04	3.05
Q60FE5	*Flna*	59.2	2	2.04	4.35
O60437	*Ppl*	27.4	38	2.06	4.07
Q3KQU3	*Map7d1*	1.9	1	2.10	2.14
P53814	*Smtn*	7.1	5	2.12	2.03
Q99996	*Akap9*	1.3	2	2.13	1.49
Q7Z3J3	*Rgpd3; Rgpd4; Rgpd8; Rgpd5*	4.5	2	2.15	2.14
P04792	*Hspb1*	68.3	11	2.16	6.81
P21333	*Flna*	59.4	3	2.18	5.26
Q9UNX3	*Rpl26l1*	27.6	1	2.19	1.51
P54652	*Hspa2*	13.3	1	2.24	2.76
P21291	*Csrp1*	37.9	3	2.27	3.10
O94832	*Myo1d*	7.8	7	2.28	1.80
Q8TBL5	*Larp4*	10.4	1	2.31	1.91
P17275	*Junb*	27.1	5	2.31	1.61
Q86UP2	*Ktn1*	4	2	2.52	2.35
Q8NEU8	*Appl2*	6	1	2.66	4.60
Q9UHR4	*Baiap2l1*	10	3	2.70	2.29
P61026	*Rab10*	11.5	2	2.72	1.34
P05783	*Krt18*	88.8	33	2.79	2.17
O00151	*Pdlim1*	19.8	3	2.84	4.28
E9PMS6	*Lmo7*	31.5	0	2.85	5.63
P09493; H0YKP3	*Tpm1*	62.3	0	2.88	1.41
Q9P0K7	*Rai14*	11.8	9	2.91	3.10
P06756	*Itgav*	1.3	1	3.09	3.00
Q96CF2	*Chmp4c*	11.6	1	3.33	2.75
Q9NWM3	*Cuedc1*	17.9	2	3.34	1.78
Q96PY6	*Nek1*	1.3	1	3.46	4.06
Q15654	*Trip6*	10.7	1	3.50	2.44
A0A075B730	*Eppk1*	51.5	5	3.70	1.76
F8W8M4	*Ablim1*	17.5	8	3.84	4.77
Q5SZC9	*Abracl*	23.9	1	3.85	1.44
Q8IWY7		2.1	1	3.86	1.95
Q8TEQ6	*Gemin5*	0.9	1	4.01	1.70
Q4G0J3	*Larp7*	7.9	3	5.67	1.90
Q8N3V7	*Synpo*	3.4	2	5.78	2.53
Q9UMR2	*Ddx19a; Ddx19b*	16.5	1	7.32	2.01
Q9UM54	*Myo6*	32.1	1	8.16	1.55
Q9BRP0	*Ovol2*	6.5	1	8.39	3.49
Q7Z3Z5	*Tnrc11; Med12*	2.1	3	8.70	2.00

Q8TED0	*Utp15*	8.8	3	9.74	2.03
Q05682	*Cald1*	5.3	4	13.81	5.82
Q9UNF0	*Pacsin2*	5.5	2	14.25	1.51
Q15008	*Psmd6*	19.4	2	15.67	3.09
Q5H8X8	*Uts2*	5.8	1	15.98	2.11
Q9UJY1	*Hspb8*	41.3	5	21.97	5.32